Fall 12-22-2010

6- and 5-Halodecaboranes: Selective Syntheses From ClOSO-B10H10(2-) and Use as Polyborane Building Blocks

William C. Ewing
University of Pennsylvania, wce@sas.upenn.edu

6- and 5-Halodecaboranes: Selective Syntheses From ClOSO-B10H10(2-) and Use as Polyborane Building Blocks

Abstract
Decaborane halogenated in the 6-position has been synthesized in high yields via the super-acid induced cage-opening reactions of closo-B10H10(2-) salts. These 6-halogenated compounds were then isomerized to their 5-substituted isomers through base catalysis. The isomerization was driven by the energy differences between the anionic-forms of each respective isomer. These reactions provided 5-halodeboranes in high yields. The bridging-hydrogens of the halodecaboranyl anions were fluxional at a range of temperatures. Variable-temperature NMR studies supported computationally proposed fluxional mechanisms. Both 5- and 6-halodecaboranes were reacted with alcohols yielding boranyl ethers. The mechanisms of substitution, where reactions with 6- and 5-halodecaboranes yielded 5- and 6-boranyl ethers, respectively, were explained computationally and confirmed through isotopic-labeling studies.

The regeneration of the polymeric products of ammonia-borane dehydrogenation was carried out through a process that included digestion of the polymer, complexation of the digestate with a base, reduction of B-X bonds to B-H bonds, and finally displacement of the base with ammonia. While digestion schemes proved unable to digest all forms of the dehydrogenated materials, portions of the polymer digested to boron-trihalides were quantitatively regenerated to ammonia borane, with complete separation and collection of by-products.

Degree Type
Dissertation

Degree Name
Doctor of Philosophy (PhD)

First Advisor
Larry G. Sneddon

Keywords
Substituted Decaboranes, Halogenated Decaboranes, Polyboranes, Hydrogen Storage, Boranyl Ethers, Variable Temperature NMR

Subject Categories
Chemistry | Inorganic Chemistry

6- AND 5-HALODECABORANES: SELECTIVE SYNTHESES FROM *closo*-$B_{10}H_{10}^{2-}$ AND USE AS POLYBORANE BUILDING BLOCKS

William C. Ewing

A DISSERTATION

in

Chemistry

Presented to the Faculties of the University of Pennsylvania in Partial Fulfillment of the Requirements for the Degree of Doctor of Philosophy

2010

____

Professor Larry G. Sneddon
Supervisor of Dissertation

____

Professor Gary Molander
Graduate Group Chair

Committee Members:

Dr. I. Dmochowski, Professor of Chemistry
Dr. D. Berry, Professor of Chemistry
Dr. P. Walsh, Professor of Chemistry

Acknowledgment

I would like to gratefully acknowledge Professor James E. Davis and Professor Larry G. Sneddon, the men responsible for my discovery and re-discovery of chemistry. Similar acknowledgement is deserved of my parents, Peter and Deborah Ewing, whose support, if not patience, has been unwavering. Acknowledgement is also due the friends and colleagues, too numerous to mention, known to spike the too-oft bland punch served at the cantina of the day-to-day.

> “But then they danced down the street like dingledodies, and I shambled after as I've been doing all my life after people who interest me, because the only people for me are the mad ones, the ones who are mad to live, mad to talk, mad to be saved, desirous of everything at the same time, the ones who never yawn or say a commonplace thing, but burn, burn, burn, like fabulous yellow roman candles exploding like spiders across the stars and in the middle you see the blue centerlight pop and everybody goes ‘Awww!’”
>
> \- J. Kerouac

ABSTRACT

6- AND 5-HALODECABORANES: SELECTIVE SYNTHESES FROM *closo*-$B_{10}H_{10}^{2-}$ AND USE AS POLYBORANE BUILDING BLOCKS

William C. Ewing

Larry G. Sneddon

Decaborane halogenated at the 6-position (6-X-$B_{10}H_{13}$, X = Cl, Br, I) was synthesized through cage-opening reactions of *closo*-$B_{10}H_{10}^{2-}$ induced by treatment with hydrogen halides absorbed in ionic liquid mixtures known to greatly enhance HX acidity. The previously unknown member of the 6-halogenated series, 6-F-$B_{10}H_{13}$, was synthesized in excellent yields by reaction of the *closo*-$B_{10}H_{10}^{2-}$ with triflic acid in the presence of 1-fluoropentane. Triflic acid also induced the cage-opening of *closo*-$B_{10}H_{10}^{2-}$ to 6-Cl-$B_{10}H_{13}$ when performed in CH_2Cl_2.

The 6-halogenated isomers were used as starting materials in the syntheses of 5-X-$B_{10}H_{13}$ (X = Cl, Br, I). Base catalyzed isomerization reactions yielded equilibrium mixtures of 5-X-$B_{10}H_{13}$ and 6-X-$B_{10}H_{13}$ with ratios dictated by the free energy difference between the respective anions, 5-X-$B_{10}H_{12}^{-}$ and 6-X-$B_{10}H_{12}^{-}$, strongly favoring the 5-substituted isomer. Pure 5-X-$B_{10}H_{13}$ was isolated in good yields by selective crystallization or by chromatography. These syntheses represent a significant step forward in the chemistry of this isomer, and provide the first path by which these compounds may be synthesized in useful quantities.

Calculations on the 5- and 6-halogenated anions identified fluxional processes by which bridging hydrogens move about the open face of the cage, explaining the results of variable-temperature NMR studies on these compounds. Variable-temperature NMR was also used to validate similar processes previously proposed for the parent $B_{10}H_{13}^{-}$.

As proof of the utility of 5-X-$B_{10}H_{13}$ and 6-X-$B_{10}H_{13}$ as starting materials for further functionalization a new class of boranyl ether compounds, selectively substituted at the 6- or 5-position, were synthesized using the reaction of the halogenated species with alcohols. A range of alcohols, with various pendant functional groups, were tethered to the cage via a rare B-O-C organic/inorganic ether linkage. The regiochemistry of the reaction was unique in that reaction of 5-X-$B_{10}H_{13}$ with alcohols selectively yielded 6-RO-$B_{10}H_{13}$ ethers, and 6-X-$B_{10}H_{13}$ with the same alcohols yielded 5-RO-$B_{10}H_{13}$ compounds. A plausible reaction mechanism explaining this regiochemistry was found using DFT calculations, which subsequent experiments with deuterated starting materials supported.

Table of Contents

Chapter 1

Introduction and Outline of the Dissertation

1.1 Outline of the Dissertation

The major goal of the research presented in this dissertation was to develop new synthetic routes to functionalized decaborane ($B_{10}H_{14}$) derivatives. These new synthetic pathways now allow the cage to be used as a building block by the wider chemistry community.

Chapter 2 details the use of strongly acidic conditions to affect the cage-opening reactions of *closo*-$B_{10}H_{10}^{2-}$salts, selectively yielding *nido*-6-X-$B_{10}H_{13}$ (**6X**) compounds (X = F, Cl, Br, I). Halodecaboranes have been previously synthesized, but never regioselectively in high yields. In contrast, the methods presented in Chapter 2 provide a pathway whereby the **6X** cages can be synthesized as single isomers in high yields. The synthesis of the previously unknown 6-F-$B_{10}H_{13}$ is presented and discussed, as well as the syntheses and mechanistic implications of two 6-X-9-(C_2H_5)-$B_{10}H_{12}$ compounds (X = Br, I).

The work presented in **Chapter 3** demonstrates that the **6X** compounds synthesized in Chapter 2 may be used as starting materials in the syntheses of the 5-X-$B_{10}H_{13}$ (**5X**, X = Cl, Br, I) isomer. Treatment of **6X** with catalytic quantities of base promoted movement of the halide, resulting in the formation of **5X**. These reactions provided **5X** in yields far surpassing those found in the literature, and represent a major step forward in the availability of these compounds. Reactions with Proton Sponge, a strong Bronsted- but weak Lewis-base, provided evidence that the isomerization proceeded via the 6-X-$B_{10}H_{12}^-$ anion, to an equilibrium mixture of the two anions, favoring 5-X-$B_{10}H_{12}^-$. DFT calculations indicated that the free energy (ΔG^o) differences between the 6-X-$B_{10}H_{12}^-$ and 5-X-$B_{10}H_{12}^-$ drove the isomerization reactions, and the predicted equilibrium constants, based on calculated values of ΔG^o, were a good match for the observed ratios of compounds at equilibrium.

Chapter 4 describes computational (DFT) and spectroscopic (variable-temperature NMR) studies of the fluxional behavior of $B_{10}H_{13}^-$ and its halogenated derivatives (5-Cl-, 6-Cl-, and 6-F-$B_{10}H_{12}^-$). The results of the VT-NMR examination of $B_{10}H_{13}^-$ provided evidence for a previously proposed mechanism whereby the three bridging-protons on the anion rapidly move about the open face of the cage, producing apparent C_{2v} symmetry on the NMR time scale at elevated temperatures. Similar VT-NMR studies of 6-X-$B_{10}H_{12}^-$ (X = Cl, F) indicated similar fluxional pathways, which were also explained with DFT calculations.

The work presented in **Chapter 5** demonstrated that both **5X** and **6X** can be used as starting points in the syntheses of functionalized decaboranes. The syntheses of 6- and 5-RO-$B_{10}H_{13}$ mixed organic/inorganic ethers via nucleophilic substitution reactions are described and represent an expansion of the known chemistry of decaborane. Prior to this work, examples of decaboranyl ethers were limited, with organic groups limited to short alkyl chains. The robust chemistry in Chapter 5 allowed for the syntheses of decaboranyl-cages tethered to a wide variety of functional groups. While in textbook substitution reactions the incoming nucleophile takes the place of the exiting leaving-group, the substitution of the halogen on 6- and 5-X-$B_{10}H_{13}$ yielded 5-RO- and 6-RO-$B_{10}H_{13}$ decaboranyl ethers, respectively. A mechanism was computationally identified that involves attack of alcohol at the B5/B6 site adjacent to the halogenated vertex, movement of the terminal-hydrogen at this vertex into a bridging-position, and movement of the bridging-hydrogen at this spot into the position of the vacating halogen. This mechanism explained the regiochemistry, contained no steps with energies unattainable under reaction conditions, and is supported by the results of studies with isotopically labeled halodecaboranes.

Chapter 6 describes efforts aimed at the rehydrogenation of the polymeric product of the dehydrogenation of ammonia borane. Ammonia borane is considered a potentially useful chemical hydrogen storage material; however, its eventual utility may ultimately be determined by whether or not efficient methods can be found to rehydrogenate spent products. Chapter 6 details a process by which polymeric spent-fuel was digested into monomeric units by strong acids, followed by complexation of boron to Lewis bases, rehydrogenation using metal hydrides, and final displacement of the Lewis base by ammonia. While digestion steps were unable to completely degrade the polymeric spent fuels into monomeric units, regeneration of ammonia borane from the halogenated intermediate BBr_3 was quantitative. The system promoted near-quantitative separation and recovery of all products and by-products.

Polyhedral boranes are fascinating molecular systems, but their chemistry is not as widely followed in the general chemical community as perhaps they warrant. As such, a brief introduction to the types of compounds this dissertation describes is offered here.

1.2 Introduction: Decadecaborate and Decaborane.

The decaborate anion ($B_{10}H_{10}^{2-}$) and neutral decaborane ($B_{10}H_{14}$) are the two most important parent boron hydride species to the work presented in this dissertation. As such, the basics of their structure and chemistry will be reviewed briefly.

1.2.1 *closo*-$B_{10}H_{10}^{2-}$

The $B_{10}H_{10}^{2-}$ anion, depicted in **Figure 1.1**, was first reported by Hawthorne and Pitochelli in 1959,[1] a year before the discovery of the related, and more frequently studied, $B_{12}H_{12}^{2-}$ icosahedron.[2] The bicapped square antiprism (D_{4d}) consists of two staggered 4-membered rings of boron atoms (**Figure 1.1**, B2-B9) and two capping boron vertices (B1, B10). Each boron vertex bears one bond to a terminal-hydrogen atom. The ^{11}B NMR of the anion reflects the two different boron environments, displaying an intensity-2 peak at ~ -1 ppm, and an intensity-8 peak at ~ -31 ppm.

The chemistry of the $B_{10}H_{10}^{2-}$ anion has recently been reviewed.[3] For this reason, the treatment of the chemistry of the anion here is not exhaustive, as the details not included in this dissertation are already compiled and available. A brief overview of the synthesis of the anion and known substitution reaction is provided here, in hopes that future work combining chemistry in this dissertation with substituted-*closo*-cages might lead to useful *nido*-products. The electronic structure of the compound is also discussed, as the three dimensional delocalization of charge (3-dimensional aromaticity) was the reason that our cage-opening reactions required the forcing conditions we employed. A general discussion of the cage-opening reactions of $B_{10}H_{10}^{2-}$ is saved for **Chapter 2**.

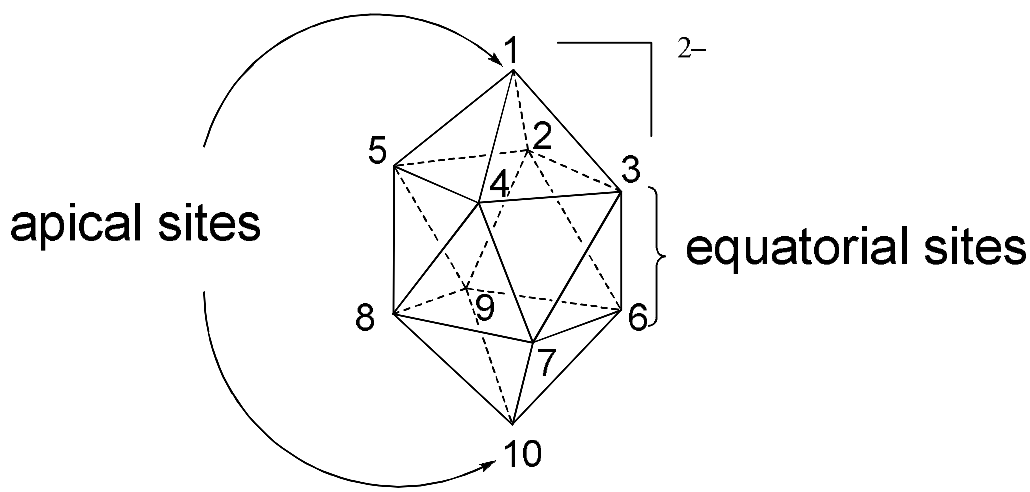

Figure 1.1. The $B_{10}H_{10}^{2-}$ deltahedron.

1.2.1.1 Syntheses

The most common synthesis of *closo*-$B_{10}H_{10}^{2-}$ is from the 6,9-bis-adducts of decaborane (**Section 1.2.2.4**). For example, the reaction of the bis-acetonitrile adduct of *nido*-decaborane with triethylamine, or the bis-dimethylsulfide adduct with liquid ammonia yielded $[Et_3NH^+]_2[B_{10}H_{10}^{2-}]$[4] and $[NH_4^+]_2[B_{10}H_{10}^{2-}]$[5], respectively (**Eq. 1**). However, due to the fact that this synthesis requires the use of $B_{10}H_{14}$, a compound generally synthesized through a hazardous diborane (B_2H_6) pyrolysis, the usefulness of these syntheses is limited.

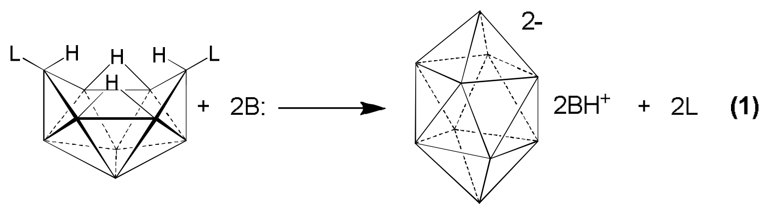

As will be discussed in **Chapter 2**, there are known routes to $B_{10}H_{10}^{2-}$ compounds via the controlled pyrolysis of the cheap and readily available borohydride $[NEt_4^+][BH_4^-]$ that have the potential to make these cages more readily available. These methods are of particular importance to this work, as our syntheses of open *nido*-halodecaboranes start from *closo*-$B_{10}H_{10}^{2-}$. The borohydride-based syntheses, combined with the chemistry in this dissertation, provide safe, convenient routes to halodecaboranes.

1.2.1.2 Electronic structure and bonding

The bonding in $B_{10}H_{10}^{2-}$, as with many similar deltahedral boranes, has been the focus of a good deal of theoretical speculation. At the very least it can be said that the basic notions of valence-bond theory fail to explain the three-dimensional delocalization of electrons throughout the cage.

Wade's generalization regarding the electron counts in polyhedral boranes dictate that *closo*-boranes, such as $B_{10}H_{10}^{2-}$, must have n+1 pairs of skeletal bonding electrons, where n is the number of boron vertices in the cage (e.g. if n = 10, 11 skeletal pairs).[6] Boron, having 3 valence electrons, contributes 2 of these to cage skeletal bonding, since one electron is used in forming a conventional 2-center, 2-electron bond with the terminal hydrogen. In $B_{10}H_{10}^{2-}$ the 20 skeletal electrons provided by the cage-borons, plus the extra 2 electrons accounting for the dianionic charge, sum to 22 electrons, or 11 pairs, in accordance with Wade's rule on these architectures.

While Wade's initial formulation was empirical, he justified it with molecular orbital theory.[7] Each boron on the surface of the deltahedron was assumed to be *sp* hybridized with the *sp*-hybrid orbital radially oriented on the surface of the cage, and the two unhybridized *p*-orbitals laying tangential on the surface of the deltahedron. The 2n tangential orbitals combined to form 2n surface-molecular orbitals, n of which were bonding and n of which were anti-bonding. The mixing of the radial orbitals produces one strongly bonding molecular orbital, and hence n+1 total bonding orbitals, requiring n+1 electron pairs.

Molecular orbital studies to more explicitly describe the orbital interactions have been carried out by Jemmis and Hoffmann.[8] Using the "Ring and Cap" formulation, first employed by Jemmis and Schleyer to describe aromaticity in three dimensions,[9] the authors depicted the molecular orbital interactions of *closo*-$B_nH_n^{2-}$ species as the interaction between ring-like fragments (in $B_{10}H_{10}^{2-}$, the 4-membered equatorial rings in **Figure 1.1**) and capping atoms (apical borons). The authors constructed an interaction diagram between two *nido*-$B_5H_5^{-}$ fragments explicitly depicting the 11 bonding molecular orbitals of $B_{10}H_{10}^{2-}$.[5] The bonding depicted was slightly more complicated than Wade's generalized counting scheme predicted, as there were two (instead of one) filled, radial bonding orbitals on account of second-order stabilizing interactions from higher energy fragment MOs. However, the end result was in agreement with Wade's rules.

Several years after the initial publication of his rules, Wade published a study on *closo*-$B_nH_n^{2-}$ anions, using extended Hückel molecular orbital calculations to predict relative stabilities. These calculations predicted, in agreement with experimentally known trends in stability, $B_{10}H_{10}^{2-}$, $B_{12}H_{12}^{2-}$ and $B_6H_6^{2-}$ to be of higher stability than the remainder of the *closo*-$B_nH_n^{2-}$ family (n = 5-12). Recent thermochemical calculations have reiterated this stability, predicting *closo*-$B_{10}H_{10}^{2-}$ to have the second most negative heat of formation, more positive than only $B_{12}H_{12}^{2-}$, among the *closo*-$B_nH_n^{2-}$ series (n = 5-12).[10]

When thinking of the three dimensionally electronically-delocalized structures of the *closo*-$B_nH_n^{2-}$ anions, questions regarding whether or not these structures can be termed "aromatic" are often raised. The limited reactivity of the *closo*-cages in general, and $B_{10}H_{10}^{2-}$ and $B_{12}H_{12}^{2-}$ in particular, points to aromatic stabilization. Hückel's familiar 4n + 2 rule detailed the electron counts necessary for aromatic stabilization in 2-dimensions, rather than the 3-dimensions of deltahedral boranes. Jemmis and Schleyer extended Hückel's 4n+2 rule to 3-dimensions, terming it the 4n+2 interstitial electron rule,[11] putting into play orbitals from capping interactions over planar rings, not unlike those found in *closo*-boranes. Aihara published an oft-cited study of the aromaticity of boranes in 3-dimensions in which he envisioned the bonding in polyhedral structures as combinations, not of single atomic orbitals as might be used in an LCAO calculation, but of 3-center bonding orbitals that composed the triangular faces of the deltahedron. Using linear combinations of these orbitals he was able to compute a metric he termed "resonance energy", defined as "the extra stabilization energy gained by a circular migration of bonding electrons from face to face through successive resonance integrals".[12] His calculations indicated that all *closo*-$B_nH_n^{2-}$ (n = 6-12) were aromatic (ie. had positive resonance energies), and that, of the bunch, $B_{10}H_{10}^{2-}$ and $B_{12}H_{12}^{2-}$ had the largest total resonance energies.

Nucleus Independent Chemical Shift (NCIS) has been used to gauge aromaticity in planar molecules[13] and is easily applied to three dimensional structures as well. Not surprisingly, the largest negative values of NCIS (most aromatic character) within the *closo*-$B_nH_n^{2-}$ group (n = 5-12) are for n = 12, 10, and 6.[14]

1.2.1.3. Substitution reactions.

A number of derivatives of $B_{10}H_{10}^{2-}$ with boron-carbon bonds are known, many of which are derived from the carbonyl derivative 2-(OC)-$B_{10}H_9^-$. This compound was synthesized in high yields through the reaction of $B_{10}H_{10}^{2-}$ with oxalyl chloride (**Eq. 2**).[15] The 1,10-$(OC)_2$-$B_{10}H_{18}$ neutral dicarbonyl species was similarly prepared.[16]

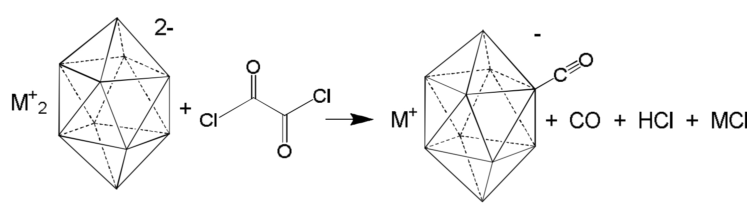

(2)

Carbonyl groups on both the mono- and di-substituted cages were capable of further functionalization, yielding a large number of functionalized cages (carboxylic acid, amino, ester, alkyl, etc.), including bio-relevant compounds of interest in Boron Nuetron Capture Therapy.[3]

Of the numerous derivatives of $B_{10}H_{10}^{2-}$ bearing a B-N bond perhaps the most intriguing is the diazonium derivatives made available through the reaction shown in **Eq. 3**.[16]

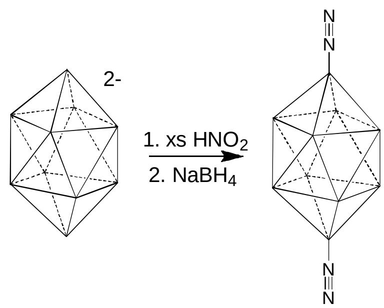

(3)

This compound is an important starting material for other syntheses, as the apical N_2 groups are easily displaced by a number of nucleophiles, leading to several disubstituted derivatives.[3] Non-diazo routes to several cages bearing amines, nitriles, and isothiocyanate have been utilized and recently reviewed.[3]

The syntheses of the 2-hydroxylated derivatives of $B_{10}H_{10}^{2-}$ have been achieved through the hydrolysis of the solvent-adducts formed when $B_{10}H_{10}^{2-}$ was treated with HCl or trifluoroacetic acid in 1-methylpyrrolidin-2-one (NMP) or N,N'-dimethylformamide (DMF).[17] Other successful routes to 2-HO-$B_{10}H_9^{2-}$ include the formation, and subsequent hydrolysis of the ester formed by treatment of the cage with carboxylic acids (**Eq. 4**).[3] Treatment of the hydroxyl derivatives with alkyl halides led to the formation of a range of alkoxide substituted $B_{10}H_9OR^{2-}$ derivatives.[3]

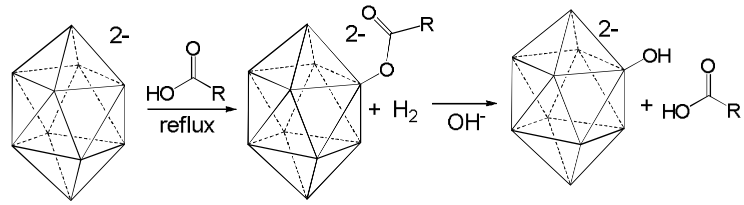

(4)

Cyclic oxonium derivatives are available through the treatment of $B_{10}H_{10}^{2-}$ with acids in cyclic ethers (THF, dioxane, tetrahydropyran, **Eq. 5**). These compounds may then be ring-opened by nucleophiles to provide linkers to other molecular structures.[3]

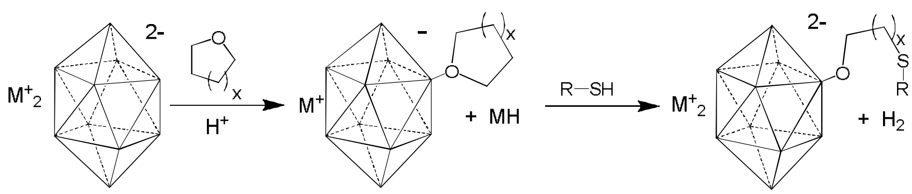

(5)

Halogenated species, $B_{10}H_{(10-y)}X_{(y)}$, were produced primarily as a mixture of mono- and poly-halogenated isomers.[3] Reactions of $B_{10}H_{10}^{2-}$ with elemental Cl_2, Br_2, or I_2 (at room temperature) yielded mixtures which could be chromatographically separated.[3] A single isomer, 2-X-$B_{10}H_{10}^{2-}$ (X = Cl, Br), was produced through the in-situ reaction of carbocations with $B_{10}H_{10}^{2-}$ in 1,2-$X_2C_2H_4$ solvents.[18] The specifically iodinated 2-I-$B_{10}H_9^{2-}$ was formed in the reaction of I_2 with $B_{10}H_{10}^{2-}$ in ethanol at -70 ^{o}C.[19]

1.2.2. *nido*-$B_{10}H_{14}$.

The structure of the compound commonly referred to as simply decaborane, *nido*-$B_{10}H_{14}$, is shown in **Figure 1.2**. The structure has C_{2v} symmetry, and shows 4 peaks in the ^{11}B NMR in a ratio of 2 (~ -12 ppm):2 (~ -10 ppm):4 (~ -1 ppm):2 (~40 ppm). It is a white crystalline solid that melts at ~99 ^{o}C and sublimes under vacuum.

The recent use of decaborane is dominated by those seeking to incorporate *ortho*-carborane moieties into bioactive agents for Boron Neutron Capture Therapy. Just a few recent examples of these chemistries are shown in ref. 20. These applications, though important, and a potential driving force for the functionalization of decaborane, are much more biochemical than synthetic in nature, and will not be covered, in depth, in this introduction.

The list of chemistries herein described is not meant to be comprehensive, but rather is written as a set of reactions that either yield products similar to the substituted decaboranes presented in this dissertation, or, perhaps more importantly, employ the decaborane cage as a starting point for other chemistries.

1.2.2.1 Synthesis

As mentioned previously, the most common synthesis of $B_{10}H_{14}$ is through the thermal pyrolysis of B_2H_6.[21] A laser driven thermal pyrolysis of B_2H_6 and B_5H_9 has been reported to yield $B_{10}H_{14}$ in ~65% yield.[22] Shore synthesized $B_{10}H_{14}$ through the action of Lewis acids on $B_9H_{14}^-$,[23] while Dunks and Ordonez reported a synthesis based on the oxidation of $B_{11}H_{14}^-$, which they synthesized from $NaBH_4$.[24]

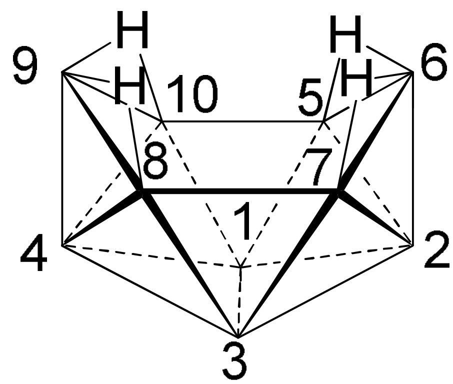

Figure 1.2. The structure and numbering scheme for decaborane (*nido*-$B_{10}H_{14}$).

1.2.2.2 Electronic structure and bonding

Decaborane, with 10 boron vertices donating 2 electrons each to the bonding skeleton, and 4 bridging hydrogens donating 4 electrons, has 24 total skeletal electrons, or 12 pairs. This is in accord with Wade's rules, which state that a *nido*-structure will have n+2 pairs of skeletal bonding electrons, where n is the number of vertices in the deltahedron.[6]

Wade viewed *nido*-structures as equivalent to *closo*-structures with one boron-vertex removed.[6] In this respect $B_{10}H_{14}$ is intrinsically related to $B_{11}H_{11}^{2-}$ (also C_{2v}, **Eq 6.**).

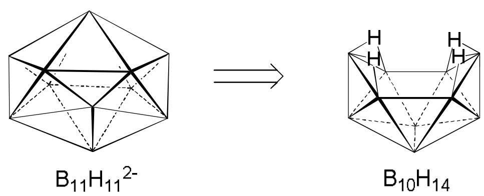

(6)

Since the locations of the new bridging hydrogens are symmetry-related to the original *closo*-structure, Wade postulated that the two structures had the same number of skeletal bonding orbitals and hence needed an identical electron count. The two electrons which would have been donated by the now-removed vertex needed to be replaced, meaning the *nido*-structure required n+2 pairs of bonding skeletal electrons.[6]

Wade's EHMO calculations predicted that the extra electron pair, formerly of the removed vertex, was situated in the HOMO of the new *nido*-structure, which rings the open face of the molecule.[25] This result confirmed a prediction made through the use of tensor surface harmonic theory, suggesting that the extra pair of electrons was stabilized by residing on the largest possible ring.[26]

1.2.2.3 Substitution of a terminal B-H

From the late-1950s to the mid-1970s there was intense interest in the synthesis of substituted decaboranes (R-$B_{10}H_{13}$). Since that time, the focus has shifted into its use as a starting material for carborane, and other heteroborane syntheses.

The hydridic nature of the terminal-hydrogens on the $B_{10}H_{14}$ skeleton makes them amenable to substitution via Friedel-Crafts chemistry. This will be discussed in the following chapters as it pertains to cage-halogenation, however a small number of other derivatives was achieved by these methods. Specifically, cages were alkylated at one or more positions through treatment of ethyl- or methyhalides and aluminum chloride.[27] As described by Lipscomb, these electrophilic substitutions, both alkylations and halogenations, tended to occur at boron vertices 1-4, as these are the most electron-rich boron atoms in the cage.[28]

The bridging hydrogens on decaborane, on the other hand, are Bronsted-acidic, with pK_as, measured in water/ethanolic mixures, of 2.4-3.2.[29] Deprotonation of the bridging hydrogen in decaborane yielded $B_{10}H_{13}^-$, the nucleophilic character of which was employed to affect substitution chemistry and salt elimination. Similarly, the reaction of decaborane with methyl Grignard reagents formed a decaboranyl Grignard reagent, capable of nucleophilic activity (**Eq. 7**).[30]

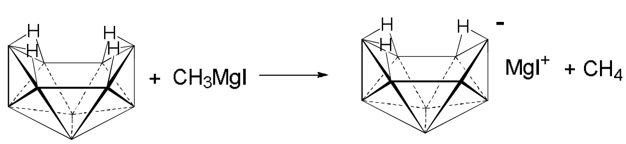

(**7**)

The reaction of the either the sodium salt $Na^+[B_{10}H_{13}^-]$[31] or the Grignard ($MgIB_{10}H_{13}$)[9,32] with benzyl halides yielded 6-benzyldecaborane (6-$C_6H_5CH_2$-$B_{10}H_{13}$). The benzyl product was deprotonated and reacted again with another equivalent of benzyl halide to yield decaborane benzylated at both the 6- and 9-positions (6,9-$(C_6H_5CH_2)_2$-$B_{10}H_{12}$). The same benzylation reaction between the sodium salt and 3-fluorobenzyl chloride yielded a mixture of 6- and 5-(3-F-C_6H_4)-$B_{10}H_{13}$.[33] Allyl-[34] and alkyldecaboranes,[35] with unknown regiochemistry were the products of the reactions of allyl- and alkylhalides and $MgBrB_{10}H_{13}$. Interestingly, Gaines found that the treatment of $B_{10}H_{13}^-$ with an equivalent of alkyllithium followed by acidification yielded 6-R-$B_{10}H_{13}$ selectively.[36]

Non-carbon electrophiles have been substituted on the borane skeleton through salt elimination reactions using either the sodium salt or the Grignard. The tridecaboranyl phosphine, $P(B_{10}H_{13})_3$, was synthesized through the addition of 3 equivalents of $Na^+[B_{10}H_{13}^-]$ to PCl_3.[37] Similar salt eliminations yielded (Cl_2(O)P)-$B_{10}H_{13}$, from reaction with $POCl_3$, and phosphazine derivatives $Br_5P_3N_3(B_{10}H_{13})$, $Br_4P_3N_3(B_{10}H_{13})_2$, $Br_3P_3N_3(B_{10}H_{13})_3$, and $P_3N_3(B_{10}H_{13})_6$ but again without information on the regiochemistry of cage-substitution.[38] The silylated derivative $Me_3SiB_{10}H_{13}$ was also synthesized by the reaction of Me_3SiCl with $Na^+[B_{10}H_{13}^-]$.[39]

Both $(Ph_2P)B_{10}H_{13}$ and $(Ph_2As)B_{10}H_{13}$ have been synthesized through salt elimination reactions of EPh_2Cl (E = P, As) with the decaboranyl Grignard or sodium salt.[40] The crystallographically determined structure of the phosphino-derivative was surprising in that the phosphine was not terminally situated on a cage boron, but instead bridged the B5-B6 bond, much like a bridging hydrogen.[41]

Hydroboration of unsaturated organics with terminal B-H vertices is another way in which decaborane may be functionalized through C-substitution of the terminal hydrides. Transition metal hydroboration of alkenes on decaborane using platinum catalysts yielded symmetrically substituted 6,9-R-$B_{10}H_{12}$ (R = alkyl) compounds,[42] whereas the use of Cp_2TiCl_2 as catalyst stopped after only one hydroboration, yielding 6-R-$B_{10}H_{13}$.[43] Hydroboration was found to proceed smoothly when run in ionic liquids, yielding a number of new functionalized decaboranyl cages with a range of pendant functionalities mono-substituted at B6.[44] Hydroboration of terminal alkynes yielded 6,9-bisalkenyl-decaborane, substituted at either the terminal *or* internal carbon of the alkyne, depending on which catalyst system was employed.[45]

1.2.2.4 6,9-L_2-$B_{10}H_{12}$.

nido-Decaborane is known to form adducts with 2-electon donors, forming formally *arachno*-structures (10 vertices, 13 pairs of cage electrons) with the formula 6,9-L_2-$B_{10}H_{12}$ (for instance, **Eq. 8**). A wide range of adducts including sulfides, nitriles, phosphines, amines, anilines, arsines, pyridines has been made and characterized, with sulfides and nitriles forming the strongest adducts.[46]

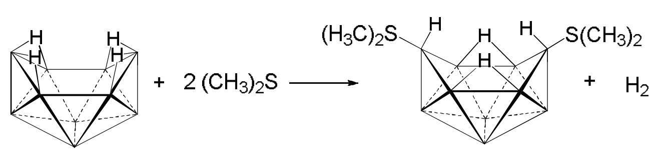

(**8**)

While reaction of $B_{10}H_{14}$ with pyridine under normal conditions was found to form 6,9-$(C_5H_5N)_2$-$B_{10}H_{13}$ complex, when run at low temperature (pyridine condensed at -196 °C and slowly warmed to room temperature) the formation of $[C_5H_5NH^+][B_{10}H_{13}^-]$ was observed followed by the eventual formation of 6,6-$(C_5H_5N)_2$-$B_{10}H_{13}$ (**Eq. 9**) in high purity and good yield.[47]

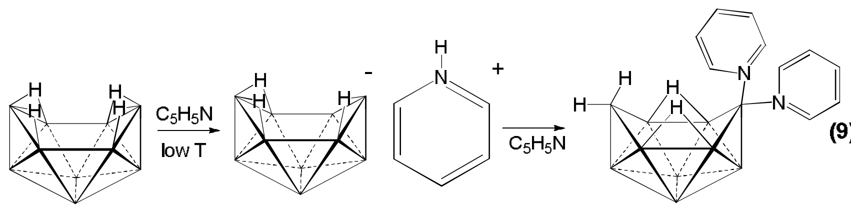

(9)

1.2.2.5 Incorporation of Heteroatoms

Though there are numerous methods for the preparation of $C_2B_{10}H_{12}$ and C-substituted derivatives, the most frequently employed method involves the addition of acetylenes to the 6,9-bis-adduct (**Eq. 10**).[48] Sneddon and Li reported a convenient, high-yield ionic liquid based route to *ortho*-carboranes from $B_{10}H_{14}$.[49]

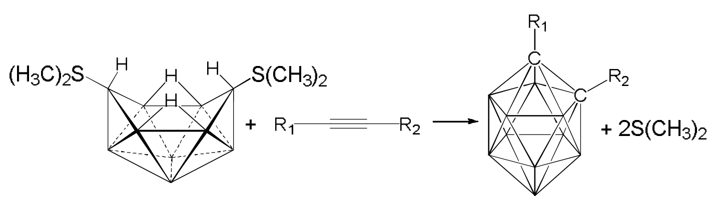

(**10**)

The Brellochs reaction[50] (**Eq. 11**), deboronation of decaborane and carbon insertion, has made available a variety of functionalized RCB_9H_{11} monocarbaboranes.[51] While this reaction is efficient, and gives high yields, for the parent decaborane, the strongly basic reaction conditions may prohibit its use with some functionalized or more highly acidic decaborane derivatives.

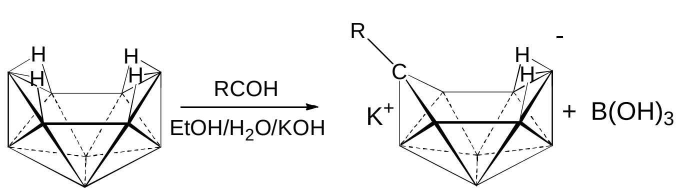

(11)

Carbon has also been inserted into the decaborane skeleton to form 7-RNH_2-7-$CB_{10}H_{12}$ through the addition of isocyanides or the cyanide ion (**Eq. 12**).[52]

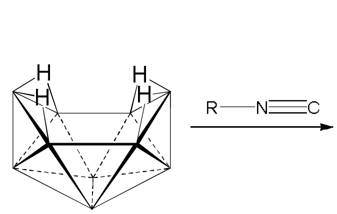

(12)

When the $B_{10}H_{13}^-$ anion was treated with acetonitrile the cage incorporated the C≡N triple bond, yielding the azacarborane *arachno*-7-CH_3-7,12-$CNB_{10}H_{13}^-$.[53]

Azaboranes have been synthesized from decaborane in a number of ways. The reaction of $NaNO_2$ with $B_{10}H_{14}$, followed by acidification yielded the neutral *arachno*-4-NB_8H_{14}.[54] When the addition of $NaNO_2$ was followed by I_2-oxidation *nido*-6-NB_9H_{12} was produced in good yield.[55] Phosphorous has been inserted into the B_{10}-framework through the reaction of decaborane with PCl_3 to give *closo*-1,2-$P_2B_{10}H_{10}$, which underwent a carborane-like isomerization to *closo*-1,7-$P_2B_{10}H_{10}$ at elevated temperatures.[56] Sneddon and Shedlow found that a similar reaction of $RPCl_2$ with Proton Sponge and decaborane gave phosphorous insertion to *nido*-7-$RPB_{10}H_{11}^-$, which could then be acidified to the neutral *nido*-7-$RPB_{10}H_{11}$, all in near quantitative yields (**Eq. 13**).[57] Group-V trihalides were also used to synthesize *closo*-1,2-$Sb_2B_{10}H_{10}$[58] and *closo*-1,2-$As_2B_{10}H_{10}$.[59]

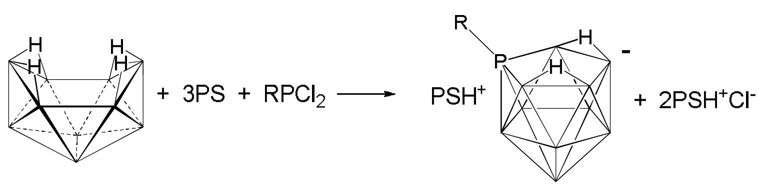

(13)

Muetterties found that the reaction of $B_{10}H_{14}$ with polyammonium sulfide led to the near-quantitative conversion to *arachno*-$B_9H_{12}S^-$.[60] Much more recently, it was found that the reaction of decaborane with elemental sulfur, in the presence of triethylamine yielded the triethylammonium salt of *nido*-7-$SB_{10}H_{11}^{-}$, which when treated with triethylammonium borane (Et_3N-BH_3) incorporated another boron to yield *closo*-1-$SB_{11}H_{11}$.[61] Sneddon and Shedlow were again able to improve on these syntheses through the reaction of $B_{10}H_{14}$ with SCl_2 and Proton Sponge, producing both *nido*-7-$SB_{10}H_{11}^{-}$ and protonated *nido*-7-$SB_{10}H_{12}$ in excellent yields. In the chalcogen family both $SeB_{10}H_{12}$ and $TeB_{10}H_{12}$ were formed through the reactions of decaborane with polysodium selenide and polysodium telluride.[61]

1.3 Conclusion.

The preceding discussion on the chemistry of $B_{10}H_{10}^{2-}$ and $B_{10}H_{14}$ provides an overview of the kinds of systems that will be presented in this dissertation. Functionalization of the parent $B_{10}H_{10}^{2-}$, in combination with the chemistry to be presented, may yield many interesting functionalized decaboranyl derivatives. Likewise, the functionalization of the decaborane derivatives discussed in the coming chapters, in conjunction with the reactions of decaborane just discussed, may yield a number of functionalized, useful products.

1.4 References.

1. Hawthrowne, M. F.; Pitochelli, A. R. *J. Am. Chem. Soc.* **1959**, *81*, 5583-5584.

2. Hawthrowne, M. F.; Pitochelli, A. R. *J. Am. Chem. Soc.* **1960**, *82*, 3328-3329.

3. Sivaev, I. B.; Prikaznov, A. V.; Naoufal, D. *Collect. Czech. Chem. Comm.* **2010**, *75*, 1149-1199 and references therein.

4. Hawthorne, M. F.; Pitochelli, A. R. *J. Am. Chem. Soc.* **1959**, *81*, 5519.

5. Muetterties, E. L.; Balthis, J. H.; Chia, Y. T.; Knoth, W. H.; Miller, H. C. *Inorg. Chem.* **1964**, *3*, 444-451.

6. Wade, K.; *Chem. Comm.* **1971**, *792-793*.

7. Wade, K. *Adv. Inorg. Chem. Radiochem.* **1976**, *18*, 1-66.

8. Balakrishnarajan, M. M.; Hoffmann, R.; Pancharatna, P. D.; Jemmis, E. D. *Inorg. Chem.* **2003**, *42*, 4650-4659.

9. Jemmis, E. D.; Schleyer, P. v. R. *J. Am. Chem. Soc.* **1982**, *104*, 4781-4788.

10. Nguyen, M. T.; Matus, M. H.; Dixon, D, A. *Inorg. Chem.* **2007**, *46*, 7561-7570.

11. Jemmis, E. D.; Schleyer, P. v. R. *J. Am. Chem. Soc.* **1982**, *104*, 4781-4788.

12. Aihara, J. *J. Am. Chem. Soc.* **1978**, *100*, 3339-3342.

13. Subramanian, G.; Jiao, H.; Schleyer, P. v. R. *Agnew. Chem. Intl. Ed. Engl.* **1996,** *35*, 2638-2641.

14. Schleyer, P. v. R.; Subramanian, G.; Jiao, H.; Najafian, K.; Hofmann, M. Are Boron Compounds Aromatic? An Analysis of their Magnetic Properties. In *Advances in Boron Chemistry*; Siebert, W. Ed.; Royal Society of Chemistry: Cambridge, 1997. 3-14.

15. Hertler, W. R.; Knoth, W. H.; Muetterties, E. L. *Inorg. Chem.* **1965**, *4*, 288-293.

16. Knoth, W. H.; Sauer, J. C.; Miller, H. C.; Muetterties, E. L. *J. Am. Chem. Soc.* **1964**, *86*, 115-116. (b) Knoth, W. H. *J. Am. Chem. Soc.* **1966**, *88*, 935-939.

17. (a) Knoth, W. H.; Sauer, J. C.; England, D. C.; Hertler, W. R.; Muetterties, E. L. *J. Am. Chem. Soc.* **1964**, *86*, 3973-3983. (b) Zhizhin, K. Y.; Mustyatsa, V. N.; Malinina, E. A.; Polyakova, I. N.; Kuznetsov, N. T. *Russ. J. Inorg. Chem.* **2005**, *50*, 29-35.

18. Retivov, V. M.; Matveev, E. Y.; Liskovii, M. V.; Ravgonyaeva, G. A.; Ochertyanova, L. I.; Zhizhin, K. Y.; Kuznetsov, N. T. *Russ. Chem. Bull.* **2010**, *59*, 550-555.

19. Zakharkin, L. I.; Guseva, V. V.; Petrovskii, P. V. *Zh. Obschch. Khim.* **2001**, *71*, 1082.

20. Sivaev, I. B.; Bregadze, V. V. *Eur. J. Inorg. Chem.* **2009**, 1433-1450.

21. Hughes, R. L.; Smith, I. C.; Lawless, E. W. In *Production of Boranes and Related Research*; Holzmann, R. T., Ed.; Academic Press: New York, 1967; pp 104-114.

22. Hartford Jr., A. Atencio, J. H. *Inorg. Chem.* **1980**, *19*, 3060-3062.

23. Toft, M. A.; Leach, J. B.; Himpsl, F. L.; Shore, S. G. *Inorg. Chem.* **1982**, *21*, 1952-1957.

24. (a) Dunks, G. B.; Ordonez, K. P. *J. Am. Chem. Soc.* **1978**, *100*, 2555-2556. (b) Dunks, G. B.; Barker, K.; Hedaya, E.; Hefner, C.; Palmer-Ordonez, K.; Remec, P. *Inorg. Chem.* **1981**, *20*, 1692-1697.

25. Porterfield, W. W.; Jones, M. E.; Wade, K. *Inorg. Chem.* **1990**, *29*, 2919-2923.

26. (a) Stone, A. J.; *Inorg. Chem.* **1981**, *20*, 563-571. (b) Stone, A. J.; Alderton, M. J. *Inorg. Chem.* **1982**, *21*, 2297-2302.

27. (a) Williams, R. L.; Dunstan, I.; Blay, N. J. *J. Chem. Soc.* **1960**, 5006-5012. (b) Blay, N. J. ; Dunstan, I.; Williams, R. L. *J. Chem. Soc.* **1960**, 430-433. (c) Cueilleron, J.; Gulliot, P. *Bull. Soc. Chim. Fr.* **1960**, 2044-2052.

28. Lipscomb, W. N. *Boron Hydrides*; W. A. Benjamin: New York, 1963; pp 179-180.

29. Heřmánek, S.; Plotova, H.; Plešek, J. *Collect. Czech. Chem. Comm.* **1975**, *40*, 3593-3601.

30. Siegel, B.; Mack, J. L.; Lowe, J. V.; Gallahan, J. *J. Am. Chem. Soc.* **1958**, 4523-4526.

31. Palchak, R. J. F.; Norman, J, H.; Williams, R. E. *J. Am. Chem. Soc.* **1961**, *83*, 3380-3384.

32. (a) Dunstan, I.; Blay, N. J.; Williams, R. L. *J. Chem. Soc.* **1960**, 5016-5019. (b) Siegel, B.; Mack, J. L. *J. Phys. Chem.* **1960**, *63*, 1212-1213.

33. Plzák, Z.; Štibr, B.; Plešek, J.; Heřmánek, S. *Collect. Czech. Chem. Comm.* **1975**, *40*, 3602-3607.

34. Emery, F. W.; Harold, P. L.; Owen, A. J. *J. Chem Soc.* **1964**, 426-430.

35. Gallagan, J.; Siegel, B. *J. Am. Chem. Soc.* **1959**, *81*, 504.

36. Bridges, A. N., Powell, D. R.; Dopke, J. A.; Desper, J. M.; Gaines, D. F. *Inorg. Chem.*, **1998**, *37,* 503-509.

37. Kuznetzov, N. T.; Klimchuk, G. S. *Russ. J. Inorg. Chem.* **1969**, *14*, 1424-1427.

38. (a) Kuznetzov, N. T. *Izv. Akad. Nauk SSSR Neorgan. Materialy* **1966**, *2,* 2258-2259. (b) Kuznetzov, N. T. *Izv. Akad. Nauk SSSR Neorgan. Materialy* **1967**, *3,* 587-588.

39. Amberger, E.; Liedl, P. *J. Organomet. Chem.* **1969**, *18,* 345-347.

40. (a) Muetterties, M. L.; Aftandilian, V. D. *Inorg. Chem.* **1962**, *1*, 731-734. (b) Schroeder, H. *Inorg. Chem.* **1963**, *2,* 390-393.

41. Friedman, L. B.; Perry, S. L. *Inorg. Chem.* **1973**, *12*, 288-293.

42. Mazighi, K.; Carroll, P. J.; Sneddon, L. G. *Inorg. Chem.* **1993**, *32*, 1963-1969.

43. Pender, M. J.; Wideman, T.; Carroll, P. J.; Sneddon, L. G. *Inorg. Chem.* **1998**, *120,* 9108-9109.

44. Kusari, U.; Carroll, P. J; Sneddon L. G. *Inorg. Chem.* **2008**, *47*, 9203-9215.

45. Chatterjee, S.; Carroll, P. J.; Sneddon, L. G. *Inorg. Chem.* **2010**, *49*, 3095-3097.

46. Pace, R. J.; Williams, J.; Williams, R. L. *J. Chem. Soc.* **1961**, 2196-2204.

47. Cendrowski-Guillaume, S. M.; O'Loughlin, J. L.; Pelczer, I.; Spencer, J. T. *Inorg. Chem.* **1995**, *34,* 3935-3941.

48. Grimes, R. N. *Carboranes*; Academic Press: New York, 1970; pp 54-55.

49. Li, Y.; Carroll, P. J.; Sneddon, L. G. *Inorg. Chem.* **2008**, *47*, 9193-9202.

50. Brellochs B. in: *Contemporary Boron Chemistry* M. G. Davidson, A. K. Hughes, T. B. Marder and K. Wade, Eds.; Royal Society of Chemistry, Cambridge (U.K.) 2000; p. 212.

51. Franken, A.; Kilner, C. A.; Thornton-Pett, M.; Kennedy, J. D. *Collect. Czech. Chem. Comm.* **2002**, *67*, 869-912.

52. (a) Hyatt, D. E.; Owen, D. A.; Todd, L. *J. Am. Chem. Soc.* **1966**, *5*, 1749-1751. (b) Knoth, W. H. *J. Am Chem. Soc.* **1967**, *89*, 1274. (c) Batsanov, A. S.; Fox, M. A.; Goeta, A. E.; Howard, J. A. K.; Hughes, A. K.; Malget, J. M. *J. Chem. Soc. Dalton Trans.* **2002**, 2624-2631.

53. Willie, A. E.; Su, K.; Carroll, P. J.; Sneddon, L. G. *J. Am. Chem. Soc.* **1996**, *118*, 6407-6421.

54. Base, K.; Plesek, J., Hermanek, S.; Huffman, J.; Ragatz, P.; Schaeffer, R. *J. Chem. Soc. Chem. Comm.* **1975**, 934-935.

55. Kester, J. G.; Huffman, J. C. Todd, L. J. *Inorg. Chem.* **1988**, *27*, 4528-4523.

56. Little, J. L.; Kester, J. G.; Huffman, J. C., Todd, L. J. *Inorg. Chem.* **1989**, *28*, 1087-1091.

57. Shedlow, A. M.; Sneddon, L. G. *Inorg. Chem.* **1998**, *37*, 5269-5277.

58. Little, J. L. *Inorg. Chem.* **1979,** *18*, 1598-1600.

59. Hanusa, T. P.; de Parisi, N. R.; Kester, J. G.; Arafat, A.; Todd, L. J. *Inorg. Chem.* **1987**, *46*, 4100-4102.

60. (a) Hertler, W. R.; Klanberg, F.; Muetterties, E. L. *Inorg. Chem*. **1967**, *6*, 1696-706.

(b) Rudolph, R. W.; Pretzer, W. R. *Inorg. Synth.* **1983**, 22, 226-231.

61. Machacek, J.; Plesek, J.; Holub, J.; Hnyk, D.; Vsetcka, V.; Cisarova, I.; Kaupp, M.; Stibr, B. *Dalton Trans.* **2006**, 1024-1029.

62. Little, J. L., Friesen, G. D.; Todd, L. J. *Inorg. Chem.* **1977**, *16*, 869-872.

Chapter 2

Crystallographic Characterizations and New High Yield Synthetic Routes via Super Acid Induced Cage-Opening Reactions of *closo*-$B_{10}H_{10}^{2-}$ Salts for the Complete Series of 6-X-$B_{10}H_{13}$ Halodecaboranes (X = F, Cl, Br, I)

Abstract

The high yield syntheses of 6-X-$B_{10}H_{13}$, X = Cl (88%), Br (96%) and I (84%) resulted from the cage-opening reactions of the $(NH_4^+)_2B_{10}H_{10}^{2-}$ salt with ionic-liquid based superacidic hydrogen halides, while both the previously unknown 6-F-$B_{10}H_{13}$ derivative (77%) and 6-Cl-$B_{10}H_{13}$ (92%) were synthesized in high yields via the reactions of $(NH_4^+)_2B_{10}H_{10}^{2-}$ with triflic acid in the presence of 1-fluoropentane and dichloromethane, respectively. Structural characterizations of the halogenated cages confirm the predicted structures and indicate strong halogen backbonding interactions with the B6-boron. Reactions of $(NH_4^+)_2B_{10}H_{10}^{2-}$ with triflic acid in bromo- and iodoethane yielded mixtures of 6-X-$B_{10}H_{13}$ and 6-X-9-C_2H_5-$B_{10}H_{12}$. This result is at odds with a previously proposed mechanism of the reaction of *closo*-$B_{10}H_{10}^{2-}$ with strong acids.

2.1 Introduction

Decaborane ($B_{10}H_{14}$), when compared to lighter, neutral polyhedral boranes, is widely available and relatively stable. As discussed in **Chapter 1**, there exist a number of potential applications for the B_{10}-skeleton; however, in order to fulfill this potential, systematic routes toward its functionalization must be discovered and optimized.

Halogenation of decaborane is one way to provide a functional handle, useful in further selective functionalization of the *nido*-B10 skeleton. In organic chemistry, carbon-halogen bonds serve as reactive starting points for many reactions (S_N1, S_N2, S_N2_{Ar}, Pd-coupling, etc.). There are several examples of Pd-coupling reactions utilizing B-I bonds on carboranes, yielding useful functionalized carboranyl-derivatives.[1] Metallocarboranes have also been functionalized at boron via transition-metal coupling reactions at boron-halide bonds.[2] Halodecaboranes are not currently utilized as starting points for similar borane functionalization, primarily on account of the absence of efficient methods for their high-yield, *selective* syntheses.

Since the 1960's, Friedel-Crafts[3] and direct halogenation[4] reactions of decaborane have been known, producing mixtures of halodecaboranes substituted at B1 and/or B2, off of the open face (for the numbering scheme see **Eq. 1**). Alternatively, the reactions of anhydrous HX (X = F, Cl, Br, I) with 6,9-$(R_2S)_2$-$B_{10}H_{12}$, or $B_{10}H_{14}$ in the presence of R_2S (R = Me, Et), have been shown to yield mixtures of 5-X-$B_{10}H_{13}$ and 6-X-$B_{10}H_{13}$ from which additional purification is required to give discreet products (**Eq. 2**).[5-7]

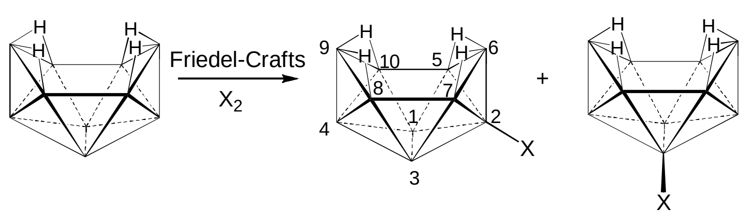

(**1**)

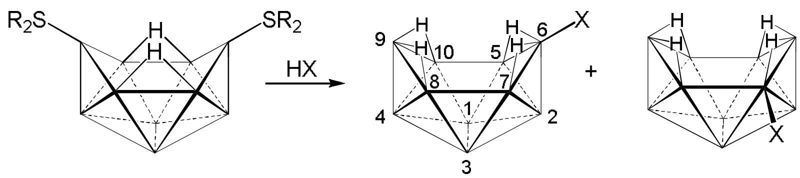

(**2**)

Aside from the problematic lack of regioselectivity in these reactions, all of the syntheses require $B_{10}H_{14}$, a compound most commonly produced by a hazardous diborane-pyrolysis reaction.[8] However, 6-(Cl, Br, I)-$B_{10}H_{13}$ have also been obtained in moderate yields (Cl, 45%; Br, 45%; I, 30%) via the hydrolysis of $(AlX_3)_n$-$B_{10}H_{10}^{2-}$ adducts.[9,10] Since *closo*-$B_{10}H_{10}^{2-}$ anions can be synthesized from the thermolysis of borohydrides instead of diborane,[11,12] synthetic routes based on the use of *closo*-$B_{10}H_{10}^{2-}$ anions as starting points could have significant advantages over $B_{10}H_{14}$ based schemes. This possibility stimulated the study described in this chapter of *closo*-$B_{10}H_{10}^{2-}$ cage-opening reactions.

2.2. Experimental

Materials. AlX_3 (X = Cl, Br, I) was purchased from Aldrich and either sublimed prior to use (X = Cl) or used as received (X = Br, I). 1-Butyl-3-methylimidazolium halides (Cl, Br, I) were purchased from Aldrich and azeotropically dried with toluene prior to use. Anhydrous HBr and HCl, tributyltin hydride, ethyl bromide and ethyl iodide (Aldrich) were used as received. Ampules of trifluoromethanesulfonic acid (Aldrich) were opened in air and immediately loaded into a nitrogen purged Schlenk-flask with a Teflon screw-top, and stored under dry N_2. CH_2Cl_2, hexanes, and pentane (Fisher) were used as received. Silica gel (Fisher) was acidified prior to use as described elsewhere.[6]

$(NH_4^+)_2B_{10}H_{10}^{2-}$ from stock was dried prior to use by heating to 100 ^oC under vacuum for 20 h.

Physical Methods. ^{11}B NMR at 128.3 MHz and ^1H NMR at 400.1 MHz spectra were obtained on a Bruker DMX-400 spectrometer equipped with appropriate decoupling accessories. All ^{11}B chemical shifts were referenced to $BF_3{\cdot}OEt_2$ (0.0 ppm), with a negative sign indicating an upfield shift. All proton chemical shifts were measured relative to internal residual protons from the lock solvents (99.9% $CDCl_3$) and then referenced to $(CH_3)_4Si$ (0.0 ppm). High- and low-resolution mass spectra employing chemical ionization with negative ion detection were obtained on a Micromass AutoSpec high-resolution mass spectrometer. IR spectra were obtained on a Perkin-Elmer Spectrum 100 FT-IR spectrometer.

6-Fluorodecaborane, 6-F-$B_{10}H_{13}$ (1). Under flowing N_2, a 3-neck flask equipped with an addition funnel was charged with $(NH_4^+)_2B_{10}H_{10}^{2-}$ (0.30 g, 1.94 mmol). Pentane (10.0 mL) and 1-fluoropentane (0.44 mL, 3.85 mmol) were added and the resulting suspension was stirred at room temperature while trifluoromethanesulfonic acid (0.57 mL, 6.27 mmol) was added dropwise through the addition funnel. The reaction mixture gradually turned yellow while it was being stirred at room temperature for 5 h. Pentane (20.0 mL) was added and the solution was filtered. The volatiles were vacuum evaporated through U-traps cooled at 0 °C and -78 °C with the product and solvent collecting at -78 °C. Vacuum evaporation of the solvent from this trap at -30 °C then left behind 0.21 g (1.50 mmol, 77% yield) of white solid **1**, mp = 48-49 °C. Crystals suitable for X-ray diffraction were grown by slow evaporation of hexane. Exact mass for $^{19}F^{11}B_{10}{}^1H_{13}$: (obs./calc.): 142.1913/142.1931. ^{11}B NMR (128.4 MHz, CD_2Cl_2), (mult, assign, J in Hz):

20.7 (s, B6), 6.7 (d, B9, *J*BH = 153), 4.2 (d, B1,3, *J*BH = 148), 1.5 (d, B8,10, *J*BH = 164), -11.3 (d, B5,7, *J*BH = 161), -35.3 (d, B2, *J*BH = 154), -44.2 (d, B4, *J*BH = 158). $^{1}H\{^{11}B\}$ NMR (400 MHz, CD_2Cl_2) 3.96 (1H, s), 3.33 (2H, s), 3.25 (2H, s), 2.56 (2H, s), 1.38 (1H, s), 0.37 (1H, s), -0.48 (2H, d, *J*FH = 21.0), -1.71 (2H, s). ^{19}F NMR (282.4 MHz, CDCl3), δ (mult): -141 (m).

6-Chlorodecaborane, 6-Cl-$B_{10}H_{13}$ (2).

Method 1. Under inert conditions, 6.00 g (45.0 mmol) of $AlCl_3$ was mixed with 6.00 g (34.4 mmol) of BmimCl to create a monophasic ionic liquid, to which was added 0.20 g (1.30 mmol) of $(NH_4^+)_2B_{10}H_{10}^{2-}$. The inhomogenous mixture was heated at 75 °C under a slow flow of HCl metered through a bubbler. After 2 h, the solution was removed from heat and vacuum was applied for 10 min to remove excess HCl. The ionic liquid was then extracted several times with hexanes until the extracts showed no traces of product by ^{11}B NMR. The extracts were filtered to remove any solids and solvent was vacuum evaporated at -30 °C to give a pale-yellow solid. No attempts were made to recycle the ionic liquid. The solid was sublimed at room temperature for 3 h onto a -78 °C cold finger. After sublimation, the cold finger was warmed to room temperature and the collected white solid washed with pentane into a tared flask. Following vacuum evaporation of the pentane at -30 °C, 0.18 g (1.14 mmol, 88%) of white, crystalline solid **2** was obtained, mp = 30-32 °C (lit. 28-29).[7] ^{11}B NMR (128.4 MHz, CH_2Cl_2): δ (mult, assign, *J* in Hz): 17.5 (s, B6), 8.2 (d, B9,1,3, *J*BH = ~150), 0.9 (d, B8,10, *J*BH = 158), -3.9 (d, B5,7, *J*BH = 161), -33.4 (d, B2, *J*BH = 160), -40.6 (d, B4, *J*BH = 160). $^{1}H\{^{11}B\}$ NMR (400 MHz, $CDCl_3$): δ 4.00 (1H,s), 3.56 (2H, s), 3.23 (2H, s), 2.94 (2H, s), 1.33 (1H, s), 0.57 (1H, s), -0.72 (2H, s), -1.79 (2H, s).

Method 2. Under flowing N_2, a 3-neck flask was charged with 0.50 g (3.25 mmol) of $(NH_4^+)_2B_{10}H_{10}^{2-}$ and 30.0 mL of CH_2Cl_2. Under vigorous stirring, 1.15 mL of trifluoromethanesulfonic acid (12.9 mmol) was added dropwise at room temperature. The mixture was stirred for 2 h at room temperature, filtered to remove solids and then the solvent vacuum evaporated at -35 °C. The remaining crude yellow oil was dissolved in pentane, transferred to a sublimer, and the pentane vacuum evaporated at -30 °C. Sublimation from the remaining oil at room temperature for 3 h onto a -78 °C cold finger gave 0.46 g (2.94 mmol, 90% yield) of white flakey solid **2**, mp = 30-32 °C (lit. 28-29),[7] which was identified by its ^1H and ^{11}B NMR (listed above).

6-Bromodecaborane, 6-Br-$B_{10}H_{13}$ (3). Under inert conditions, 15.0 g (56.2 mmol) of $AlBr_3$ was mixed with 10.0 g (45.6 mmol) of BmimBr, to which was added 0.75 g (4.87 mmol) of $(NH_4^+)_2B_{10}H_{10}^{2-}$. The inhomogenous mixture was heated at 75 °C under a slow flow of HBr metered through a bubbler. After 2 h, the solution had become monophasic and was removed from heat. Vacuum was applied for 10 min to remove excess HBr. The ionic liquid was then extracted several times with hexanes until the extracts showed no traces of product by ^{11}B NMR. The extracts were filtered to remove any solids and solvent was vacuum evaporated at -30 °C to give a pale-yellow solid. No attempts were made to recycle the ionic liquid. The solid was sublimed at 45 °C onto a -78 °C cold finger. After sublimation, the cold finger was warmed to room temperature and the collected white solid washed with pentane into a tared flask. Following vacuum evaporation of the pentane at -30 °C, 0.93 g (4.63 mmol, 96%) of white, crystalline solid **3** was obtained, mp = 34-35 °C (lit. 32-34).[7] ^{11}B NMR (128.4 MHz, CH_2Cl_2) δ (mult, assign, *J* in Hz): 9.6 (s, B6), 9.6 (d, B9, *J*BH = ~175), 8.2 (d, B1,3, *J*BH = ~145), 0.0 (d, B8,10, *J*BH = 170), -2.1 (d, B5,7, *J*BH = 178), -34.1 (d, B2, *J*BH = 158), -39.4 (d, B4, *J*BH = 157). $^{1}H\{^{11}B\}$ NMR (400 MHz, $CDCl_3$) δ 4.03 (1H, s), 3.65 (2H, s), 3.23 (2H, s), 3.08 (2H, s), 1.34 (1H, s), 0.74 (1H, s), -0.77 (2H, s), -1.86 (2H, s).

6-Iododecaborane, 6-I-$B_{10}H_{13}$ (4). Under inert conditions, 6.10 g (15.0 mmol) of AlI_3 was mixed with 3.00 g (11.3 mol) of BmimI, to which was added 0.20 g (1.30 mmol) of $(NH_4^+)_2B_{10}H_{10}^{2-}$. The inhomogenous mixture was heated at 85 °C under a slow flow of HCl metered through a bubbler. After 2 h, all starting material had been consumed and the mixture was removed from heat. Vacuum was applied for 10 min to remove excess HCl. The ionic liquid was then extracted several times with hexanes until the extracts showed no traces of product by ^{11}B NMR. The extracts were filtered to remove any solids and the solvent was vacuum evaporated at 0 °C to give a pale-yellow solid. No attempts were made to recycle the ionic liquid. The solid was sublimed at 45 °C onto a 0 °C cold finger. After sublimation, the cold finger was warmed to room temperature and the collected yellow solid washed with pentane into a tared flask. Following vacuum evaporation of the pentane at 0 °C, 0.27 g (1.10 mmol, 84%) of pale yellow, crystalline solid **4** was obtained, mp = 70-72 °C (lit. 75-76).[7] ^{11}B NMR (128.4 MHz, $CDCl_3$) δ (mult, assign, *J* in Hz): 10.7 (d, B1,3, *J*BH = ~145), 9.9 (d, B9, *J*BH = ~170), 1.2 (d, B5,7 *J*BH = ~145), 0.5 (d, B8,10, *J*BH = ~190), -6.8 (s, B6), -34.0 (d, B2, *J*BH = 163), -37.7 (d, B4, *J*BH = 157). $^{1}H\{^{11}B\}$ NMR (400 MHz, $CDCl_3$) δ 4.04 (1H, s), 3.72 (2H, s), 3.25 (2H, s), 3.22 (2H, s), 1.33 (1H, s), 1.00 (1H, s), -0.83 (2H, s), -1.99 (2H, s).

6-Br-9-C_2H_5-$B_{10}H_{12}$ (5). Trifluoromethanesulfonic acid (0.52 mL, 5.84 mmol) was added dropwise via syringe to a rapidly stirring suspension of $(NH_4^+)_2B_{10}H_{10}^{2-}$ (200 mg, 1.30 mmol) in ethylbromide (5 mL). The reaction was stirred at room temperature for 2 h, at which point analysis by ^{11}B NMR indicated conversion of the starting material into a mixture of **4** and 6-Br-9-C_2H_5-$B_{10}H_{12}$ (**5**) with in ratio of ~1:3 (**4**:**5**). CH_2Cl_2 (~10 mL) was added to the mixture and it was then extracted with water. The organic layer was dried ($MgSO_4$), filtered, concentrated in vacuo, and chromatographed on acidified silica gel using a 5% CH_2Cl_2 in hexanes eluent yielding **5** (57 mg, 0.25 mmol, 19%) as a clear oil. Exact mass for $^{12}C^{11}B_{10}{}^{1}H_{17}{}^{81}Br$: (obs./calc.): 232.1422/232.1428. ^{11}B NMR (128.4 MHz, $CDCl_3$) δ (mult, assign, *J* in Hz): 26.0 (s, B9), 8.5 (s, B6), 7.5 (d, B1,3 *J*BH = 159), -0.8 (d, B5,7, *J*BH = ~190), -2.5 (d, B8,10 *J*BH = ~180), -36.4 (d, B2, *J*BH = ~125), -37.2 (d, B4, *J*BH = ~140). $^{1}H\{^{11}B\}$ NMR (400 MHz, $CDCl_3$) δ 3.53 (s, 2BH), 3.09 (s, 2BH), 2.99 (s, 2BH), 1.44 (m, CH_2), 1.22 (t, CH_3, *J* = 7.2), 1.13 (s, 1BH), 0.89 (s, 1BH), -0.67 (s, 2BHB), -1.42 (s, 2BHB). IR (KBr, cm^{-1}) 2965 (m), 2935 (w), 2911 (w), 2878 (w), 2579 (vs), 1970 (w), 1913 (w), 1524 (m), 1461 (s), 1414 (s), 1379 (w), 1287 (w), 1122 (w), 1095 (m), 1035 (w), 980 (s), 952 (w), 939 (m), 912 (w), 887 (m), 854 (w), 838 (w), 819 (m), 800 (w), 775 (w), 721 (m), 701 (m), 674 (m), 596 (w).

6-I-9-C_2H_5-$B_{10}H_{12}$ (6). Trifluoromethanesulfonic acid (0.52 mL, 5.84 mmol) was added dropwise via syringe to a rapidly stirring suspension of $(NH_4^+)_2B_{10}H_{10}^{2-}$ (200 mg, 1.30 mmol) in ethyliodide (5 mL). The reaction was stirred at room temperature for 2 h, at which point analysis by ^{11}B NMR indicated conversion of the starting material into a mixture of **4** and 6-I-9-C_2H_5-$B_{10}H_{12}$ (**6**) with in ratio of ~2:3 (**4**:**6**). CH_2Cl_2 (~10 mL) was added to the mixture and it was then extracted with water. The organic layer was dried ($MgSO_4$) and filtered. The solvent was removed in vacuo, and the resultant oil was dried for several hours on under high-vaccuum. The oil was redissolved in pentane and recrystallized twice from pentane. The second crystallization yielded crystals suitable for X-ray diffraction. Further purification and characterization were not performed.

Collection and Reduction of the Data. Crystallographic data and structure refinement information are summarized in **Table 2.2.1**. The data for 6-F-$B_{10}H_{13}$ (**1**, Penn3320), 6-Cl-$B_{10}H_{13}$ (**2**, Penn3322), 6-Br-$B_{10}H_{13}$ (**3**, Penn3321), 6-I-$B_{10}H_{13}$ (**4**, Penn3327), and 6-I-9-(C_2H_5)-$B_{10}H_{12}$ (**6**, Penn3341) were collected on a Rigaku Mercury CCD area detector employing graphite-monochromated Mo-K_α radiation. Rotation frames were integrated using CrystalClear,[13] producing a list of unaveraged F^2 and $\sigma(F^2)$ values which were then passed to the CrystalStructure[14] program package for further processing and structure solution on a Dell Pentium 4 computer. The intensity data were corrected for Lorentz and polarization effects and for absorption using REQAB.[15]

Solution and Refinement of the Structures. The structures were solved by direct methods (SIR97[16]). Refinement was by full-matrix least squares based on F^2 using SHELXL-97.[17] All reflections were used during refinement (values of F^2 that were experimentally negative were replaced with $F^2 = 0$). For **1-4** and **6** all non-hydrogen atoms were refined anisotropically and hydrogen atoms were refined isotropically except for H4 and H4'in **1** which were included as constant contributions to the structure factors and were not refined. Cartesian coordinates, bond lengths, and bond angles for the solved structures are provided in **Tables 2.2.2-2.2.11**.

Table 2.2.1. Crystallographic and refinement data for compounds **1-4**.

	1	**2**	**3**	**4**	**6**
Empirical formula	$B_{10}H_{13}F$	$B_{10}H_{13}Cl$	$B_{10}H_{13}Br$	$B_{10}H_{13}I$	$C_2B_{10}H_{17}I$
Formula weight	140.20	156.65	201.11	248.10	276.16
Crystal class	Monoclinic	Monoclinic	Monoclinic	Monoclinic	Monoclinic
space group	P2/n	$P2_1/c$	$P2_1/c$	$P2_1/n$	$P2_1/c$
Z	4	4	4	4	4
a, Å	12.639(3)	12.444(2)	12.391(2)	7.1901	11.760(2)
b, Å	5.6456(11)	7.6026(10)	7.7367(9)	14.5748(14)	13.025(2)
c, Å	12.645(3)	11.147(2)	11.203(2)	9.7529(11)	8.315(2)
β, deg	107.966(5)	115.766(4)	114.947(3)	103.429(3)	108.561(4)
V, $Å^3$	858.3(3)	949.7(3)	973.8(3)	994.2(2)	1207.4
D_{calc}, g/cm^3	1.085	1.096	1.372	1.658	1.519
μ, cm^{-1}	0.59	3.17	41.38	31.4	25.94
λ, Å (Mo-K_α)	0.71070	0.71073	0.71073	0.71073	0.71073
Crystal size, mm	0.35 x 0.10 x 0.04	0.44 x 0.15 x 0.10	0.45 x 0.12 x 0.05	0.32 x 0.28 x 0.12	0.46 x 0.35 x 0.10
F(000)	288	320	392	464	528
2θ angle, deg	5.48-50.02	6.48-50.04	6.4-54.92	5.12-54.9	6.04-55.02
Temperature, K	143(1)	143(1)	143(1)	143(1)	143(1)
hkl collected	$-15 \leq h \leq 10$; $-6 \leq k \leq 6$; $-15 \leq l \leq 14$	$-14 \leq h \leq 13$; $-8 \leq k \leq 9$; $-11 \leq l \leq 13$	$-16 \leq h \leq 15$; $-9 \leq k \leq 8$; $-14 \leq l \leq 9$	$-9 \leq h \leq 9$; $-16 \leq k \leq 18$; $-9 \leq l \leq 12$	$-14 \leq h \leq 15$; $-16 \leq k \leq 16$; $-8 \leq l \leq 10$
No. meas reflns	6460	5753	6052	7060	15697
No. of unique reflns	1513 (R_{int}=0.0214)	1661 (R_{int}=0.0184)	2200 (R_{int}=0.0291)	2259 (R_{int}=0.0204)	2742 (R_{int}=0.0268)
No. parameters	159	153	153	153	187
R^a indices (F>2σ)	R_1=0.0405 wR_2=0.1092	R_1=0.0333 wR_2=0.0864	R_1=0.0370 wR_2=0.0989	R_1=0.0290 wR_2=0.0698	R_1=0.0241 wR_2=0.0585
R^a indices (all data)	R_1=0.0432 wR_2=0.1124	R_1=0.0373 wR_2=0.0908	R_1=0.0494 wR_2=0.1483	R_1=0.0315 wR_2=0.0725	R_1=0.0253 wR_2=0.0592
GOF^b	1.122	1.041	1.117	0.927	1.100
final difference peaks, e/$Å^3$	+0.155, -0.153	+0.199, -0.204	+0.686, -1.127	+0.574, -1.576	+1.314, -1.255

$^a R_1 = \Sigma||F_o| - |F_c||/\Sigma|F_o|$; $wR_2 = \{\Sigma w(F_o^2 - F_c^2)^2/\Sigma w(F_o^2)^2\}^{1/2}$
^{b}GOF = $\{\Sigma w(F_o^2 - F_c^2)^2/(n-p)\}^{1/2}$ where n = no. of reflns; p = no. of params refined

Table 2.2.2. Bond lengths for **1**.

B1-B7#1	1.746(3)	B1-B5	1.757(3)	B1-B2#1	1.778(3)
B1-B1#1	1.782(3)	B1-B2	1.783(3)	B1-H1	1.10(2)
B2-B6	1.718(2)	B2-B1#1	1.778(3)	B2-B5	1.800(3)
B2-B7	1.800(3)	B2-H2	1.02(3)	B5-B6	1.784(3)
B5-B7#1	1.994(4)	B5-H5	1.04(2)	B5-H56	1.24(2)
B6-F1	1.279(3)	B6-B7	1.803(3)	B6-H56	1.30(2)
B6-H67	1.25(2)	B6-H6	1.0962	B7-B1#1	1.746(3)
B7-B5#1	1.994(4)	B7-H7	1.02(2)	B7-H67	1.28(2)
B1'-B7'#2	1.750(3)	B1'-B5'	1.757(3)	B1'-B2'	1.770(3)
B1'-B1'#2	1.771(3)	B1'-B2'#2	1.783(3)	B1'-H1'	1.11(2)
B2'-B6'	1.720(3)	B2'-B1'#2	1.783(3)	B2'-B5'	1.789(3)
B2'-B7'	1.799(3)	B2'-H2'	1.12(2)	B5'-B6'	1.784(3)
B5'-B7'#2	1.990(4)	B5'-H5'	1.11(2)	B5'-H56'	1.24(2)
B6'-F1'	1.278(3)	B6'-B7'	1.798(3)	B6'-H56'	1.32(2)
B6'-H67'	1.32(2)	B6'-H6'	1.0991	B7'-B1'#2	1.750(3)
B7'-B5'#2	1.990(4)	B7'-H7'	1.11(2)	B7'-H67'	1.25(2)

Table 2.2.3 Bond angles for **1**.

B7#1-B1-B5	69.38(14)	B7#1-B1-B2#1	61.41(12)	B5-B1-B2#1	118.42(13)
B7#1-B1-B1#1	108.22(13)	B5-B1-B1#1	107.69(12)	B2#1-B1-B1#1	60.12(12)
B7#1-B1-B2	118.53(14)	B5-B1-B2	61.12(11)	B2#1-B1-B2	114.53(12)
B1#1-B1-B2	59.83(12)	B7#1-B1-H1	113.2(10)	B5-B1-H1	113.0(10)
B2#1-B1-H1	118.8(9)	B1#1-B1-H1	129.5(10)	B2-B1-H1	118.1(9)
B6-B2-B1#1	110.73(13)	B6-B2-B1	110.49(12)	B1#1-B2-B1	60.05(12)
B6-B2-B5	60.91(10)	B1#1-B2-B5	106.00(14)	B1-B2-B5	58.73(10)
B6-B2-B7	61.62(11)	B1#1-B2-B7	58.44(11)	B1-B2-B7	105.8(2)
B5-B2-B7	105.30(14)	B6-B2-H2	118.2(14)	B1#1-B2-H2	123.1(13)

B1-B2-H2	121.0(13)	B5-B2-H2	121.9(12)	B7-B2-H2	125.3(12)
B1-B5-B6	108.6(2)	B1-B5-B2	60.14(11)	B6-B5-B2	57.27(11)
B1-B5-B7#1	55.05(10)	B6-B5-B7#1	117.1(2)	B2-B5-B7#1	106.06(14)
B1-B5-H5	125.6(11)	B6-B5-H5	113.1(11)	B2-B5-H5	119.7(11)
B7#1-B5-H5	124.8(11)	B1-B5-H56	127.5(10)	B6-B5-H56	47.0(9)
B2-B5-H56	101.4(8)	B7#1-B5-H56	92.0(10)	H5-B5-H56	106.4(14)
F1-B6-B2	130.1(2)	F1-B6-B5	124.1(2)	B2-B6-B5	61.82(10)
F1-B6-B7	128.2(2)	B2-B6-B7	61.42(10)	B5-B6-B7	105.8(2)
F1-B6-H56	108.5(9)	B2-B6-H56	103.1(8)	B5-B6-H56	44.1(8)
B7-B6-H56	117.1(10)	F1-B6-H67	110.3(9)	B2-B6-H67	104.3(9)
B5-B6-H67	118.1(9)	B7-B6-H67	45.4(9)	H56-B6-H67	94.7(13)
F1-B6-H6	5.9	B2-B6-H6	125.3	B5-B6-H6	126.7
B7-B6-H6	123.9	H56-B6-H6	114.2	H67-B6-H6	110.6
B1#1-B7-B2	60.15(11)	B1#1-B7-B6	108.26(14)	B2-B7-B6	56.96(11)
B1#1-B7-B5#1	55.57(11)	B2-B7-B5#1	106.23(13)	B6-B7-B5#1	116.42(14)
B1#1-B7-H7	121.2(11)	B2-B7-H7	126.2(12)	B6-B7-H7	121.9(13)
B5#1-B7-H7	115.9(13)	B1#1-B7-H67	127.7(9)	B2-B7-H67	98.8(8)
B6-B7-H67	44.1(8)	B5#1-B7-H67	93.6(9)	H7-B7-H67	109.9(14)
B5-H56-B6	88.9(12)	B6-H67-B7	90.4(13)	B7'#2-B1'-B5'	69.15(13)
B7'#2-B1'-B2'	118.25(13)	B5'-B1'-B2'	60.96(11)	B7'#2-B1'-B1'#2	107.73(12)
B5'-B1'-B1'#2	107.82(13)	B2'-B1'-B1'#2	60.45(13)	B7'#2-B1'-B2'#2	61.23(11)
B5'-B1'-B2'#2	118.11(13)	B2'-B1'-B2'#2	114.71(12)	B1'#2-B1'-B2'#2	59.75(11)
B7'#2-B1'-H1'	114.7(8)	B5'-B1'-H1'	115.0(8)	B2'-B1'-H1'	117.9(8)
B1'#2-B1'-H1'	127.5(8)	B2'#2-B1'-H1'	117.8(8)	B6'-B2'-B1'	111.28(12)
B6'-B2'-B1'#2	111.02(12)	B1'-B2'-B1'#2	59.79(12)	B6'-B2'-B5'	61.08(11)
B1'-B2'-B5'	59.16(11)	B1'#2-B2'-B5'	105.9(2)	B6'-B2'-B7'	61.39(11)
B1'-B2'-B7'	105.64(14)	B1'#2-B2'-B7'	58.51(10)	B5'-B2'-B7'	104.72(14)
B6'-B2'-H2'	120.3(11)	B1'-B2'-H2'	120.0(11)	B1'#2-B2'-H2'	119.9(11)
B5'-B2'-H2'	124.7(11)	B7'-B2'-H2'	124.5(10)	B1'-B5'-B6'	108.9(2)

B1'-B5'-B2'	59.89(11)	B6'-B5'-B2'	57.56(11)	B1'-B5'-B7'#2	55.27(10)
B6'-B5'-B7'#2	117.55(14)	B2'-B5'-B7'#2	106.04(13)	B1'-B5'-H5'	120.8(11)
B6'-B5'-H5'	120.0(13)	B2'-B5'-H5'	123.8(12)	B7'#2-B5'-H5'	117.6(14)
B1'-B5'-H56'	127.7(9)	B6'-B5'-H56'	47.6(10)	B2'-B5'-H56'	102.0(10)
B7'#2-B5'-H56'	91.6(10)	H5'-B5'-H56'	110.0(14)	F1'-B6'-B2'	129.2(2)
F1'-B6'-B5'	126.1(2)	B2'-B6'-B5'	61.36(10)	F1'-B6'-B7'	126.8(2)
B2'-B6'-B7'	61.47(10)	B5'-B6'-B7'	105.0(2)	F1'-B6'-H56'	111.5(9)
B2'-B6'-H56'	102.3(9)	B5'-B6'-H56'	44.0(9)	B7'-B6'-H56'	115.6(8)
F1'-B6'-H67'	112.4(10)	B2'-B6'-H67'	102.4(9)	B5'-B6'-H67'	115.1(10)
B7'-B6'-H67'	44.2(8)	H56'-B6'-H67'	92.6(12)	F1'-B6'-H6'	1.8
B2'-B6'-H6'	127.5	B5'-B6'-H6'	125.1	B7'-B6'-H6'	127.2
H56'-B6'-H6'	112.0	H67'-B6'-H6'	114.0	B1'#2-B7'-B6'	108.91(14)
B1'#2-B7'-B2'	60.27(10)	B6'-B7'-B2'	57.13(11)	B1'#2-B7'-B5'#2	55.58(10)
B6'-B7'-B5'#2	117.20(14)	B2'-B7'-B5'#2	106.35(14)	B1'#2-B7'-H7'	119.9(8)
B6'-B7'-H7'	123.4(9)	B2'-B7'-H7'	127.8(8)	B5'#2-B7'-H7'	113.3(9)
B1'#2-B7'-H67'	126.9(11)	B6'-B7'-H67'	47.3(9)	B2'-B7'-H67'	101.2(9)
B5'#2-B7'-H67'	90.8(11)	H7'-B7'-H67'	110.5(13)	B5'-H56'-B6'	88.5(13)
B6'-H67'-B7'	88.5(12)				

Table 2.2.4. Bond lengths for **2**.

Cl1-B6	1.764(2)	B1-B10	1.747(2)	B1-B5	1.757(2)
B1-B3	1.774(2)	B1-B4	1.777(2)	B1-B2	1.785(2)
B1-H1	1.07(2)	B2-B6	1.723(2)	B2-B3	1.779(2)
B2-B5	1.797(2)	B2-B7	1.803(2)	B2-H2	1.07(2)
B3-B7	1.744(2)	B3-B8	1.750(2)	B3-B4	1.774(2)
B3-H3	1.07(2)	B4-B9	1.729(2)	B4-B8	1.791(2)
B4-B10	1.791(2)	B4-H4	1.07(2)	B5-B6	1.797(2)
B5-B10	1.987(2)	B5-H5	1.05(2)	B5-H56	1.27(2)
B6-B7	1.786(2)	B6-H56	1.29(2)	B6-H67	1.26(2)
B7-B8	1.992(2)	B7-H7	1.07(2)	B7-H67	1.20(2)

B8-B9	1.792(2)	B8-H8	1.04(2)	B8-H89	1.25(2)
B9-B10	1.794(2)	B9-H9	1.11(2)	B9-H89	1.29(2)
B9-H910	1.27(2)	B10-H10	1.07(2)	B10-H910	1.30(2)

Table 2.2.5. Bond angles for **2**.

B10-B1-B5	69.07(10)	B10-B1-B3	107.35(11)	B5-B1-B3	107.49(11)
B10-B1-B4	61.08(9)	B5-B1-B4	118.14(11)	B3-B1-B4	59.93(9)
B10-B1-B2	117.81(11)	B5-B1-B2	60.98(9)	B3-B1-B2	59.97(9)
B4-B1-B2	114.47(11)	B10-B1-H1	115.2(10)	B5-B1-H1	114.6(10)
B3-B1-H1	127.9(9)	B4-B1-H1	118.3(10)	B2-B1-H1	117.8(10)
B6-B2-B3	109.78(11)	B6-B2-B1	110.48(11)	B3-B2-B1	59.71(9)
B6-B2-B5	61.34(9)	B3-B2-B5	105.55(11)	B1-B2-B5	58.74(9)
B6-B2-B7	60.81(9)	B3-B2-B7	58.29(9)	B1-B2-B7	105.54(11)
B5-B2-B7	105.07(10)	B6-B2-H2	118.2(8)	B3-B2-H2	123.1(8)
B1-B2-H2	122.1(8)	B5-B2-H2	122.9(8)	B7-B2-H2	124.3(8)
B7-B3-B8	69.51(9)	B7-B3-B4	118.57(11)	B8-B3-B4	61.10(9)
B7-B3-B1	108.55(11)	B8-B3-B1	108.28(11)	B4-B3-B1	60.13(9)
B7-B3-B2	61.54(9)	B8-B3-B2	118.99(11)	B4-B3-B2	114.96(11)
B1-B3-B2	60.32(9)	B7-B3-H3	112.8(9)	B8-B3-H3	113.8(9)
B4-B3-H3	118.9(9)	B1-B3-H3	128.6(9)	B2-B3-H3	117.2(9)
B9-B4-B3	110.59(11)	B9-B4-B1	110.96(11)	B3-B4-B1	59.94(9)
B9-B4-B8	61.19(9)	B3-B4-B8	58.79(9)	B1-B4-B8	106.33(11)
B9-B4-B10	61.25(9)	B3-B4-B10	105.46(11)	B1-B4-B10	58.63(9)
B8-B4-B10	105.11(11)	B9-B4-H4	119.9(10)	B3-B4-H4	121.4(10)
B1-B4-H4	119.7(10)	B8-B4-H4	125.0(10)	B10-B4-H4	123.3(10)
B1-B5-B6	108.40(12)	B1-B5-B2	60.28(9)	B6-B5-B2	57.30(8)
B1-B5-B10	55.24(8)	B6-B5-B10	115.95(11)	B2-B5-B10	106.04(10)
B1-B5-H5	123.7(9)	B6-B5-H5	119.6(9)	B2-B5-H5	126.0(9)
B10-B5-H5	117.9(9)	B1-B5-H56	126.7(8)	B6-B5-H56	46.1(7)
B2-B5-H56	100.6(7)	B10-B5-H56	91.2(8)	H5-B5-H56	108.0(12)
B2-B6-Cl1	130.81(11)	B2-B6-B7	61.80(9)	Cl1-B6-B7	125.55(11)
B2-B6-B5	61.36(9)	Cl1-B6-B5	126.99(11)	B7-B6-B5	105.80(11)
B2-B6-H56	103.3(7)	Cl1-B6-H56	110.1(7)	B7-B6-H56	117.0(8)
B5-B6-H56	44.8(7)	B2-B6-H67	100.7(8)	Cl1-B6-H67	111.7(8)

B7-B6-H67	42.3(8)	B5-B6-H67	115.2(8)	H56-B6-H67	93.8(11)
B3-B7-B6	108.48(11)	B3-B7-B2	60.17(9)	B6-B7-B2	57.39(8)
B3-B7-B8	55.38(8)	B6-B7-B8	116.67(10)	B2-B7-B8	106.38(10)
B3-B7-H7	125.3(9)	B6-B7-H7	118.7(8)	B2-B7-H7	127.3(9)
B8-B7-H7	117.2(8)	B3-B7-H67	124.9(8)	B6-B7-H67	45.0(8)
B2-B7-H67	99.0(8)	B8-B7-H67	90.8(8)	H7-B7-H67	108.3(12)
B3-B8-B4	60.11(9)	B3-B8-B9	108.76(11)	B4-B8-B9	57.69(9)
B3-B8-B7	55.11(8)	B4-B8-B7	106.05(11)	B9-B8-B7	116.68(11)
B3-B8-H8	122.6(8)	B4-B8-H8	127.4(8)	B9-B8-H8	121.1(8)
B7-B8-H8	115.5(9)	B3-B8-H89	128.9(8)	B4-B8-H89	101.4(8)
B9-B8-H89	46.0(8)	B7-B8-H89	93.4(8)	H8-B8-H89	106.6(11)
B4-B9-B8	61.12(9)	B4-B9-B10	61.09(9)	B8-B9-B10	104.94(11)
B4-B9-H9	130.6(8)	B8-B9-H9	127.7(8)	B10-B9-H9	125.4(8)
B4-B9-H89	103.1(8)	B8-B9-H89	44.3(8)	B10-B9-H89	118.4(8)
H9-B9-H89	109.8(11)	B4-B9-H910	104.5(7)	B8-B9-H910	117.2(7)
B10-B9-H910	46.3(7)	H9-B9-H910	108.1(10)	H89-B9-H910	95.1(11)
B1-B10-B4	60.28(9)	B1-B10-B9	109.33(11)	B4-B10-B9	57.66(9)
B1-B10-B5	55.69(8)	B4-B10-B5	106.62(11)	B9-B10-B5	117.39(11)
B1-B10-H10	123.7(9)	B4-B10-H10	125.6(9)	B9-B10-H10	118.1(10)
B5-B10-H10	117.8(10)	B1-B10-H910	128.2(7)	B4-B10-H910	100.0(7)
B9-B10-H910	45.0(7)	B5-B10-H910	93.2(7)	H10-B10-H910	107.0(11)

Table 2.2.6. Bond lengths for **3**.

Br1-B6	1.929(4)	B1-B5	1.754(5)	B1-B10	1.763(6)
B1-B3	1.772(6)	B1-B2	1.783(5)	B1-B4	1.787(5)
B1-H1	1.14(4)	B2-B6	1.710(5)	B2-B3	1.782(5)
B2-B5	1.785(5)	B2-B7	1.794(5)	B2-H2	1.08(4)
B3-B7	1.739(5)	B3-B8	1.746(5)	B3-B4	1.769(6)
B3-H3	0.97(4)	B4-B9	1.716(6)	B4-B8	1.783(5)
B4-B10	1.807(6)	B4-H4	1.08(4)	B5-B6	1.789(5)
B5-B10	1.994(6)	B5-H5	1.09(5)	B5-H56	1.26(4)

B6-B7	1.783(5)	B6-H56	1.34(4)	B6-H67	1.20(4)
B7-B8	2.000(5)	B7-H7	0.96(5)	B7-H67	1.21(5)
B8-B9	1.792(5)	B8-H8	1.00(4)	B8-H89	1.12(5)
B9-B10	1.795(5)	B9-H9	1.07(4)	B9-H89	1.25(5)
B9-H910	1.28(3)	B10-H10	1.11(4)	B10-H910	1.43(4)

Table 2.2.7. Bond angles for **3**.

B5-B1-B10	69.1(2)	B5-B1-B3	107.4(3)	B10-B1-B3	107.3(3)
B5-B1-B2	60.6(2)	B10-B1-B2	117.5(3)	B3-B1-B2	60.2(2)
B5-B1-B4	118.1(3)	B10-B1-B4	61.2(2)	B3-B1-B4	59.6(2)
B2-B1-B4	114.2(3)	B5-B1-H1	111(2)	B10-B1-H1	117(2)
B3-B1-H1	129(2)	B2-B1-H1	114(2)	B4-B1-H1	123(2)
B6-B2-B3	109.7(2)	B6-B2-B1	110.7(3)	B3-B2-B1	59.6(2)
B6-B2-B5	61.5(2)	B3-B2-B5	105.6(3)	B1-B2-B5	58.9(2)
B6-B2-B7	61.1(2)	B3-B2-B7	58.2(2)	B1-B2-B7	105.8(2)
B5-B2-B7	105.8(2)	B6-B2-H2	120(2)	B3-B2-H2	122(2)
B1-B2-H2	121(2)	B5-B2-H2	124(2)	B7-B2-H2	124(2)
B7-B3-B8	70.0(2)	B7-B3-B4	118.9(3)	B8-B3-B4	61.0(2)
B7-B3-B1	108.7(3)	B8-B3-B1	108.8(3)	B4-B3-B1	60.6(2)
B7-B3-B2	61.2(2)	B8-B3-B2	119.1(3)	B4-B3-B2	115.2(3)
B1-B3-B2	60.2(2)	B7-B3-H3	113(2)	B8-B3-H3	116(2)
B4-B3-H3	120(2)	B1-B3-H3	127(2)	B2-B3-H3	115(2)
B9-B4-B3	110.8(3)	B9-B4-B8	61.5(2)	B3-B4-B8	58.9(2)
B9-B4-B1	111.0(3)	B3-B4-B1	59.8(2)	B8-B4-B1	106.5(3)
B9-B4-B10	61.2(2)	B3-B4-B10	105.5(3)	B8-B4-B10	105.5(3)
B1-B4-B10	58.7(2)	B9-B4-H4	121(2)	B3-B4-H4	119(2)
B8-B4-H4	123(2)	B1-B4-H4	120(2)	B10-B4-H4	126(2)
B1-B5-B2	60.5(2)	B1-B5-B6	108.4(3)	B2-B5-B6	57.1(2)
B1-B5-B10	55.7(2)	B2-B5-B10	106.6(3)	B6-B5-B10	115.8(3)

B1-B5-H5	123(2)	B2-B5-H5	121(2)	B6-B5-H5	117(2)
B10-B5-H5	122(2)	B1-B5-H56	128(2)	B2-B5-H56	103(2)
B6-B5-H56	48(2)	B10-B5-H56	90(2)	H5-B5-H56	108(3)
B2-B6-B7	61.8(2)	B2-B6-B5	61.3(2)	B7-B6-B5	106.1(3)
B2-B6-Br1	130.7(2)	B7-B6-Br1	125.2(2)	B5-B6-Br1	126.9(2)
B2-B6-H56	103(2)	B7-B6-H56	118(2)	B5-B6-H56	44(2)
Br1-B6-H56	110(2)	B2-B6-H67	101(2)	B7-B6-H67	43(2)
B5-B6-H67	116(2)	Br1-B6-H67	111(2)	H56-B6-H67	95(3)
B3-B7-B6	108.4(3)	B3-B7-B2	60.6(2)	B6-B7-B2	57.1(2)
B3-B7-B8	55.1(2)	B6-B7-B8	116.4(3)	B2-B7-B8	106.5(2)
B3-B7-H7	126(3)	B6-B7-H7	118(2)	B2-B7-H7	127(2)
B8-B7-H7	118(2)	B3-B7-H67	125(2)	B6-B7-H67	42(2)
B2-B7-H67	96(2)	B8-B7-H67	93(2)	H7-B7-H67	109(4)
B3-B8-B4	60.2(2)	B3-B8-B9	108.4(3)	B4-B8-B9	57.4(2)
B3-B8-B7	54.8(2)	B4-B8-B7	105.9(3)	B9-B8-B7	116.5(3)
B3-B8-H8	127(2)	B4-B8-H8	125(2)	B9-B8-H8	116(2)
B7-B8-H8	121(2)	B3-B8-H89	130(3)	B4-B8-H89	100(3)
B9-B8-H89	44(3)	B7-B8-H89	96(3)	H8-B8-H89	103(3)
B4-B9-B8	61.1(2)	B4-B9-B10	61.9(2)	B8-B9-B10	105.7(3)
B4-B9-H9	132(2)	B8-B9-H9	125(2)	B10-B9-H9	127(2)
B4-B9-H89	98(2)	B8-B9-H89	38(2)	B10-B9-H89	119(2)
H9-B9-H89	109(3)	B4-B9-H910	110(2)	B8-B9-H910	116(2)
B10-B9-H910	52(2)	H9-B9-H910	106(3)	H89-B9-H910	95(3)
B1-B10-B9	108.5(3)	B1-B10-B4	60.1(2)	B9-B10-B4	56.9(2)
B1-B10-B5	55.2(2)	B9-B10-B5	117.1(3)	B4-B10-B5	105.9(3)
B1-B10-H10	124(2)	B9-B10-H10	120(2)	B4-B10-H10	128(2)
B5-B10-H10	116(2)	B1-B10-H910	126(2)	B9-B10-H910	45.1(14)
B4-B10-H910	99(2)	B5-B10-H910	92.5(13)	H10-B10-H910	108(3)

Table 2.2.8. Bond lengths for **4**.

I1-B6	2.143(3)	B1-B5	1.749(5)	B1-B10	1.756(5)

B1-B3	1.773(5)	B1-B4	1.774(5)	B1-B2	1.780(5)
B1-H1	1.07(4)	B2-B6	1.723(4)	B2-B3	1.785(5)
B2-B5	1.791(5)	B2-B7	1.796(5)	B2-H2	1.06(4)
B3-B7	1.755(5)	B3-B8	1.759(5)	B3-B4	1.774(5)
B3-H3	1.11(3)	B4-B9	1.722(5)	B4-B8	1.789(5)
B4-B10	1.790(5)	B4-H4	1.08(4)	B5-B6	1.789(5)
B5-B10	1.981(5)	B5-H5	1.06(4)	B5-H56	1.26(3)
B6-B7	1.791(5)	B6-H56	1.33(4)	B6-H67	1.29(3)
B7-B8	1.984(5)	B7-H7	1.05(4)	B7-H67	1.26(3)
B8-B9	1.791(5)	B8-H8	1.09(3)	B8-H89	1.19(4)
B9-B10	1.793(5)	B9-H13	1.06(4)	B9-H89	1.25(5)
B9-H910	1.29(4)	B10-H10	1.10(4)	B10-H910	1.21(4)

Table 2.2.9. Bond angles for **4**.

B5-B1-B10	68.8(2)	B5-B1-B3	108.0(2)	B10-B1-B3	108.0(2)
B5-B1-B4	117.6(2)	B10-B1-B4	60.9(2)	B3-B1-B4	60.0(2)
B5-B1-B2	61.0(2)	B10-B1-B2	117.9(2)	B3-B1-B2	60.3(2)
B4-B1-B2	114.4(2)	B5-B1-H1	117(2)	B10-B1-H1	116(2)
B3-B1-H1	126(2)	B4-B1-H1	117(2)	B2-B1-H1	118(2)
B6-B2-B1	110.4(2)	B6-B2-B3	110.4(2)	B1-B2-B3	59.6(2)
B6-B2-B5	61.2(2)	B1-B2-B5	58.6(2)	B3-B2-B5	105.6(2)
B6-B2-B7	61.2(2)	B1-B2-B7	105.7(2)	B3-B2-B7	58.7(2)
B5-B2-B7	105.2(2)	B6-B2-H2	119(2)	B1-B2-H2	123(2)
B3-B2-H2	121(2)	B5-B2-H2	126(2)	B7-B2-H2	122(2)
B7-B3-B8	68.7(2)	B7-B3-B4	117.6(2)	B8-B3-B4	60.8(2)
B7-B3-B1	107.8(2)	B8-B3-B1	107.6(2)	B4-B3-B1	60.0(2)
B7-B3-B2	61.0(2)	B8-B3-B2	117.4(2)	B4-B3-B2	114.2(2)
B1-B3-B2	60.0(2)	B7-B3-H3	114(2)	B8-B3-H3	114(2)
B4-B3-H3	118(2)	B1-B3-H3	128(2)	B2-B3-H3	119(2)
B9-B4-B3	111.5(2)	B9-B4-B1	111.3(2)	B3-B4-B1	59.9(2)
B9-B4-B8	61.3(2)	B3-B4-B8	59.2(2)	B1-B4-B8	106.2(2)
B9-B4-B10	61.4(2)	B3-B4-B10	106.4(2)	B1-B4-B10	59.0(2)
B8-B4-B10	105.3(2)	B9-B4-H4	116(2)	B3-B4-H4	120(2)

B1-B4-H4	126(2)	B8-B4-H4	119(2)	B10-B4-H4	127(2)
B1-B5-B2	60.4(2)	B1-B5-B6	108.8(2)	B2-B5-B6	57.5(2)
B1-B5-B10	55.8(2)	B2-B5-B10	106.7(2)	B6-B5-B10	116.5(2)
B1-B5-H5	125(2)	B2-B5-H5	126(2)	B6-B5-H5	118(2)
B10-B5-H5	118(2)	B1-B5-H56	127(2)	B2-B5-H56	102(2)
B6-B5-H56	48(2)	B10-B5-H56	90(2)	H5-B5-H56	106(3)
B2-B6-B5	61.3(2)	B2-B6-B7	61.4(2)	B5-B6-B7	105.5(2)
B2-B6-I1	128.7(2)	B5-B6-I1	125.4(2)	B7-B6-I1	126.6(2)
B2-B6-H56	103(2)	B5-B6-H56	44.7(14)	B7-B6-H56	117(2)
I1-B6-H56	111(2)	B2-B6-H67	103(2)	B5-B6-H67	116(2)
B7-B6-H67	45(2)	I1-B6-H67	112(2)	H56-B6-H67	93(2)
B3-B7-B6	108.7(2)	B3-B7-B2	60.4(2)	B6-B7-B2	57.4(2)
B3-B7-B8	55.7(2)	B6-B7-B8	115.9(2)	B2-B7-B8	106.4(2)
B3-B7-H7	121(3)	B6-B7-H7	123(3)	B2-B7-H7	128(3)
B8-B7-H7	114(2)	B3-B7-H67	126(2)	B6-B7-H67	46(2)
B2-B7-H67	101(2)	B8-B7-H67	90(2)	H7-B7-H67	110(3)
B3-B8-B4	60.0(2)	B3-B8-B9	109.0(2)	B4-B8-B9	57.5(2)
B3-B8-B7	55.5(2)	B4-B8-B7	106.2(2)	B9-B8-B7	117.2(2)
B3-B8-H8	124(2)	B4-B8-H8	127(2)	B9-B8-H8	119(2)
B7-B8-H8	117(2)	B3-B8-H89	132(2)	B4-B8-H89	100(2)
B9-B8-H89	44(2)	B7-B8-H89	97(2)	H8-B8-H89	103(3)
B4-B9-B8	61.2(2)	B4-B9-B10	61.2(2)	B8-B9-B10	105.2(2)
B4-B9-H13	132(2)	B8-B9-H13	123(2)	B10-B9-H13	130(2)
B4-B9-H89	101(2)	B8-B9-H89	42(2)	B10-B9-H89	121(2)
H13-B9-H89	104(3)	B4-B9-H910	101(2)	B8-B9-H910	118(2)
B10-B9-H910	42(2)	H13-B9-H910	113(2)	H89-B9-H910	101(3)
B1-B10-B4	60.0(2)	B1-B10-B9	108.8(2)	B4-B10-B9	57.4(2)
B1-B10-B5	55.4(2)	B4-B10-B5	105.9(2)	B9-B10-B5	116.7(2)
B1-B10-H10	122(2)	B4-B10-H10	127(2)	B9-B10-H10	121(2)
B5-B10-H10	116(2)	B1-B10-H910	129(2)	B4-B10-H910	101(2)
B9-B10-H910	46(2)	B5-B10-H910	93(2)	H10-B10-H910	108(3)
B5-H56-B6	87(2)	B6-H67-B7	89(2)	B8-H89-B9	95(3)
B9-H910-B10	91(2)				

Table 2.2.10 Bond lengths for **6**.

I1-B6	2.156(2)	B1-B5	1.749(3)	B1-B10	1.755(3)
B1-B4	1.782(3)	B1-B3	1.785(3)	B1-B2	1.789(3)
B1-H1	1.03(2)	B2-B6	1.720(3)	B2-B5	1.785(3)
B2-B3	1.788(3)	B2-B7	1.790(3)	B2-H2	1.09(2)
B3-B7	1.749(3)	B3-B8	1.764(3)	B3-B4	1.782(3)
B3-H3	1.07(2)	B4-B9	1.743(3)	B4-B8	1.793(3)
B4-B10	1.797(3)	B4-H4	1.09(2)	B5-B6	1.794(3)
B5-B10	1.978(3)	B5-H5	1.09(2)	B5-H56	1.29(2)
B6-B7	1.786(3)	B6-H56	1.34(2)	B6-H67	1.26(3)
B7-B8	1.990(3)	B7-H7	1.07(2)	B7-H67	1.26(3)
B8-B9	1.796(3)	B8-H8	1.04(2)	B8-H89	1.27(2)
B9-C11	1.581(3)	B9-B10	1.815(3)	B9-H89	1.32(2)
B9-H910	1.34(2)	B10-H10	1.03(2)	B10-H910	1.25(2)
C11-C12	1.523(3)	C11-H11a	0.97(2)	C11-H11b	0.87(3)
C12-H12a	0.94(4)	C12-H12b	0.95(4)	C12-H12c	0.89(3)

Table 2.2.11. Bond angles for **6**.

B5-B1-B10	68.73(13)	B5-B1-B4	117.4(2)	B10-B1-B4	61.04(13)
B5-B1-B3	107.3(2)	B10-B1-B3	107.6(2)	B4-B1-B3	59.94(13)
B5-B1-B2	60.60(12)	B10-B1-B2	117.4(2)	B4-B1-B2	114.1(2)
B3-B1-B2	60.02(13)	B5-B1-H1	112.0(13)	B10-B1-H1	117.0(12)
B4-B1-H1	122.6(13)	B3-B1-H1	128.4(13)	B2-B1-H1	114.5(12)
B6-B2-B5	61.52(12)	B6-B2-B1	110.8(2)	B5-B2-B1	58.59(12)
B6-B2-B3	110.2(2)	B5-B2-B3	105.6(2)	B1-B2-B3	59.89(13)
B6-B2-B7	61.15(13)	B5-B2-B7	105.5(2)	B1-B2-B7	106.1(2)
B3-B2-B7	58.54(12)	B6-B2-H2	117.5(13)	B5-B2-H2	123.9(13)
B1-B2-H2	122.8(13)	B3-B2-H2	122.6(12)	B7-B2-H2	122.7(13)
B7-B3-B8	69.01(14)	B7-B3-B4	118.2(2)	B8-B3-B4	60.74(12)
B7-B3-B1	108.0(2)	B8-B3-B1	107.1(2)	B4-B3-B1	59.94(13)
B7-B3-B2	60.80(13)	B8-B3-B2	116.9(2)	B4-B3-B2	114.2(2)

B1-B3-B2	60.09(13)	B7-B3-H3	113.7(10)	B8-B3-H3	118.3(12)
B4-B3-H3	120.3(11)	B1-B3-H3	126.4(11)	B2-B3-H3	115.5(12)
B9-B4-B1	111.8(2)	B9-B4-B3	111.8(2)	B1-B4-B3	60.11(13)
B9-B4-B8	61.01(12)	B1-B4-B8	105.9(2)	B3-B4-B8	59.13(13)
B9-B4-B10	61.65(12)	B1-B4-B10	58.74(13)	B3-B4-B10	106.0(2)
B8-B4-B10	104.3(2)	B9-B4-H4	119.1(11)	B1-B4-H4	117.8(11)
B3-B4-H4	122.3(11)	B8-B4-H4	128.6(11)	B10-B4-H4	120.6(11)
B1-B5-B2	60.81(13)	B1-B5-B6	109.3(2)	B2-B5-B6	57.46(12)
B1-B5-B10	55.80(12)	B2-B5-B10	107.1(2)	B6-B5-B10	116.7(2)
B1-B5-H5	124.5(12)	B2-B5-H5	124.3(12)	B6-B5-H5	117.0(12)
B10-B5-H5	119.4(12)	B1-B5-H56	130.2(10)	B2-B5-H56	103.7(10)
B6-B5-H56	48.4(10)	B10-B5-H56	91.9(10)	H5-B5-H56	104(2)
B2-B6-B7	61.35(13)	B2-B6-B5	61.02(12)	B7-B6-B5	105.3(2)
B2-B6-I1	129.57(14)	B7-B6-I1	126.64(13)	B5-B6-I1	125.82(14)
B2-B6-H56	104.6(9)	B7-B6-H56	119.5(10)	B5-B6-H56	45.7(9)
I1-B6-H56	107.7(10)	B2-B6-H67	103.3(11)	B7-B6-H67	44.7(12)
B5-B6-H67	117.5(8)	I1-B6-H67	110.5(9)	H56-B6-H67	96.1(14)
B3-B7-B6	109.0(2)	B3-B7-B2	60.66(13)	B6-B7-B2	57.51(13)
B3-B7-B8	55.85(12)	B6-B7-B8	115.1(2)	B2-B7-B8	106.28(14)
B3-B7-H7	122.6(12)	B6-B7-H7	121.2(12)	B2-B7-H7	127.6(12)
B8-B7-H7	116.3(12)	B3-B7-H67	127.2(8)	B6-B7-H67	44.9(12)
B2-B7-H67	99.8(11)	B8-B7-H67	91.0(11)	H7-B7-H67	108.3(14)
B3-B8-B4	60.13(12)	B3-B8-B9	110.2(2)	B4-B8-B9	58.13(12)
B3-B8-B7	55.14(12)	B4-B8-B7	106.3(2)	B9-B8-B7	119.1(2)
B3-B8-H8	124.7(13)	B4-B8-H8	127.0(12)	B9-B8-H8	116.9(12)
B7-B8-H8	116.8(12)	B3-B8-H89	128.3(9)	B4-B8-H89	102.0(9)
B9-B8-H89	47.3(9)	B7-B8-H89	92.5(9)	H8-B8-H89	105(2)
C11-B9-B4	131.8(2)	C11-B9-B8	127.2(2)	B4-B9-B8	60.86(13)
C11-B9-B10	127.9(2)	B4-B9-B10	60.63(13)	B8-B9-B10	103.5(2)
C11-B9-H89	110.5(9)	B4-B9-H89	102.6(9)	B8-B9-H89	45.1(9)
B10-B9-H89	114.0(9)	C11-B9-H910	114.7(10)	B4-B9-H910	99.6(10)
B8-B9-	110.8(10)	B10-B9-H910	43.4(10)	H89-B9-	88.8(14)

H910				H910	
B1-B10-B4	60.21(13)	B1-B10-B9	109.8(2)	B4-B10-B9	57.72(12)
B1-B10-B5	55.48(12)	B4-B10-B5	106.01(14)	B9-B10-B5	117.6(2)
B1-B10-H10	121.1(11)	B4-B10-H10	129.0(12)	B9-B10-H10	122.0(11)
B5-B10-H10	113.5(12)	B1-B10-H910	124.6(11)	B4-B10-H910	100.7(11)
B9-B10-H910	47.5(11)	B5-B10-H910	88.5(11)	H10-B10-H910	111(2)
C12-C11-B9	113.8(2)	C12-C11-H11a	110.4(13)	B9-C11-H11a	106.3(14)
C12-C11-H11b	108(2)	B9-C11-H11b	109(2)	H11a-C11-H11b	110(2)
C11-C12-H12a	108(2)	C11-C12-H12b	120(2)	H12a-C12-H12b	100(3)
C11-C12-H12c	112(2)	H12a-C12-H12c	111(3)	H12b-C12-H12c	105(3)

Computational Methods. Density Functional Theory (DFT) calculations were performed using the Gaussian 03 package.[18] The optimized ground-state, transition-state and intermediate geometries and both the electronic and free energy values were obtained at the B3LYP/6-311G(d) level without constraints for all H, C, B and F atoms. The NMR chemical shifts were calculated at the B3LYP/6-311G(d) level using the GIAO option within Gaussian 03 and are referenced to $BF_3{\cdot}O(C_2H_5)_2$ using an absolute shielding constant of 102.24 ppm. Harmonic vibrational analyses were carried out on the optimized geometries at the same level to establish the nature of stationary points. The optimized Cartesian coordinates for **1** and $B_{10}H_{13}^+$ are given in **Tables 2.2.12** and **2.2.13**.

Table 2.2.12. DFT optimized Cartesian coordinates for **1** (B3LYP/6-311G(d))

Atom	X	Y	Z
F	2.9444	-0.0000	-0.6604
B1	-0.6780	-0.8914	1.1181
B2	0.8547	0.0000	1.2077
B3	-0.6780	0.8914	1.1181
B4	-2.0111	0.0000	0.3360
B5	0.6614	-1.4320	0.1252
B6	1.6528	0.0000	-0.3095
B7	0.6614	1.4320	0.1252
B8	-1.2521	1.4233	-0.4449
B9	-1.8305	-0.0000	-1.3748
B10	-1.2521	-1.4233	-0.4448
H1	-0.9369	-1.6243	2.0136
H2	1.5031	-0.0000	2.1985
H3	-0.9369	1.6243	2.0135
H4	-3.0895	0.0000	0.8239
H5	1.2049	-2.4738	0.2599
H7	1.2050	2.4738	0.2599
H8	-1.7547	2.4765	-0.6379
H9	-2.6492	-0.0000	-2.2278
H10	-1.7547	-2.4765	-0.6378
H56	0.9978	-0.9802	-1.0415
H67	0.9978	0.9802	-1.0415
H89	-0.9642	0.9667	-1.6604
H910	-0.9643	-0.9667	-1.6604

Table 2.2.13. DFT optimized Cartesian coordinates for Hawthorne's cationic intermediate $B_{10}H_{13}^{+}$ (B3LYP/6-311G(d))

Atom	X	Y	Z
B1	1.653692	0.000000	0.471572
B2	-1.329305	0.000000	0.851122
B3	0.183546	-0.896345	1.050930
B4	0.183546	0.896345	1.050930
B5	1.039811	1.500860	-0.358656
B6	-0.978888	1.435661	-0.159800
B7	-0.978888	-1.435660	-0.159800
B8	1.039811	-1.500860	-0.358656
B9	-1.859634	0.000000	-0.794337
B10	1.409101	0.000000	-1.146328
H11	-1.165187	-0.993915	-1.387385
H12	-1.165187	0.993914	-1.387385
H13	0.969910	1.001196	-1.764552
H14	0.969909	-1.001197	-1.764551
H15	-2.929957	0.000000	-1.287042
H16	-1.505976	2.489498	-0.123991
H17	-1.505976	-2.489498	-0.123991
H18	-2.096258	0.000000	1.751406
H19	1.612064	2.514520	-0.527383
H20	1.612064	-2.514521	-0.527383
H21	2.701979	0.000000	1.023006
H22	0.344332	-1.659487	1.942181
H23	0.344332	1.659487	1.942181

2.3 Results and Discussion

2.3.1 Super-acidic Ionic Liquid Synthesis and Characterization of 6-X-$B_{10}H_{13}$

Acid-induced opening of *closo*-$B_{10}H_{10}^{2-}$ was first achieved by the reaction of $(NH_4^+)_2B_{10}H_{10}^{2-}$ with HCl in the presence of Et_2S to produce 6,9-$(Et_2S)_2$-$B_{10}H_{12}$.[19] Of more interest was Hawthorne's report that *closo*-$B_{10}H_{10}^{2-}$ salts could be opened to selectively form 6-R-$B_{10}H_{13}$ (R = triflate, phenyl, cyclohexyl) compounds if treated with triflic acid (**Eqs. 3** and **4**).[20] Similar strongly acidic conditions (conc. sulfuric acid in hexanes), were used to synthesize 6-(HO)-$B_{10}H_{13}$ from the $(NH_4^+)_2B_{10}H_{10}^{2-}$ salt.[21]

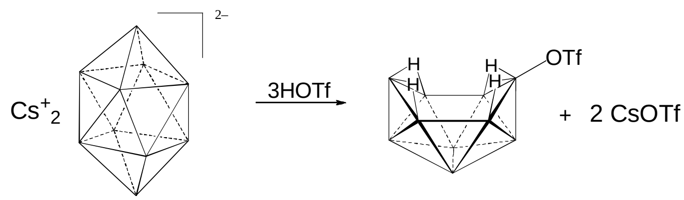

(**3**)

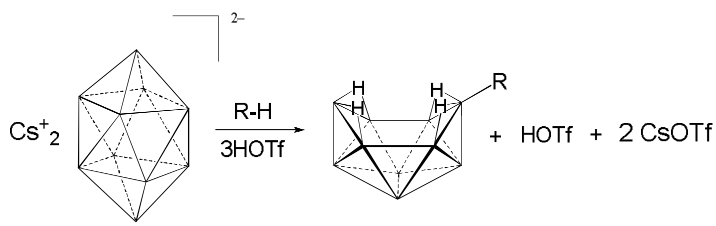

(**4**)

We found that $(NH_4^+)_2B_{10}H_{10}^{2-}$ was unreactive with anhydrous haloacids (HCl, HBr) in non-coordinating solvents such as CH_2Cl_2 or in ionic liquids, such as 1-butyl-3-methylimidazolium chloride (Bmim.Cl), thus indicating that a higher reactivity is required to induce cage opening. It has been previously shown that an ionic liquid formed by the addition of 55 mol% $AlCl_3$ to Bmim.Cl greatly enhances the acidity and the reactivity of dissolved HCl (**Eq. 5**) through the Cl-scavenging action of the Lewis-acidic $Al_2Cl_7^-$ anion.[22]

$$Al_2Cl_7^- + HCl \rightleftharpoons 2AlCl_4^- + H^+ \quad (\mathbf{5})$$

Treatment of *closo*-$B_{10}H_{10}^{2-}$ with hydrogen halides in such an ionic liquid mixture yielded the cage-opened compounds *nido*-6-X-$B_{10}H_{13}$. The products were selectively halogenated at B6 (**Eq. 6**) and were stable in the highly acidic medium at temperatures below ~100 ^{o}C.

In the synthesis of **2**, 0.20 g (1.30 mmol) of $(NH_4^+)_2B_{10}H_{10}^{2-}$ was added to 6.00 g (34.3 mmol) of Bmim.Cl and 6.00 g (45.0 mmol) of $AlCl_3$. The excess of ionic liquid, specifically the $AlCl_3$ component of the ionic liquid, is essential, as a buildup of Cl^- (NH_4Cl^- in **Eq. 6**) from the protonation of the $B_{10}H_{10}^{2-}$ decreases the acidity of the ionic liquid mixture.[23] After the mixture was stirred at 75 °C for 2 h under flowing HCl, the excess HCl was removed in vacuo and the product was extracted out of the ionic liquid with hexanes, followed by purification via sublimation. An analogous 2 h reaction and workup of 0.75 g (4.87 mmol) of $(NH_4^+)_2B_{10}H_{10}^{2-}$ in an $AlBr_3$ (15.0 g, 56.2 mmol)/Bmim.Br (10.0 g, 45.6 mmol)/HBr (flowing) system produced 0.93 g of (4.68 mmol, 96%) of **3**.

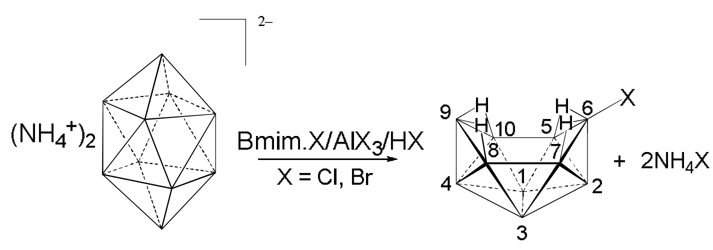

(**6**)

The iodinated derivative (**4**) was initially synthesized using an AlI_3/Bmim.I/HI system, but it was then found that substantially improved yields were obtained when HCl was utilized in place of HI (**Eq. 7**). Thus, the 2 h reaction of 0.20 g (1.30 mmol) of $(NH_4^+)_2B_{10}H_{10}^{2-}$ in AlI_3 (6.10 g, 1.10 mmol)/Bmim.I (3.00 g, 1.50 mmol)/HCl (flowing) at 70 °C produced 0.27 g (1.10 mmol, 84%) of **4**. The reaction of HCl with AlI_3 should produce H^+ and nucleophilic complex anions, e.g. $Al_2I_6Cl^-$.[22,23] Owing to the stronger Al-Cl versus Al-I bonds in these anions, cage-iodation should be favored and, indeed, no formation of 6-Cl-$B_{10}H_{13}$ was experimentally observed in this reaction.

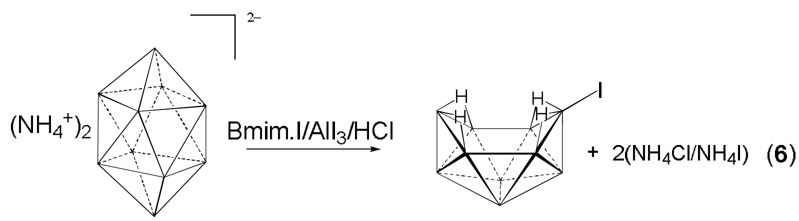

The NMR and IR spectra of the isolated products **2-4** match literature values, as do their melting points.[5,7] As shown in the ORTEP drawings in **Figures 2.3.1-2.3.3**, crystallographic determinations of compounds **2-4** confirmed their previously proposed structures, where the halogens are bonded at the terminal-position of the B6 on the decaborane open-face. The B-B intracage bond lengths in these compounds do not significantly vary between the three halogenated cages. The observed B-X bond lengths **2** (B-Cl, 1.764(2) Å), **3** (B-Br, 1.929(4) Å) and **4** (B-I, 2.143(3) Å) are consistent with those found in other halo-polyboranes and indicate significant multiple bond character. **Table 2.3.1** shows a comparison of the B-X bond lengths in **2-4** with B-X bond lengths in BX_3 compounds, where significant π-backbonding is known to exist, and B-X bonds on Lewis acid-base adducts which lack the unhybridized p-orbital necessary for backbonding. As expected, the B-X bonds on sp^2 hybridized boron atoms are shorter than those on sp^3 hybridized boron atoms. The B-X bonds in compounds **2-4** are intermediate between the two extremes, but in each case much more closely resemble the lengths in sp^2 hybridized compounds, suggesting strong X to B, π-backbonding.

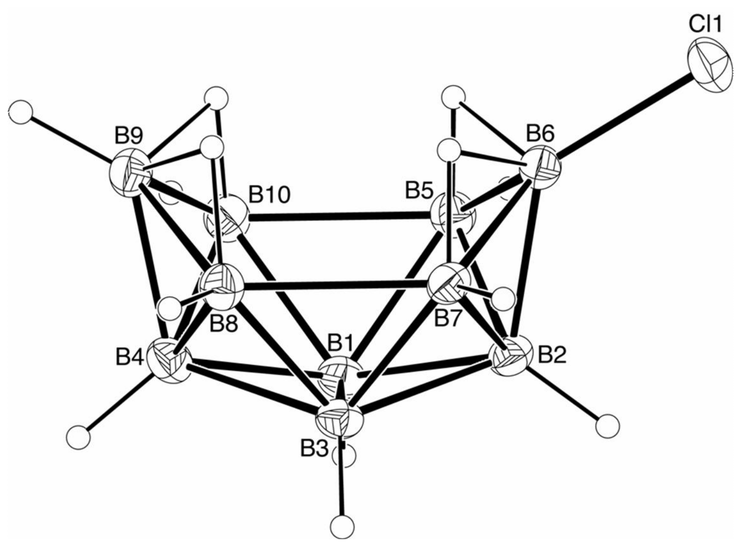

Figure 2.3.1. The crystallographically determined structure of **2**. Selected bond lengths (Å) and bond angles (º): B6-Cl, 1.764(2); B5-B6, 1.797(2); B6-B7, 1.786(2) ; B7-B8, 1.992(2) ; B8-B9, 1.792(2) ; B9-B10, 1.794(2); B10-B5, 1.987(2): B6-B2, 1.723(2); B9-B4, 1.729(2); Cl-B6-B2, 130.81(11); B7-B6-B5, 105.80(11); B8-B9-B10, 104.94(11).

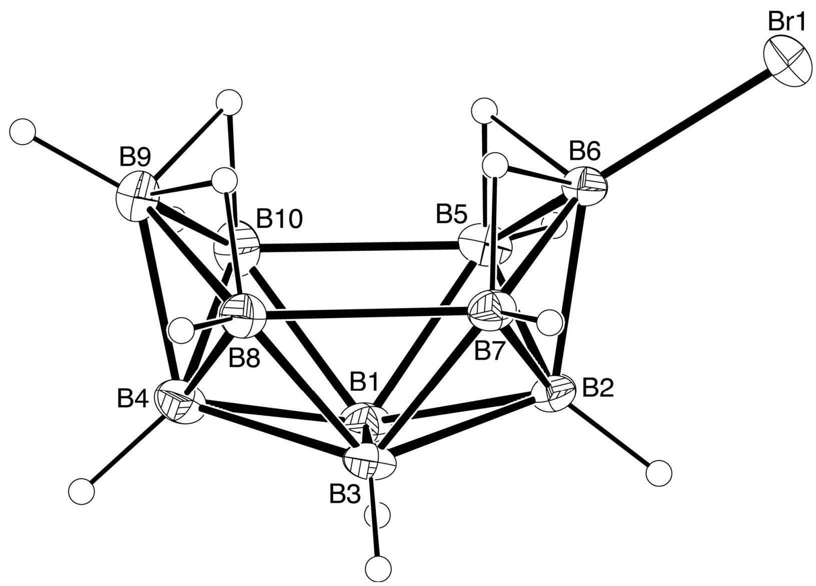

Figure 2.3.2. The crystallographically determined structure of **3**. Selected bond lengths (Å) and bond angles (º): B6-Br, 1.929(4); B5-B6, 1.789(5); B6-B7, 1.783(5); B7-B8, 2.000(5); B8-B9, 1.792(5); B9-B10, 1.795(5); B10-B5, 1.994(6); B6-B2, 1.710(5); B9-B4, 1.716(6); Br-B6-B2, 130.7(2); B7-B6-B5, 106.1(3); B8-B9-B10, 105.7(3).

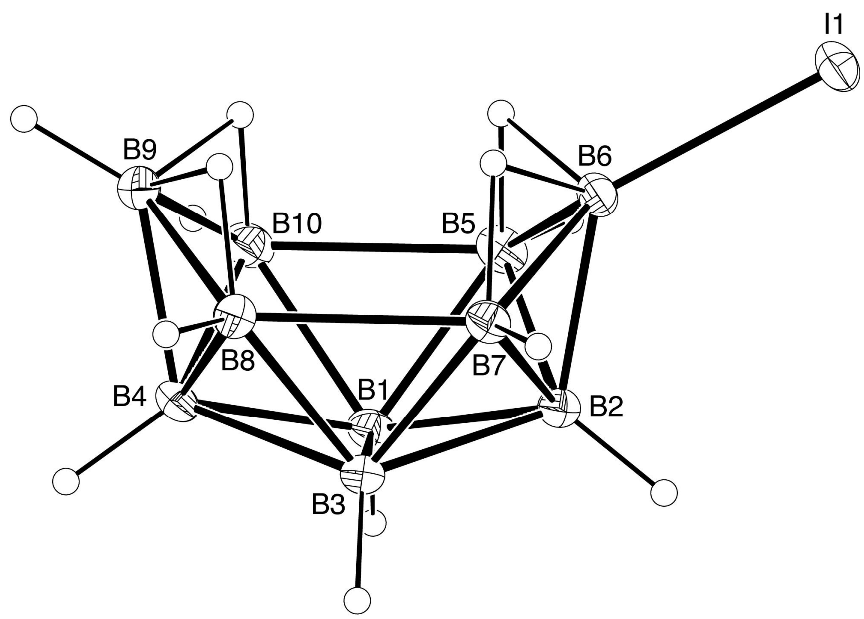

Figure 2.3.3. The crystallographically determined structure of **4**. Selected bond lengths (Å) and bond angles (º): B6-I, 2.143(3); B5-B6, 1.789(5); B6-B7, 1.791(5); B7-B8, 1.984(5); B8-B9, 1.791(5); B9-B10, 1.793(5); B10-B5, 1.981(5); B6-B2, 1.723(4); B9-B4, 1.722(5); I-B6-B2, 128.7(2); B7-B6-B5, 105.5(2); B8-B9-B10, 105.2(2).

Table 2.3.1. A comparison of boron-halogen bond lengths for compounds **2-4** with sp^2 and sp^3 hybridized B-X bonds. For: X = Cl, E = NH_3; X = Br, E = P(n-propyl)$_3$; X = I, E = $P(C_2H_3)_3$.

	Cl	Br	I
6-X-$B_{10}H_{13}$	1.764(2)	1.929(4)	2.143(3)
BX_3	1.75(2)[24]	1.8985(5)[25]	2.1251(3)[26]
E-BX_3	1.837 (avg)[27]	2.009(3)[28]	2.228 (avg)[29]

2.3.2 Triflic-acid Based Synthesis and Characterization of 6-X-$B_{10}H_{13}$

The previously unknown final compound of the series, 6-F-$B_{10}H_{13}$ (**1**), could not be synthesized by a similar ionic liquid route, as the combination of AlF_3, BmimF and HF does not form a superacidic ionic liquid. Instead, the synthesis of **1** was achieved by the dropwise addition of triflic acid (0.69 mL, 7.76 mmol) to a rapidly stirred suspension of 0.30 g (1.94 mmol) of $(NH_4^+)_2B_{10}H_{10}^{2-}$ and 1-fluoropentane (0.44 mL, 3.88 mmol) in 25 mL of pentane, followed by 3 h reaction at room temperature. Filtration of the reaction mixture, solvent evaporation at -20 ^{o}C, and sublimation of the remaining residue **1** in 77% yield.

The ^{11}B (**Figure 2.3.4**) and ^{1}H NMR spectra of **1** exhibit the characteristic patterns observed for **2**-**4**. Specifically, the ^{11}B spectrum resembles the 1:1:2:2:2:1:1 peak pattern seen in the spectrum of **2**. The low field shift (20.7 ppm) of the singlet resonance of the fluoride-substituted B6-boron is consistent with the trend observed in **2-4** where the B6 resonance shifts to progressively lower field as the electronegativity of the halogen increases (**2**, 18.2 ppm; **3**, 10.8 ppm; **4,** -5.6 ppm).[7] The DFT/GIAO calculated ^{11}B chemical shifts for **1** are in excellent agreement with the experimental values (**Figure 2.3.4**, caption).

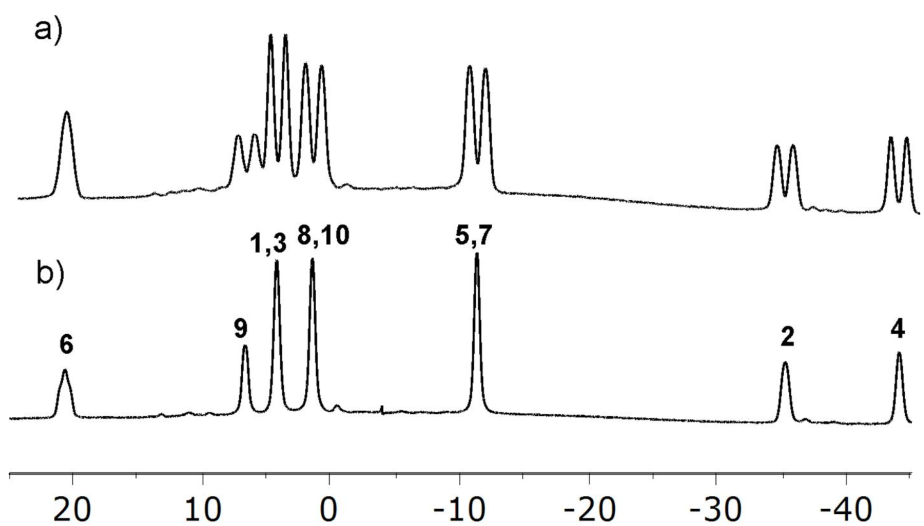

Figure 2.3.4. [11]B NMR spectra (128.4 MHz, $CDCl_3$) of **1** (a) [1]H-coupled and (b) [1]H-decoupled. Assignments and chemical shifts (exp./calc. ppm): B6 (20.7/18.7), B9 (6.7/3.5), B1,3 (4.2/6.2), B8,10 (2.1/1.5), B5,7 (-11.3/-11.7), B2 (-35.3/-37.1), B4 (-44.2/-45.7). DFT/GIAO calculations were performed at the B3LYP/311G* level.

A single-crystal x-ray determination of a twinned crystal of **1** (**Figure 2.3.5**) confirmed the proposed structure, but because of disorder the bond-distances are averaged and cannot be used for comparisons. Nevertheless, the calculated value for the B-F bond length (1.337 Å) in the DFT optimized geometry is closer to that of BF_3 (1.313(1) Å)[29] than BF_4^- (1.386(2) Å)[30] again suggesting strong multiple bond character.

An analogous 2 h reaction of $(NH_4^+)_2B_{10}H_{10}^{2-}$ with triflic acid in CH_2Cl_2 also gave excellent yields (92%) of **2**. Reactions with CH_2Br_2 and CH_2I_2 likewise produced **3** and **4**, but owing to the low volatility of CH_2Br_2 and CH_2I_2 and the corresponding R-OTf byproducts, product isolation was difficult making these reactions less useful than their ionic-liquid based syntheses.

a.

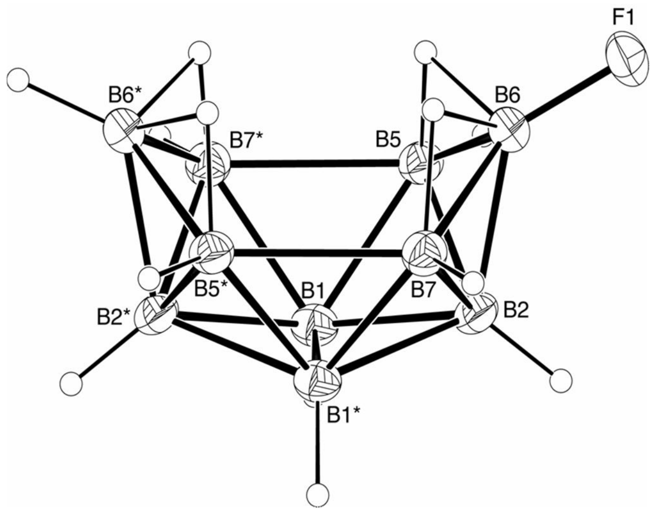

b.

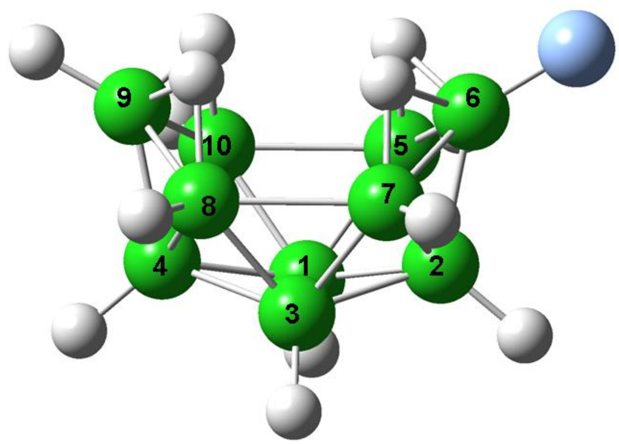

Figure 2.3.5. (a) An ORTEP drawing showing one of the two independent molecules in the crystallographically determined structure of **1**. (b) DFT optimized (B3LYP/6-311G*) geometry of **1**. Selected bond lengths (Å) and bond angles (°): B6-F, 1.338; B5-B6, 1.795; B6-B7, 1.795; B7-B8, 1.997; B8-B9, 1.796; B9-B10, 1.796; B10-B5, 1.997; B6-B2, 1.714; B9-B4, 1.720; F-B6-B2, 132.9; B7-B6-B5, 105.8; B8-B9-B10, 104.8.

2.3.3 Is Hawthorne's Cage-Opening Mechanism Valid?

When initially reporting the triflic acid-induced cage opening of *closo*-$B_{10}H_{10}^{2-}$ to *nido*-6-R-$B_{10}H_{13}$, Hawthorne postulated that the reaction in **Eq. 2** goes through a pathway wherein *closo*-$B_{10}H_{10}^{2-}$ is triply protonated to form the transient, highly electrophilic $B_{10}H_{13}^{+}$ cationic species, with a lobe of positive-charge localized at the naked B6 vertex (**Eq. 7**).[14] Following the proposed mechanism, this cation can affect electrophilic substitution on aromatics, activate C-H bonds on some alkanes, or add surrounding anions. The distinguishing, and controversial, feature of Hawthorne's proposed mechanism is the decaboranyl cation. In recent, unpublished results, Shore and Meyers reported the syntheses of *closo*-$[1,7,9\text{-}(Me_2S)_3\text{-}B_{12}H_9]^{+}$ and *closo*-$[1,2,10\text{-}(Me_2S)_3\text{-}B_{10}H_7]^{+}$ both as BF_4^{-}salts,[31] but this is the only reported case where borane cages have been shown capable of taking a positive charge. Aside from these compounds, cationic polyhedral boranes are unknown. With this in mind, if the cation is formed, it is likely very highly reactive, and able to perform energetically challenging tasks such as C-H activation.

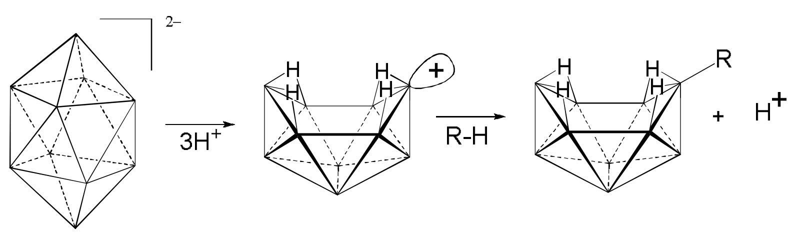

(**7**)

This mechanism can be used to explain the abstraction of F^{-} from fluoroalkanes in the synthesis of **1**. The reaction of *closo*-$B_{10}H_{10}^{2-}$ with triflic acid in cyclohexane led to C-H activation and addition of the cyclohexyl ring to B6 (**Eq. 3**),[20] but when presented with the electron-rich fluoride in 1-fluoropentane the electrophilic intermediate might activate the C-F bond, adding the electron rich fluorine at B6 (**Eq. 8**).

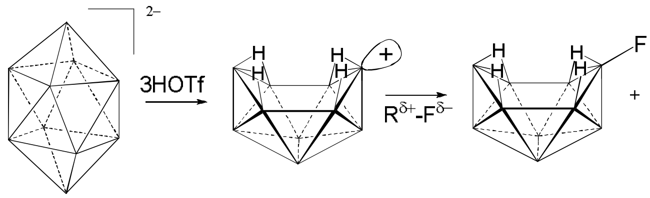

(**8**)

The DFT-calculated LUMO of the $B_{10}H_{13}^{+}$ cation is centered at B6 (**Figure 2.3.6**), positioned for regiospecific electrophilic attack, consistent with Hawthorne's mechanism. However, efforts to computationally identify relevant steps along the mechanistic pathway, from the protonated *closo*-structure to the cationic *nido*-structure, were unsuccessful.

A result inconsistent with Hawthorne's mechanism was also found in the reaction of *closo*-$B_{10}H_{10}^{2-}$ with triflic acid in the presence of non-fluorinated haloalkanes. When the cage-opening reaction was run using ethylbromide as solvent, a mixture of two products was formed (**Eq. 9**).

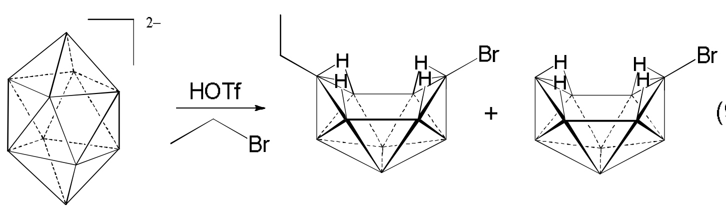

(**9**)

As expected, **3** was identified in the reaction mixture, but along with this was found 6-Br-9-(C_2H_5)-$B_{10}H_{12}$ (**5**) with a ratio of ~ 1:3 (**3**:**5**). The identity **5** was confirmed by ^{11}B (**Figure 2.3.7**) and ^{1}H NMR as well as high-resolution mass spec. The 1:1:2:2:2:1:1 ratio of peaks is seen in other 6-substituted compounds (for example: **1**, **Figure 2.3.4**) and is indicative of the same (C_s) symmetry. The existence of the two low-field singlets supports the assignment as a 6,9-asymetrically substituted decaborane compound. The same reaction run with ethyliodide as solvent yielded a ~ 2:3 mixture of **3**:6-I-9-(C_2H_5)-$B_{10}H_{12}$ (**6**). The crystallographic determination of the strructure of **6** (**Figure 2.3.8**) confirmed the proposed structure.

The reaction to form compounds **5** and **6,** where non-hydrogen substituents are added to two positions of the product decaborane, is not explained by Hawthorne's mechanism. The cationic intermediate, formed through triple protonation, is unable to add 2 separate groups at vertices on opposite sides of the compound. Instead, the formation of **5** and **6** suggests a route where C-X is broken with both fragments (alkyl and halide) being added at once as part of the cage-opening process. A mechanism such as this, where the two electrons from the C-X bond are part of the *closo* to *nido* transformation not only avoids exotic cationic species, but also conforms to Wade's electron counting rules.[32]

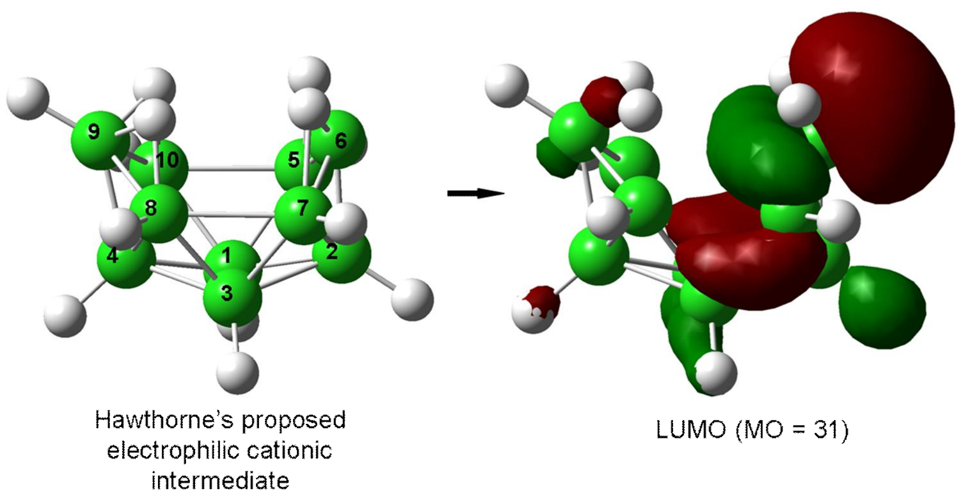

Figure 2.3.6. The structure and visualized LUMO of Hawthorne's $B_{10}H_{13}^{+}$ electrophilic intermediate.[20]

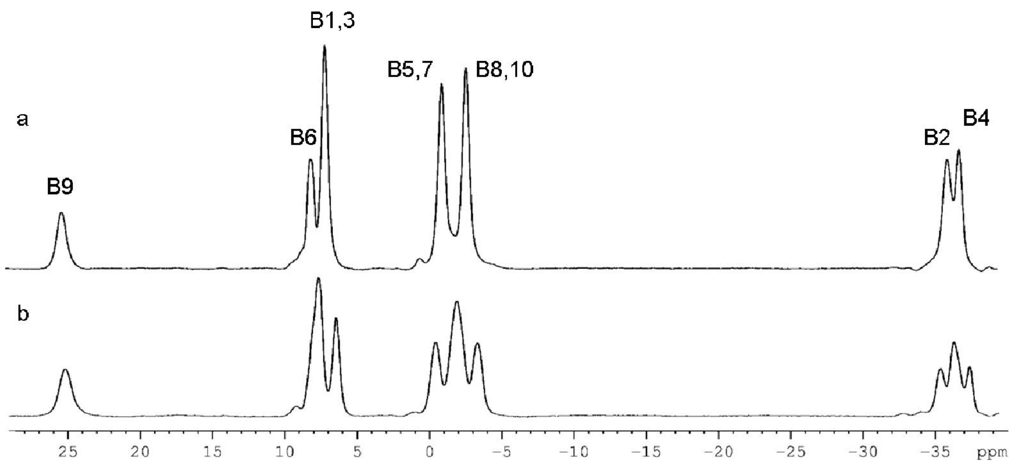

Figure 2.3.7. (a) $^{11}B\{^{1}H\}$ NMR and (b) ^{11}B NMR spectra of 6-Br-9-C_2H_5-$B_{10}H_{12}$ (**5**). Peak assignments were confirmed with ^{11}B-^{11}B COSY 2D NMR.

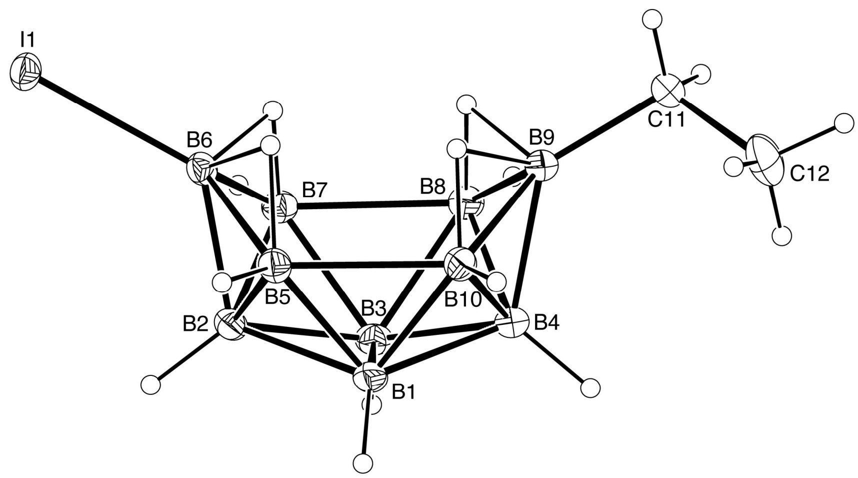

Figure 2.3.8. An ORTEP drawing of the crystallographically determined structure of **6**. Selected bond lengths (Å) and bond angles (º): B6-I, 2.156(2); B5-B6, 1.794(3); B10-B5, 1.978(3); B9-B10, 1.815(3); C11-B9, 1.581(3); B6-B2, 1.720(3); B9-B4, 1.743(3); B5-B1, 1.749(3); B10-B1, 1.755(3); I-B6-B2, 129.57(14); C11-B9-B4, 131.8(2); B7-B6-B5, 105.3(2); B8-B9-B10, 103.5(2); B6-B5-B10, 116.7(2); B9-B10-B5, 117.6(2).

2.4. Conclusions

This chapter has reported the high yield, selective syntheses of 6-halogenated decaboranes **1-4**. Easy accessibility to these molecules should now allow for extensive investigations of their chemistry and possible applications in polyborane and carborane transformations. A number of possible pathways for the functionalization of the B-X bond are possible. Likewise, the application of super-acidic ionic liquids to affect cage-opening reactions, like those previously found to occur with triflic acid, indicates the generality of cage-opening reactions of *closo*-$B_{10}H_{10}^{2-}$ with very strong acids. Many new decaborane derivatives are potentially available through the use of strongly acidic conditions.

The mechanism of the cage opening reaction was explored computationally but, at the current time, is still unknown. Reactions which yield products substituted with both alkyl- and halo-portions of alkylhalides cast doubt on Hawthorne's proposed mechanism, and its exotic cationic intermediate. The actual process by which *closo*-$B_{10}H_{10}^{2-}$ is protonated, before accepting the two electrons necessary to go from *closo*- to *nido*-, is an interesting problem worthy of further investigation.

With these methods for the selective synthesis of the 6-substituted compounds now in hand, the next chapter will describe their use as starting materials for the high-yield syntheses of the 5-halogenated isomers.

2.5 References.

1. (a) Severyugina, Y.; Julius, R. L.; Hawthorne, M. F. *Inorg. Chem.* **2010**, *49*, 10627-10634. (b) Himmelspach, A.; Finze, M. *Eur. J. Inorg. Chem.* **2010**, *13*, 2012-2024. (c) Zheng, Z.; Jiang, W.; Zinn, A. A.; Knobler, C. B.; Hawthorne, M. F. *Inorg. Chem.* **1995**, *34*, 2095-2100. (d) Beletskaya, I. P.; Bregadze, V. I.; Ivushkin, V. A.; Zhigareva, G. G.; Petrovskii, P. V.; Sivaev, I. B. *Russ. J. Org. Chem.* **2005**, *41*, 1359-1366. (e) Eriksson, L.; Beletskaya, I. P.; Bregadze, V. I.; Sivaev, I. B.; Sjoberg, S. *J. of Organomet. Chem.* **2002**, *657*, 267-272. (f) Franken, A.; Kilner, C. A.; Thornton-Pett, M.; Kennedy, J. D. *J. Organomet. Chem.* **2002**, *657*, 176-179. (g) Jiang, W.; Harwell, D. E.; Mortimer, M. D.; Knobler, C. B.; Hawthorne, M. F. *Inorg. Chem.* **1996**, *35*, 4355-4359. (h) Li, J.; Logan, C. F.; Jones Jr., M. *Inorg. Chem.* **1991**, *30*, 4866-8.

2. Butterick III, R.; Carroll, P. J.; Sneddon, L. G. *Organometallics* **2008**, *27*, 4419-4427. (b) Beletskaya, I. P.; Bregadze, V. I.; Ivushkin, V. A.; Petrovskii, P. V.; Sivaev, I. B.; Sjoeberg, S.; Zhigareva, G. G. *J .Organomet. Chem.* **2004**, *689*, 2920-2929. (c) Malaba, D.; Sabat, M.; Grimes, R. N. *Eur. J. Inorg. Chem.* **2001**, *10*, 2557-2562.

3. (a) Cohen, M. S. U.S. Patent 3,106,446, 1963. (b) Wunz, P. R. U.S. Patent 3,046,086, 1962. (c) Clark, S. L.; Fidler, D. A. U.S. Patent 3,010,783, 1961. (d) Cohen, M. S.; Pearl, C. E. U.S. Patent 2,990,239, 1961. (e) Hillman, M.; Mangold, D. J. *Inorg. Chem*. **1965**, *4*, 1356-1357. (f) Williams R. E.; Pier, E. *Inorg. Chem.* **1965**, *9*, 1357-1358. (g) Sequiera, A.; Hamilton, W. C. *Inorg. Chem.* **1967**, *6*, 1281-1286.

4. (a) Stock, A. *Hydrides of Boron and Silicon*; Cornell University Press: Ithaca, NY, 1933. (b) Hillman, M. *J. Am. Chem. Soc.* 1960, *82*, 1096-1099.

5. (a) Plešek J.; Štíbr B.; Heřmánek S. *Coll. Czech. Chem.Comm.* **1966**, *31*, 4744-4745. (b) Štíbr B.; Plešek J.; Heřmánek S. *Coll. Czech. Chem.Comm.* **1969**, *34*, 194-205.

6. Stuchlík, J.; Plešek J.; Heřmánek S.; Štíbr B. *Coll. Czech. Chem. Comm.* **1970**, *35*, 339-343.

7. Sprecher R. F.; Aufderheide, B. E.; Luther III, G. W.; Carter J. C. *J. Am. Chem. Soc.* **1974**, *96*, 4404-4410.

8. Hughes, R. L.; Smith, I. C.; Lawless, E. W. in *Production of Boranes and Related Research*; Holzmann, R. T.; Academic Press: New York, NY, 1967; pp 102-114.

9. Bonnetot, B.; Miele, P.; Naofal, D.; Mongeot, H. *Coll. Czech. Chem. Comm.* **1997**, *62*, 1273-1278.

10. Mongeot, H.; Atchekazi, J.; Bottentot, B.; Colombier, M. *Bull. Soc. Chim. Fr.* **1987**, 75-77.

11. Makhlouf, J. M.; Hough, W. V.; Hefferan, G. T. *Inorg. Chem.* **1967**, *6*, 1196-1198.

12. (a) Colombier, M.; Atchekazï, J.; Mongeot, H. *Inorg. Chim. Acta.* **1985**, *115*, 11-16. (b) Mongeot, T.; Bonnetot, B.; Atchekzai, J.; Colombier, M.; Vigot-Vieillard, C. *Bull. Soc. Chim. Fr.* **1986**, 385-389.

13. CrystalClear: Rigaku Corporation, 1999.

14. CrystalStructure: Crystal Structure Analysis Package

15. REQAB4: Jacobsen, R. A. 1994.

16. *SIR97*: Altomare, A.; Burla, M. C.; Camalli, M.; Cascarano, M.; Giacovazzo, C.; Guagliardi, A.; Moliterni, A.; Polidori, G. J.; Spagna, R. *J. Appl. Cryst.* **1999**, *32*, 115-119.

17. Sheldrick, G. M. *SHELXL-97*: Program for the Refinement of Crystal Structures; University of Göttingen: Germany, 1997.

18. Frisch, M. J.; Trucks, G. W.; Schlegel, H. B.; Scuseria, G. E.; Robb, M. A.; Cheeseman, J. R.; Montgomery, J. A., Jr.; Vreven, T; Kudin, K. N.; Burant, J. C.; Millam, J. M.; Iyengar, S. S.; Tomasi, J.; Barone, V.; Mennucci, B.; Cossi, M.; Scalmani, G.; Rega, N.; Petersson, G. A.; Nakatsuji, H.; Hada, M.; Ehara, M.; Toyota, K.; Fukuda, R.; Hasegawa, J.; Ishida, M.; Nakajima, T.; Honda, Y.; Kitao, O.; Nakai, H.; Klene, M.; Li, X.; Knox, J. E.; Hratchian, H. P.; Cross, J. B.; Adamo, C.; Jaramillo, J.; Gomperts, R.; Stratmann, R. E.; Yazyev, O.; Austin, A. J.; Cammi, R.; Pomelli, C.; Ochterski, J. W.; Ayala, P. Y.; Morokuma, K.; Voth, G. A.; Salvador, P.; Dannenberg, J. J.; Zakrzewski, V. G.; Dapprich, S.; Daniels, A. D.; Strain, M. C.; Farkas, O.; Malick, D. K.; Rabuck, A. D.; Raghavachari, K.; Foresman, J. B.; Ortiz, J. V.; Cui, Q.; Baboul, A. G.; Clifford, S.; Cioslowski, J.; Stefanov, B. B.; Liu, G.; Liashenko, A.; Piskorz, P.; Komaromi, I.; Martin, R. L.; Fox, D. J.; Keith, T.; Al-Laham, M. A.; Peng, C. Y.;Nanayakkara, A.; Challacombe, M.; Gill, P. M. W.; Johnson, B.; Chen, W.; Wong, M. W.; Gonzalez, C.; Pople, J. A. *Gaussian 03*, revision B.05; Gaussian, Inc.: Pittsburgh PA, 2003.

19. Marshall, M. D.; Hunt, R. M.; Hefferan, G. T.; Adams, R. M.; Makhlouf. J. M. *J. Am Chem. Soc.* **1967**, *89*, 3361-3362.

20. Hawthorne, M. F.; Mavunkal, I. J.; Knobler, C. B. *J. Am. Chem. Soc.* **1992**, *114*, 4427-4429.

21. Naoufal, D.; Kodieh, M.; Cornu, D.; Miele, P. *J. Organomet. Chem.* **2005**, *690*, 2787-2789.

22. Smith, G. P.; Dworkin, A. S.; Pagni, R. M.; Zingg, S. P. *J. Am. Chem. Soc.* **1989**, *111*, 525-530.

23. King, D.; Mantz, R.; Osteryoung, R. *J. Am. Chem. Soc.* 1996, *118*, 11933-11938.

24. Atoji, M.; Lipscomb, W. N. *J. Phys. Chem.* 1957, *27*, 195.

35. Konaka, S.; Ito, T.; Morino, Y. *Bull. Chem. Soc. Japan* 1966, *39*, 1146-1154.

26. Krossing, I.; Bihlmeier, A.; Raabe, I.; Trapp, N. *Angew. Chem.* **2003**, *115*, 1569-1572.

27. Avent, A. G.; Hitchcock, P B.; Lappert, M. F.; Liu, D.; Mignani, G.; Richard, C.; Roche, E. *J. Chem. Soc. Chem. Comm.* **1995,** 855-856.

28. Aubauer, C.; Davidge, K.; Klapotke, T.; Mayer, P.; Piotrowski, H.; Schulz, A. *Z. Anorg. Allg. Chem.* **2000**, *626*, 2373-2378.

28. Monkowius, U.; Nogai, S.; Schmidbaur, H. *Dalton Trans.* **2003**, 987-991.

29. Kuchitsu, K.; Konaka, S. *J. Chem. Phys.* **1966**, *45*, 4342-4347.

30. Brunton, G. *Acta Cryst.* **1968**, *B24*, 1703-1704.

31. Hamilton, E. J.; Leung, H. T.; Kultyshev, R. G.; Shore, S. G.; Chen, X.; Meyers, E. A. *Abstracts of Papers*, 239th ACS National Meeting, San Francisco, CA, March 21-25, 2010; American Chemical Society: Washington, D. C. INOR-121.

32. Wade, K. *Chem. Comm.* **1971**, 792-793.

Chapter 3

Efficient Syntheses of 5-X-$B_{10}H_{13}$ Halodecaboranes via the Photochemical (X = I) and/or Base-Catalyzed (X = Cl, Br, I) Isomerization Reactions of 6-X-$B_{10}H_{13}$

Abstract

High yield syntheses of the 5-X-$B_{10}H_{13}$ (**5X**) halodecaboranes have been achieved through the photochemical (X = I) or base-catalyzed (X = Cl, Br, I) isomerization reactions of their 6-X-$B_{10}H_{13}$ (**6X**) isomers. **5I** was obtained in 80% isolated yield upon the UV photolysis of **6I**. Treatment of **6X** (X = Cl, Br, I) with catalytic amounts of triethylamine at 60 ^{o}C led to the formation of 78:22 (Cl), 82:18 (Br) and 86:14 (I) ratio **5X**:**6X** equilibrium mixtures. The **5X** isomers were then separated from these mixtures by selective crystallization (Br and I) or column chromatography (Cl), with the supernatant mixtures in each case then subjected to another round of isomerization/separation to harvest a second crop of **5X**. The combined isolated yields of pure products after two cycles were 71% 5-Cl-$B_{10}H_{13}$, 83% 5-Br-$B_{10}H_{13}$ and 68% 5-I-$B_{10}H_{13}$. The previously proposed structures of 5-Br-$B_{10}H_{13}$ and 5-I-$B_{10}H_{13}$ were crystallographically confirmed. Deprotonation of **6X** and **5X** with bis(dimethylamino)naphthalene (PS) resulted in the formation of [PSH^+][**6X$^-$**] and [PSH^+][**5X$^-$**]. DFT/GIAO calculations and crystallographic determinations of [PSH^+][**6Cl$^-$**] and [PSH^+][**6Cl$^-$**] confirmed bridge-deprotonation at a site adjacent to the

halogen-substituted borons. NMR studies of the 6-Br-$B_{10}H_{13}$ isomerization induced by stoichiometric amounts of PS showed that following initial deprotonation to form 6-Br-$B_{10}H_{12}^{-}$, isomerization occurred at 60 °C to form an equilibrium mixture of 6-Br-$B_{10}H_{12}^{-}$ and 5-Br-$B_{10}H_{12}^{-}$. DFT calculations also showed that the observed 5-X-$B_{10}H_{13}$/6-X-$B_{10}H_{13}$ equilibrium ratios in the triethylamine-catalyzed reactions were consistent with the energetic differences of the 5-X-$B_{10}H_{12}^{-}$ and 6-X-$B_{10}H_{12}^{-}$ anions. These results strongly support a mechanistic pathway for the base-catalyzed **6X** to **5X** conversions involving the formation and subsequent isomerizations of the **6X**$^{-}$ anions. While triethylamine did not catalyze the isomerization reactions of either 6-(C_6H_{13})-$B_{10}H_{13}$ or 6,9-$(C_6H_{13})_2$-$B_{10}H_{12}$, it catalyzed the isomerization of 6-X-9-(C_6H_{13})-$B_{10}H_{12}$ to 5-X-9-(C_6H_{13})-$B_{10}H_{12}$ resulting from halo, but not alkyl rearrangement.

3.1 Introduction

Decaborane ($B_{10}H_{14}$) is the most widely available neutral polyborane and is a key starting material for the production of numerous polyborane compounds having applications in fields ranging from materials to medicine.[1,2] The incorporation of decaborane into a wider range of more complex molecules with tuned properties will depend upon the development of new efficient methods for its selective functionalization. **Chapter 2** detailed the syntheses of 6-X-$B_{10}H_{13}$ (**6X**) (X = F, Cl, Br, I)[3] halodecaboranes by the cage-opening reactions of *closo*-$B_{10}H_{10}^{2-}$ salts. Since *closo*-$B_{10}H_{10}^{2-}$ can be prepared through the pyrolysis of borohydrides,[4] rather than from the hazardous diborane pyrolysis generally employed for the synthesis of the parent decaborane, halodecaboranes prepared by this route could prove attractive alternative starting materials for decaborane-based syntheses.

The 5-X-$B_{10}H_{13}$ (**5X**) (X = Cl, Br, I) halodecaboranes have previously[5,6] been produced in low yields as mixtures with their 6-X-$B_{10}H_{13}$ isomers. For example, the reactions of 6,9-$(Me_2S)_2$-$B_{10}H_{12}$ with anhydrous HCl and HBr yielded 5:95 **5Cl**/**6Cl** and 20:80 **5Br**/**6Br** mixtures in 60% and 96% yields, respectively. Separation of the minor 5-X-$B_{10}H_{13}$ products in these mixtures was then achieved by preparative thin layer chromatography, but isolated yields of the pure products were not reported.[6] An earlier paper reported **5Br** yields of ~30% following column chromatographic separation of a 43:57 ratio **5Br**/**6Br** mixture generated using the same HBr reaction.[7] The reaction of 6,9-$(Me_2S)_2$-$B_{10}H_{12}$ with HI gave a much more favorable, 63:37, **5I**/**6I** ratio, but with only a low 16% total yield of the monoiododecaborane mixture.[6] This chapter reports the simple photochemical and/or base-catalyzed isomerization reactions of 6-X-$B_{10}H_{13}$ that provide the first efficient synthetic routes to the 5-X-$B_{10}H_{13}$ (X = Cl, Br, I) halodecaboranes, making these chiral, functionalized boranes readily available for use in the construction of decaborane-based compounds and materials.

3.2 Experimental

General Synthetic Procedures and Materials. The decaborane-derivatives, 6-F-$B_{10}H_{13}$ (**6F**),[3] 6-Cl-$B_{10}H_{13}$ (**6Cl**),[3] 6-Br-$B_{10}H_{13}$ (**6Br**),[3] 6-I-$B_{10}H_{13}$ (**6I**),[3] 6-(C_6H_{13})-$B_{10}H_{13}$[8] and 6,9-$(C_6H_{13})_2$-$B_{10}H_{12}$[9], were prepared by the literature methods or as described in **Chapter 2**. Tetrabutylammonium chloride (Fluka) was azeotropically dried with toluene and stored in an inert environment. Proton Sponge (1,8-bis(dimethylamino)naphthalene, Aldrich) was sublimed prior to use and stored away from light. Triethylamine and pentane (Fisher) were dried over CaH_2 and distilled prior to use. Dichlorobenzene and chlorobenzene (Fisher) were dried over CaH_2, filtered and stored in a N_2 filled dry box. Toluene was dried by passing through an activated alumina column prior to use. Propylamine, diisopropylethylamine, dibutylsulfide (Aldrich), triphenylphosphine, $PtBr_2$ (Strem), and 1-hexene (Acros) were used as received. All other solvents were used as received unless noted otherwise. Silica gel (Fisher) was pretreated with acetic acid vapors and dried *in vacuo* as described elsewhere.[7]

Physical Methods. ^{11}B NMR at 128.3 MHz and ^{1}H NMR at 400.1 MHz spectra were obtained on a Bruker DMX-400 spectrometer equipped with appropriate decoupling accessories. All ^{11}B chemical shifts are referenced to $BF_3{\cdot}OEt_2$ (0.0 ppm), with a negative sign indicating an upfield shift. All proton chemical shifts were measured relative to internal residual protons from the lock solvents (99.9% $CDCl_3$) and then referenced to $(CH_3)_4Si$ (0.0 ppm). High- and low-resolution mass spectra employing chemical ionization with negative ion detection were obtained on a Micromass AutoSpec high-resolution mass spectrometer. IR spectra were obtained on a Perkin-Elmer Spectrum 100 FT-IR spectrometer. Melting points were determined using a standard melting point apparatus and are uncorrected. Ultraviolet irradiation was performed with a water-cooled 450 W medium-pressure Hanovia lamp.

Photolytic Reactions

5-I-$B_{10}H_{13}$. In a N_2 filled dry-box, **6I** (30.0 mg, 0.12 mmol) was dissolved in dry, degassed pentane (3 mL) in a 10 mL quartz tube equipped with a stirbar and Schlenk adapter. The stirred, room temperature solution was then subjected to UV-irradiation for

12 h. The solution turned slightly pink and a small amount of white precipitate appeared. Analysis by ^{11}B NMR showed quantitative conversion to **5I**. The solution was filtered, concentrated and the product recrystallized from pentane (2 mL) at -78 °C to give 24 mg (0.10 mmol, 80%) of pure **5I**. For **5I**: mp 56-58 °C (lit. 56.5-57.5 °C).[6] The ^{11}B NMR[6] and IR[10] spectra of **5I** were consistent with those previously reported. $^{1}H\{^{11}B\}$ NMR (400.1 MHz, $CDCl_3$): δ 4.18 (s, 1H), 4.08 (s, 1H), 4.01 (s, 1H), 3.51 (s, 2H), 3.37 (s, 1H), 3.17 (s, 1H), 1.25 (s, 1H), 0.83 (s, 1H), -0.39 (s, 1H), -1.50 (s, 2H), -1.92 (s, 1H).

Photolysis of 6Br and 6Cl. No isomerization was observed by ^{11}B NMR when separate solutions of **6Br** (30 mg, 0.15 mmol) and **6Cl** (30 mg, 0.19 mmol) in dry, degassed pentane (3 mL) were UV-irradiated for 24 h.

Base-Catalyzed Reactions

5-I-$B_{10}H_{13}$ (5I). A 100 mL round bottom flask equipped with a side arm and stirbar was charged with **6I** (785 mg, 3.16 mmol) and dry toluene (20 mL) under dry N_2 on a Schlenk line. The solution was rapidly stirred while triethylamine (8 µL, 0.06 mmol, 3 mol%) was added. The flask was sealed and the solution stirred at 60 °C for 4 h at which point ^{11}B NMR analysis showed 86% conversion to **5I**. The solution was cooled at 0 °C while the toluene was removed *in vacuo*. The addition of hexanes (20 mL) to the remaining material caused the separation of a yellow oil from the hexanes layer. The yellow oil was washed 2 times with hexanes (10 mL). The hexanes layers were collected, filtered and concentrated to give a yellowish solid (704 mg). This solid was recrystallized twice from hexanes (5 mL) at -40 °C to give pure **5I** (468 mg, 1.89 mmol) as a pale yellow solid. The supernatant solution from the crystallization, which was shown by ^{11}B NMR analysis to contain a mixture of **5I** and **6I**, was held at 0 °C and concentrated *in vacuo*. The resulting yellow solid was dissolved in dry toluene (10 mL) and subjected to a second isomerization by reaction with triethylamine (3-4 μL, 0.02 mmol) at 60 °C for 12 h. Workup as described above yielded a second crop of **5I** (70 mg, 0.28 mmol). The total yield of the pure pale yellow solid **5I**, isolated after 2 isomerizations was 538 mg (2.33 mmol, 68%).

An alternative synthesis of **5I** employed a combined TEA-catalyzed/photolytic method. A solution of **6I** (500 mg, 2.02 mmol) in dry toluene (20 mL) was reacted with triethylamine (8 μl, 0.06 mmol, 3%) at 60 ^{o}C for 4 h, and worked up as in the first step of the TEA catalyzed synthesis of **5I** described above to give an initial yield of 309 mg (1.25 mmol) of pure **5I**. The supernatant solution from the recrystallization, which was shown by ^{11}B NMR to be a mixture of **6I** and **5I**, was then transferred to a 50 mL quartz tube and photolyzed for 24 h. An additional crop of **5I** (101 mg, 0.40 mmol) was then collected. The combined yield from the two-step TEA/photolytic reaction was 410 mg (1.65 mmol, 82%) of pure **5I**.

5-Br-$B_{10}H_{13}$ (5Br). Analysis by ^{11}B NMR showed 82% conversion to **5Br** after a solution of **6Br** (400 mg, 2.00 mmol) in dry toluene (20 mL) was reacted with triethylamine (8 μL, 0.06 mmol, 3 mol%) for 6 h at 60 °C. The mixture was cooled at 0 °C while the toluene was removed *in vacuo*. The addition of pentane (20 mL) caused the formation of a small amount of white precipitate. The pentane solution was filtered and concentrated at -20 °C yielding a clear oil. The oil was recrystallized twice from pentane (5.0 mL) at -78 °C yielding **5Br** (232 mg, 1.15 mmol) as a white solid. The supernatant solution from the recrystallization was concentrated at -20 °C. The resulting solid was dissolved in dry toluene (10 mL) and subjected to a second isomerization reaction with triethylamine (~2-3 μL, 0.02 mmol) for 6 h at 60 ^{o}C. Workup and recrystallization as described above yielded a second crop of **5Br** (100 mg, 0.5 mmol). The combined yield of pure **5Br**, mp 46-47 °C (lit. 46-48 °C),[6] from the two isomerization reactions was 332 mg (1.65 mmol, 83%). The ^{11}B NMR[6] and IR[10] spectra of **5Br** were consistent with those previously reported. ^{1}H{^{11}B} NMR (400.1 MHz, $CDCl_3$): δ 4.03 (s, 2H), 3.96 (s, 1H), 3.64 (s, 1H), 3.37 (s, 1H), 3.17 (s, 2H), 1.18 (s, 1H), 0.77 (s, 1H), -0.10 (s, 1H), -1.44 (s, 1H), -1.65 (s, 1H), -1.99 (s, 1H).

5-Cl-$B_{10}H_{13}$ (5Cl). Analysis by ^{11}B NMR showed 78% conversion to **5Cl** after a solution of **6Cl** (242 mg, 1.57 mmol) in dry toluene (10 mL) was reacted with triethylamine (7 μL, 0.05 mmol, 3%) for 12 h at 60 °C. The solution was cooled at 0 °C while the toluene was removed *in vacuo*. After the remaining yellow oil was dissolved in a minimal amount of a 2%-CH_2Cl_2 in hexanes solution, it was chromatographed on a column containing acetic-acid treated silica gel with a 2%-CH_2Cl_2/hexanes eluent. Fractions containing only **5Cl**, as determined by ^{11}B NMR, were collected and concentrated *in vacuo* at -20 °C, yielding white solid **5Cl** (109 mg, 0.71 mmol, 45 %), which then melted into a clear oil above 0 °C. Other fractions which contained **6Cl** and/or **5Cl/6Cl** were combined and concentrated *in vacuo* at -20 ^{o}C to give 100 mg (0.65 mmol) of a **5Cl/6Cl** mixture. This material was subjected to a second isomerization with triethylamine (~2-3 μL, 0.02 mmol) for 12 h at 60 ^{o}C. Workup and chromatographic separation yielded a second crop of **5Cl** (62 mg, 0.40 mmol). The total combined yield of **5Cl** from both isomerizations was 171 mg (1.11 mmol, 71%). The ^{11}B NMR[6] spectrum of **5Cl** was consistent with that previously reported. ^{1}H{^{11}B} NMR (400.1 MHz, $CDCl_3$): δ 4.03 (s, 1H), 3.92 (s, 2H), 3.71 (s, 1H), 3.30 (s, 1H), 3.09 (s, 2H), 1.14

(s, 1H), 0.72 (s, 1H), 0.03 (s, 1H), -1.45 (s, 1H), -1.78 (s, 1H), -2.05 (s, 1H). IR (KBr, cm^{-1}) 2581 (s), 1890 (w), 1558 (w), 1497 (m), 1438 (w), 1098 (w), 1043 (w), 1012 (w), 992 (w), 960 (m), 923 (s), 880 (m), 851 (m), 808 (m), 777 (m), 740 (w), 710 (m), 654 (w), 623 (w), 599 (w), 573 (w).

Attempted Base-Promoted Isomerization of 6-F-$B_{10}H_{13}$. Analysis by ^{11}B NMR showed no evidence of isomerization after a solution of 6-F-$B_{10}H_{13}$ (150 mg, 1.07 mmol) in dry toluene (10 mL) was reacted with triethylamine (5 μL, 0.03 mmol, 3%) at 60 °C for 4 h. Even after the solution was then stirred for 15 h at 80 °C, only trace (< 2%) isomerization to 5-F-$B_{10}H_{13}$ was observed.

Isomerization of 6I with other Bases. Analysis by ^{11}B NMR of separate reactions of **6I** (200 mg, 0.80 mmol) in dry toluene (10 mL) at 60 °C under N_2 showed: (a) only trace isomerization to **5I** (<3%) after reaction with dibutylsulfide (7 μL, 0.04 mmol, 5%) for 3 days, (b) conversion to a 60:40 **5I**:**6I** mixture after 12 h and a 85:15 **5I**:**6I** mixture after 20 h of reaction with triphenylphosphine (11 mg, 0.04 mmol, 5%), (c) conversion to 86:14 and 85:15 **5I**/**6I** mixtures when reacted with diisopropylethylamine (7 μL, 0.04 mmol, 5%) and propylamine (8 μL, 0.10 mmol, 5%) for 4 h, (d) conversion to a 87:13 **5I**:**6I** mixture when reacted with tetrabutylammonium chloride (42.0 mg, 0.15 mmol, 4 mol%) at 60 °C for 10 h.

TEA-Catalyzed Isomerization of 5I. Analysis by ^{11}B NMR showed the formation of an 86:14 ratio **5I**/**6I** mixture after **5I** (200 mg, 0.80 mmol) was reacted with triethylamine (5 μL, 0.03 mmol, 4%) for 12 h at 60 °C in dry toluene (15 mL).

TEA-Catalyzed Isomerization of 5Br. Analysis by ^{11}B NMR showed the formation of an 83:17 ratio **5Br**/**6Br** mixture after **5Br** (180 mg, 0.90 mmol) was reacted with triethylamine (5 μL, 0.03 mmol, 4%) for 12 h at 60 °C in dry toluene (15 mL).

TEA-Catalyzed Isomerization of 5Cl. Analysis by ^{11}B NMR showed the formation of a 78:22 ratio **5Cl**/**6Cl** mixture after **5Cl** (130 mg, 0.80 mmol) was reacted with triethylamine (5 μL, 0.03 mmol, 4%) for 12 h at 60 °C in dry toluene (10 mL).

Isomerization of 6-Br-$B_{10}H_{12}^-$ (6Br$^-$) to 5-Br-$B_{10}H_{12}^-$ (5Br$^-$). In an N_2 filled dry box, **6Br** (100 mg, 0.49 mmol) was reacted with PS (105 mg, 0.49 mmol) in 4 mL of dry dichlorobenzene to form the soluble [PSH^+][**6Br$^-$**] salt. An aliquot of this solution was transferred to a resealable thick-walled, high-pressure NMR tube, with the isomerization of **6Br$^-$** to **5Br$^-$** then followed by ^{11}B NMR with the NMR probe heated at 60 °C. After 130 min, no further changes in the relative concentrations of the two anions were observed. The tube was opened, cooled at 0 °C and acidified with conc. H_2SO_4 (1 drop). The ^{11}B NMR spectrum of the acidified mixture showed an 81:19 **5Br**/**6Br** ratio.

Attempted Base Isomerizations of 6-(C_6H_{13})-$B_{10}H_{13}$ and 6,9-(C_6H_{13})$_2$-$B_{10}H_{12}$. Analysis by ^{11}B NMR showed that no isomerization had occurred when separate samples of 6-(C_6H_{13})-$B_{10}H_{13}$ (200 mg, 0.97 mmol) and 6,9-(C_6H_{13})$_2$-$B_{10}H_{12}$ (200 mg, 0.69 mmol) were reacted in dry toluene (10 mL) at 60 °C for 12 h with (7 μL, 0.05 mmol, 5%) and (5 μL, 0.03 mmol, 5%) of triethylamine, respectively.

6-X-9-(C_6H_{13})-$B_{10}H_{12}$ (X = Cl, I) Syntheses. A stirred mixture of **6Cl** (115 mg, 0.74), 1-hexene (15 mL), and $PtBr_2$ (13.0 mg, 0.04 mmol) was reacted for 4 days at room temperature under N_2. The 1-hexene was removed *in vacuo* and the resulting oil was dissolved in a minimal amount of hexanes. After purification by column chromatography on acetic acid treated silica gel using a 5%-CH_2Cl_2 in hexanes eluent, the eluent was removed *in vacuo* to give 6-Cl-9-(C_6H_{13})-$B_{10}H_{12}$ as a light-brown oil (97 mg, 0.40 mmol, 53%). For 6-Cl-9-(C_6H_{13})-$B_{10}H_{12}$: HRMS: *m/z* calcd for $^{12}C_6{}^1H_{25}{}^{11}B_{10}{}^{37}Cl$ 244.2545, found 244.2563. ^{11}B NMR (128.3 MHz, $CDCl_3$): δ 25.3 (s, 1B), 16.4 (s, 1B), 6.8 (d, 152, 2B), -1.9 (d, *J* = ~100, 4B), -35.9 (d, *J* = 164, 1B), -37.9 (d, *J* = 148, 1B). $^1H\{^{11}B\}$ NMR (400.1 MHz, $CDCl_3$): δ 3.45 (s, 2H), 2.98 (s, 4H), 1.59 (m, 2H), 1.44 (m, 4H), 1.35 (m, 4H), 1.13 (s, 1H), 0.93 (t, *J* = 6.4, 3H), 0.70 (s, 1H), -0.61 (s, 2H), -1.34 (s, 2H). IR (KBr, cm^{-1}) 2957 (m), 2926 (s), 2857 (m), 2581 (s), 1971 (vw), 1920 (vw), 1869 (vw), 1523 (w), 1466 (m), 1412 (m), 1096 (w), 1058 (w), 1036 (m), 984 (s), 913 (vw), 898 (m), 859 (vw), 828 (w), 721 (w), 703 (w), 676 (w), 594 (vw). .

An analogous reaction of **6I** (300 mg, 1.21 mmol), 1-hexene (15 mL), and $PtBr_2$ (24.0 mg, 0.06 mmol) gave 6-I-9-(C_6H_{13})-$B_{10}H_{12}$ as a light-brown oil (112 mg, 0.34 mmol, 28%). For 6-I-9-(C_6H_{13})-$B_{10}H_{12}$ HRMS: *m/z* calcd for $^{12}C_6{}^1H_{25}{}^{11}B_{10}{}^{127}I$ 334.1931, found 334.1948. ^{11}B NMR (128.3 MHz, $CDCl_3$): δ 26.5 (s, 1B), 9.4 (d, *J* = 147, 2B), 2.4 (d, *J* = 162, 2B), -2.5 (d, *J* = 148, 2B), -8.0 (s, 1B), -35.0 (d, *J* = 150, 1B), -36.2 (d, *J* = 154, 1B). $^1H\{^{11}B\}$ NMR (400.1 MHz, $CDCl_3$): δ 3.60 (s, 2H), 3.26 (s, 2H), 2.96 (s, 2H), 1.59 (m, 2H), 1.40 (m, 4H), 1.34 (m, 4H), 1.14 (s, 2H), 0.93 (t, *J* = 6.6, 3H), -0.76 (s, 2H), -1.54 (s, 2H). IR (KBr, cm^{-1}) 2957 (m), 2926 (s), 2856 (m), 2579 (s), 1965 (vw), 1906 (vw), 1865 (vw), 1520 (w), 1463 (m), 1455 (m), 1411 (m), 1262 (vw), 1213 (vw), 1096 (w), 974 (m), 942 (w), 910 (vw), 887 (w), 814 (w), 720 (w), 698 (w), 674 (w), 581 (w).

TEA-Catalyzed Isomerizations of 6-X-9-(C_6H_{13})-$B_{10}H_{12}$ (X = Cl, I). Analysis by ^{11}B NMR showed ~70% conversion to 5-Cl-9-(C_6H_{13})-$B_{10}H_{12}$ after reaction of 6-Cl-9-

(C_6H_{13})-$B_{10}H_{12}$ (92 mg, 0.38 mmol) with triethylamine (3 μL, 0.02 mmol, 5%) in dry toluene (8 mL) under N_2 for 18 h at 60 °C and ~93% conversion to 5-I-9-(C_6H_{13})-$B_{10}H_{12}$ after reaction of 6-I-9-(C_6H_{13})-$B_{10}H_{12}$ (84 mg, 0.25 mmol) with triethylamine (~2 μL, 0.01 mmol, 5%) in dry toluene (6 mL) under N_2 for 4 h at 60 °C. In both cases, the toluene was removed *in vacuo* and the remaining light-brown oil was dissolved in a minimal amount of 2%-CH_2Cl_2 in hexanes. Chromatographic separations on acetic acid treated silica gel with 2%-CH_2Cl_2 in hexanes elution gave 5-Cl-9-(C_6H_{13})-$B_{10}H_{12}$ (40 mg, 0.17 mmol, 43%) and 5-I-9-(C_6H_{13})-$B_{10}H_{12}$ (43 mg, 0.13 mmol, 51%) as a light-brown oils. For 5-Cl-6-(C_6H_{13})-$B_{10}H_{12}$: HRMS *m/z* calcd for $^{12}C_6{}^1H_{25}{}^{11}B_{10}{}^{37}Cl$ 244.2545, found 244.2655. ^{11}B NMR (128.3 MHz, $CDCl_3$): δ 27.1 (s, 1B), 11.5 (s, 1B), 11.5 (d, *J* = ~110, B), 10.2 (d, *J* = 154, 1B), 6.2 (d, *J* = 158, 1B), 0.8 (d, *J* = 145, 1B), -3.7 (d, *J* = ~115, 1B), -4.3 (d, *J* = ~125, 1B), -34.6 (d, *J* = 155, 1B), -37.4 (d, *J* = 159, 1B). $^1H\{^{11}B\}$ NMR (400.1 MHz, $CDCl_3$): δ 3.80 (s, 2H), 3.58 (s, 2H), 3.01 (s, 2H), 2.83 (s, 1H), 1.59 (m, 2H), 1.43 (m, 4H), 1.34 (bm, 4H), 0.92 (t, *J* = 6.1, 3H), 0.86 (s, 1H), 0.12 (s, 1H), -1.00 (s, 1H), -1.59 (s, 1H), -1.68 (s, 1H). IR (KBr, cm^{-1}) 2957 (m), 2927 (s), 2857 (s), 2579 (s), 1963 (bw), 1542 (w), 1466 (m), 1414 (w), 1098 (w), 1033 (vw), 972 (w), 955 (w), 923 (m), 880 (w), 845 (m), 793 (w), 708 (w). For 5-I-6-(C_6H_{13})-$B_{10}H_{12}$: HRMS *m/z* calcd for $^{12}C_6{}^1H_{25}{}^{11}B_{10}{}^{127}I$ 334.1931, found 334.1924. ^{11}B NMR (128.3 MHz, $CDCl_3$): δ 25.9 (s, 1B), 12.3 (d, *J* = 160, 1B), 10.9 (d, *J* = ~165, 1B), 9.0 (d, *J* = 153, 1B), 0.4 (d, *J* = 151, 1B), -0.7 (d, *J* = 144, 1B), -3.7 (d, *J* = 139, 1B), -14.0 (s, 1B), -33.8 (d, *J* = 156, 1B), -37.0 (d, *J* = 159, 1B). $^1H\{^{11}B\}$ NMR (400.1 MHz, $CDCl_3$): δ 4.07 (s, 2H), 3.38 (s, 2H), 3.28 (s, 1H), 2.92 (s, 1H), 1.58 (m, 2H), 1.41 (m, 4H), 1.33 (bm, 4H), 1.28 (s, 1H), 1.08 (s, 1H), 0.92 (t, *J* = 6.4, 3H), -0.28 (s, 1H), -1.03 (s, 1H), -1.44 (s, 2H). IR (KBr, cm^{-1})

2957 (m), 2926 (s), 2856 (m), 2579 (s), 1891 (bw), 1532 (w), 1463 (m), 1411 (w), 1378 (w), 1261 (w), 1213 (vw), 1096 (m), 1008 (w), 962 (w), 972 (w), 908 (m), 866 (w), 827 (m), 806 (w), 787 (w) 704 (m), 640 (w), 603 (w), 569 (w).

Crystallographic Data. Single crystals of **5Br** and **5I** were grown via slow solvent evaporation from heptane at -20 °C. Crystals of [PSH$^+$][**6Cl$^-$**] and [PSH$^+$][**5Cl$^-$**] grew from chlorobenzene solutions at 10 ^{o}C.

Collection and Reduction of the Data. Crystallographic data and structure refinement information are summarized in **Table 3.2.1**. X-ray intensity data for **5Br** (Penn3340), **5I** (Penn3334), [PSH$^+$][**6Cl$^-$**] (Penn3358), and [PSH$^+$][**5Cl$^-$**] (Penn3359) were collected on a Rigaku R-AXIS IIC area detector employing graphite-monochromated Mo-K_α radiation. Indexing was performed from a series of twelve 0.5^o rotation images with exposures of 30 seconds and a 36 mm crystal-to-detector distance. Oscillation images were processed using CrystalClear,[11] producing a list of unaveraged F^2 and $\sigma(F^2)$ values which were then passed to the CrystalStructure[12] program package for further processing and structure solution on a Dell Pentium III computer. The intensity data were corrected for Lorentz and polarization effects and for absorption.

Solution and Refinement of the Structures. The structures were solved by direct methods (SIR97[13]). Refinement was by full-matrix least squares based on F^2 using SHELXL-97.[14] All reflections were used during refinement (values of F^2 that were experimentally negative were replaced with $F^2 = 0$). In the case of **5I**, [PSH$^+$][**6Cl$^-$**], and [PSH$^+$][**5Cl$^-$**] non-hydrogen atoms were refined anisotropically and hydrogen atoms were refined isotropically. In the case of **5Br**, non-hydrogen atoms were refined anisotropically and hydrogen atoms were included as constant contributions to the structure factors and were not refined. The crystallographically determined bond lengths and angles for **5Br**, **5I**, **6Cl⁻** and **5Cl⁻** are given in **Tables 3.2.2-3.2.9**.

Table 3.2.1. Crystallographic data for **5I**, **5Br**, **6Cl⁻** and **5Cl⁻**.

	5I	**5Br**	**[PSH⁺][6Cl⁻]**	**[PSH⁺][5Cl⁻]**
Empirical formula	$B_{10}H_{13}I$	$B_{10}H_{13}Br$	$C_{14}B_{10}H_{31}N_2Cl$	$C_{14}B_{10}H_{31}N_2Cl$
formula weight	248.10	201.11	370.96	370.96
Crystal class	Monoclinic	Orthorhombic	Monoclinic	Monoclinic
space group	$P2_1/c$	$Pca2_1$	$P2_1/c$	$P2_1/n$
Z	4	8	4	4
a, Å	12.803(3)	11.214(7)	9.1706(15)	9.4491(11)
b, Å	7.2932(15)	12.815(14)	23.403(4)	9.9107(9)
c, Å	10.874(2)	13.507(7)	10.1822(17)	23.784(3)
β, deg	92.308(5)		98.755(5)	97.446(3)
V, Å^3	1014.5(4)	1941(3)	2159.8(6)	2208.5(4)
D_{calc}, g/cm^3	1.624	1.376	1.141	1.116
μ, cm^{-1}	30.77	40.15	1.78	1.75
λ, Å (Mo-K$_\alpha$)	0.71073	0.71073	0.71073	0.71073
Crystal size, mm	0.40 x 0.18 x 0.06	0.38 x 0.26 x 0.12	0.35 x 0.30 x 0.06	0.22 x 0.22 x 0.12
F(000)	464	784	784	784
2θ angle, deg	3.18-27.49	2.85-27.48	2.67-25.04	2.68-25.04
temperature, K	160(1)	143(1)	143(1)	143(1)
hkl collected	$-16 \le h \le 14$; $-9 \le k \le 7$; $-14 \le l \le 14$	$-12 \le h \le 14$; $-13 \le k \le 16$; $-17 \le l \le 17$	$-10 \le h \le 10$; $-27 \le k \le 25$; $-12 \le l \le 12$	$-11 \le h \le 11$; $-11 \le k \le 11$; $-28 \le l \le 28$
No. meas reflns	9143	13039	21783	31640
No. of unique reflns	2314 (R_{int}=0.0272)	4389 (R_{int}=0.0224)	3800 (R_{int}=0.0364)	3895 (R_{int}=0.0329)
No. parameters	153	200	369	369
R^a indices (F>2σ)	R_1=0.0354 wR_2=0.0945	R_1=0.0379 wR_2=0.0870	R_1=0.0478 wR_2=0.1238	R_1=0.0479 wR_2=0.1252
R^a indices (all data)	R_1=0.0389 wR_2=0.0962	R_1=0.0446 wR_2=0.0901	R_1=0.0569 wR_2=0.1320	R_1=0.0550 wR_2=0.1320
GOF^b	1.156	1.150	1.054	1.085
final difference peaks, e/Å^3	+0.963, -1.245	+1.135, -1.381	+0.179, -0.381	+0.201, -0.289

$^a R_1 = \Sigma||F_o| - |F_c||/\Sigma|F_o|$; $wR_2 = \{\Sigma w(F_o^2 - F_c^2)^2/\Sigma w(F_o^2)^2\}^{1/2}$

^{b}GOF = $\{\Sigma w(F_o^2 - F_c^2)^2/(n-p)\}^{1/2}$ where n = no. of reflns; p = no. of params refined

Table 3.2.2 Bond lengths in **5Br** (Å).

Br1-B5	1.958(4)	B1-B5	1.728(6)	B1-B10	1.754(6)
B1-B2	1.775(6)	B1-B3	1.784(6)	B1-B4	1.791(7)
B1-H1	1.10	B2-B6	1.724(6)	B2-B3	1.769(6)
B2-B7	1.774(6)	B2-B5	1.778(5)	B2-H2	1.10
B3-B8	1.743(6)	B3-B7	1.754(6)	B3-B4	1.789(7)
B3-H3	1.10	B4-B9	1.729(7)	B4-B10	1.794(6)
B4-B8	1.796(7)	B4-H4	1.10	B5-B6	1.787(6)
B5-B10	1.978(7)	B5-H56	1.18	B6-B7	1.766(6)
B6-H6	0.98	B6-H56	1.20	B6-H67	1.22
B7-B8	1.986(6)	B7-H7	1.10	B7-H67	1.23
B8-B9	1.806(7)	B8-H8	1.10	B8-H89	1.23
B9-B10	1.768(7)	B9-H9	1.07	B9-H89	1.24
B9-H910	1.29	B10-H10	1.10	B10-H910	1.12
Br1'-B5'	1.945(4)	B1'-B5'	1.740(6)	B1'-B10'	1.749(6)
B1'-B3'	1.769(6)	B1'-B4'	1.774(7)	B1'-B2'	1.790(7)
B1'-H1'	1.10	B2'-B6'	1.729(7)	B2'-B3'	1.781(7)
B2'-B5'	1.781(6)	B2'-B7'	1.785(6)	B2'-H2'	1.10
B3'-B8'	1.752(6)	B3'-B7'	1.755(7)	B3'-B4'	1.771(7)
B3'-H3'	1.10	B4'-B9'	1.708(7)	B4'-B10'	1.782(7)
B4'-B8'	1.798(7)	B4'-H4'	1.10	B5'-B6'	1.804(6)
B5'-B10'	1.975(7)	B5'-H56'	1.24	B6'-B7'	1.790(6)
B6'-H6'	1.06	B6'-H56'	1.30	B6'-H67'	1.19
B7'-B8'	1.972(7)	B7'-H7'	1.10	B7'-H67'	1.39
B8'-B9'	1.792(7)	B8'-H8'	1.10	B8'-H89'	1.32
B9'-B10'	1.787(7)	B9'-H9'	1.02	B9'-H89'	1.29
B9'-H910'	1.28	B10'-H10'	1.10	B10'-H910'	1.17

Table 3.2.3 Bond angles in **5Br** (°).

B5-B1-B10	69.2(3)	B5-B1-B2	61.0(2)	B10-B1-B2	117.6(3)
B5-B1-B3	107.5(3)	B10-B1-B3	107.2(3)	B2-B1-B3	59.6(2)
B5-B1-B4	118.1(3)	B10-B1-B4	60.8(3)	B2-B1-B4	114.1(3)
B3-B1-B4	60.1(3)	B5-B1-H1	116.4	B10-B1-H1	116.9
B2-B1-H1	117.6	B3-B1-H1	125.8	B4-B1-H1	117.5
B6-B2-B3	111.3(3)	B6-B2-B7	60.6(3)	B3-B2-B7	59.3(2)
B6-B2-B1	110.8(3)	B3-B2-B1	60.5(2)	B7-B2-B1	106.2(3)
B6-B2-B5	61.3(2)	B3-B2-B5	106.0(3)	B7-B2-B5	104.4(3)
B1-B2-B5	58.2(2)	B6-B2-H2	118.4	B3-B2-H2	121.2
B7-B2-H2	124.0	B1-B2-H2	121.7	B5-B2-H2	124.2
B8-B3-B7	69.2(3)	B8-B3-B2	118.4(3)	B7-B3-B2	60.5(3)
B8-B3-B1	108.1(3)	B7-B3-B1	106.7(3)	B2-B3-B1	59.9(2)
B8-B3-B4	61.1(3)	B7-B3-B4	117.3(3)	B2-B3-B4	114.5(3)
B1-B3-B4	60.1(3)	B8-B3-H3	115.9	B7-B3-H3	117.3
B2-B3-H3	117.4	B1-B3-H3	125.8	B4-B3-H3	117.4
B9-B4-B3	110.0(3)	B9-B4-B1	109.7(3)	B3-B4-B1	59.8(3)
B9-B4-B10	60.2(3)	B3-B4-B10	105.3(3)	B1-B4-B10	58.6(3)
B9-B4-B8	61.6(3)	B3-B4-B8	58.2(2)	B1-B4-B8	105.5(3)
B10-B4-B8	104.8(3)	B9-B4-H4	119.0	B3-B4-H4	122.3
B1-B4-H4	122.1	B10-B4-H4	124.1	B8-B4-H4	123.7
B1-B5-B2	60.8(2)	B1-B5-B6	110.0(3)	B2-B5-B6	57.8(2)
B1-B5-Br1	120.9(3)	B2-B5-Br1	125.6(3)	B6-B5-Br1	120.4(3)
B1-B5-B10	56.0(2)	B2-B5-B10	106.8(3)	B6-B5-B10	116.8(3)
Br1-B5-B10	116.4(2)	B1-B5-H56	130.0	B2-B5-H56	98.0
B6-B5-H56	42.0	Br1-B5-H56	108.4	B10-B5-H56	95.9
B2-B6-B7	61.1(2)	B2-B6-B5	60.8(2)	B7-B6-B5	104.3(3)
B2-B6-H6	130.8	B7-B6-H6	123.0	B5-B6-H6	130.9
B2-B6-H56	99.8	B7-B6-H56	117.9	B5-B6-H56	40.9
H6-B6-H56	113.5	B2-B6-H67	95.9	B7-B6-H67	43.9
B5-B6-H67	102.8	H6-B6-H67	119.5	H56-B6-H67	87.8
B3-B7-B6	110.0(3)	B3-B7-B2	60.2(3)	B6-B7-B2	58.3(2)
B3-B7-B8	55.1(2)	B6-B7-B8	118.6(4)	B2-B7-B8	106.5(3)
B3-B7-H7	140.6	B6-B7-H7	108.4	B2-B7-H7	141.0

B8-B7-H7	111.3	B3-B7-H67	115.2	B6-B7-H67	43.4
B2-B7-H67	93.0	B8-B7-H67	85.8	H7-B7-H67	98.5
B3-B8-B4	60.7(3)	B3-B8-B9	108.6(3)	B4-B8-B9	57.4(3)
B3-B8-B7	55.7(2)	B4-B8-B7	106.2(3)	B9-B8-B7	114.6(3)
B3-B8-H8	139.5	B4-B8-H8	140.2	B9-B8-H8	111.0
B7-B8-H8	112.6	B3-B8-H89	126.8	B4-B8-H89	98.3
B9-B8-H89	43.3	B7-B8-H89	92.0	H8-B8-H89	89.1
B4-B9-B10	61.7(3)	B4-B9-B8	61.0(3)	B10-B9-B8	105.4(3)
B4-B9-H9	132.0	B10-B9-H9	125.7	B8-B9-H9	127.4
B4-B9-H89	101.5	B10-B9-H89	117.6	B8-B9-H89	42.9
H9-B9-H89	109.9	B4-B9-H910	95.6	B10-B9-H910	39.1
B8-B9-H910	109.9	H9-B9-H910	116.9	H89-B9-H910	93.7
B1-B10-B9	109.6(3)	B1-B10-B4	60.6(3)	B9-B10-B4	58.1(3)
B1-B10-B5	54.8(2)	B9-B10-B5	117.0(3)	B4-B10-B5	106.2(3)
B1-B10-H10	140.2	B9-B10-H10	109.4	B4-B10-H10	140.5
B5-B10-H10	112.2	B1-B10-H910	120.1	B9-B10-H910	46.9
B4-B10-H910	99.0	B5-B10-H910	85.7	H10-B10-H910	92.9
B5-H56-B6	97.1	B6-H67-B7	92.7	B8-H89-B9	93.8
B9-H910-B10	93.9	B5'-B1'-B10'	69.0(3)	B5'-B1'-B3'	107.6(3)
B10'-B1'-B3'	107.4(3)	B5'-B1'-B4'	117.7(3)	B10'-B1'-B4'	60.8(3)
B3'-B1'-B4'	60.0(3)	B5'-B1'-B2'	60.6(3)	B10'-B1'-B2'	117.1(3)
B3'-B1'-B2'	60.1(3)	B4'-B1'-B2'	114.1(3)	B5'-B1'-H1'	116.5
B10'-B1'-H1'	117.0	B3'-B1'-H1'	125.5	B4'-B1'-H1'	117.7
B2'-B1'-H1'	117.8	B6'-B2'-B3'	111.1(3)	B6'-B2'-B5'	61.8(2)
B3'-B2'-B5'	105.3(3)	B6'-B2'-B7'	61.2(3)	B3'-B2'-B7'	59.0(2)
B5'-B2'-B7'	105.1(3)	B6'-B2'-B1'	111.0(3)	B3'-B2'-B1'	59.4(3)
B5'-B2'-B1'	58.3(2)	B7'-B2'-B1'	105.5(3)	B6'-B2'-H2'	117.9
B3'-B2'-H2'	122.0	B5'-B2'-H2'	123.9	B7'-B2'-H2'	123.7
B1'-B2'-H2'	122.2	B8'-B3'-B7'	68.4(3)	B8'-B3'-B1'	108.5(3)
B7'-B3'-B1'	107.7(3)	B8'-B3'-B4'	61.4(3)	B7'-B3'-B4'	117.2(3)
B1'-B3'-B4'	60.1(3)	B8'-B3'-B2'	117.8(3)	B7'-B3'-B2'	60.6(3)
B1'-B3'-B2'	60.6(3)	B4'-B3'-B2'	114.7(3)	B8'-B3'-H3'	116.5
B7'-B3'-H3'	117.3	B1'-B3'-H3'	124.7	B4'-B3'-H3'	117.4
B2'-B3'-H3'	117.3	B9'-B4'-B3'	111.1(3)	B9'-B4'-B1'	111.5(3)
B3'-B4'-B1'	59.9(3)	B9'-B4'-B10'	61.6(3)	B3'-B4'-B10'	105.9(3)

B1'-B4'-B10'	58.9(3)	B9'-B4'-B8'	61.4(3)	B3'-B4'-B8'	58.8(2)
B1'-B4'-B8'	106.3(3)	B10'-B4'-B8'	105.4(3)	B9'-B4'-H4'	117.9
B3'-B4'-H4'	121.9	B1'-B4'-H4'	121.4	B10'-B4'-H4'	123.6
B8'-B4'-H4'	123.6	B1'-B5'-B2'	61.1(2)	B1'-B5'-B6'	109.8(3)
B2'-B5'-B6'	57.7(2)	B1'-B5'-Br1'	121.0(3)	B2'-B5'-Br1'	124.0(3)
B6'-B5'-Br1'	119.8(3)	B1'-B5'-B10'	55.7(2)	B2'-B5'-B10'	106.9(3)
B6'-B5'-B10'	116.4(3)	Br1'-B5'-B10'	117.9(2)	B1'-B5'-H56'	121.0
B2'-B5'-H56'	98.3	B6'-B5'-H56'	46.2	Br1'-B5'-H56'	116.0
B10'-B5'-H56'	85.7	B2'-B6'-B7'	60.9(3)	B2'-B6'-B5'	60.5(2)
B7'-B6'-B5'	104.0(3)	B2'-B6'-H6'	129.9	B7'-B6'-H6'	125.9
B5'-B6'-H6'	127.9	B2'-B6'-H56'	98.7	B7'-B6'-H56'	109.2
B5'-B6'-H56'	43.6	H6'-B6'-H56'	118.1	B2'-B6'-H67'	106.7
B7'-B6'-H67'	50.8	B5'-B6'-H67'	112.1	H6'-B6'-H67'	110.7
H56'-B6'-H67'	82.2	B3'-B7'-B2'	60.4(3)	B3'-B7'-B6'	109.5(3)
B2'-B7'-B6'	57.9(3)	B3'-B7'-B8'	55.7(2)	B2'-B7'-B8'	107.1(3)
B6'-B7'-B8'	117.9(3)	B3'-B7'-H7'	140.4	B2'-B7'-H7'	140.9
B6'-B7'-H7'	109.2	B8'-B7'-H7'	110.9	B3'-B7'-H67'	123.4
B2'-B7'-H67'	95.6	B6'-B7'-H67'	41.7	B8'-B7'-H67'	92.1
H7'-B7'-H67'	91.7	B3'-B8'-B9'	108.1(3)	B3'-B8'-B4'	59.8(3)
B9'-B8'-B4'	56.8(3)	B3'-B8'-B7'	55.9(3)	B9'-B8'-B7'	116.2(3)
B4'-B8'-B7'	105.9(3)	B3'-B8'-H8'	140.2	B9'-B8'-H8'	110.7
B4'-B8'-H8'	141.2	B7'-B8'-H8'	111.9	B3'-B8'-H89'	129.3
B9'-B8'-H89'	45.8	B4'-B8'-H89'	100.5	B7'-B8'-H89'	93.6
H8'-B8'-H89'	85.8	B4'-B9'-B10'	61.3(3)	B4'-B9'-B8'	61.8(3)
B10'-B9'-B8'	105.4(3)	B4'-B9'-H9'	130.4	B10'-B9'-H9'	126.2
B8'-B9'-H9'	126.6	B4'-B9'-H89'	106.7	B10'-B9'-H89'	119.2
B8'-B9'-H89'	47.3	H9'-B9'-H89'	106.9	B4'-B9'-H910'	98.9
B10'-B9'-H910'	40.6	B8'-B9'-H910'	115.3	H9'-B9'-H910'	112.7
H89'-B9'-H910'	95.8	B1'-B10'-B4'	60.3(3)	B1'-B10'-B9'	109.0(3)
B4'-B10'-B9'	57.2(3)	B1'-B10'-B5'	55.3(2)	B4'-B10'-B5'	106.2(3)
B9'-B10'-B5'	117.4(3)	B1'-B10'-H10'	140.3	B4'-B10'-H10'	141.1
B9'-B10'-H10'	109.7	B5'-B10'-H10'	111.7	B1'-B10'-H910'	126.8
B4'-B10'-H910'	99.7	B9'-B10'-H910'	45.7	B5'-B10'-H910'	92.1
H10'-B10'-H910'	87.6	B5'-H56'-B6'	90.1	B6'-H67'-B7'	87.4
B8'-H89'-B9'	87.0	B9'-H910'-B10'	93.6		

Table 3.2.4. Bond lengths in **5I** (Å).

I1-B5	2.166(5)	B1-B5	1.742(7)	B1-B10	1.755(6)
B1-B4	1.774(7)	B1-B3	1.780(6)	B1-B2	1.782(7)
B1-H1	1.08(5)	B2-B6	1.715(7)	B2-B5	1.781(7)
B2-B3	1.787(8)	B2-B7	1.791(7)	B2-H2	1.08(5)
B3-B8	1.747(8)	B3-B7	1.759(8)	B3-B4	1.775(7)
B3-H3	1.27(6)	B4-B9	1.729(7)	B4-B8	1.780(7)
B4-B10	1.783(7)	B4-H4	1.07(6)	B5-B6	1.788(7)
B5-B10	1.968(7)	B5-H56	1.19(5)	B6-B7	1.781(9)
B6-H6	1.06(6)	B6-H56	1.38(5)	B6-H67	1.28(5)
B7-B8	1.986(9)	B7-H7	1.16(7)	B7-H67	1.27(6)
B8-B9	1.784(8)	B8-H8	1.03(6)	B8-H89	1.26(6)
B9-B10	1.789(7)	B9-H9	1.07(5)	B9-H89	1.27(6)
B9-H910	1.27(6)	B10-H10	1.10(5)	B10-H910	1.16(6)

Table 3.2.5. Bond angles in **5I** (^{o}).

B5-B1-B10	68.5(3)	B5-B1-B4	116.8(3)	B10-B1-B4	60.7(3)
B5-B1-B3	107.3(3)	B10-B1-B3	107.5(3)	B4-B1-B3	59.9(3)
B5-B1-B2	60.7(3)	B10-B1-B2	117.4(3)	B4-B1-B2	114.2(3)
B3-B1-B2	60.2(3)	B5-B1-H1	112(3)	B10-B1-H1	114(3)
B4-B1-H1	121(3)	B3-B1-H1	130(3)	B2-B1-H1	117(3)
B6-B2-B5	61.5(3)	B6-B2-B1	111.2(3)	B5-B2-B1	58.5(3)
B6-B2-B3	110.9(4)	B5-B2-B3	105.3(3)	B1-B2-B3	59.8(3)
B6-B2-B7	61.0(3)	B5-B2-B7	104.7(3)	B1-B2-B7	106.0(4)
B3-B2-B7	58.9(3)	B6-B2-H2	122(3)	B5-B2-H2	126(3)
B1-B2-H2	119(3)	B3-B2-H2	118(3)	B7-B2-H2	124(3)
B8-B3-B7	69.0(3)	B8-B3-B4	60.7(3)	B7-B3-B4	117.4(4)
B8-B3-B1	107.4(3)	B7-B3-B1	107.5(4)	B4-B3-B1	59.9(3)
B8-B3-B2	117.3(4)	B7-B3-B2	60.7(3)	B4-B3-B2	113.9(3)
B1-B3-B2	60.0(3)	B8-B3-H3	122(3)	B7-B3-H3	111(3)
B4-B3-H3	126(3)	B1-B3-H3	125(3)	B2-B3-H3	109(3)
B9-B4-B1	111.2(3)	B9-B4-B3	111.0(4)	B1-B4-B3	60.2(3)
B9-B4-B8	61.1(3)	B1-B4-B8	106.2(4)	B3-B4-B8	58.9(3)

B9-B4-B10	61.2(3)	B1-B4-B10	59.1(3)	B3-B4-B10	106.4(3)
B8-B4-B10	105.2(4)	B9-B4-H4	119(3)	B1-B4-H4	122(3)
B3-B4-H4	120(3)	B8-B4-H4	123(3)	B10-B4-H4	125(3)
B1-B5-B2	60.8(3)	B1-B5-B6	109.7(3)	B2-B5-B6	57.4(3)
B1-B5-B10	56.1(2)	B2-B5-B10	107.3(3)	B6-B5-B10	117.7(3)
B1-B5-I1	122.0(3)	B2-B5-I1	124.4(3)	B6-B5-I1	118.7(3)
B10-B5-I1	117.5(3)	B1-B5-H56	130(2)	B2-B5-H56	105(3)
B6-B5-H56	51(2)	B10-B5-H56	90(2)	I1-B5-H56	106(2)
B2-B6-B7	61.6(3)	B2-B6-B5	61.1(3)	B7-B6-B5	104.8(4)
B2-B6-H6	133(3)	B7-B6-H6	138(3)	B5-B6-H6	117(3)
B2-B6-H56	100(2)	B7-B6-H56	117(2)	B5-B6-H56	42(2)
H6-B6-H56	100(4)	B2-B6-H67	104(3)	B7-B6-H67	45(3)
B5-B6-H67	115(3)	H6-B6-H67	116(4)	H56-B6-H67	95(3)
B3-B7-B6	109.1(4)	B3-B7-B2	60.4(3)	B6-B7-B2	57.4(3)
B3-B7-B8	55.2(3)	B6-B7-B8	116.7(4)	B2-B7-B8	106.0(3)
B3-B7-H7	121(3)	B6-B7-H7	121(3)	B2-B7-H7	125(3)
B8-B7-H7	117(3)	B3-B7-H67	127(3)	B6-B7-H67	46(3)
B2-B7-H67	100(3)	B8-B7-H67	91(3)	H7-B7-H67	110(4)
B3-B8-B4	60.4(3)	B3-B8-B9	109.7(4)	B4-B8-B9	58.0(3)
B3-B8-B7	55.8(3)	B4-B8-B7	106.5(3)	B9-B8-B7	116.9(4)
B3-B8-H8	126(3)	B4-B8-H8	127(3)	B9-B8-H8	116(3)
B7-B8-H8	119(3)	B3-B8-H89	129(3)	B4-B8-H89	101(3)
B9-B8-H89	45(3)	B7-B8-H89	93(3)	H8-B8-H89	104(4)
B4-B9-B8	60.9(3)	B4-B9-B10	60.9(3)	B8-B9-B10	104.8(3)
B4-B9-H9	129(3)	B8-B9-H9	124(3)	B10-B9-H9	128(3)
B4-B9-H89	103(3)	B8-B9-H89	45(3)	B10-B9-H89	118(2)
H9-B9-H89	109(4)	B4-B9-H910	97(3)	B8-B9-H910	113(3)
B10-B9-H910	40(3)	H9-B9-H910	118(4)	H89-B9-H910	95(4)
B1-B10-B4	60.2(3)	B1-B10-B9	109.3(3)	B4-B10-B9	57.9(3)
B1-B10-B5	55.4(2)	B4-B10-B5	105.9(3)	B9-B10-B5	116.3(3)
B1-B10-H10	124(3)	B4-B10-H10	125(3)	B9-B10-H10	118(3)
B5-B10-H10	119(3)	B1-B10-H910	125(3)	B4-B10-H910	99(3)
B9-B10-H910	45(3)	B5-B10-H910	90(3)	H10-B10-H910	110(4)
B5-H56-B6	88(3)	B6-H67-B7	89(4)	B8-H89-B9	90(4)
B9-H910-B10	95(4)				

Table 3.2.6. Bond lengths for [**6Cl⁻**][PSH+] (Å).

B1-B5	1.738(3)	B1-B2	1.748(3)	B1-B10	1.783(3)
B1-B3	1.793(3)	B1-B4	1.805(3)	B1-H1	1.11(2)
B2-B6	1.752(3)	B2-B3	1.761(3)	B2-B7	1.764(3)
B2-B5	1.798(3)	B2-H2	1.09(2)	B3-B8	1.742(3)
B3-B7	1.761(3)	B3-B4	1.785(3)	B3-H3	1.13(2)
B4-B9	1.709(3)	B4-B8	1.769(3)	B4-B10	1.810(3)
B4-H4	1.08(2)	B5-B6	1.631(3)	B5-B10	1.862(3)
B5-H5	1.11(2)	B6-B7	1.781(3)	B6-Cl1	1.811(2)
B6-H67	1.33(2)	B7-B8	2.019(3)	B7-H7	1.06(2)
B7-H67	1.26(2)	B8-B9	1.772(4)	B8-H8	1.13(2)
B8-H89	1.25(2)	B9-B10	1.787(3)	B9-H9	1.09(2)
B9-H89	1.27(2)	B9-H910	1.23(2)	B10-H10	1.10(2)
B10-H910	1.29(2)	N21-C11	1.474(2)	N21-C23	1.490(2)
N21-C24	1.495(2)	N21-H21	1.06(3)	N22-C19	1.458(2)
N22-C25	1.473(2)	N22-C26	1.482(2)	N22-H21	1.58(3)
C11-C12	1.364(3)	C11-C20	1.427(2)	C12-C13	1.403(3)
C12-H12	0.96(2)	C13-C14	1.358(3)	C13-H13	0.90(2)
C14-C15	1.413(3)	C14-H14	0.98(2)	C15-C16	1.411(3)
C15-C20	1.431(2)	C16-C17	1.357(3)	C16-H16	0.95(2)
C17-C18	1.404(3)	C17-H17	0.97(2)	C18-C19	1.371(2)
C18-H18	0.94(2)	C19-C20	1.426(2)	C23-H23a	0.96(2)
C23-H23b	0.95(2)	C23-H23c	1.04(2)	C24-H24a	0.96(2)
C24-H24b	0.96(3)	C24-H24c	0.96(3)	C25-H25a	0.98(3)
C25-H25b	0.92(3)	C25-H25c	1.00(3)	C26-H26a	0.95(3)
C26-H26b	0.94(3)	C26-H26c	1.04(3)		

Table 3.2.7. Bond angles in [**6Cl⁻**][PSH$^+$] (^{o}).

B5-B1-B2	62.08(13)	B5-B1-B10	63.84(13)	B2-B1-B10	112.25(15)
B5-B1-B3	107.21(15)	B2-B1-B3	59.66(12)	B10-B1-B3	103.80(14)
B5-B1-B4	115.09(15)	B2-B1-B4	113.15(15)	B10-B1-B4	60.58(13)
B3-B1-B4	59.49(12)	B5-B1-H1	125.2(10)	B2-B1-H1	124.4(10)
B10-B1-H1	119.1(10)	B3-B1-H1	122.2(10)	B4-B1-H1	109.7(10)
B1-B2-B6	104.91(15)	B1-B2-B3	61.44(13)	B6-B2-B3	109.00(15)
B1-B2-B7	107.03(15)	B6-B2-B7	60.88(12)	B3-B2-B7	59.93(12)
B1-B2-B5	58.71(12)	B6-B2-B5	54.69(11)	B3-B2-B5	106.01(15)
B7-B2-B5	102.11(14)	B1-B2-H2	121.9(11)	B6-B2-H2	123.0(11)
B3-B2-H2	120.7(11)	B7-B2-H2	123.4(11)	B5-B2-H2	126.0(11)
B8-B3-B7	70.42(14)	B8-B3-B2	119.96(16)	B7-B3-B2	60.11(12)
B8-B3-B4	60.20(13)	B7-B3-B4	115.49(16)	B2-B3-B4	113.48(16)
B8-B3-B1	109.21(16)	B7-B3-B1	105.23(15)	B2-B3-B1	58.90(12)
B4-B3-B1	60.61(13)	B8-B3-H3	113.1(10)	B7-B3-H3	117.8(11)
B2-B3-H3	118.7(10)	B4-B3-H3	118.2(11)	B1-B3-H3	127.1(11)
B9-B4-B8	61.25(14)	B9-B4-B3	110.70(16)	B8-B4-B3	58.68(13)
B9-B4-B1	113.22(16)	B8-B4-B1	107.42(15)	B3-B4-B1	59.91(12)
B9-B4-B10	60.97(13)	B8-B4-B10	102.84(15)	B3-B4-B10	103.01(15)
B1-B4-B10	59.09(12)	B9-B4-H4	119.3(11)	B8-B4-H4	124.7(11)
B3-B4-H4	121.6(12)	B1-B4-H4	118.3(11)	B10-B4-H4	126.3(12)
B6-B5-B1	110.83(16)	B6-B5-B2	61.23(12)	B1-B5-B2	59.21(12)
B6-B5-B10	111.47(15)	B1-B5-B10	59.23(12)	B2-B5-B10	106.42(14)
B6-B5-H5	122.5(11)	B1-B5-H5	117.3(11)	B2-B5-H5	122.4(11)
B10-B5-H5	119.1(11)	B5-B6-B2	64.08(13)	B5-B6-B7	108.46(16)
B2-B6-B7	59.89(12)	B5-B6-Cl1	128.63(15)	B2-B6-Cl1	129.80(14)
B7-B6-Cl1	120.70(14)	B5-B6-H67	118.6(9)	B2-B6-H67	101.7(10)
B7-B6-H67	45.0(9)	Cl1-B6-H67	106.8(9)	B3-B7-B2	59.96(12)
B3-B7-B6	107.70(15)	B2-B7-B6	59.22(12)	B3-B7-B8	54.34(11)
B2-B7-B8	106.38(15)	B6-B7-B8	114.84(15)	B3-B7-H7	124.7(11)
B2-B7-H7	128.6(11)	B6-B7-H7	122.4(11)	B8-B7-H7	114.3(11)
B3-B7-H67	123.2(10)	B2-B7-H67	104.1(10)	B6-B7-H67	48.2(10)
B8-B7-H67	87.2(10)	H7-B7-H67	107.8(15)	B3-B8-B4	61.12(13)
B3-B8-B9	109.77(16)	B4-B8-B9	57.69(13)	B3-B8-B7	55.24(12)

B4-B8-B7	104.46(14)	B9-B8-B7	112.95(15)	B3-B8-H8	119.4(11)
B4-B8-H8	125.6(11)	B9-B8-H8	122.5(11)	B7-B8-H8	118.7(11)
B3-B8-H89	130.3(10)	B4-B8-H89	101.7(11)	B9-B8-H89	46.0(11)
B7-B8-H89	91.3(11)	H8-B8-H89	108.4(15)	B4-B9-B8	61.06(14)
B4-B9-B10	62.32(13)	B8-B9-B10	103.65(15)	B4-B9-H9	128.4(12)
B8-B9-H9	128.1(12)	B10-B9-H9	126.3(12)	B4-B9-H89	103.9(11)
B8-B9-H89	44.8(11)	B10-B9-H89	116.4(10)	H9-B9-H89	110.6(15)
B4-B9-H910	104.9(10)	B8-B9-H910	113.3(10)	B10-B9-H910	46.0(10)
H9-B9-H910	111.3(16)	H89-B9-H910	91.1(14)	B1-B10-B9	110.58(16)
B1-B10-B4	60.33(12)	B9-B10-B4	56.72(12)	B1-B10-B5	56.93(12)
B9-B10-B5	123.83(16)	B4-B10-B5	109.05(15)	B1-B10-H10	124.3(10)
B9-B10-H10	114.4(10)	B4-B10-H10	125.6(11)	B5-B10-H10	115.3(10)
B1-B10-H910	130.1(10)	B9-B10-H910	43.3(10)	B4-B10-H910	97.1(10)
B5-B10-H910	98.9(10)	H10-B10-H910	105.2(14)	C11-N21-C23	113.43(15)
C11-N21-C24	111.61(15)	C23-N21-C24	110.71(16)	C11-N21-H21	100.8(13)
C23-N21-H21	111.5(13)	C24-N21-H21	108.3(13)	C19-N22-C25	112.89(15)
C19-N22-C26	111.02(15)	C25-N22-C26	111.16(18)	C12-C11-C20	122.24(17)
C12-C11-N21	119.56(16)	C20-C11-N21	118.19(15)	C11-C12-C13	120.0(2)
C11-C12-H12	118.6(14)	C13-C12-H12	121.4(14)	C14-C13-C12	120.13(19)
C14-C13-H13	121.2(14)	C12-C13-H13	118.6(14)	C13-C14-C15	121.47(19)
C13-C14-H14	120.5(12)	C15-C14-H14	118.0(12)	C16-C15-C14	121.12(17)
C16-C15-C20	119.41(16)	C14-C15-C20	119.47(17)	C17-C16-C15	121.21(17)
C17-C16-H16	121.6(12)	C15-C16-H16	117.2(12)	C16-C17-C18	120.09(18)
C16-C17-H17	122.9(12)	C18-C17-H17	117.0(12)	C19-C18-C17	120.87(18)
C19-C18-H18	119.0(12)	C17-C18-H18	120.1(12)	C18-C19-C20	120.70(16)
C18-C19-N22	120.59(15)	C20-C19-N22	118.70(14)	C19-C20-C11	125.63(15)
C19-C20-C15	117.71(15)	C11-C20-C15	116.66(15)	N21-C23-H23a	110.5(14)
N21-C23-H23b	108.5(13)	H23a-C23-H23b	110(2)	N21-C23-H23c	108.0(13)
H23a-C23-H23c	108.2(19)	H23b-C23-H23c	111.2(18)	N21-C24-H24a	107.6(13)
N21-C24-H24b	105.5(14)	H24a-C24-H24b	109.4(19)	N21-C24-H24c	109.6(15)
H24a-C24-H24c	114(2)	H24b-C24-H24c	110(2)	N22-C25-H25a	108.9(15)
N22-C25-H25b	108.8(14)	H25a-C25-H25b	110(2)	N22-C25-H25c	112.1(14)
H25a-C25-H25c	108(2)	H25b-C25-H25c	108(2)	N22-C26-H26a	110.6(15)
N22-C26-H26b	107.2(15)	H26a-C26-H26b	107(2)	N22-C26-H26c	108.6(16)
H26a-C26-H26c	112(2)	H26b-C26-H26c	112(2)	B6-H67-B7	86.8(13)

B8-H89-B9	89.2(15)	B9-H910-B10	90.7(14)	N21-H21-N22	159(2)

Table 3.2.8. Bond lengths for [**5Cl⁻**][PSH$^+$] (Å).

B1-B5	1.737(3)	B1-B2	1.755(3)	B1-B3	1.787(3)
B1-B10	1.796(3)	B1-B4	1.804(3)	B1-H1	1.11(2)
B2-B6	1.754(3)	B2-B7	1.764(3)	B2-B3	1.767(3)
B2-B5	1.790(3)	B2-H2	1.16(2)	B3-B8	1.737(3)
B3-B7	1.770(3)	B3-B4	1.784(3)	B3-H3	1.13(2)
B4-B9	1.702(3)	B4-B8	1.766(3)	B4-B10	1.800(3)
B4-H4	1.11(2)	B5-B6	1.644(3)	B5-B10	1.844(3)
B5-Cl1	1.844(2)	B6-B7	1.775(3)	B6-H6	1.12(2)
B6-H67	1.27(2)	B7-B8	2.028(3)	B7-H7	1.08(2)
B7-H67	1.24(2)	B8-B9	1.773(3)	B8-H8	1.12(2)
B8-H89	1.293(19)	B9-B10	1.791(3)	B9-H9	1.05(2)
B9-H89	1.279(19)	B9-H910	1.235(18)	B10-H10	1.09(2)
B10-H910	1.280(18)	N21-C11	1.470(2)	N21-C23	1.488(3)
N21-C24	1.491(2)	N21-H21	1.06(2)	N22-C19	1.462(2)
N22-C26	1.474(3)	N22-C25	1.479(2)	N22-H21	1.58(2)
C11-C12	1.370(3)	C11-C20	1.424(2)	C12-C13	1.405(4)
C12-H12	0.92(2)	C13-C14	1.348(4)	C13-H13	0.91(3)
C14-C15	1.413(3)	C14-H14	1.03(3)	C15-C16	1.410(3)
C15-C20	1.431(2)	C16-C17	1.348(4)	C16-H16	0.94(2)
C17-C18	1.398(3)	C17-H17	0.94(3)	C18-C19	1.362(3)
C18-H18	0.91(2)	C19-C20	1.422(2)	C23-H23a	0.96(3)
C23-H23b	0.97(2)	C23-H23c	0.95(3)	C24-H24a	0.97(3)
C24-H24b	0.96(3)	C24-H24c	0.95(3)	C25-H25a	1.07(3)
C25-H25b	0.93(2)	C25-H25c	0.99(3)	C26-H26a	0.92(3)
C26-H26b	1.03(2)	C26-H26c	0.98(3)		

Table 3.2.9. Bond angles for [**5Cl⁻**][PSH^{+}] (°).

B5-B1-B2	61.67(13)	B5-B1-B3	106.26(15)	B2-B1-B3	59.85(13)
B5-B1-B10	62.90(11)	B2-B1-B10	111.69(15)	B3-B1-B10	103.49(14)
B5-B1-B4	113.26(14)	B2-B1-B4	113.03(15)	B3-B1-B4	59.57(12)
B10-B1-B4	60.00(12)	B5-B1-H1	122.1(10)	B2-B1-H1	124.1(10)
B3-B1-H1	126.3(10)	B10-B1-H1	117.7(10)	B4-B1-H1	113.2(10)
B6-B2-B1	106.22(16)	B6-B2-B7	60.61(13)	B1-B2-B7	107.08(16)
B6-B2-B3	109.47(15)	B1-B2-B3	60.99(13)	B7-B2-B3	60.18(12)
B6-B2-B5	55.25(13)	B1-B2-B5	58.66(12)	B7-B2-B5	101.16(15)
B3-B2-B5	104.86(15)	B6-B2-H2	123.4(11)	B1-B2-H2	120.9(11)
B7-B2-H2	123.5(11)	B3-B2-H2	119.5(11)	B5-B2-H2	127.8(11)
B8-B3-B2	120.26(16)	B8-B3-B7	70.63(13)	B2-B3-B7	59.82(13)
B8-B3-B4	60.20(13)	B2-B3-B4	113.40(15)	B7-B3-B4	115.11(16)
B8-B3-B1	109.93(15)	B2-B3-B1	59.16(13)	B7-B3-B1	105.40(15)
B4-B3-B1	60.68(12)	B8-B3-H3	111.5(10)	B2-B3-H3	118.0(10)
B7-B3-H3	114.7(10)	B4-B3-H3	120.9(10)	B1-B3-H3	129.4(10)
B9-B4-B8	61.43(13)	B9-B4-B3	110.66(15)	B8-B4-B3	58.57(12)
B9-B4-B10	61.44(12)	B8-B4-B10	103.83(14)	B3-B4-B10	103.44(15)
B9-B4-B1	114.11(14)	B8-B4-B1	107.84(15)	B3-B4-B1	59.74(12)
B10-B4-B1	59.77(11)	B9-B4-H4	118.7(10)	B8-B4-H4	125.2(10)
B3-B4-H4	122.6(10)	B10-B4-H4	124.5(11)	B1-B4-H4	117.5(10)
B6-B5-B1	112.22(16)	B6-B5-B2	61.28(14)	B1-B5-B2	59.66(12)
B6-B5-B10	113.82(15)	B1-B5-B10	60.12(12)	B2-B5-B10	107.92(14)
B6-B5-Cl1	121.75(14)	B1-B5-Cl1	117.67(13)	B2-B5-Cl1	124.80(13)
B10-B5-Cl1	115.92(13)	B5-B6-B2	63.47(13)	B5-B6-B7	106.75(16)
B2-B6-B7	59.96(13)	B5-B6-H6	127.2(11)	B2-B6-H6	130.2(11)
B7-B6-H6	124.1(12)	B5-B6-H67	117.8(9)	B2-B6-H67	101.5(10)
B7-B6-H67	44.3(10)	H6-B6-H67	108.7(14)	B2-B7-B3	60.00(13)
B2-B7-B6	59.42(13)	B3-B7-B6	108.37(16)	B2-B7-B8	106.32(15)
B3-B7-B8	53.91(12)	B6-B7-B8	116.19(15)	B2-B7-H7	131.3(11)
B3-B7-H7	123.9(11)	B6-B7-H7	123.7(11)	B8-B7-H7	111.1(11)
B2-B7-H67	102.5(10)	B3-B7-H67	125.0(10)	B6-B7-H67	45.9(10)
B8-B7-H67	90.9(10)	H7-B7-H67	106.9(15)	B3-B8-B4	61.23(13)
B3-B8-B9	109.59(15)	B4-B8-B9	57.49(12)	B3-B8-B7	55.45(12)

B4-B8-B7	104.27(14)	B9-B8-B7	112.06(14)	B3-B8-H8	121.2(10)
B4-B8-H8	127.3(10)	B9-B8-H8	121.9(10)	B7-B8-H8	118.8(10)
B3-B8-H89	129.7(9)	B4-B8-H89	101.5(9)	B9-B8-H89	46.1(8)
B7-B8-H89	90.0(9)	H8-B8-H89	106.9(13)	B4-B9-B8	61.08(13)
B4-B9-B10	61.98(12)	B8-B9-B10	103.96(15)	B4-B9-H9	127.8(11)
B8-B9-H9	129.3(12)	B10-B9-H9	124.5(12)	B4-B9-H89	105.6(9)
B8-B9-H89	46.8(9)	B10-B9-H89	117.0(9)	H9-B9-H89	111.2(14)
B4-B9-H910	104.7(8)	B8-B9-H910	115.1(8)	B10-B9-H910	45.6(8)
H9-B9-H910	109.6(15)	H89-B9-H910	91.8(12)	B9-B10-B1	110.26(15)
B9-B10-B4	56.58(12)	B1-B10-B4	60.23(12)	B9-B10-B5	122.59(15)
B1-B10-B5	56.97(11)	B4-B10-B5	108.49(15)	B9-B10-H10	117.4(11)
B1-B10-H10	121.6(11)	B4-B10-H10	125.7(11)	B5-B10-H10	114.4(11)
B9-B10-H910	43.6(8)	B1-B10-H910	131.0(8)	B4-B10-H910	97.6(8)
B5-B10-H910	98.7(8)	H10-B10-H910	107.0(13)	B6-H67-B7	89.9(14)
B8-H89-B9	87.1(12)	B9-H910-B10	90.8(12)	C11-N21-C23	113.47(17)
C11-N21-C24	111.14(15)	C23-N21-C24	111.78(19)	C11-N21-H21	102.4(12)
C23-N21-H21	109.9(12)	C24-N21-H21	107.6(12)	C19-N22-C26	113.11(15)
C19-N22-C25	110.55(14)	C26-N22-C25	111.64(18)	C12-C11-C20	121.12(18)
C12-C11-N21	120.79(17)	C20-C11-N21	118.01(14)	C11-C12-C13	120.4(2)
C11-C12-H12	119.6(14)	C13-C12-H12	120.1(14)	C14-C13-C12	120.5(2)
C14-C13-H13	120.5(18)	C12-C13-H13	119.0(19)	C13-C14-C15	121.2(2)
C13-C14-H14	122.7(15)	C15-C14-H14	116.1(15)	C16-C15-C14	121.3(2)
C16-C15-C20	119.30(19)	C14-C15-C20	119.4(2)	C17-C16-C15	121.3(2)
C17-C16-H16	120.6(14)	C15-C16-H16	118.1(14)	C16-C17-C18	120.1(2)
C16-C17-H17	122.4(17)	C18-C17-H17	117.5(17)	C19-C18-C17	121.1(2)
C19-C18-H18	119.2(14)	C17-C18-H18	119.8(14)	C18-C19-C20	120.82(17)
C18-C19-N22	120.59(16)	C20-C19-N22	118.55(14)	C19-C20-C11	125.26(15)
C19-C20-C15	117.37(16)	C11-C20-C15	117.37(16)	N21-C23-H23a	109.7(17)
N21-C23-H23b	108.6(13)	H23a-C23-H23b	108(2)	N21-C23-H23c	107.2(15)
H23a-C23-H23c	113(2)	H23b-C23-H23c	110(2)	N21-C24-H24a	104.6(15)
N21-C24-H24b	107.1(14)	H24a-C24-H24b	108(2)	N21-C24-H24c	108.1(16)
H24a-C24-H24c	115(2)	H24b-C24-H24c	113(2)	N22-C25-H25a	108.3(14)
N22-C25-H25b	109.1(15)	H25a-C25-H25b	108(2)	N22-C25-H25c	107.8(15)
H25a-C25-H25c	113(2)	H25b-C25-H25c	111(2)	N22-C26-H26a	113.9(16)
N22-C26-H26b	105.9(13)	H26a-C26-H26b	113(2)	N22-C26-H26c	104.4(15)

H26a-C26-H26c	112(2)	H26b-C26-H26c	107(2)

Computational Methods. Density Functional Theory (DFT) calculations were performed using the Gaussian 03 package.[15] All ground state, transition state, and intermediate geometries and both electronic and free energies were obtained using the B3LYP/6-311G(d) level without constraints for all H, C, B and Cl atoms. Both the B3LYP/6-311G(d) level and B3LYP/SDD pseudopotential were used for Br atoms, and only the B3LYP/SDD pseudopotential was used for I atoms. The NMR chemical shifts were calculated at the B3LYP/6-311G(d) level using the GIAO option within Gaussian 03 and are referenced to $BF_3 \cdot O(C_2H_5)_2$ using an absolute shielding constant of 102.24 ppm. Harmonic vibrational analyses were carried out on the optimized geometries at the same level to establish the nature of stationary points. True first-order saddle points possessed only one imaginary frequency. Intrinsic reaction coordinate (IRC) calculations were carried out in both the forward and reverse directions to confirm the reaction pathways from the located transition states. All optimized geometries and energies (free and electronic) are given in **Tables 3.2.10-3.2.40.**

Table 3.2.10. DFT optimized (B3LYP/6-311G(d)) coordinates for 6-F-$B_{10}H_{13}$.

Center Number	Atomic Number	X	Y	Z
1	5	-0.67787	-0.89149	1.118304
2	5	0.854866	0.00000	1.207452
3	5	-0.67787	0.891492	1.118304
4	5	-2.01124	0.00000	0.336083
5	5	0.661412	-1.43197	0.125147
6	5	1.6527	0.00000	-0.30981
7	5	0.661412	1.431972	0.125147
8	5	-1.25238	1.423166	-0.44482
9	5	-1.83035	0.00000	-1.37485
10	5	-1.25238	-1.42317	-0.44482
11	1	-0.93685	-1.62445	2.013636
12	1	1.503167	0.00000	2.198292
13	1	-0.93685	1.624449	2.013636
14	1	-3.08972	0.00000	0.823643
15	1	1.204796	-2.47383	0.26006
16	9	2.944321	0.00000	-0.66024
17	1	1.204796	2.473834	0.26006
18	1	-1.75472	2.476514	-0.6378
19	1	-2.64878	0.00000	-2.22813
20	1	-1.75472	-2.47651	-0.6378
21	1	0.998208	-0.98051	-1.04182
22	1	0.998208	0.98051	-1.04182
23	1	-0.96400	0.966908	-1.66024
24	1	-0.96400	-0.96691	-1.66024

Table 3.2.11. DFT optimized (B3LYP/6-311G(d)) coordinates for 6-F-$B_{10}H_{12}^{-}$.

Center Number	Atomic Number	X	Y	Z
1	5	0.620579	0.995232	1.111407
2	5	-0.82533	0.019874	1.27489
3	5	0.734841	-0.79844	1.169212
4	5	1.963785	0.128275	0.256011
5	5	-0.73473	1.407616	0.097162
6	5	-1.57763	0.060835	-0.33021
7	5	-0.63187	-1.39497	0.212033
8	5	1.314572	-1.4058	-0.35373

9	5	1.734097	-0.02871	-1.43004
10	5	0.97192	1.3906	-0.60762
11	1	1.004326	1.734109	1.967813
12	1	-1.46042	-0.01312	2.28524
13	1	1.080627	-1.47647	2.088805
14	1	3.075024	0.251555	0.669709
15	1	-1.26167	2.466012	0.296631
16	9	-2.87906	-0.11319	-0.7352
17	1	-1.13401	-2.4674	0.346615
18	1	1.899642	-2.43886	-0.44614
19	1	2.585097	-0.01303	-2.26158
20	1	1.42376	2.435649	-0.9648
21	1	-0.88301	-0.95679	-0.96403
22	1	0.993625	-1.10942	-1.61986
23	1	0.73741	0.73384	-1.77723

Table 3.2.12. DFT optimized (B3LYP/6-311G(d)) coordinates for 5-F-$B_{10}H_{13}$.

Center Number	Atomic Number	X	Y	Z
1	5	0.223092	-0.53149	1.143129
2	5	0.703583	1.160501	0.75064
3	5	-0.9991	0.764554	1.046815
4	5	-1.46191	-0.92745	0.696692
5	5	1.397433	-0.25198	-0.11319
6	5	1.027836	1.311908	-0.93907
7	5	-0.58717	1.787693	-0.3086
8	5	-2.02186	0.427683	-0.33886
9	5	-1.59212	-1.18135	-1.00093
10	5	-0.08556	-1.6441	-0.17052
11	1	0.688066	-1.02597	2.115278
12	1	1.315743	1.803382	1.533753
13	1	-1.55551	1.314514	1.937411
14	1	-2.15702	-1.51944	1.449754
15	9	2.661628	-0.71668	-0.08884
16	1	1.809325	2.009685	-1.4863
17	1	-0.90925	2.921369	-0.40883
18	1	-3.13731	0.807259	-0.44276
19	1	-2.2895	-1.89704	-1.63242
20	1	0.273553	-2.77125	-0.17389
21	1	1.153393	0.093363	-1.41424

22	1	-0.15731	1.457645	-1.52297
23	1	-1.67477	0.039481	-1.54902
24	1	-0.3352	-1.36278	-1.43682

Table 3.2.13. DFT optimized (B3LYP/6-311G(d)) coordinates for 5-F-$B_{10}H_{12}^{-}$.

Center Number	Atomic Number	X	Y	Z
1	5	0.314412	-0.44139	1.154861
2	5	0.676366	1.221081	0.704046
3	5	-1.00269	0.783727	1.02481
4	5	-1.36832	-0.95227	0.728093
5	5	1.397357	-0.18549	-0.20818
6	5	0.983106	1.182609	-1.0411
7	5	-0.58723	1.750447	-0.40244
8	5	-2.0715	0.330686	-0.27316
9	5	-1.57044	-1.24584	-0.9417
10	5	0.046266	-1.5273	-0.23075
11	1	0.732576	-0.93156	2.160062
12	1	1.254813	1.95727	1.44441
13	1	-1.57863	1.329959	1.916354
14	1	-1.99789	-1.59132	1.512635
15	9	2.702383	-0.66405	-0.07729
16	1	1.634564	1.928511	-1.71148
17	1	-1.00671	2.847444	-0.60239
18	1	-3.21413	0.662022	-0.3129
19	1	-2.26534	-2.04541	-1.48198
20	1	0.431235	-2.65438	-0.26964
21	1	-0.2495	1.20705	-1.54897
22	1	-1.79626	-0.05864	-1.51079
23	1	-0.35278	-1.25581	-1.47203

Table 3.2.14. DFT optimized (B3LYP/6-311G(d)) coordinates for 6-Cl-$B_{10}H_{13}$.

Center Number	Atomic Number	X	Y	Z
1	5	1.1874	0.891222	1.09301
2	5	-0.33695	0.00000	1.333693
3	5	1.1874	-0.89122	1.09301
4	5	2.427581	0.00000	0.171192
5	5	-0.24755	1.428066	0.246486
6	5	-1.27574	0.00000	-0.10928

7	5	-0.24755	-1.42807	0.246486
8	5	1.590971	-1.42373	-0.52496
9	5	2.060003	0.00000	-1.51028
10	5	1.590971	1.423731	-0.52496
11	1	1.539759	1.625049	1.955031
12	1	-0.88442	0.00000	2.382911
13	1	1.539759	-1.62505	1.955031
14	1	3.552726	0.00000	0.538626
15	1	-0.77682	2.471363	0.416098
16	17	-3.03864	0.00000	-0.35779
17	1	-0.77682	-2.47136	0.416098
18	1	2.069281	-2.4769	-0.77173
19	1	2.775132	0.00000	-2.4516
20	1	2.069281	2.476897	-0.77173
21	1	-0.730100	0.96620	-0.88394
22	1	-0.730100	-0.96620	-0.88394
23	1	1.163242	-0.96857	-1.69526
24	1	1.163242	0.968572	-1.69526

Table 3.2.15. DFT optimized (B3LYP/6-311G(d)) coordinates for 6-Cl-$B_{10}H_{12}^{-}$.

Center Number	Atomic Number	X	Y	Z
1	5	1.171144	1.032119	1.026345
2	5	-0.27597	0.115545	1.4073
3	5	1.237551	-0.76626	1.156681
4	5	2.384992	0.081397	0.073785
5	5	-0.2887	1.43511	0.154376
6	5	-1.19811	0.086968	-0.0913
7	5	-0.25724	-1.35013	0.407547
8	5	1.619622	-1.44561	-0.4006
9	5	1.950616	-0.12904	-1.5673
10	5	1.356584	1.345773	-0.72418
11	1	1.668741	1.798843	1.794375
12	1	-0.78662	0.150778	2.4843
13	1	1.670928	-1.41699	2.058133
14	1	3.538242	0.176294	0.3579
15	1	-0.75936	2.519268	0.341846
16	17	-3.00657	-0.06369	-0.38134
17	1	-0.76044	-2.40581	0.625056

18	1	2.145263	-2.50603	-0.52458
19	1	2.672428	-0.18099	-2.5106
20	1	1.792836	2.363215	-1.16709
21	1	-0.64797	-0.93594	-0.76563
22	1	1.138525	-1.17978	-1.61612
23	1	0.936591	0.670513	-1.80807

Table 3.2.16. DFT optimized (B3LYP/6-311G(d)) coordinates for 5-Cl-$B_{10}H_{13}$.

Center Number	Atomic Number	X	Y	Z
1	5	-0.06697	-0.43561	1.153392
2	5	0.132044	1.301767	0.752015
3	5	-1.49085	0.634304	1.0356
4	5	-1.65693	-1.11087	0.696849
5	5	1.048315	0.022363	-0.11363
6	5	0.431143	1.499631	-0.93396
7	5	-1.24007	1.706595	-0.32171
8	5	-2.43174	0.121072	-0.35178
9	5	-1.73353	-1.39679	-0.9998
10	5	-0.16839	-1.58993	-0.16055
11	1	0.461162	-0.84239	2.132648
12	1	0.63021	2.0392	1.531775
13	1	-2.13501	1.092798	1.918973
14	1	-2.2421	-1.80982	1.451615
15	17	2.812903	-0.28734	-0.0429
16	1	1.090589	2.294782	-1.5068
17	1	-1.74614	2.769688	-0.43415
18	1	-3.593	0.313433	-0.46655
19	1	-2.29905	-2.22772	-1.62183
20	1	0.372	-2.64123	-0.15011
21	1	0.769756	0.291513	-1.3881
22	1	-0.75809	1.435418	-1.52889
23	1	-2.019	-0.21825	-1.56107
24	1	-0.46582	-1.37541	-1.43044

Table 3.2.17. DFT optimized (B3LYP/6-311G(d)) coordinates for 5-Cl-$B_{10}H_{12}^{-}$.

Center Number	Atomic Number	X	Y	Z
1	5	-0.00268	-0.34679	1.172942
2	5	0.125029	1.342927	0.694124
3	5	-1.47928	0.67366	1.02104
4	5	-1.58737	-1.09461	0.730587
5	5	1.006042	0.039194	-0.19041
6	5	0.422485	1.325677	-1.04736
7	5	-1.21042	1.682295	-0.41443
8	5	-2.47247	0.070462	-0.27283
9	5	-1.75297	-1.42268	-0.93917
10	5	-0.09858	-1.45661	-0.2375
11	1	0.465928	-0.76355	2.186276
12	1	0.603853	2.156952	1.421276
13	1	-2.12194	1.146037	1.908394
14	1	-2.11621	-1.81761	1.515806
15	17	2.841062	-0.27223	-0.03922
16	1	0.98049	2.111918	-1.75053
17	1	-1.77753	2.710207	-0.61548
18	1	-3.64976	0.238469	-0.31138
19	1	-2.33645	-2.32451	-1.44869
20	1	0.432884	-2.52118	-0.26514
21	1	-0.81137	1.203502	-1.55968
22	1	-2.15295	-0.29447	-1.51449
23	1	-0.56397	-1.2854	-1.48462

Table 3.2.18. DFT optimized (B3LYP/SDD for Br, 6-311G(d) for B, H) coordinates for 6-Br-$B_{10}H_{13}$.

Center Number	Atomic Number	X	Y	Z
1	5	-1.78035	-1.20927	0.891772
2	5	-1.41014	0.291344	0.00000
3	5	-1.78035	-1.20927	-0.89177
4	5	-1.41029	-2.70987	0.00000
5	5	-0.44466	-0.21532	1.428076
6	5	0.284038	0.586579	0.00000
7	5	-0.44466	-0.21532	-1.42808
8	5	-0.44466	-2.2076	-1.42335

9	5	0.282458	-3.02129	0.0000
10	5	-0.44466	-2.2076	1.423349
11	1	-2.71119	-1.2013	1.62605
12	1	-2.16652	1.201238	0.00000
13	1	-2.71119	-1.2013	-1.62605
14	1	-2.18395	-3.60568	0.00000
15	1	-0.39157	0.336251	2.471979
16	35	1.293567	2.26247	0.000000
17	1	-0.39157	0.336251	-2.47198
18	1	-0.40213	-2.74345	-2.47688
19	1	0.875877	-4.04365	0.00000
20	1	-0.40213	-2.74345	2.476881
21	1	0.788726	-0.20207	0.96591
22	1	0.788726	-0.20207	-0.96591
23	1	0.799217	-2.26458	-0.96945
24	1	0.799217	-2.26458	0.969445

Table 3.2.19. DFT optimized (B3LYP/SDD for Br 6-311G(d) for B, H) coordinates for 6-Br-$B_{10}H_{12}^{-}$.

Center Number	Atomic Number	X	Y	Z
1	5	1.864559	1.058905	0.969464
2	5	0.430649	0.17383	1.463838
3	5	1.918521	-0.7353	1.154745
4	5	3.009267	0.063259	-0.02141
5	5	0.359074	1.454442	0.171517
6	5	-0.56508	0.106364	0.020499
7	5	0.37602	-1.32284	0.51523
8	5	2.201222	-1.46894	-0.40027
9	5	2.474203	-0.19316	-1.62471
10	5	1.952693	1.315274	-0.79845
11	1	2.413542	1.844085	1.681514
12	1	-0.01532	0.24851	2.566688
13	1	2.397595	-1.36318	2.048979
14	1	4.178097	0.151465	0.191398
15	1	-0.08779	2.549306	0.349313
16	35	-2.57423	-0.03565	-0.18235
17	1	-0.12199	-2.36624	0.791938
18	1	2.707028	-2.53893	-0.52164

19	1	3.134727	-0.28739	-2.60856
20	1	2.371988	2.312625	-1.29882
21	1	-0.08984	-0.94128	-0.65085
22	1	1.64651	-1.23443	-1.58877
23	1	1.457725	0.613947	-1.83125

Table 3.2.20. DFT optimized (B3LYP/SDD for Br, 6-311G(d) for B, H) coordinates for 5-Br-$B_{10}H_{13}$.

Center Number	Atomic Number	X	Y	Z
1	5	-0.63126	-0.40238	1.161812
2	5	-0.51881	1.339052	0.75458
3	5	-2.10947	0.589344	1.029474
4	5	-2.17808	-1.16292	0.695048
5	5	0.458938	0.1069	-0.10627
6	5	-0.22375	1.548987	-0.9299
7	5	-1.90607	1.671036	-0.3288
8	5	-3.01055	0.022201	-0.36283
9	5	-2.22837	-1.45744	-1.00132
10	5	-0.65814	-1.56258	-0.15264
11	1	-0.09071	-0.78012	2.145439
12	1	-0.06454	2.10453	1.533776
13	1	-2.7834	1.017848	1.905604
14	1	-2.72994	-1.89116	1.447136
15	35	2.414585	-0.12389	-0.02084
16	1	0.396612	2.371368	-1.50742
17	1	-2.46805	2.705044	-0.44726
18	1	-4.17919	0.152727	-0.48864
19	1	-2.74607	-2.31989	-1.62205
20	1	-0.06644	-2.58532	-0.12942
21	1	0.185611	0.353404	-1.37699
22	1	-1.4049	1.422703	-1.53258
23	1	-2.57099	-0.29922	-1.56883
24	1	-0.9607	-1.37666	-1.42506

Table 3.2.21. DFT optimized (B3LYP/SDD for Br, 6-311G(d) for B, H) coordinates for 5-Br-$B_{10}H_{12}^{-}$.

Center Number	Atomic Number	X	Y	Z
1	5	-0.58406	-0.31328	1.180185
2	5	-0.53186	1.377649	0.694968
3	5	-2.1061	0.636061	1.016813
4	5	-2.12847	-1.13605	0.729946
5	5	0.397986	0.112984	-0.18377
6	5	-0.22865	1.371718	-1.04578
7	5	-1.87893	1.653408	-0.42039
8	5	-3.06422	-0.01679	-0.27905
9	5	-2.27323	-1.47609	-0.94019
10	5	-0.61931	-1.4294	-0.23358
11	1	-0.10321	-0.70521	2.196884
12	1	-0.09153	2.214005	1.420203
13	1	-2.77256	1.081585	1.900217
14	1	-2.62547	-1.88131	1.514811
15	35	2.435653	-0.11982	-0.01894
16	1	0.296412	2.176344	-1.75213
17	1	-2.49196	2.653752	-0.62493
18	1	-4.24753	0.097252	-0.32314
19	1	-2.8136	-2.40634	-1.44575
20	1	-0.04237	-2.46963	-0.25334
21	1	-1.45589	1.192934	-1.56268
22	1	-2.72352	-0.37084	-1.51965
23	1	-1.09239	-1.28971	-1.48333

Table 3.2.22. DFT optimized (B3LYP/SDD for I, 6-311G(d) for B, H) coordinates for 6-I-$B_{10}H_{13}$.

Center Number	Atomic Number	X	Y	Z
1	5	-2.3907	-0.89049	1.062495
2	5	-0.8831	0.00000	1.416587
3	5	-2.3907	0.890493	1.062495
4	5	-3.5559	0.000000	0.047133
5	5	-0.8971	-1.42667	0.328184
6	5	0.15071	0.000000	0.038783
7	5	-0.8971	1.426669	0.328184
8	5	-2.6688	1.422609	-0.58272

9	5	-3.0566	0.000000	-1.60202
10	5	-2.6688	-1.42261	-0.58272
11	1	-2.8091	-1.62417	1.894557
12	1	-0.4203	0.00000	2.505457
13	1	-2.8091	1.624168	1.894557
14	1	-4.7064	0.00000	0.325119
15	1	-0.385	-2.47273	0.527927
16	53	2.31439	0.00000	-0.11272
17	1	-0.385	2.472727	0.527926
18	1	-3.1257	2.476128	-0.86598
19	1	-3.6929	0.00000	-2.5982
20	1	-3.1257	-2.47613	-0.86598
21	1	-0.3101	-0.96404	-0.76431
22	1	-0.3101	0.964036	-0.76431
23	1	-2.1463	0.968947	-1.71236
24	1	-2.1463	-0.96895	-1.71236

Table 3.2.23. DFT optimized (B3LYP/SDD for I, 6-311G(d) for B, H) coordinates for 6-I-$B_{10}H_{12}^{-}$.

Center Number	Atomic Number	X	Y	Z
1	5	2.39128	1.07279	0.936281
2	5	0.96292	0.202964	1.479312
3	5	2.44129	-0.71826	1.152277
4	5	3.50775	0.0551	-0.06269
5	5	0.86762	1.463218	0.169228
6	5	-0.0592	0.112846	0.059574
7	5	0.88112	-1.30934	0.560914
8	5	2.68661	-1.48063	-0.39571
9	5	2.932	-0.22771	-1.6474
10	5	2.44093	1.297691	-0.83778
11	1	2.95928	1.868414	1.620979
12	1	0.54509	0.298919	2.590987
13	1	2.93922	-1.33144	2.046232
14	1	4.68143	0.141632	0.121297
15	1	0.43128	2.563238	0.33594
16	53	-2.2868	-0.02446	-0.11515
17	1	0.38791	-2.34829	0.859367
18	1	3.18412	-2.55507	-0.50941

19	1	3.56353	-0.34241	-2.64773
20	1	2.84953	2.283744	-1.36775
21	1	0.3856	-0.94049	-0.6064
22	1	2.10057	-1.26572	-1.57075
23	1	1.91179	0.580527	-1.8397

Table 3.2.24. DFT optimized (B3LYP/SDD for I, 6-311G(d) for B, H) coordinates for 5-I-$B_{10}H_{13}$.

Center Number	Atomic Number	X	Y	Z
1	5	-1.0967	-0.39272	1.162824
2	5	-1.0139	1.348496	0.754627
3	5	-2.5939	0.569705	1.026752
4	5	-2.6284	-1.18322	0.694156
5	5	-0.0155	0.135152	-0.10727
6	5	-0.7251	1.563605	-0.93002
7	5	-2.4089	1.65643	-0.32969
8	5	-3.481	-0.01562	-0.36577
9	5	-2.6696	-1.48047	-1.00224
10	5	-1.0979	-1.55542	-0.15019
11	1	-0.5558	-0.75992	2.150011
12	1	-0.5782	2.122662	1.535607
13	1	-3.2753	0.986478	1.902847
14	1	-3.1657	-1.92115	1.447338
15	53	2.15634	-0.07505	-0.01313
16	1	-0.1236	2.393579	-1.51637
17	1	-2.9912	2.679238	-0.44808
18	1	-4.6512	0.093784	-0.49681
19	1	-3.1701	-2.35368	-1.62204
20	1	-0.4914	-2.5691	-0.12218
21	1	-0.288	0.371075	-1.37346
22	1	-1.9059	1.413748	-1.53202
23	1	-3.0321	-0.33044	-1.57133
24	1	-1.4034	-1.37831	-1.42374

Table 3.2.25. DFT optimized (B3LYP/SDD for I, 6-311G(d) for B, H) coordinates for 5-I-$B_{10}H_{12}^{-}$.

Center Number	Atomic Number	X	Y	Z
1	5	-1.0564	-0.30568	1.182796
2	5	-1.029	1.385667	0.693929
3	5	-2.5929	0.620231	1.016855
4	5	-2.588	-1.15114	0.729633
5	5	-0.0886	0.133167	-0.18429
6	5	-0.7284	1.384163	-1.04734
7	5	-2.3825	1.64072	-0.42123
8	5	-3.5406	-0.04598	-0.27927
9	5	-2.7293	-1.49449	-0.94085
10	5	-1.0739	-1.42248	-0.23554
11	1	-0.5753	-0.68955	2.201615
12	1	-0.6012	2.228638	1.418074
13	1	-3.2654	1.057485	1.899478
14	1	-3.0731	-1.90396	1.514387
15	53	2.16917	-0.07344	-0.012
16	1	-0.2171	2.192016	-1.7588
17	1	-3.0102	2.631965	-0.62484
18	1	-4.7253	0.051117	-0.32282
19	1	-3.2579	-2.43374	-1.44161
20	1	-0.4865	-2.45637	-0.25325
21	1	-1.9555	1.187628	-1.56312
22	1	-3.1971	-0.39786	-1.52068
23	1	-1.5537	-1.2959	-1.48615

Table 3.2.26. DFT optimized (B3LYP/6-311G(d)) coordinates for 6-Cl-9-Et-$B_{10}H_{12}$.

Center Number	Atomic Number	X	Y	Z
1	5	-0.2045	-1.83777	0.890598
2	5	-1.6483	-1.28947	0.000176
3	5	-0.2046	-1.83795	-0.89033
4	5	1.32745	-1.65951	0.000047
5	5	-1.0277	-0.39104	1.427148
6	5	-1.7451	0.428694	0.000035
7	5	-1.0278	-0.39128	-1.42703
8	5	0.95144	-0.63568	-1.42019
9	5	1.88686	-0.0202	-0.00013
10	5	0.9516	-0.63543	1.420136
11	1	-0.3246	-2.76183	1.624085
12	1	-2.6441	-1.92909	0.000257
13	1	-0.3248	-2.76216	-1.62361
14	1	2.11826	-2.54202	0.000128
15	1	-1.5706	-0.27567	-2.47098
16	1	1.49117	-0.67212	-2.47329
17	1	1.49143	-0.67174	2.473188
18	1	3.87697	0.230778	-0.873
19	1	3.87737	0.230299	0.871985
20	6	3.3344	0.612021	-0.00028
21	1	2.89006	2.571503	0.882656
22	1	4.41202	2.517514	0.000001
23	6	3.38265	2.150745	0.000125
24	1	2.88967	2.57198	-0.88196
25	1	-0.89137	0.832405	0.96398
26	1	1.145212	0.576913	0.969066
27	1	1.145154	0.576736	-0.96936
28	1	-0.89139	0.832194	-0.96409
29	17	-3.15993	1.513003	-9.2E-05
30	1	-1.57034	-0.27519	2.471141

Table 3.2.27. DFT optimized (B3LYP/6-311G(d)) coordinates for 5-Cl-9-Et-$B_{10}H_{12}$.

Center Number	Atomic Number	X	Y	Z
1	5	-0.9332	0.527455	-1.24737
2	5	-1.7129	1.345939	0.144711
3	5	-0.2465	2.0359	-0.58884
4	5	0.81397	0.855406	-1.40081
5	5	-1.4885	-0.43557	0.101645
6	5	-1.3398	0.529608	1.614171
7	5	-0.3677	1.963382	1.151393
8	5	1.30368	1.644884	0.132675
9	5	1.74325	-0.06137	-0.26364
10	5	0.21725	-0.75472	-0.92401
11	1	-1.5689	0.386911	-2.23721
12	1	-2.7641	1.872867	0.01144
13	1	-0.3109	3.128212	-1.0457
14	1	1.27687	1.107082	-2.46214
15	17	-2.7692	-1.68582	-0.03137
16	1	-1.9900	0.383507	2.589747
17	1	-0.4037	2.911693	1.85776
18	1	2.17946	2.43134	0.259103
19	1	0.2622	-1.75282	-1.55789
20	1	3.91287	0.112096	-0.4724
21	1	3.25032	-1.30821	-1.23989
22	6	3.18689	-0.69706	-0.33222
23	1	2.92341	-2.40032	1.024694
24	1	4.60500	-1.94839	0.768457
25	6	3.595088	-1.54746	0.884351
26	1	3.583558	-0.96445	1.810934
27	1	-0.86661	-0.66364	1.259816
28	1	0.862434	-1.0066	0.18091
29	1	1.614449	0.636379	0.899358
30	1	-0.12971	0.945724	1.973905

Table 3.2.28. DFT optimized coordinates (B3LYP/6-311G(d)) for 6-Cl-9-Et-$B_{10}H_{11}^{-}$.

Center Number	Atomic Number	X	Y	Z
1	5	-0.2995	-1.8636	0.923275
2	5	-1.688	-1.34147	-0.01634
3	5	-0.2333	-1.86338	-0.8791
4	5	1.27422	-1.62956	0.057196
5	5	-1.0922	-0.38411	1.411501
6	5	-1.6748	0.413825	0.095339
7	5	-1.0773	-0.39234	-1.38407
8	5	0.94621	-0.69826	-1.41252
9	5	1.81229	-0.00284	0.002947
10	5	0.77411	-0.51255	1.394123
11	1	-0.3174	-2.83678	1.614722
12	1	-2.691	-1.98327	-0.07715
13	1	-0.3113	-2.80157	-1.61242
14	1	2.09802	-2.49039	0.117424
15	1	-1.5696	-0.22561	-2.45402
16	1	1.51007	-0.79315	-2.4573
17	1	1.33856	-0.45919	2.444195
18	1	3.8671	0.129209	-0.79525
19	1	3.79024	0.185001	0.9479
20	6	3.30302	0.561978	0.040438
21	1	2.91794	2.562439	0.843947
22	1	4.47788	2.421029	0.030349
23	6	3.43204	2.093892	-0.00181
24	1	2.9909	2.509317	-0.91455
25	1	1.010816	0.66665	0.824477
26	1	1.153035	0.549614	-1.03304
27	1	-0.80984	0.775471	-0.86072
28	17	-3.05511	1.623985	-0.01699
29	1	-1.63797	-0.38022	2.47661

Table 3.2.29. DFT optimized (B3LYP/6-311G*) coordinates for 5-Cl-9-Et-$B_{10}H_{11}^{-}$.

Center Number	Atomic Number	X	Y	Z
1	5	-1.002	0.515747	-1.21275
2	5	-1.713	1.375768	0.149023
3	5	-0.2444	2.026725	-0.58905
4	5	0.7795	0.776076	-1.3669
5	5	-1.4692	-0.41328	0.181739
6	5	-1.2852	0.440414	1.583987
7	5	-0.3857	1.930154	1.176041
8	5	1.32309	1.655712	0.070026
9	5	1.72348	-0.07247	-0.21341
10	5	0.13355	-0.77769	-0.70206
11	1	-1.5642	0.38625	-2.25553
12	1	-2.752	1.949644	0.040532
13	1	-0.2858	3.11174	-1.08373
14	1	1.24096	0.944384	-2.45382
15	17	-2.843	-1.66227	-0.02309
16	1	-1.836	0.342166	2.638137
17	1	-0.3357	2.878001	1.89568
18	1	2.20023	2.459475	0.124525
19	1	0.22023	-1.82422	-1.26418
20	1	3.88826	0.070022	-0.62766
21	1	3.14774	-1.37842	-1.26106
22	6	3.16928	-0.72174	-0.38291
23	1	3.01418	-2.34783	1.075273
24	1	4.67818	-1.94506	0.64763
25	6	3.684669	-1.51825	0.827713
26	1	3.759949	-0.88908	1.72165
27	1	0.880792	-0.90912	0.38853
28	1	1.696589	0.694007	0.893765
29	1	-0.04761	0.870743	1.860716

Table 3.2.30. DFT optimized (B3LYP/SDD for I, 6-311G(d) for B, H, C) coordinates for 5-I-9-Et-$B_{10}H_{12}$.

Center Number	Atomic Number	X	Y	Z
1	5	-0.3467	0.622851	1.318614
2	5	0.13249	1.995063	0.272394
3	5	-1.5329	1.886942	0.896882
4	5	-2.0859	0.232456	1.259487
5	5	0.61879	0.310934	-0.10507
6	5	0.2004	1.507247	-1.37658
7	5	-1.2841	2.311501	-0.78045
8	5	-2.7566	1.154791	-0.12145
9	5	-2.5098	-0.63486	-0.18087
10	5	-0.8707	-0.86031	0.540718
11	1	0.2234	0.474222	2.345823
12	1	0.87666	2.821233	0.676509
13	1	-1.9308	2.771265	1.579219
14	1	-2.67	0.009888	2.266254
15	53	2.64403	-0.50914	-0.03323
16	1	0.90425	1.859746	-2.25707
17	1	-1.5829	3.352048	-1.25771
18	1	-3.8566	1.581071	-0.20672
19	1	-0.5662	-1.93262	0.935746
20	1	0.23259	0.16659	-1.35774
21	1	-1.0542	1.518137	-1.82088
22	1	-2.6094	0.337598	-1.12838
23	1	-1.3025	-1.03677	-0.67535
24	6	-3.5673	-1.7759	-0.46795
25	1	-3.30869	-2.63487	0.162719
26	1	-3.46141	-2.14002	-1.49844
27	6	-5.03378	-1.38199	-0.22254
28	1	-5.35281	-0.57061	-0.88204
29	1	-5.69964	-2.23013	-0.40188
30	1	-5.19314	-1.04793	0.805641

Table 3.2.31. DFT optimized (B3LYP/SDD for I, 6-311G(d) for B, H, C) coordinates for 5-I-9-Et-$B_{10}H_{11}^{-}$.

Center Number	Atomic Number	X	Y	Z
1	5	-0.31852	0.623533	1.283883
2	5	0.116869	2.005003	0.281624
3	5	-1.54429	1.881603	0.879875
4	5	-2.07159	0.194999	1.175456
5	5	0.553839	0.32371	-0.18188
6	5	0.191151	1.40099	-1.37598
7	5	-1.23799	2.315423	-0.81469
8	5	-2.79537	1.180009	-0.1051
9	5	-2.52998	-0.58887	-0.28237
10	5	-0.83024	-0.79948	0.303386
11	1	0.158916	0.426831	2.356427
12	1	0.847546	2.852613	0.688808
13	1	-1.95486	2.741252	1.597489
14	1	-2.64234	-0.10383	2.17886
15	53	2.66611	-0.50412	-0.01767
16	1	0.817399	1.777479	-2.3176
17	1	-1.58706	3.343089	-1.30493
18	1	-3.89882	1.623577	-0.12862
19	1	-0.56533	-1.91986	0.604529
20	1	-1.09267	1.436529	-1.76616
21	1	-2.71291	0.407691	-1.17066
22	1	-1.39084	-0.88888	-0.89747
23	6	-3.60653	-1.74513	-0.51402
24	1	-3.25053	-2.63793	0.01482
25	1	-3.63408	-2.03535	-1.57381
26	6	-5.03486	-1.42008	-0.0499
27	1	-5.45058	-0.56615	-0.593
28	1	-5.71239	-2.26838	-0.2028
29	1	-5.05621	-1.16368	1.012728

Table 3.2.32. DFT optimized (B3LYP/SDD for I, 6-311G(d) for B, H, C) coordinates for 6-I-9-Et-$B_{10}H_{12}$.

Center Number	Atomic Number	X	Y	Z
1	5	1.408372	-2.03289	0.890198
2	5	-0.13634	-1.91399	0.000344
3	5	1.408251	-2.03324	-0.88967
4	5	2.825081	-1.42592	0.000053
5	5	0.210002	-0.88012	1.426251
6	5	-0.70437	-0.28917	0.000055
7	5	0.20979	-0.88067	-1.42607
8	5	2.174311	-0.5508	-1.41999
9	5	2.89401	0.304857	-0.00026
10	5	2.174482	-0.55023	1.419763
11	1	1.556162	-2.95239	1.624361
12	1	-0.9071	-2.81173	0.000482
13	1	1.555961	-2.95312	-1.62338
14	1	3.835103	-2.0456	0.000115
15	1	-0.3386	-0.91517	-2.47254
16	1	2.701825	-0.43219	-2.47317
17	1	2.702171	-0.43116	2.472791
18	1	-0.02705	0.338793	-0.96127
19	1	2.012255	0.666348	-0.96963
20	1	2.012092	0.666627	0.968917
21	6	4.112204	1.309938	-0.00035
22	1	4.737745	1.088872	-0.87287
23	1	4.738038	1.088642	0.871918
24	6	3.744927	2.804599	0.000094
25	1	3.158601	3.078243	0.883089
26	1	4.63862	3.433558	-0.00063
27	1	3.157024	3.078443	-0.88178
28	53	-2.72883	0.49529	-4.2E-05
29	1	-0.33824	-0.91414	2.472822
30	1	-0.02724	0.339201	0.961159

Table 3.2.33. DFT optimized (B3LYP/SDD for I, 6-311G(d) for B, H, C) coordinates for 6-I-9-Et-$B_{10}H_{11}^{-}$.

Center Number	Atomic Number	X	Y	Z
1	5	-1.43825	1.710732	1.142081
2	5	0.1077	1.89798	0.323727
3	5	-1.37788	2.069056	-0.62482
4	5	-2.76338	1.152867	0.042903
5	5	-0.20108	0.51458	1.469568
6	5	0.698779	0.261608	0.120777
7	5	-0.0288	1.113513	-1.25778
8	5	-2.02562	0.709351	-1.50377
9	5	-2.67985	-0.513	-0.35966
10	5	-2.00096	0.018329	1.225524
11	1	-1.80956	2.462687	1.991423
12	1	0.813714	2.838463	0.514931
13	1	-1.59515	3.109208	-1.16721
14	1	-3.83879	1.660494	0.135993
15	1	0.550639	1.343667	-2.26928
16	1	-2.51386	0.821043	-2.58387
17	1	-2.56531	-0.4292	2.174522
18	1	0.117511	-0.17262	-0.98274
19	1	-1.78652	-0.57703	-1.37147
20	1	-1.74682	-1.02291	0.447241
21	6	-3.85577	-1.55181	-0.65929
22	1	-3.44099	-2.54132	-0.89763
23	1	-4.37145	-1.22913	-1.5727
24	6	-4.88729	-1.7082	0.469748
25	1	-5.34476	-0.74784	0.722256
26	1	-5.6907	-2.39906	0.188296
27	1	-4.42665	-2.09209	1.383995
28	53	2.800412	-0.50194	-0.01984
29	1	0.231885	0.463468	2.582483

Table 3.2.34. Calculated free energies (ΔG in kcal/mol, 333 K (60 °C)) and electronic energies (ΔE in kcal/mol, 333 K (60 °C)) at B3LYP/6-311G(d) for the isomerization of 6-F-$B_{10}H_{13}$.

Free Energy (ΔG)					
	G (in	**ΔG**		**G (in Hartrees)**	**ΔG**
6F	-356.218740	0.00	**6F⁻**	-355.724520	0.00
5F	-356.218539	0.13	**5F⁻**	-355.722225	1.44
Electronic Energy (ΔE)					
	E (in Hartrees)	**ΔE**		**E (in Hartrees)**	**ΔE**
6F	-356.181139	0.00	**6F⁻**	-355.686966	0.00
5F	-356.181056	0.05	**5F⁻**	-355.684758	1.38

Table 3.2.35. Calculated free energies (ΔG in kcal/mol, 333 K (60 °C)) and electronic energies (ΔE in kcal/mol, 333 K (60 °C)) at B3LYP/6-311G(d) for the isomerization of 6-Cl-$B_{10}H_{13}$.

Free Energy (ΔG)					
	G (in	**ΔG**		**G (in Hartrees)**	**ΔG**
6Cl	-716.562203	0.00	**6Cl⁻**	-716.075427	0.00
5Cl	-716.561951	0.16	**5Cl⁻**	-716.076238	-0.51
Electronic Energy (ΔE)					
	E (in Hartrees)	**ΔE**		**E (in Hartrees)**	**ΔE**
6Cl	-716.523473	0.00	**6Cl⁻**	-716.036704	0.00
5Cl	-716.523347	0.08	**5Cl⁻**	-716.037670	-0.61

Table 3.2.36. Calculated free energies (ΔG in kcal/mol, 333 K (60 ^{o}C)) and electronic energies (ΔE in kcal/mol, 333 K (60 ^{o}C)) at B3LYP/6-311G(d) for B and H atoms, and the SDD psuedopotential for Br, for the isomerization of 6-Br-$B_{10}H_{13}$.

Free Energy (ΔG)					
	G (in	**ΔG**		**G (in Hartrees)**	**ΔG**
6Br	-269.710274	0.00	**6Br$^-$**	-269.225964	0.00
5Br	-269.710066	0.13	**5Br$^-$**	-269.227775	-1.14
Electronic Energy (ΔE)					
	E (in Hartrees)	**ΔE**		**E (in Hartrees)**	**ΔE**
6Br	-269.670158	0.00	**6Br$^-$**	-269.185890	0.00
5Br	-269.670197	-0.02	**5Br$^-$**	-269.187876	-1.25

Table 3.2.27. Calculated free energies (ΔG in kcal/mol, 333 K (60 ^{o}C)) and electronic energies (ΔE in kcal/mol, 333 K (60 ^{o}C)) at B3LYP/6-311G(d) for the isomerization of 6-Br-$B_{10}H_{13}$.

Free Energy (ΔG)					
	G (in	**ΔG**		**G (in Hartrees)**	**ΔG**
6Br	-2830.480242	0.00	**6Br$^-$**	-2829.994781	0.00
5Br	-2830.479833	0.25	**5Br$^-$**	-2829.996097	-0.83
Electronic Energy (ΔE)					
	E (in Hartrees)	**ΔE**		**E (in Hartrees)**	**ΔE**
6Br	-2830.440131	0.00	**6Br$^-$**	-2829.954739	0.00
5Br	-2830.439962	0.11	**5Br$^-$**	-2829.956202	-0.92

Table 3.2.38. Calculated free energies (ΔG in kcal/mol, 333 K (60 ^{o}C)) and electronic energies (ΔE in kcal/mol, 333 K (60 ^{o}C)) at B3LYP/6-311G(d) for B and H atoms, and the SDD psuedopotential for I, for the isomerization of 6-I-$B_{10}H_{13}$.

Free Energy (ΔG)					
	G (in	**ΔG**		**G (in Hartrees)**	**ΔG**
6I	-267.742269	0.00	**6I⁻**	-267.260231	0.00
5I	-267.742367	-0.06	**5I⁻**	-267.262667	-1.53
Electronic Energy (ΔE)					
	E (in Hartrees)	**ΔE**		**E (in Hartrees)**	**ΔE**
6I	-267.701465	0.00	**6I⁻**	-267.219251	0.00
5I	-267.701618	-0.10	**5I⁻**	-267.221864	-1.64

Table 3.2.39. Calculated free energies (ΔG in kcal/mol, 333 K(60 ^{o}C)) and electronic energies (ΔE in kcal/mol, 333 K (60 ^{o}C)) at B3LYP/6-311G(d) for the isomerization of 6-Cl-9-Et-$B_{10}H_{12}$.

Free Energy (ΔG)					
	G (in Hartrees)	**ΔG**		**G (in Hartrees)**	**ΔG**
6-Cl-9-Et	-795.158218	0.00	**6-Cl-9-Et⁻**	-794.669352	0.00
5-Cl-9-Et	-795.159263	-0.66	**5-Cl-9-Et⁻**	-794.669447	-0.06
Electronic Energy (ΔE)					
	E (in Hartrees)	**ΔE**		**E (in Hartrees)**	**ΔE**
6-Cl-9-Et	-795.120428	0.00	**6-Cl-9-Et⁻**	-794.631196	0.00
5-Cl-9-Et	-795.121399	-0.61	**5-Cl-9-Et⁻**	-794.631332	-0.09

Table 3.2.40. Calculated free energies (ΔG in kcal/mol, 333 K(60 °C)) and electronic energies (ΔE in kcal/mol, 333 K (60 °C)) at B3LYP/6-311G(d) for B, C and H atoms, and the SDD psuedopotential for I, for the isomerization of 6-I-9-Et-$B_{10}H_{12}$.

Free Energy (ΔG)					
	G (in	**ΔG**		**G (in Hartrees)**	**ΔG**
6-I-9-Et	-346.345708	0.00	**6-I-9-Et⁻**	-345.859158	0.00
5-I-9-Et	-346.345105	0.38	**5-I-9-Et⁻**	-345.862464	-2.07
Electronic Energy (ΔE)					
	E (in Hartrees)	**ΔE**		**E (in Hartrees)**	**ΔE**
6-I-9-Et	-346.299631	0.00	**6-I-9-Et⁻**	-345.812887	0.00
5-I-9-Et	-346.298866	0.48	**5-I-9-Et⁻**	-345.815891	-1.89

3.3 Results and Discussion

3.3.1 Photochemical Isomerization of 6I to 5I. UV-vis spectroscopy revealed that the **6X** and **5X** (X = Cl, Br, I) derivatives and the parent $B_{10}H_{14}$ had absorption maxima between 250 and 350 nm. However, while neither **6Br** nor **6Cl** were photochemically reactive, ^{11}B NMR analysis showed that ultraviolet irradiation of pentane solutions of ~30-50 mg samples of **6I** for 24 h at room temperature gave quantitative conversions to **5I (Eq. 1).** Reaction workup with product recrystallization from cold pentane gave ~80% isolated yields of pure **5I**.

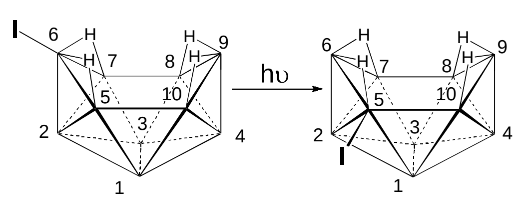

(1)

Although small scale **6I** photolysis reactions were quite suitable for **5I** syntheses, larger scale reactions proved to be less satisfactory, requiring substantially longer times and giving lower **5I** yields as a result of the formation of other unidentified side-products.

3.3.2 Base Catalyzed Isomerizations of 6-X-$B_{10}H_{13}$ and 5-X-$B_{10}H_{13}$. The syntheses of the 5-X-$B_{10}H_{13}$ (X = Cl, Br, I) halodecaboranes were readily achieved by treatment of their corresponding 6-X-$B_{10}H_{13}$ isomers with catalytic amounts (3%) of triethylamine (TEA) at 60 ^{o}C (**Eq. 2**).

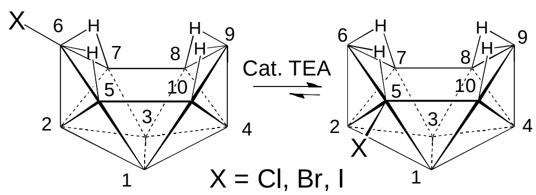

(**2**)

The ^{11}B NMR spectra in **Figure 3.3.1** monitored the progress of the isomerization of **6I** to **5I**. **Figure 3.3.1a** shows the spectrum of pure **6I** immediately after the addition of TEA. The reaction can be followed by the appearance of the B5 singlet resonance of **5I** (-15.2 ppm) and the corresponding decrease of the B6 singlet resonance of **6I** (-8.2 ppm). After 20 min, (**Figure 3.3.1b**) the -15.2 ppm resonance was clearly evident and after 40 min (**Figure 3.3.1c**) there were nearly equal amounts of **6I** and **5I**. No change in the ratio of the two isomers (~86:14 **5I/6I**) was observed after 80 min (**Figure 3.3.1e**). Recrystallization of the mixture yielded pure **5I**, the spectrum of which is shown in **Figure 3.3.1f**. The supernatant solution from the recrystallization, a solution enriched in **6I**, was subjected to a second isomerization reaction with TEA and workup. The total isolated yield of **5I** after two isomerizations was 68%.

A second photolytic-step could also be used to drive the TEA-catalyzed isomerization of **6I** to completion. For example, in one experiment 500 mg of **6I** was initially isomerized with 3% TEA to yield 309 mg (62%) of recrystallized **5I**. When the supernatant material from the recrystallization, which contained a mixture of **6I** and **5I**, was then irradiated for 24 h in dry, degassed pentane, near quantitative conversion to **5I** was observed by ^{11}B NMR. Recrystallization from this solution then gave an additional 101 mg of **5I**, for a total isolated yield from the two steps of 410 mg (82%) of pure **5I**.

Both **6Br** and **6Cl** were also found to undergo TEA-catalyzed isomerizations to their **5Br** and **5Cl** isomers. After 6 h at 60 °C, ^{11}B NMR analysis of the **6Br** reaction indicated the formation of an ~82:18 ratio **5Br**/**6Br** mixture. Separation of **5Br** by selective crystallization, followed by a second round of isomerization and crystallization of the supernatant mixture, gave a combined 83% isolated yield of **5Br**. Reaction of **6Cl** with TEA for 12 h at 60 ^{o}C produced a ~78:22 ratio **5Cl/6Cl** mixture. **5Cl** was most easily separated from this mixture by column chromatography. After isolation of pure **5Cl**, fractions from the column containing **6Cl** and mixtures of **5Cl** and **6Cl** were combined and subjected to a second isomerization and chromatographic separation to ultimately give a 71% total yield of pure **5Cl**.

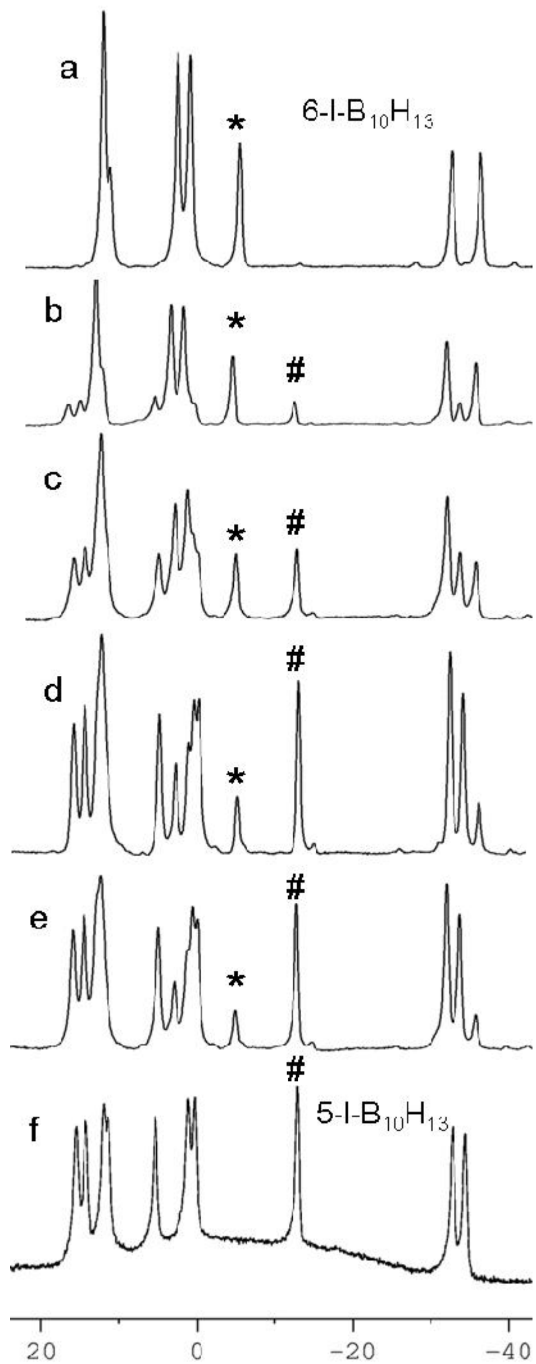

Figure 3.3.1. Isomerization of **6I** with 4 mol% TEA in toluene at 60 °C monitored by $^{11}B\{^{1}H\}$ NMR after: (**a**) 0 min, (**b**) 20 min, (**c**) 40 min, (**d**) 60 min, (**e**) 80 min, and (**f**) recrystallized, pure **5I**. ***** indicates 6-boron resonance in **6I**; **#** indicates 5-boron resonance in **5I**.

The melting points and ^{11}B NMR[6] and IR[10] spectra of **5I**, **5Br**, and **5Cl** match their reported values. COSY ^{11}B-^{11}B 2D NMR allowed for the assignment of ^{11}B resonances. **Figure 3.3.2** allows for definitive assignment of all resonances in **5Br**. The B5 resonance, a singlet in the ^{1}H-coupled ^{11}B NMR spectrum, is unambiguously assigned as the peak at ~2.0 ppm. This peak shows the expected cross-peaks with B2, B1 and weak cross-peaks with B6 and B10. The weakness of the cross-peak with B6 is not unusual as cross-peaks between neighboring boron atoms are weak, or often absent, when the two are bridged by hydrogen.[16] For this reason, the B6 resonance lacks the expected cross-peak with B7, and the B9 resonance lacks cross-peaks with anything, save B4. The weakness of the cross-peak between B5 and B10 is on account of the longer length of the B5-B10 bond (1.978(7) Å, discussed later). Cross-peaks between B8 and B7 are weak for this reason as well (B8-B7, 1.986(6) Å). The coincident B1/B3 peak shows cross-peaks with all resonances except B6 and B9, and the B4 and B2 resonances each show the appropriate cross-peaks to boron atoms on their respective side of the molecule.

In the COSY ^{11}B-^{11}B 2D spectrum of **5I** (**Figure 3.3.3**), the halogenated B5 has moved upfield, as found in the series of 6-halodecaboranes.[3] The B5-B6 cross-peak is not evident in this spectrum, on account of the bridging-hydrogen between them; however, the B5 resonance still shows the expected cross-peaks with B1, B2 and B10. In this spectrum, the B6 and B9 resonances, differentiated by cross-peaks with B2 and B4, respectively, have swapped relative position with the B6 resonance coming at lower field. Likewise, the B1 and B3 peaks, coincident in the spectrum of **5Br**, are separate in the **5I** spectrum, with the B1 resonance occupying lower field.

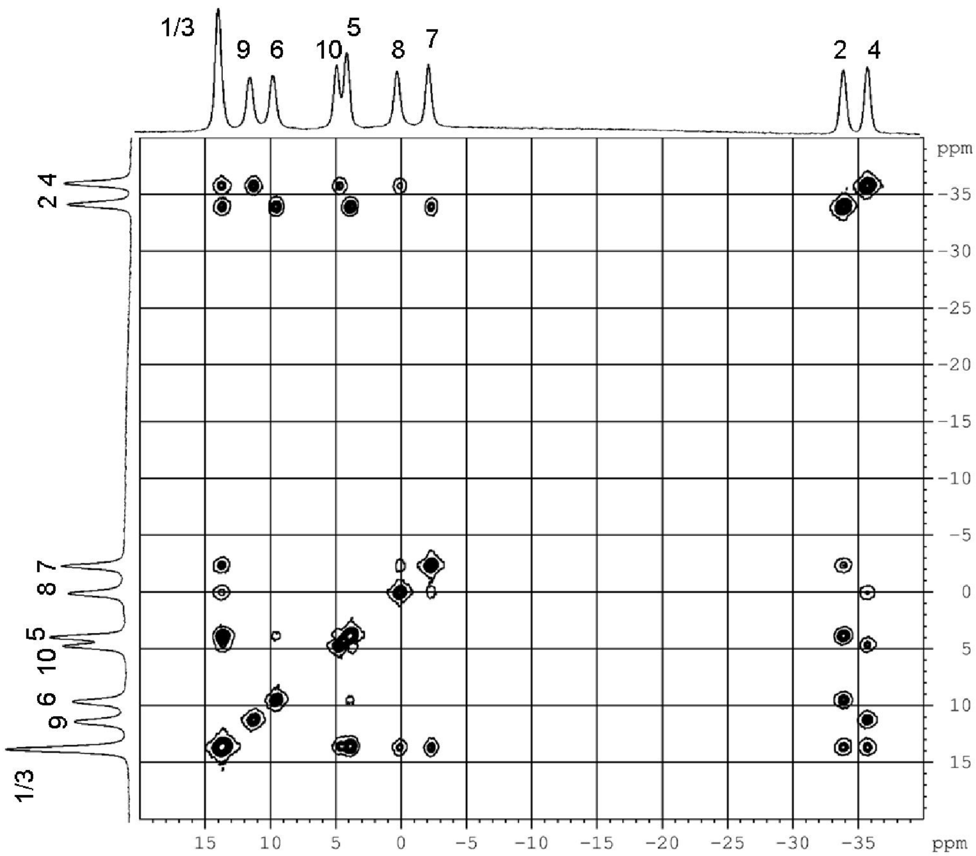

Figure 3.3.2. COSY ^{11}B-^{11}B 2D NMR spectrum of **5Br**.

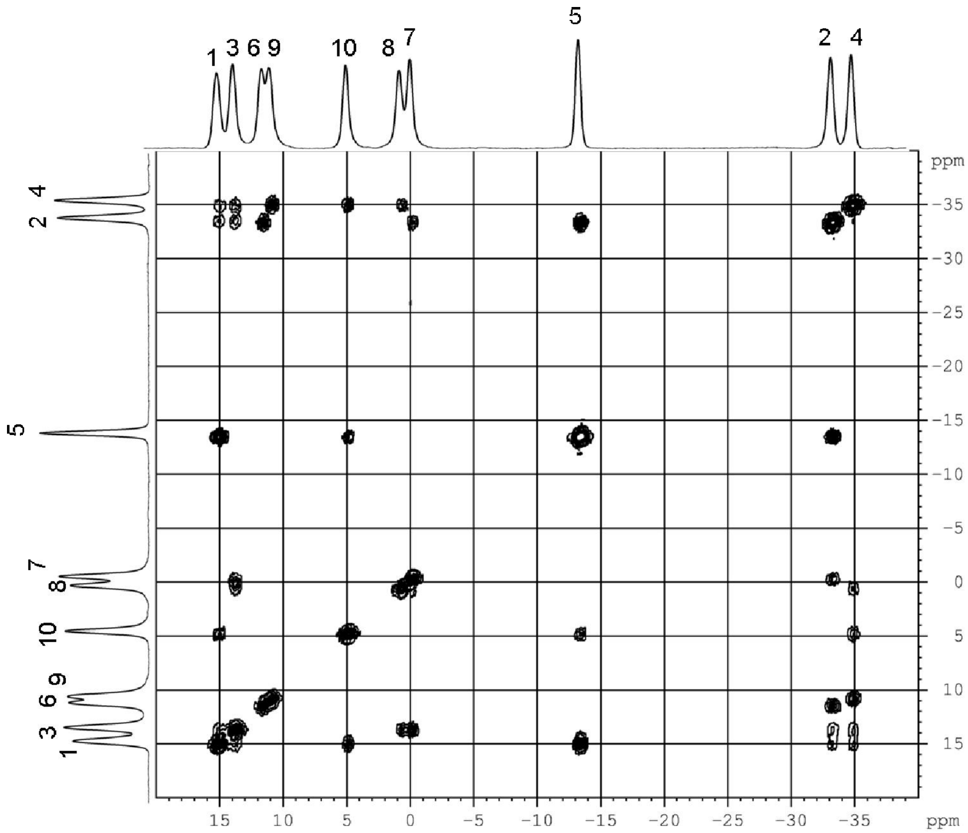

Figure 3.3.3. COSY ^{11}B-^{11}B 2D NMR spectrum of **5I.**

The ^{1}H NMR spectra of the **5X** compounds are consistent with C_1 symmetry, displaying 9 terminal B-H resonances (the two furthest downfield are coincident) and 4 individual bridging hydrogens, with 3 upfield and one downfield of 0.0 ppm. As shown in **Figure 3.3.4**, ^{11}B-^{1}H HCOR 2D NMR allowes for the assignment of these bridging protons, as well as the other proton resonances. The downfield bridging resonance is the bridge between the substituted B5 and B6. The intermediate two bridging resonances are each connected to a neighbor of B5, and the highest field resonance (μH, B8-B9) is the furthest from the halogenated vertex.

The proposed structures of **5I** and **5Br** were crystallographically confirmed, as shown in the ORTEP drawings in **Figure 3.3.5**. The halogen identity and position seem to have little effect on the B-B bonding within the cage, as evidenced by the fact the corresponding cage distances and angles in **5I**, **5Br**, **6I** and **6Br** are all quite similar. However, the B-X distances in **5Br** (1.958(4) Å and 1.945(4) Å for the two independent molecules) and **5I** (2.166(5) Å) are longer (either greater than, or just under 3σ) than those of **6Br** (1.929(4) Å) and **6I** (2.143(3) Å), respectively, suggesting less halogen π-backbonding to the cage[3] and potentially greater reactivity for **5I** and **5Br**. Analysis of populated molecular orbitals confirm the existence of π-character in the B-X bond (**Figure 3.3.6**).

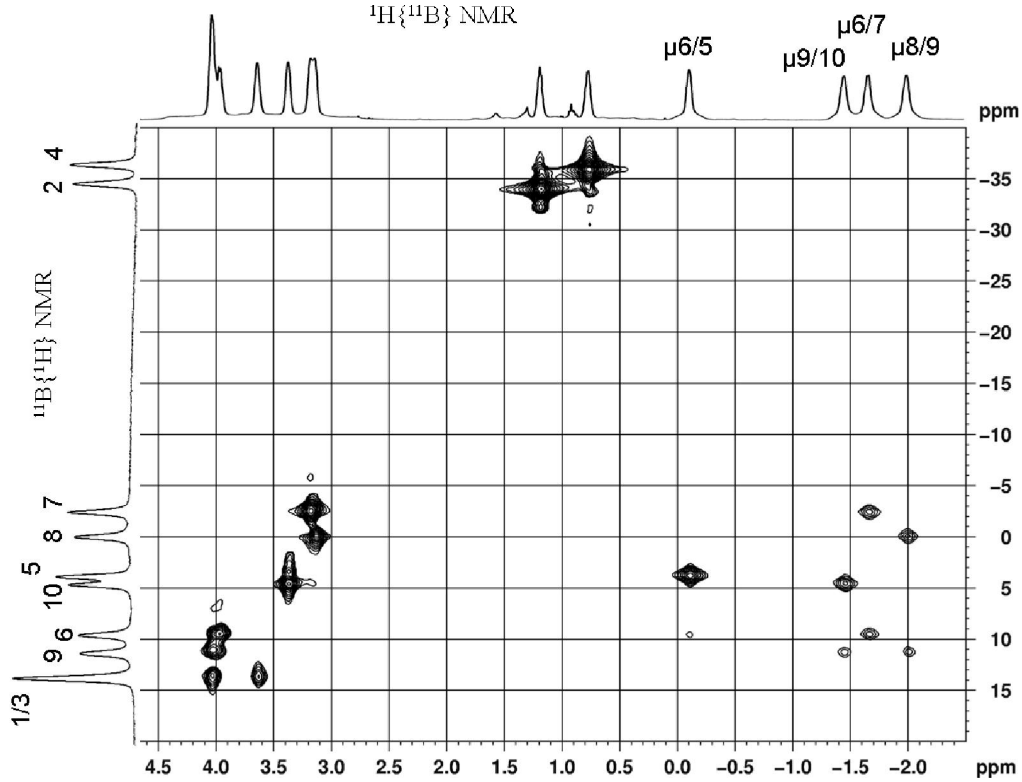

Figure 3.3.4. ^{11}B-^1H HCOR 2D NMR of **6Br**. The vertical axis shows the $^{11}B\{^1H\}$ NMR spectrum; the horizontal axis shows the $^1H\{^{11}B\}$ NMR spectrum.

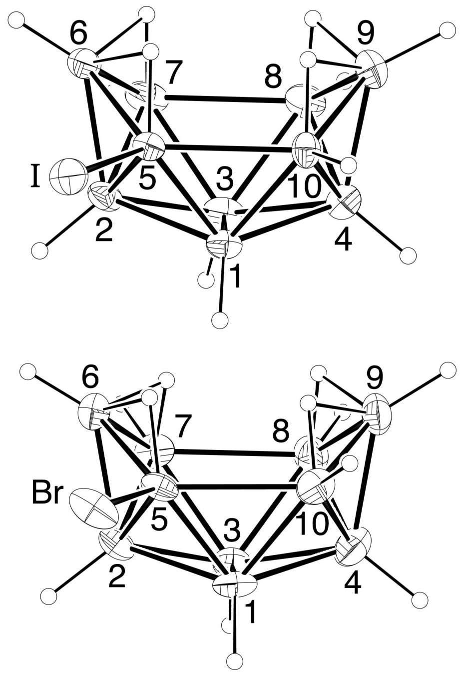

Figure 3.3.5. ORTEP drawings of the crystallographically determined structure of **5I** (top) and one of the two independent structures of **5Br** (bottom). Selected bond lengths (Å) and bond angles (deg): **5I**: B5-I, 2.166(5); B5-B6, 1.788(7); B6-B7, 1.781(9); B7-B8, 1.986(9); B8-B9, 1.784(8); B9-B10, 1.789(7); B10-B5, 1.968(7); B6-B2, 1.715(7); B9-B4, 1.729(7); I-B5-B6, 118.7(3); B2-B5-B6, 57.4(3); B4-B10-B9, 57.9(3); B5-B6-B7, 104.8(4); B8-B9-B10, 104.8(3). **5Br**: B5-Br, 1.958(4); B5-B6, 1.787(6); B6-B7, 1.766(6); B7-B8, 1.986(6); B8-B9, 1.806(7); B9-B10, 1.768(7); B10-B5, 1.978(7); B6-B2, 1.724(6); B9-B4, 1.729(7); Br-B5-B6, 120.4(3); B2-B5-B6, 57.8(2); B4-B10-B9, 58.1(3); B5-B6-B7, 104.3(3); B8-B9-B10, 105.4(3).

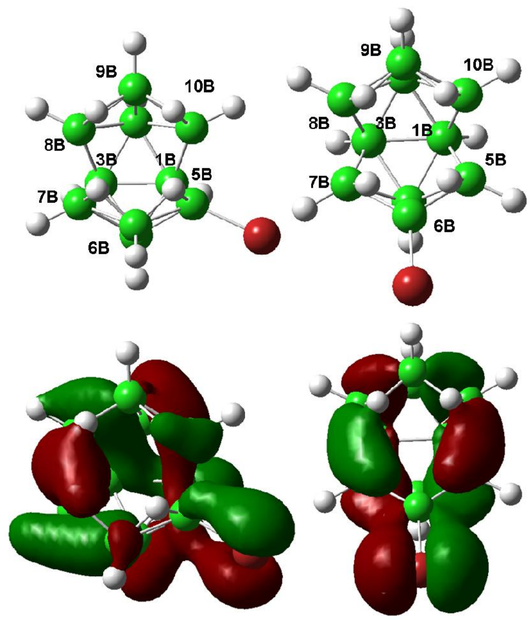

Figure 3.3.6. One molecular orbital (MO = 47) contributing to B-X π-backbonding in **5Br** and **6Br**, calculated at the B3LYP/6-311G(d) level of theory.

When pure samples of **5Cl**, **5Br** and **5I** were reacted for 12 h with 4 mol% of TEA in toluene at 60 °C, **5X/6X** mixtures were again produced (**Eq. 3**) with the observed isomer ratios identical to those obtained in the reactions starting with the 6-X-isomer (**Eq. 2**). This result suggests that these ratios correspond to thermodynamic equilibrium mixtures of the two isomers.

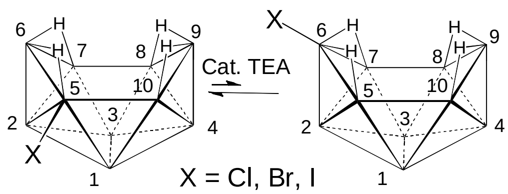

(**3**)

However, as can be seen in **Figure 3.3.7**, DFT calculations of the relative free energy of the 6-X-$B_{10}H_{13}$ and 5-X-$B_{10}H_{13}$ isomers, show that isomerization is nearly energetically neutral for these compounds, with the largest energy difference of +0.25 kcal/mol for the **6Br** reaction in fact favoring the **6Br** isomer. Based on these calculations, an equilibrium ratio near 1:1 would have been expected rather than the observed ratios favoring the **5X** isomers.

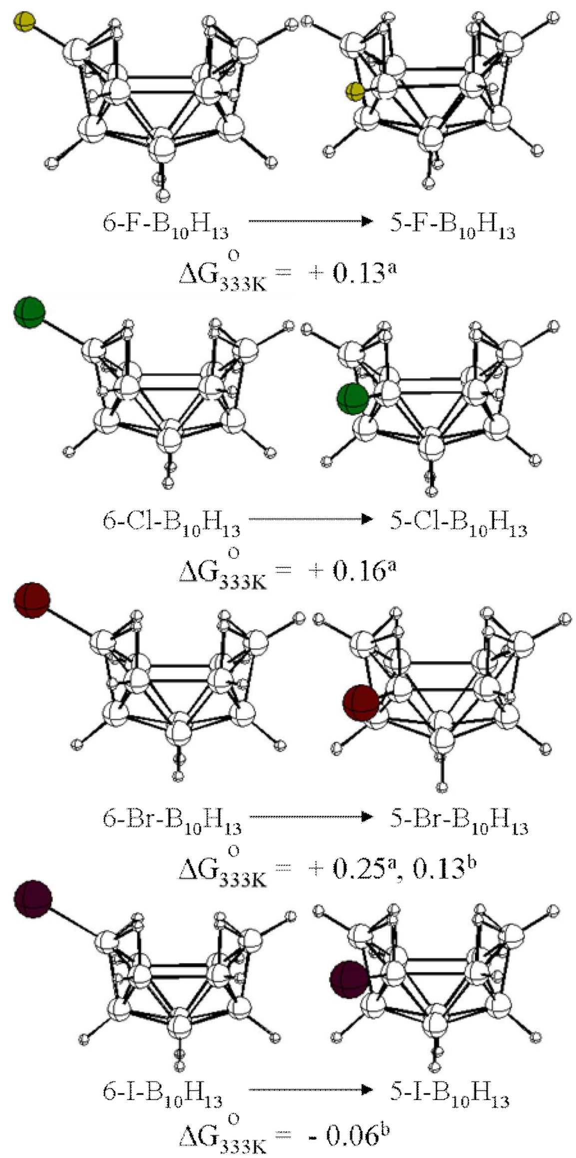

Figure 3.3.7. DFT optimized geometries of 6-X- and 5-X-$B_{10}H_{13}$ and the calculated free energy changes for the isomerization of 6-X- to 5-X-$B_{10}H_{13}$ at 60 ^{o}C. [a]Optimization and free energy calculation utilized the B3LYP/6-311G(d) basis set. [b]Optimization and free energy calculation utilized the B3LYP/6-311G(d) basis set for all H and B atoms, and the SDD pseudopotential for all halogen electrons

The questions that then arise are: (1) What is the activating role of the bases in these isomerization reactions? and (2) What determines the equilibrium isomer ratio? Decaborane is known to form adducts at the B6 and B9 positions with strong Lewis bases.[17] On the other hand, strong Brønsted bases readily abstract an acidic bridging-hydrogen to produce the $B_{10}H_{13}^-$ anion.[18] A reaction of **6I** with a catalytic amount of dibutylsulfide, a strong Lewis but weak Brønsted base, [19] at 60 °C for 3 days gave only a trace of **5I**. A reaction of **6I** with triphenylphosphine, also a strong Lewis base but a somewhat better Brønsted base than dibutylsulfide,[20] reached 60% **5I** after 12 h at 60 °C and 85% **5I** after 20 h. This reaction was substantially slower than the TEA (stronger Brønsted base, pK_a = 10.68[21]) catalyzed isomerization, which was complete after only 80 min. Amines with greater (diisopropylethylamine) or lesser (propylamine) steric bulk but comparable Brønsted basicity[19,22] showed nearly identical rates and yields as TEA, again providing evidence that adduct formation (i.e. Lewis basicity) is not a driving force in the isomerization. Further support for this hypothesis was found by the observation that **6I** also isomerized in the presence of catalytic amounts of tetrabutylammonium chloride to form the ~87:13 **5I**/**6I** ratio after 10 h at 60 °C. While HCl is a strong acid in water, it is only partially disassociated in many organic solvents (for example in dichloroethane: pKa = 10.8, HCl)[23] and it has been previously demonstrated that the Brønsted basicity of chloride ion is sufficient to deprotonate decaborane in organic solvents.[8] It is also significant that no halogen exchange was seen in the **6I** isomerizations with the chloride ion, providing evidence that halo dissociation/association is not a step in the halo isomerization reaction.

When the **6X** and **5X** compounds were each reacted with stoichiometric amounts of the non-nucleophilic, strong Brønsted base (pKa ~12) bis(dimethylamino)naphthalene, Proton Sponge (PS),[24] immediate deprotonation to form their 6-X-$B_{10}H_{12}^-$ (**6X⁻**) and 5-X-$B_{10}H_{12}^-$ (**5X⁻**) anions resulted. DFT calculations showed that the structures shown in **Figure 3.3.8a** for **6Cl⁻** and **Figure 3.3.9a** for **5Cl⁻**, where deprotonation occurred at a site adjacent to the halogen-substituted borons, are the energetically favored isomers for these anions. As can be seen in **Figures 3.3.8b** and **3.3.9b**, crystallographic determinations of the [PSH^+][**6Cl⁻**] and [PSH^+][**5Cl⁻**] salts confirmed these predictions. The intracage distances and angles in both anions are similar to those found in the crystallographic determinations of the parent [Et_3NH^+][$B_{10}H_{13}^-$][25] and [$PhCH_2NMe_3^+$][$B_{10}H_{13}^-$][26] salts with the unbridged B5-B6 distances (**6Cl⁻**, 1.631(3) Å; **5Cl⁻**, 1.644(3) Å) significantly shortened relative to those of the hydrogen-bridged B6-B7, B8-B9 and B9-B10 borons. The B5-B10 distance in **5Cl⁻** (1.844(3) Å) is also considerably shortened relative to its corresponding B7-B8 distance (2.208(3) Å). The B5-Cl distance in **5Cl⁻** (1.844(2) Å) is significantly longer than the B6-Cl distance in **6Cl⁻** (1.811(2) Å) with both of the distances being longer than the B6-Cl distance of **6Cl** (1.764(2) Å)[3] suggesting reduced Cl to B π back-donation in the more electron-rich anions.

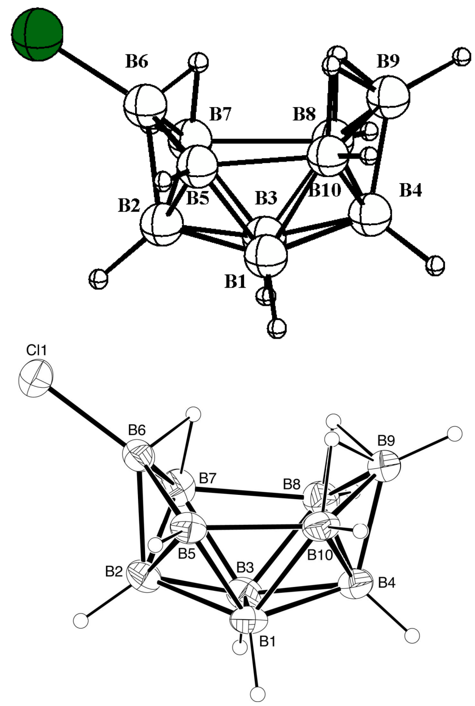

Figure 3.3.8. (top) DFT (B3LYP/6-311G(d)) optimized geometry and (bottom) crystallographically determined structure of **6Cl^{-}.** Selected bond lengths (Å) and bond angles (º): (**top**) B6-Cl, 1.838; B5-B6, 1.645; B6-B7, 1.789; B7-B8, 2.046; B8-B9, 1.790; B9-B10, 1.800; B10-B5, 1.867; B6-B2, 1.760; B9-B4, 1.711; B2-B5, 1.820; B1-B5, 1.748; B1-B10, 1.788; B1-B4, 1.812; B3-B7, 1.771; B3-B8, 1.741; B1-B3, 1.804; Cl-B6-B2, 130.65; B7-B6-B5, 109.03; B8-B9-B10, 103.67; Cl-B6-B5, 129.41; Cl-B6-B7, 119.72; B6-B5-B10, 112.19; B6-B7-B8, 114.20; B7-B8-B9, 113.13; B5-B10-B9, 123.40. (**bottom**) B6-Cl, 1.811(2); B5-B6, 1.631(3); B6-B7, 1.781(3); B7-B8, 2.019(3); B8-B9, 1.772(4); B9-B10, 1.787(3); B10-B5, 1.862(3): B6-B2, 1.752(3); B9-B4, 1.709(3); B2-B5, 1.798(3); B1-B5, 1.738(3); B1-B10, 1.783(3); B1-B4, 1.805(3); B3-B7, 1.761(3); B3-B8, 1.742(3); B1-B3, 1.793(3); Cl-B6-B2, 129.80(14); B7-B6-B5, 108.46(16); B8-B9-B10, 103.65(15); Cl-B6-B5, 128.63(15); Cl-B6-B7, 120.70(14); B6-B5-B10, 111.47(15); B6-B7-B8, 114.84(15); B7-B8-B9, 112.95(15); B5-B10-B9, 123.83(16).

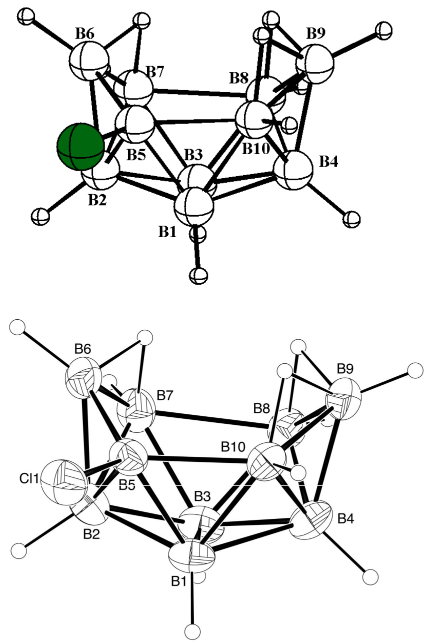

Figure 3.3.9. (top) DFT (B3LYP/6-311G(d)) optimized geometry and (bottom) crystallographically determined structure of **5Cl⁻**. Selected bond lengths (Å) and bond angles (º): (**top**) B5-Cl, 1.867; B5-B6, 1.652; B6-B7, 1.787; B7-B8, 2.052; B8-B9, 1.786; B9-B10, 1.797; B10-B5, 1.860; B6-B2, 1.767; B9-B4, 1.710; B2-B5, 1.805; B2-B7, 1.768; B1-B5, 1.739; B1-B10, 1.797; B1-B4, 1.807; B3-B7, 1.775; B3-B8, 1.739; B1-B3, 1.801; Cl-B5-B2, 124.08; B7-B6-B5, 107.12; B8-B9-B10, 103.94; Cl-B5-B1, 118.00; Cl-B5-B6, 121.26; B6-B5-B10, 113.78; B6-B7-B8, 115.44; B7-B8-B9, 112.52; B5-B10-B9, 122.77. (**bottom**) B5-Cl, 1.844(2); B5-B6, 1.644(3); B6-B7, 1.775(3); B7-B8, 2.028(3); B8-B9, 1.773(3); B9-B10, 1.791(3); B10-B5, 1.844(3): B6-B2, 1.754(3); B9-B4, 1.702(3); B2-B5, 1.790(3); B2-B7, 1.764(3); B1-B5, 1.737(3); B1-B10, 1.796(3); B1-B4, 1.804(3); B3-B7, 1.770(3); B3-B8, 1.737(3); B1-B3, 1.787(3); Cl-B5-B2, 124.80(13); B7-B6-B5, 106.75(16); B8-B9-B10, 103.96(15); Cl-B5-B1, 117.67(13); Cl-B5-B6, 121.75(14); B6-B5-B10, 113.82(15); B6-B7-B8, 116.19(15); B7-B8-B9, 112.06(14); B5-B10-B9, 122.59(15).

Figure 3.3.10a shows the ^{11}B NMR spectrum of **6Br**, while **Figure 3.3.10b** is that of **6Br⁻** resulting from its reaction with one equivalent of PS. The **6Br⁻** solution was held at 60 °C in dichlorobenzene and its isomerization to **5Br⁻** monitored over time. Since the 6B resonance in **6Br⁻** and the 5B resonance in **5Br⁻** are coincident (~25 ppm), the progress of the isomerization can be most easily followed through the appearance of the 4.5 ppm resonance of **5Br⁻** along with the corresponding disappearance of the -2.0 ppm resonance of **6Br⁻**. After 90 min at 60 °C, equal amounts of the two anions were present (**Figure 3.3.10d**), and after 130 min, no further change in their relative amounts was observed (**Figure 3.3.10e**). Acidification at this point yielded same ~82:18 **5Br**:**6Br** ratio mixture that was found for the **6Br** isomerizations catalyzed with TEA (**Figure 3.3.10f**).

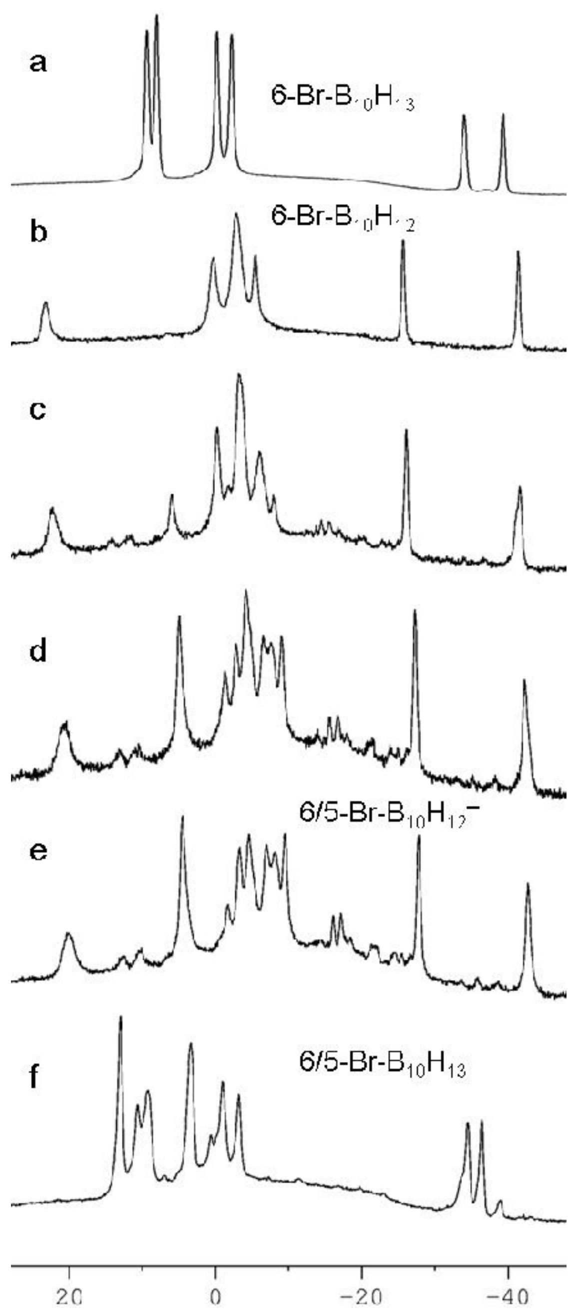

Figure 3.3.10. Deprotonation of **6Br** and isomerization of resultant **6Br⁻** at 60 °C in dichlorobenzene monitored by $^{11}B\{^{1}H\}$ NMR. (**a**) **6Br**, (**b**) 6-Br-$B_{10}H_{12}^{-}$, 0 min; (**c**) 60 min; (**d**) 90 min; (**e**) 130 min; (**f**) acidified mixture after 130 min.

The DFT calculated free energies for 6-X-$B_{10}H_{12}^-$ isomerization to 5-X-$B_{10}H_{12}^-$ at 60 ^oC (**Figure 3.3.11**) range from a positive value for **6F⁻**, to progressively more negative values as the halogen is changed from Cl to Br to I. This trend is consistent with the experimental results, in that the TEA-catalyzed reaction of **6F** gave only trace isomerization, while the reactions of **6Cl**, **6Br** and **6I** gave progressively higher equilibrium **5X**:**6X** ratios. In fact, as indicated in **Table 3.3.1**, the equilibrium constant values obtained from the calculated free energies of isomerization of these anions agree quite well with the experimentally observed values both in scale and trend ($K_I>K_{Br}>K_{Cl}>K_F$). Thus, both these calculations and the NMR study in **Figure 3.3.10** strongly support a mechanistic pathway (**Figure 3.3.12**) for the base-catalyzed **6X** to **5X** conversions involving formation and subsequent isomerization of the **6X⁻** anions with the final **6X**:**5X** equilibrium ratios determined by the energetic differences of their corresponding 6-X-$B_{10}H_{12}^-$ and 5-X-$B_{10}H_{12}^-$ anions.

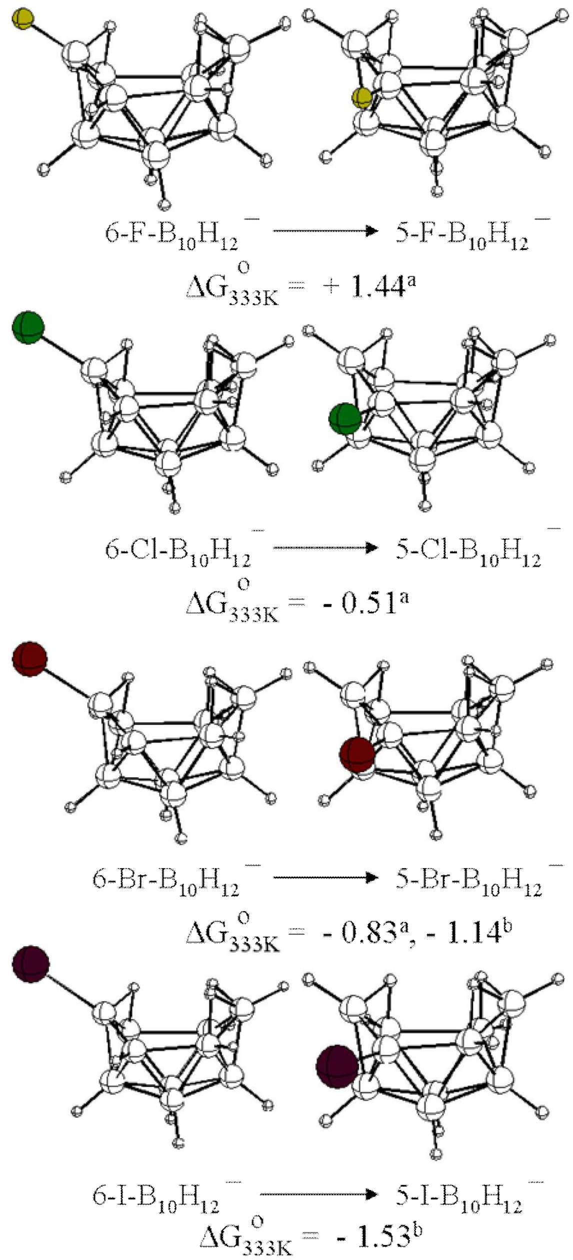

Figure 3.3.11. DFT optimized geometries of 6-X- and 5-X-$B_{10}H_{12}^{-}$ and calculated free energy changes in their isomerizations at 60 °C. [a] Optimization and free energy calculation at B3LYP/6-311G(d). [b] Optimization and free energy calculation used B3LYP/6-311G(d) for all H and B atoms, and the SDD pseudopotential for Br and I.

Table 3.3.1. Calculated and observed equilibrium constants for the isomerization of 6-X-$B_{10}H_{12}^{-}$ to 5-X-$B_{10}H_{12}^{-}$ at 60 °C. Calculated K values are derived from the DFT calculated ΔG^o of reaction at 60 °C.

X-$B_{10}H_{13}$	K_{calc} [$5X^-$]/[$6X^-$]	K_{obs} [5X]/[6X]
F	0.1[a]	<0.05
Cl	2.2[a]	3.5
Br	3.4[a]	4.9
	5.6[b]	
I	10.1[b]	6.1
6-R-X-$B_{10}H_{12}$[c]		
Cl	2.2[a]	2.9
I	23.2[b]	6.9
6-R-$B_{10}H_{13}$[c]	3.9×10^{-2}[a]	0
6,9-R_2-$B_{10}H_{12}$[c]	0.1[a]	0

[a] B3LYP/6-311G(d) level for all atoms. [b] B3LYP/6-311G(d) level for H and B atoms and the SDD pseudopotential for I. [c] R = C_2H_5 in calculated values, R = C_6H_{13} in observed values.

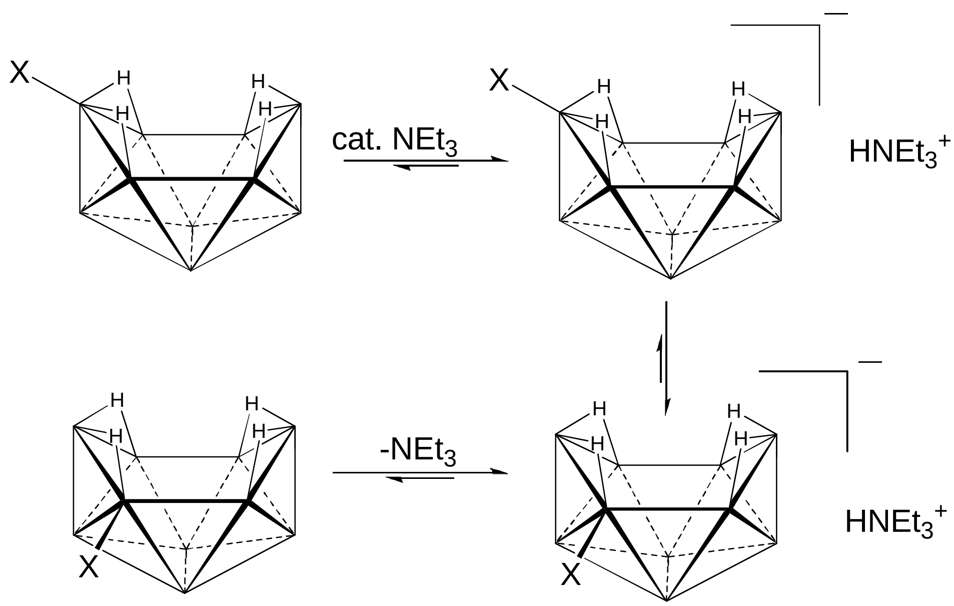

Figure 3.3.12. Proposed pathway for the base-catalyzed isomerization of 6X compounds.

3.3.3 Isomerization of 6-X-9-R-$B_{10}H_{12}$. In agreement with the DFT calculations of the relative energies of 6 and 5-substituted alkyl-isomers (Table 2), neither 6-(C_6H_{13})-$B_{10}H_{13}$ nor 6,9-(C_6H_{13})$_2$-$B_{10}H_{12}$ isomerized when reacted with 5% TEA at 60 ^{o}C (**Eq. 4**). However, when either 6-Cl-9-(C_6H_{13})-$B_{10}H_{12}$ or 6-I-9-(C_6H_{13})-$B_{10}H_{12}$ were treated with 4% TEA in toluene at 60 ^{o}C (**Eq. 5**), their ^{11}B NMR (for X = Cl, **Figure 3.3.13**) spectra showed the emergence of new C_1-symmetric species.

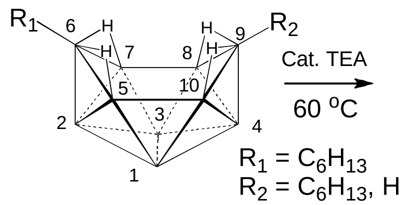

(4)

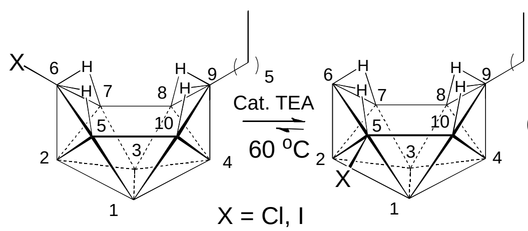

(5)

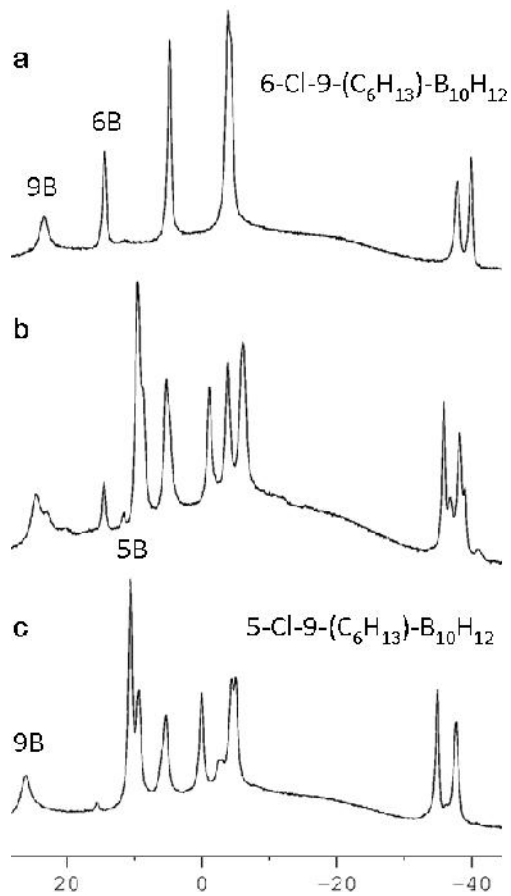

Figure 3.3.13. Isomerization of 6-Cl-9-(C_6H_{13})-$B_{10}H_{12}$ in toluene monitored by $^{11}B\{^1H\}$ NMR. (**a**) 6-Cl-(C_6H_{13})-$B_{10}H_{12}$ before base addition. (**b**) reaction mixture of 6-Cl-9-(C_6H_{13})-$B_{10}H_{12}$ and 5-Cl-9-(C_6H_{13})-$B_{10}H_{12}$ produced after 4 h at 60 °C. (**c**) 5-Cl-9-(C_6H_{13})-$B_{10}H_{12}$ isomer after column purification (spectrum taken in $CDCl_3$). Substituted boron peaks are labeled (singlet at 11.4 ppm is coincident with another resonance in (c)). DFT/GIAO calculated ^{11}B NMR shifts for the 5-Cl-9-(C_2H_5)-$B_{10}H_{12}$ model compound: 25.0 (B9), 14.5 (B5), 13.0 (B3), 11.0 (B1), 3.0 (B6), 1.9 (B10), -4.0 (B8), -4.5 (B7), -37.8 (B4), -39.5 (B2)

In principle, several different isomers resulting from either halo or alkyl migration could have formed, but DFT optimizations of the possible isomers showed that 5-X-9-R-$B_{10}H_{12}$ products (**5X-9R**) were energetically favored with the DFT/GIAO calculated chemical shifts for the model compound 5-Cl-9-(C_2H_5)-$B_{10}H_{12}$ being in excellent agreement with the experimentally observed shifts for 5-Cl-9-(C_6H_{13})-$B_{10}H_{12}$. In both reactions, equilibrium mixtures of the **5X-9R** and **6X-9R** isomers were formed with the experimentally observed ~3:1 (X = Cl) and ~7:1 (X = I) **5X-9R**:**6X-9R** equilibrium ratios again consistent with the DFT calculated differences in the free energies of the **5X-9Et$^-$** and **6X-9Et$^-$** model compounds (**Figure 3.3.14**).

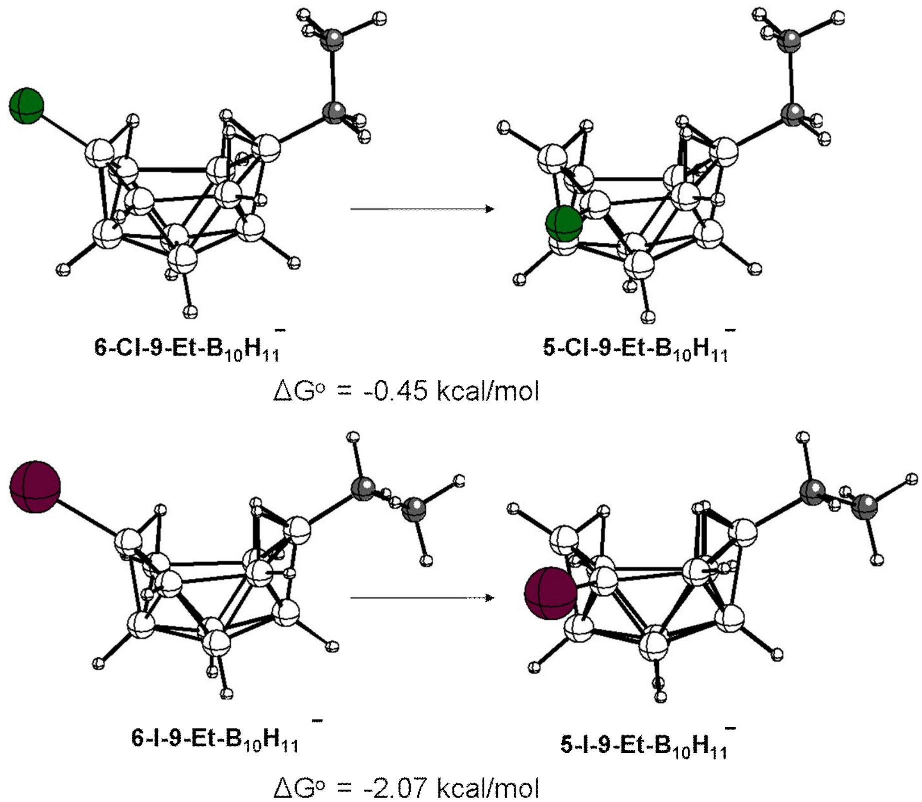

Figure 3.3.14. DFT optimized geometries and calculated free energy changes at for the isomerizations at 60 ^{o}C of (top) 6-Cl-9-(C_2H_5)-$B_{10}H_{12}$ and 5-Cl-9-(C_2H_5)-$B_{10}H_{12}$ (B3LYP/6-311G(d)) and (bottom) 6-I-9-(C_2H_5)-$B_{10}H_{11}^{-}$ and 5-I-9-(C_2H_5)-$B_{10}H_{11}^{-}$ (B3LYP/6-311G(d) for C,B, and H; B3LYP/SDD for I).

Our computational investigations of their rearrangement mechanisms have not yet yielded isomerization pathways from **6X$^-$** to **5X$^-$** or from **6X-9R$^-$** to **5X-9R$^-$** that would be energetically feasible at 60 ^{o}C. The usual mechanisms postulated to account for halo- or alkyl-isomerizations in polyhedral boranes and carboranes have involved skeletal rearrangements where the halo- or alkyl-substituent remains attached to its skeletal-boron during the isomerization. However, our computational investigations of the standard[27] skeletal-based rearrangement mechanisms, including trigonal face rotation (TFR), pentagonal face rotation (PFR), and diamond-square-diamond (DSD) transformations, have not been successful in identifying viable pathways for skeletal-rearrangement . Furthermore, energy calculations predict that a distribution of isomers, where the alkyl or halogen had migrated to other cage positions, would be produced by these skeletal-rearrangements, but these isomers were not observed experimentally. The fact that no I to Cl exchange was observed when the isomerization of **6I** to **5I** was carried out in the presence of $Bu_4N^+Cl^-$ would also seem to exclude any halo-dissociative mechanism. At this point, the combined computational and experimental results suggest a mechanism for the **6X$^-$** to **5X$^-$** and **6X-9R$^-$** to **5X-9R$^-$** isomerizations with direct transfer of the halogen from B6 to B5, perhaps involving a halogen bridging the deprotonated B5-B6 edge, may be possible.

3.4 Conclusions

In conclusion, the new methods reported herein for the syntheses of the 5-X-$B_{10}H_{13}$ halodecaboranes from their 6-X-$B_{10}H_{13}$ isomers, coupled with our previous development of high yield routes to the 6-X-$B_{10}H_{13}$ compounds from the cage-opening reactions of *closo*-$B_{10}H_{10}^{2-}$ salts, now provide the first efficient routes to these synthetically useful decaborane derivatives. These syntheses are now enabling the first systematic investigations of halodecaborane reactivities. Subsequent chapters will demonstrate that halodecaboranes readily undergo high yield transformations to a wide variety of functional decaborane derivatives of potential interest for either biomedical or materials applications.

3.5 References

1. (a) Plesek, J. *Chem. Rev.* **1992**, *92*, 269-278. (b) Packirisamy, S. *Prog. Polym. Sci.* **1996**, *21*, 707-773. (c) Wei, X.; Carroll, P. J.; Sneddon, L. G. *Chem. Mater.* **2006**, *18*, 1113-1123. (d) Teixidor, F.; Vinas, C.; Demonceau, A.; Nunez, R. *Pure Appl. Chem.* **2003**, *75*, 1305-1313. (e) Grimes, R. N. *J. Chem. Educ.* **2004**, *81*, 657-672.

2. (a) Hawthorne, M. F. *Angew. Chem., Int. Ed. Engl.* **1993**, *32*, 950-984. (b) Barth, R. F.; Soloway, A. H.; Fairchild, R. G. *Sci. Am.* **1990**, 100-107. (c) Soloway, A. H.; Tjarks, W.; Barnum, B. A.; Rong, F-G.; Barth, R. F.; Codogni, I. M.; Wilson, J. G. *Chem. Rev.* **1998**, *98*, 1515-1562.

3. Ewing, W. C.; Carroll, P. J.; Sneddon, L. G. *Inorg. Chem.* **2008**, *47*, 8580-8582.

4. (a) Colombier, M.; Atchekzai, J.; Mongeot, H. *Inorg. Chim. Acta* **1986**, *115*, 11-16. (b) Makhlouf, J. M.; Hough, W. V.; Hefferan, G. T. *Inorg. Chem.* **1967**, *6*, 1196-1198.

5. (a) Plesek, J.; Stibr, B.; Hermanek, S. *Coll. Czech. Chem. Comm.* **1966**, *31*, 4744-4745. (b) Stibr, B.; Plesek, J.; Hermanek, S. *Coll. Czech. Chem. Comm.* **1969**, *34*, 194-205.

6. Sprecher, R. F.; Aufderhiede, B. E.; Luther III, G. W.; Carter, J. C. *J. Am. Chem. Soc.* **1974**, *96*, 4404-4410.

7. Stuchlik, J.; Hermanek, S.; Plesek, J.; Stibr, B. *Coll. Czech. Chem. Comm.* **1970**, *35*, 339-343.

8. Kusari, U.; Carroll, P. J.; Sneddon, L. G. *Inorg. Chem.* **2008**, *47*, 9203-9215.

9. Mazighi, K.; Carroll, P. J.; Sneddon, L. G. *Inorg. Chem.* **1993**, *32*, 1963-1969.

10. Sedmera, S.; Hanousek, F.; Samek, Z. *Coll. Czech. Chem. Comm.* **1968**, *33*, 2169-2176.

11. *CrystalClear*: Rigaku Corporation, 1999.

12. *CrystalStructure*: Crystal Structure Analysis Package, Rigaku Corp. Rigaku/MSC (2002).

13. *SIR97*: Altomare, A.; Burla, M. C.; Camalli, M.; Cascarano, M.; Giacovazzo, C.; Guagliardi, A.; Moliterni, A.; Polidori, G. J.; Spagna, R. *J. Appl. Cryst.* **1999**, *32*, 115-119.

14. Sheldrick, G. M. *SHELXL-97*: Program for the Refinement of Crystal Structures; University of Göttingen: Germany, 1997.

15. Frisch, M. J.; Trucks, G. W.; Schlegel, H. B.; Scuseria, G. E.; Robb, M. A.; Cheeseman, J. R.; Montgomery, J. A., Jr.; Vreven, T; Kudin, K. N.; Burant, J. C.; Millam, J. M.; Iyengar, S. S.; Tomasi, J.; Barone, V.; Mennucci, B.; Cossi, M.; Scalmani, G.; Rega, N.; Petersson, G. A.; Nakatsuji, H.; Hada, M.; Ehara, M.; Toyota, K.; Fukuda, R.; Hasegawa, J.; Ishida, M.; Nakajima, T.; Honda, Y.; Kitao, O.; Nakai, H.; Klene, M.; Li, X.; Knox, J. E.; Hratchian, H. P.; Cross, J. B.; Adamo, C.; Jaramillo, J.; Gomperts, R.; Stratmann, R. E.; Yazyev, O.; Austin, A. J.; Cammi, R.; Pomelli, C.; Ochterski, J. W.; Ayala, P. Y.; Morokuma, K.; Voth, G. A.; Salvador, P.; Dannenberg, J. J.; Zakrzewski, V. G.; Dapprich, S.; Daniels, A. D.; Strain, M. C.; Farkas, O.; Malick, D. K.; Rabuck, A. D.; Raghavachari, K.; Foresman, J. B.; Ortiz, J. V.; Cui, Q.; Baboul, A. G.; Clifford, S.;

Cioslowski, J.; Stefanov, B. B.; Liu, G.; Liashenko, A.; Piskorz, P.; Komaromi, I.; Martin, R. L.; Fox, D. J.; Keith, T.; Al-Laham, M. A.; Peng, C. Y.;Nanayakkara, A.; Challacombe, M.; Gill, P. M. W.; Johnson, B.; Chen, W.; Wong, M. W.; Gonzalez, C.; Pople, J. A. *Gaussian 03,* revision B.05; Gaussian, Inc.: Pittsburgh PA, 2003.

16. Goodreau, B. H.; Spencer, J. T. *Inorg. Chem.* **1992**, *31*, 2612-2621.

17. Hawthorne, F. M.; Pitochelli, A. R. *J. Am. Chem. Soc.* **1958**, *80*, 6685.

18. Hawthorne, F. M.; Pitochelli, A. R.; Strahm, R. D.; Miller, J. J. *J. Am Chem. Soc.* **1960**, *82*, 1825-1829.

19. Bonvicini, P.; Levi, A.; Lucchini, V.; Scorrano, G. *J. Chem. Soc., Perkin Trans. 2* **1972**, 2267-2269.

20. (a) Streuli, C. A. *Anal. Chem.* **1960**, *32*, 985-987. (b) Pestovsky, O.; Shuff, A.; Bakac, A. *Organometallics* **2006**, *25*, 2894-2898.

21. Frenna, V.; Vivona, N.; Consiglio, G., Spinelli, D. *J. Chem. Soc., Perkin Trans. 2* **1985**, 1865-1868.

22. Fujii, T.; Nishida, H.; Abiru, Y.; Yamamato, M.; Kise, M. *Chem. Pharm. Bull.* **1995**, *43*, 1872-1877.

23. Bos, M.; Dahmen, E. A. M. F. *Anal. Chim. Acta* **1973**, *63*, 185-196.

24. Alder, R. W.; Bowman, P. S.; Steele, W. R. S.; Winterman, D. R. *Chem. Comm.* **1968**, 723-724.

25. Sneddon, L. G.; Huffman, J. C.; Schaeffer, R. O.; Streib, W. E. *Chem. Comm.* **1972**, 474-475.

26. Wynd, A. J.; Welch, A. J. *Acta Cryst.* **1989**, *C45*, 615-617.

27. (a) Lipscomb, W. N. *Science* **1966**, *153*, 373-378. (b) Wu, S-h.; Jones Jr., M. *J. Am. Chem. Soc.* **1989**, *111*, 5373-5384. (c) Gimarc, B. M.; Ott, J. J. *J. Am. Chem. Soc.* **1987**, *109*, 1388-1392. (d) Gimarc, B. M.; Warren, D. S.; Ott, J. J.; Brown, C. *Inorg. Chem.* **1991**, *30*, 1598-1605. (e) Wales, D. J. *J. Am. Chem. Soc.* **1993**, *115*, 1557-1567. (f) Hart, H. V.; Lipscomb, W. N. *J. Am. Chem. Soc.* **1969**, *91*, 771-772. (g) Kaesz, H. D.; Bau, R.; Beall, H. A.; Lipscomb, W. N. *J. Am. Chem. Soc.* **1967**, *89*, 4218-4220. (h) Edvenson, G. M.; Gaines, D. F. *Inorg. Chem.* **1990**, *29*, 1210-1216 and references therein

Chapter 4

Probing the Fluxional Behavior of $B_{10}H_{13}^{-}$ and Halogenated Derivatives by Variable Temperature ^{11}B NMR

Abstract

Variable-temperature NMR studies were carried out on the Proton Sponge salt of decaborane ($[PSH^{+}][B_{10}H_{13}^{-}]$) in order to observe the fluxional processes proposed for the bridging-hydrogens in the anion. While low temperature experiments failed to observe a static C_1-symmetric ground-state, high temperature NMR revealed a spectrum indicative of C_{2v} symmetry on the NMR time scale, in accordance with earlier computationally proposed fluxional processes. Similar studies were carried out the halogenated decaborate salts $[PSH^{+}][6\text{-}Cl\text{-}B_{10}H_{12}^{-}]$, $[PSH^{+}][6\text{-}F\text{-}B_{10}H_{12}^{-}]$, and $[PSH^{+}][5\text{-}Cl\text{-}B_{10}H_{12}^{-}]$, each of which revealed a C_1-symmetric ground state structure in agreement with DFT calcuations. While $[PSH^{+}][5\text{-}Cl\text{-}B_{10}H_{12}^{-}]$ showed no fluxional behavior across the range of temperatures studied, both $[PSH^{+}][6\text{-}Cl\text{-}B_{10}H_{12}^{-}]$, $[PSH^{+}][6\text{-}F\text{-}B_{10}H_{12}^{-}]$ displayed apparent C_s-symmetry in their respective high temperature ^{11}B NMR spectra, in accordance with a DFT predicted high-energy fluxional mechanism.

4.1 Introduction

The bridging hydrogens of decaborane ($B_{10}H_{14}$) are known to be acidic (Pk_a = ~2.4-3.2 in H_2O/ethanol mixtures),[1] and may be deprotonated to give $B_{10}H_{13}^{-}$ by bases such as amines or anilines.[2] The positions of the bridging hydrogens on the anion have been a subject of debate. The two postulated isomers of $B_{10}H_{13}^-$ are shown in **Figure 4.1.1**.

Crystallographic studies of the anion have shown it to take the C_1 form in the solid state.[3] However, the room-temperature ^{11}B NMR spectrum of the anion does not display the correct number of peaks required of C_1 symmetry, instead showing only 4 peaks, in 2:1:5:2 ratios, which led the authors to propose the static C_s isomer.[4] Heřmánek and co-workers agreed with this assessment, assigning the C_s structure as the static, solution phase form of the anion.[1]

This apparent conflict was resolved by Hofmann and Schleyer's computational studies (MP2/6-31G(d) level),[5] which showed that while the C_1 structure is 4.5 kcal/mol lower in energy than the C_s structure, the C_s symmetric pattern observed in the NMR could be explained by a fluxional hydrogen rearrangement that interconverts the two enantiomeric forms of the C_1 structure **Figure 4.1.2**. Averaging the chemical shifts for the boron atoms in the C_1 structure that become equivalent in the fluxional structure then gave good agreement with the experimental spectrum (calculated and averaged values are given in **Table 4.3.1**).

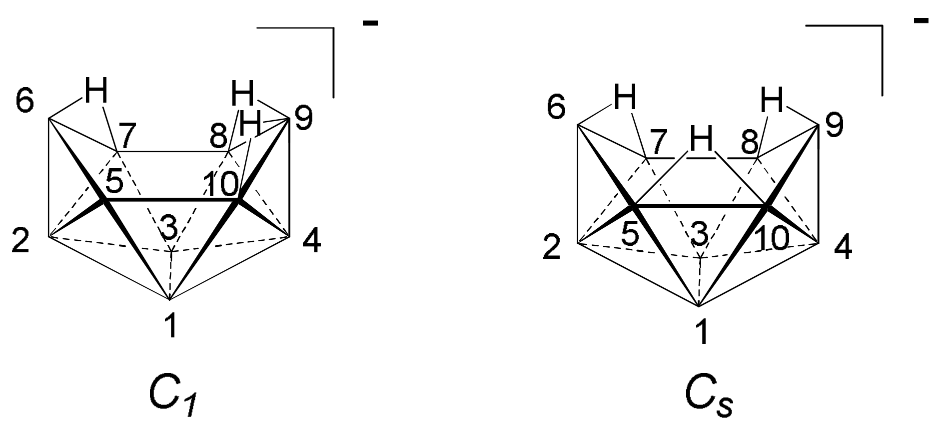

Figure 4.1.1. Drawings of the proposed C_1 and C_s structures of $B_{10}H_{13}^-$.

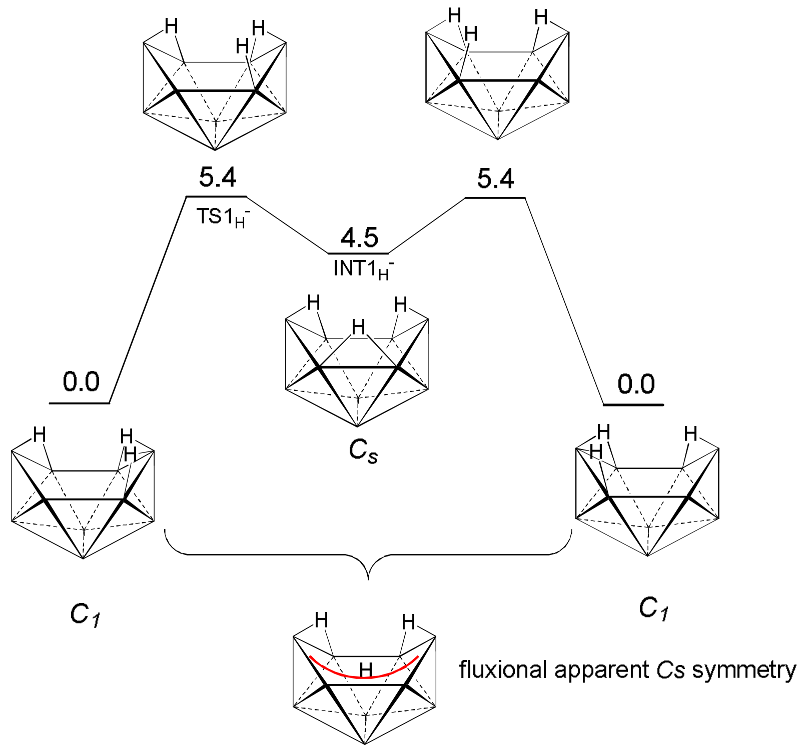

Figure 4.1.2. The fluxional form of the $B_{10}H_{13}^{-}$ anion proposed by Hofmann and Schleyer.[5] Listed electronic energies are in kcal/mol.

The transition states linking the C_1 and C_s forms of the anion were calculated to be 5.4 kcal/mol above the starting material, and therefore accessible at room temperature. Another transition state was located in which the bridging-hydrogen adjacent to the vacant bridging-position had moved into a, *endo*-position on B6/9 (**Figure 4.3.2**, $\mathbf{TS3_H^-}$). However, this transition state was of significantly higher energy (15.1 kcal/mol above starting material), and hence did not play a role in the observed solution-state structure at room temperature.[5]

Prior to the work described here, no variable-temperature (VT) NMR studies had been carried out to explore the possibility of observing either the static C_1 ground state, or a more highly fluxional compound in which the higher of the two proposed transition states might be achieved. This chapter details such VT-NMR studies on $B_{10}H_{13}^-$ as well as on several halogenated, anionic derivates.

4.2 Experimental

General Synthetic Procedures and Materials. All manipulations were carried out in a nitrogen-filled glove-box. Decaborane ($B_{10}H_{14}$) from stock was sublimed prior to use. Halodecaboranes 6-F-$B_{10}H_{13}$ (**6F**),[6] 6-Cl-$B_{10}H_{13}$ (**6Cl**),[6] 5-Br-$B_{10}H_{13}$ (**5Cl**),[7] were prepared by the literature methods, described in **Chapter 2**. Proton Sponge (1,8-bis(dimethylamino)naphthalene, Aldrich) was sublimed prior to use and stored away from light. Dichlorobenzene and chlorobenzene (Fisher) were dried over CaH_2, filtered and stored in a N_2 filled dry box. Deuterated chloroform (99.6 atom % D, ampules, Aldrich) was used as received.

Physical Methods. ^{11}B NMR at 128.3 MHz and ^{1}H NMR at 400.1 MHz spectra were obtained on a Bruker DMX-400 spectrometer equipped with appropriate decoupling accessories and variable-temperature capabilities. All ^{11}B chemical shifts are referenced to $BF_3{\cdot}OEt_2$ (0.0 ppm), with a negative sign indicating an upfield shift.

NMR studies of $B_{10}H_{13}^-$, 6-X-$B_{10}H_{12}^-$ (X = H, Cl, F) and 5-Cl-$B_{10}H_{12}^-$ (5Cl$^-$). For lower temperature studies, $B_{10}H_{14}$ (20 mg, 0.17 mmol), **6Cl** (30 mg, 0.19 mmol), **5Cl** (30 mg, 0.19 mmol) and **6F** (25 mg, 0.18 mmol) were reacted with 1 equivalent of 1,8-bis(dimethylamino)naphthalene (Proton Sponge, PS) (35 mg, 40 mg, 40 mg and 38 mg, respectively) in $CDCl_3$ (3 mL) to form [PSH^+][$B_{10}H_{13}^-$], [PSH^+][**6Cl$^-$**], [PSH^+][**5Cl$^-$**] and [PSH^+][**6F$^-$**], respectively, as bright yellow solutions. The NMR spectra of an aliquot of each sample were then recorded over the 32 ^{o}C to -53 ^{o}C range allowing at least 5 min for the sample to equilibrate at each new temperature. For the higher temperature studies, the same amounts of $B_{10}H_{14}$, **6Cl**, **5Cl**, **6F**, and PS were reacted in dichlorobenzene (3 mL) and the aliquots loaded into resealable thick-walled, high-pressure NMR tubes, with their spectra then obtained from 32 ^{o}C to 102 ^{o}C with the same 5 min equilibration time.

Computational Methods. Density Functional Theory (DFT) calculations were performed using the Gaussian 03 package.[8] All ground state, transition state, and intermediate geometries and both electronic and free energies were obtained using the B3LYP/6-311G(d) level without constraints for all H, C, B and Cl atoms. The NMR chemical shifts were calculated at the B3LYP/6-311G(d) level using the GIAO option within Gaussian 03 and are referenced to $BF_3{\cdot}O(C_2H_5)_2$ using an absolute shielding constant of 102.24 ppm. Harmonic vibrational analyses were carried out on the optimized geometries at the same level to establish the nature of stationary points. True first-order saddle points possessed only one imaginary frequency. Intrinsic reaction coordinate (IRC) calculations were carried out in both the forward and reverse directions to confirm the reaction pathways from the located transition states. All optimized geometries and energies (free and electronic) are given in **Tables 4.2.1-4.2.14.**

Table 4.2.1. DFT optimized (B3LYP/6-311G*) coordinates for **6Cl$^-$**

Center Number	Atomic Number	X	Y	Z
1	5	1.171144	1.032119	1.026345
2	5	-0.27597	0.115545	1.4073
3	5	1.237551	-0.76626	1.156681
4	5	2.384992	0.081397	0.073785
5	5	-0.2887	1.43511	0.154376
6	5	-1.19811	0.086968	-0.0913
7	5	-0.25724	-1.35013	0.407547
8	5	1.619622	-1.44561	-0.4006
9	5	1.950616	-0.12904	-1.5673
10	5	1.356584	1.345773	-0.72418
11	1	1.668741	1.798843	1.794375
12	1	-0.78662	0.150778	2.4843
13	1	1.670928	-1.41699	2.058133
14	1	3.538242	0.176294	0.3579
15	1	-0.75936	2.519268	0.341846
16	17	-3.00657	-0.06369	-0.38134
17	1	-0.76044	-2.40581	0.625056
18	1	2.145263	-2.50603	-0.52458
19	1	2.672428	-0.18099	-2.5106
20	1	1.792836	2.363215	-1.16709
21	1	-0.64797	-0.93594	-0.76563
22	1	1.138525	-1.17978	-1.61612
23	1	0.936591	0.670513	-1.80807

Table 4.2.2. DFT optimized (B3LYP/6-311G*) coordinates for **5Cl⁻**

Center Number	Atomic Number	X	Y	Z
1	5	-0.00268	-0.34679	1.172942
2	5	0.125029	1.342927	0.694124
3	5	-1.47928	0.67366	1.02104
4	5	-1.58737	-1.09461	0.730587
5	5	1.006042	0.039194	-0.19041
6	5	0.422485	1.325677	-1.04736
7	5	-1.21042	1.682295	-0.41443
8	5	-2.47247	0.070462	-0.27283
9	5	-1.75297	-1.42268	-0.93917
10	5	-0.09858	-1.45661	-0.2375
11	1	0.465928	-0.76355	2.186276
12	1	0.603853	2.156952	1.421276
13	1	-2.12194	1.146037	1.908394
14	1	-2.11621	-1.81761	1.515806
15	17	2.841062	-0.27223	-0.03922
16	1	0.98049	2.111918	-1.75053
17	1	-1.77753	2.710207	-0.61548
18	1	-3.64976	0.238469	-0.31138
19	1	-2.33645	-2.32451	-1.44869
20	1	0.432884	-2.52118	-0.26514
21	1	-0.81137	1.203502	-1.55968
22	1	-2.15295	-0.29447	-1.51449
23	1	-0.56397	-1.2854	-1.48462

Table 4.2.3. DFT optimized (B3LYP/6-311G*) coordinates for **6F⁻**

Center Number	Atomic Number	X	Y	Z
1	5	0.620579	0.995232	1.111407
2	5	-0.82533	0.019874	1.27489
3	5	0.734841	-0.79844	1.169212
4	5	1.963785	0.128275	0.256011
5	5	-0.73473	1.407616	0.097162
6	5	-1.57763	0.060835	-0.33021
7	5	-0.63187	-1.39497	0.212033
8	5	1.314572	-1.4058	-0.35373
9	5	1.734097	-0.02871	-1.43004
10	5	0.97192	1.3906	-0.60762

11	1	1.004326	1.734109	1.967813
12	1	-1.46042	-0.01312	2.28524
13	1	1.080627	-1.47647	2.088805
14	1	3.075024	0.251555	0.669709
15	1	-1.26167	2.466012	0.296631
16	9	-2.87906	-0.11319	-0.7352
17	1	-1.13401	-2.4674	0.346615
18	1	1.899642	-2.43886	-0.44614
19	1	2.585097	-0.01303	-2.26158
20	1	1.42376	2.435649	-0.9648
21	1	-0.88301	-0.95679	-0.96403
22	1	0.993625	-1.10942	-1.61986
23	1	0.73741	0.73384	-1.77723

Table 4.2.4. DFT optimized (B3LYP/6-311G*) coordinates for $\mathbf{TS1^{-}_{Cl}}$

Center Number	Atomic Number	X	Y	Z
1	5	-1.18730	-0.9108	1.111617
2	5	0.292121	0.012728	1.353719
3	5	-1.19300	0.922843	1.049497
4	5	-2.4159	-0.00948	0.149364
5	5	0.247676	-1.38034	0.155507
6	5	1.232839	-0.05809	-0.11499
7	5	0.323103	1.388903	0.267893
8	5	-1.6500	1.388711	-0.59248
9	5	-2.05460	-0.03766	-1.51389
10	5	-1.54560	-1.40627	-0.55369
11	1	-1.61280	-1.55807	2.018327
12	1	0.820072	0.012996	2.42328
13	1	-1.58080	1.675624	1.891571
14	1	-3.55210	-0.0608	0.506223
15	1	0.682161	-2.47866	0.329001
16	17	3.054522	-0.01342	-0.35701
17	1	0.799374	2.472821	0.375647
18	1	-2.05932	2.471159	-0.86879
19	1	-2.69475	-0.08148	-2.5156
20	1	-2.00512	-2.48242	-0.77998
21	1	-0.55711	-1.06182	-1.27078
22	1	0.70955	0.870377	-0.89561
23	1	-1.12272	0.895664	-1.7069

Table 4.2.5. DFT optimized (B3LYP/6-311G*) coordinates for **Int1$^-_{Cl}$**

Center Number	Atomic Number	X	Y	Z
1	5	-1.2021	-0.92588	1.100582
2	5	0.292725	-0.0148	1.331791
3	5	-1.19000	0.914462	1.053035
4	5	-2.41750	-0.01834	0.177799
5	5	0.244308	-1.38020	0.124558
6	5	1.252567	-0.02804	-0.10404
7	5	0.325441	1.388855	0.277961
8	5	-1.68860	1.3827	-0.58518
9	5	-2.09900	-0.02900	-1.51198
10	5	-1.54400	-1.38698	-0.60164
11	1	-1.59030	-1.57321	2.023195
12	1	0.836454	-0.06564	2.391656
13	1	-1.55400	1.66115	1.911542
14	1	-3.54820	-0.08071	0.553655
15	1	0.692925	-2.4728	0.285978
16	17	3.064788	-0.00428	-0.35643
17	1	0.795816	2.475026	0.386797
18	1	-2.07220	2.481845	-0.83226
19	1	-2.798400	-0.00565	-2.47649
20	1	-1.972000	-2.48361	-0.79361
21	1	-0.324200	-1.14288	-1.11035
22	1	0.715837	0.881971	-0.89831
23	1	-1.15160	0.883411	-1.697

Table 4.2.6. DFT optimized (B3LYP/6-311G*) coordinates for **TS2$^-_{Cl}$**

Center Number	Atomic Number	X	Y	Z
1	5	-1.2339	-0.92149	1.079935
2	5	0.279648	0.019956	1.346693
3	5	-1.2365	0.910734	1.036964
4	5	-2.4304	-0.03201	0.136756
5	5	0.246563	-1.38001	0.216586
6	5	1.239856	0.018898	-0.05667
7	5	0.263561	1.425697	0.28134
8	5	-1.6828	1.35458	-0.62504
9	5	-1.992	-0.10843	-1.55534
10	5	-1.5023	-1.40674	-0.60956
11	1	-1.5865	-1.57836	2.011156

12	1	0.803561	-0.00633	2.415971
13	1	-1.6143	1.655309	1.89083
14	1	-3.57	-0.05436	0.492935
15	1	0.781808	-2.42867	0.393222
16	17	3.031764	-0.00834	-0.35908
17	1	0.746241	2.504292	0.408083
18	1	-2.0919	2.441062	-0.88975
19	1	-2.6752	-0.07105	-2.53463
20	1	-1.8901	-2.52353	-0.78753
21	1	0.168136	-1.00154	-0.98659
22	1	0.72176	0.939346	-0.86859
23	1	-1.0918	0.859797	-1.69913

Table 4.2.7. DFT optimized (B3LYP/6-311G*) coordinates for **$Int2^{-}_{Cl}$**

Center Number	Atomic Number	X	Y	Z
1	5	0.301496	0.030859	1.272917
2	5	-2.4527	0.029365	0.154594
3	5	-1.276	-0.84361	1.119884
4	5	-1.2108	0.955501	1.01228
5	5	0.246462	1.447702	0.206065
6	5	-1.6121	1.346553	-0.67616
7	5	-1.6197	-1.43871	-0.48515
8	5	0.126421	-1.3868	0.139991
9	5	-1.9701	-0.19237	-1.52424
10	5	1.231121	0.001771	-0.15298
11	1	-1.0489	0.775902	-1.69974
12	1	0.78205	0.987977	-0.9264
13	1	0.679958	-0.86338	-0.97182
14	1	-2.6067	-0.17023	-2.53591
15	1	-2.0199	2.411353	-1.02164
16	1	-2.1373	-2.51664	-0.5647
17	1	-3.592	0.112456	0.501786
18	1	0.703323	-2.41644	0.297843
19	1	0.876547	0.031131	2.31587
20	1	-1.55868	-1.46466	2.099502
21	1	-1.54915	1.74016	1.845229
22	17	3.051248	-0.05151	-0.29735
23	1	0.777957	2.496629	0.378897

Table 4.2.8. DFT optimized (B3LYP/6-311G*) coordinates for $\mathbf{TS3^{-}_{Cl}}$

Center Number	Atomic Number	X	Y	Z
1	5	-1.16269	-0.92459	1.095139
2	5	0.339267	-0.00016	1.260317
3	5	-1.16228	0.924526	1.095534
4	5	2.420867	0.000496	0.185549
5	5	0.287618	-1.41202	0.242549
6	5	1.20231	-5.6E-05	-0.23521
7	5	0.28767	1.411863	0.242294
8	5	-1.6097	1.416826	-0.52313
9	5	-2.0576	0.000245	-1.48272
10	5	-1.6114	-1.41647	-0.52303
11	1	-1.5954	-1.61961	1.964563
12	1	0.9895	-0.00057	2.259368
13	1	-1.5951	1.619305	1.965101
14	1	-3.5502	0.001012	0.562657
15	1	0.740185	-2.50812	0.343246
16	17	3.074009	-6.8E-05	-0.33103
17	1	0.740808	2.507632	0.344514
18	1	-2.11039	2.463525	-0.78726
19	1	-2.72	0.000528	-2.46884
20	1	-2.1124	-2.46308	-0.78695
21	1	-1.0923	-0.96589	-1.62379
22	1	0.67631	-0.0023	-1.3078
23	1	-1.091	0.965374	-1.62371

Table 4.2.9. DFT optimized (B3LYP/6-311G*) coordinates for $\mathbf{TS1^{-}_{F}}$

Center Number	Atomic Number	X	Y	Z
1	5	-0.6683	-0.91291	1.136438
2	5	0.82111	0.016027	1.230298
3	5	-0.6862	0.918168	1.080637
4	5	-1.9959	-0.0081	0.307946
5	5	0.65432	-1.38737	0.042392
6	5	1.62368	-0.07925	-0.32838
7	5	0.73967	1.386861	0.141904
8	5	-1.3063	1.391836	-0.50009
9	5	-1.8108	-0.03233	-1.38273
10	5	-1.1987	-1.40247	-0.48811

11	1	-1.0014	-1.56435	2.07888
12	1	1.45009	0.012487	2.245539
13	1	-0.9806	1.668699	1.962213
14	1	-3.0875	-0.06131	0.78456
15	1	1.09615	-2.48892	0.190371
16	1	1.23292	2.467415	0.229394
17	1	-1.746	2.474584	-0.72699
18	1	-2.5663	-0.07024	-2.30194
19	1	-1.6828	-2.47753	-0.66757
20	1	-0.2971	-1.05355	-1.30843
21	1	0.993661	0.901516	-1.03961
22	1	-0.9105	0.898759	-1.67384
23	9	2.95958	-0.01776	-0.66379

Table 4.2.10. DFT optimized (B3LYP/6-311G*) coordinates for $\mathbf{Int1^{-}_{F}}$

Center Number	Atomic Number	X	Y	Z
1	5	-0.6884	-0.92381	1.126742
2	5	0.81667	-0.00474	1.207819
3	5	-0.6875	0.913679	1.076796
4	5	-1.9952	-0.01755	0.333005
5	5	0.65072	-1.38531	0.022536
6	5	1.64672	-0.03825	-0.30864
7	5	0.73943	1.391826	0.146571
8	5	-1.3472	1.379869	-0.50028
9	5	-1.8481	-0.03797	-1.38335
10	5	-1.1997	-1.38517	-0.53827
11	1	-0.9784	-1.5727	2.084445
12	1	1.463108	-0.05953	2.209732
13	1	-0.9555	1.660432	1.970286
14	1	3.079231	-0.07735	0.828651
15	1	1.111299	-2.47856	0.155071
16	9	2.973512	-0.00371	-0.6564
17	1	1.228039	2.473672	0.238822
18	1	-1.7601	2.477875	-0.70459
19	1	-2.6608	-0.00488	-2.25613
20	1	-1.6404	-2.48605	-0.67591
21	1	0.003035	-1.15091	-1.14734
22	1	1.002315	0.91476	-1.04393
23	1	-0.9321	0.873784	-1.66611

Table 4.2.11. DFT optimized (B3LYP/6-311G*) coordinates for **Int2$^{-}_{F}$**

Center Number	Atomic Number	X	Y	Z
1	5	-0.78635	-0.85662	1.130044
2	5	0.80144	0.002374	1.18189
3	5	-0.709	0.946411	1.048953
4	5	-2.0354	0.051209	0.291382
5	5	0.53035	-1.40151	0.04535
6	5	1.62592	-0.02928	-0.30449
7	5	0.6918	1.428658	0.129244
8	5	-1.2561	1.364334	-0.59043
9	5	-1.7172	-0.15227	-1.42721
10	5	-1.2822	-1.41891	-0.44932
11	1	-0.995	-1.4981	2.115869
12	1	1.449415	-0.01902	2.182629
13	1	0.962562	1.719024	1.922897
14	1	-3.13495	0.140003	0.749144
15	1	1.100311	-2.44295	0.155122
16	9	2.966446	-0.08872	-0.57274
17	1	1.247604	2.468534	0.291442
18	1	-1.6726	2.442214	-0.88258
19	1	-2.4602	-0.0942	-2.36323
20	1	-1.8138	-2.49283	-0.48971
21	1	0.940732	-0.88089	-1.09265
22	1	1.082456	0.992636	-1.04024
23	1	-0.7957	0.792034	-1.67112

Table 4.2.12. DFT optimized (B3LYP/6-311G*) coordinates for **TS2$^{-}_{F}$**

Center Number	Atomic Number	X	Y	Z
1	5	-0.7173	-0.92557	1.110144
2	5	0.8088	0.01311	1.217135
3	5	-0.722	0.907815	1.071793
4	5	-2.0121	-0.02717	0.309049
5	5	0.65714	-1.3874	0.090869
6	5	1.637011	0.003445	-0.26896
7	5	0.69503	1.42022	0.157473
8	5	-1.3527	1.360722	-0.52262
9	5	-1.7758	-0.0942	-1.42126
10	5	-1.1749	-1.39785	-0.54921
11	1	-0.9746	-1.5854	2.070531

12	1	1.44095	-0.02303	2.227674
13	1	-0.9951	1.647351	1.969432
14	1	-3.1019	-0.05185	0.797103
15	1	1.19349	-2.44447	0.220801
16	1	1.19346	2.495798	0.264811
17	1	-1.78398	2.450976	-0.73314
18	1	-2.5779	-0.04811	-2.30636
19	1	-1.583	-2.51391	-0.68438
20	1	0.40441	-1.04001	-1.0964
21	1	0.99849	0.958994	-1.02319
22	1	-0.8918	0.860729	-1.66493
23	9	2.94024	-0.00808	-0.66823

Table 4.2.13. DFT optimized (B3LYP/6-311G*) coordinates for **$TS3^{-}_{F}$**

Center Number	Atomic Number	X	Y	Z
1	5	-0.6537	-0.92227	1.11583
2	5	0.85686	-3.5E-05	1.150186
3	5	-0.6536	0.922228	1.115878
4	5	-1.9977	0.000051	0.334662
5	5	0.70615	-1.40687	0.127264
6	5	1.60076	0.000004	-0.41291
7	5	0.70606	1.406864	0.127233
8	5	-1.2547	1.41402	-0.45284
9	5	-1.8098	0.00004	-1.36049
10	5	-1.2549	-1.41399	-0.45283
11	1	-1.0066	-1.62174	2.018303
12	1	1.57842	-8.3E-05	2.101062
13	1	-1.0066	1.621745	2.018331
14	1	-3.0844	0.000089	0.822057
15	1	1.1594	-2.50791	0.194908
16	9	2.99166	0.000015	-0.62219
17	1	1.15937	2.507854	0.195258
18	1	-1.7771	2.462992	-0.66392
19	1	-2.5775	0.000111	-2.26785
20	1	-1.7775	-2.4629	-0.66372
21	1	-0.8638	-0.95987	-1.60566
22	1	0.90743	-0.00041	-1.4034
23	1	-0.8635	0.959786	-1.60557

Table 4.2.14. Calculated free energies (ΔG in kcal/mol, 393.15 K) and electronic energies (ΔE in kcal/mol, 393.15) at B3LYP/6-311G* for fluxional processes in **Figure 4.3.6**.

Reactions					
Free Energy (ΔG)					
	G (in Hartrees)	**ΔG**		**G (in Hartrees)**	**ΔG**
$6Cl^-$	-716.070123	0.0	**$6F^-$**	-355.719379	0.0
$TS1^-_{Cl}$	-716.060370	6.1	**$TS1^-_{F}$**	-355.708287	7.0
$Int1^-_{Cl}$	-716.061215	5.6	**$Int1^-_{F}$**	-355.709915	5.9
$TS2^-_{Cl}$	-716.057416	8.0	**$TS2^-_{F}$**	-355.708427	6.9
$Int2^-_{Cl}$	-716.063493	4.2	**$Int2^-_{F}$**	-355.714399	3.1
$TS3^-_{Cl}$	-716.050402	12.4	**$TS3^-_{F}$**	-355.693196	16.4
Electronic Energy (ΔE)					
	E (in Hartrees)	**ΔE**		**E (in Hartrees)**	**ΔE**
$6Cl^-$	-716.036700	0.0	**$6F^-$**	-355.686958	0.0
$TS1^-_{Cl}$	-716.027251	5.9	**$TS1^-_{F}$**	-355.675929	6.9
$Int1^-_{Cl}$	-716.027751	5.6	**$Int1^-_{F}$**	-355.677476	5.9
$TS2^-_{Cl}$	-716.024064	7.9	**$TS2^-_{F}$**	-355.676062	6.8
$Int2^-_{Cl}$	-716.030059	4.2	**$Int2^-_{F}$**	-355.677476	3.2
$TS3^-_{Cl}$	-716.016705	12.5	**$TS3^-_{F}$**	-355.660396	16.7

4.3 Results and Discussion

4.3.1 Fluxional Properties of the $B_{10}H_{13}^-$ anion. A selection of ^{11}B NMR spectra of $[PSH^+][B_{10}H_{13}^-]$ at various temperatures is shown in **Figure 4.3.1**. **Table 4.3.1** gives the ^{11}B NMR shifts calculated by Schleyer,[5] along with the values of peaks obtained by averaging ^{11}B resonances made equivalent by a mirror plane bisecting the B5-B10 and B7-B8 bonds (C_s avg.), and values assuming C_{2v} symmetry of the boron skeleton (the identities of the averaged peaks are listed in the caption). The table also gives the chemical shifts observed at low temperature (24 °C) and high temperature (93 °C)

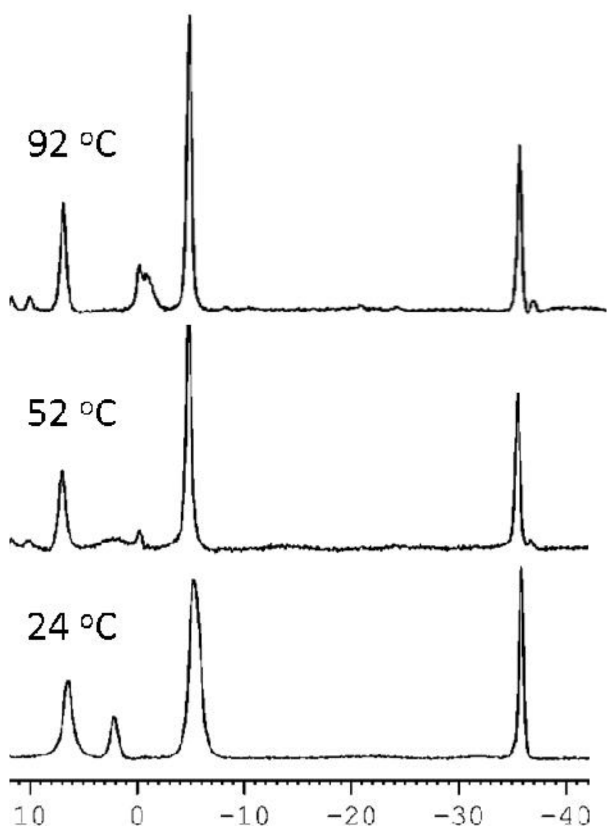

Figure 4.3.1. Variable temperature $^{11}B\{^{1}H\}$ NMR spectra of$[PSH^{+}][B_{10}H_{13}^{-}]$.

Table 4.3.1. Comparisons of the DFT predicted peaks for the ground state, C_1 structure of $[PSH^+][B_{10}H_{13}^-]$[5] and the expected chemical shifts assuming C_s and C_{2v} symmetry with the observed peaks at low and high temperature. [a] – Averaged resonances: B2,B4; B5,B10; B7,B8. [b] – Averaged resonances: B1,B3; B2,B4; B5,B10,B7,B8; B6,B9.

	B1	B2	B3	B4	B5	B6	B7	B8	B9	B10
C_1 calc.	7.3	-46.2	-4.5	-31	-8.5	-9.2	-2.5	-6.5	21.9	-5.9
C_s avg.[a]	7.3	-38.6	-4.5	-38.6	-7.2	6.4	-4.5	-4.5	6.4	-7.2
Obs. 24 ^oC	2.2	-35.8	-5.2	-35.8	-5.2	6.5	-5.2	-5.2	6.5	-5.2
C_{2v} avg.[b]	1.4	-38.6	1.4	-38.6	-5.9	6.4	-5.9	-5.9	6.4	-5.9
Obs. 92 ^oC	-0.8	-35.1	-0.8	-35.1	-4.8	6.8	-4.8	-4.8	6.8	-4.8

Even at very low temperatures (as low as -53 ^{o}C) no peaks indicative of the calculated static ground state structure were observed. Instead, the 2:1:5:2 pattern, seen at 24 ^{o}C, persisted, consistent with Schleyer's proposal of the rapid movement of a bridging proton between the two enantiomeric forms of the C_1 ground state, via the C_s intermediate (**Figure 4.1.2**).

At increased temperature, the peak at 2.2 ppm disappeared, and the large, broad peak at -5.2 ppm sharpened. Around 92 ^{o}C a new resonance emerged at -0.8 ppm. This new peak is a result of another, higher-energy, fluxional process depicted in **Figure 4.3.2**, where the fluxional proton is no long sequestered to one side of the molecule, but instead can achieve $\mathbf{TS3_H^-}$. This process, in conjunction with the lower-energy fluxional pathway, allowed for free movement of the three bridging hydrogens around the open face of the cage, and hence apparent C_{2v} symmetry (much like neutral $B_{10}H_{14}$) on the NMR time scale.

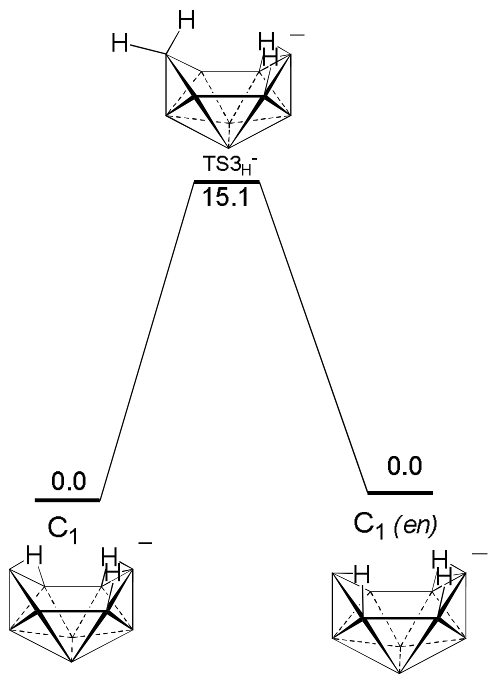

Figure 4.3.2 Depiction of the high-temperature fluxional process interchanging enantiomeric forms of $B_{10}H_{13}^-$. The energies shown (kcal/mol) were calculated by Hofmann and Schleyer.[5]

Apparent C_{2v} symmetry requires the averaging of the calculated ground-state shifts of B5, B7, B8 and B10. Likewise, in the C_{2v} structure B1 became equivalent to B3, and hence their predicted shifts were averaged. Similar to the C_s structure, the B6 and B9 resonances were averaged, as were the resonances for B2 and B4. Comparison of the averaged resonance assuming C_{2v} symmetry in **Table 4.3.1** showed excellent agreement with the observed shifts at 92 ^{o}C, indicating that at this temperature the high-energy fluxional mechanism is available.

4.3.2 Fluxional Properties of the 5- and 6-X-$B_{10}H_{12}^{-}$ anions. The DFT/GIAO calculated ^{11}B NMR chemical shifts for the lowest energy structure of **5Cl^{-}** (**Figure 4.3.3a**) match well the experimental chemical shifts observed over the -53 ^{o}C to 102 ^{o}C (**Figure 4.3.3b**). This was unsurprising, as the asymmetry of the **5Cl^{-}** structure precludes any fluxionality leading to averaged structures. There exists only one low-energy isomer, with no isoenergetic enantiomers accessible through movement of bridging-hydrogen, as was seen in [PSH^{+}][$B_{10}H_{13}^{-}$].

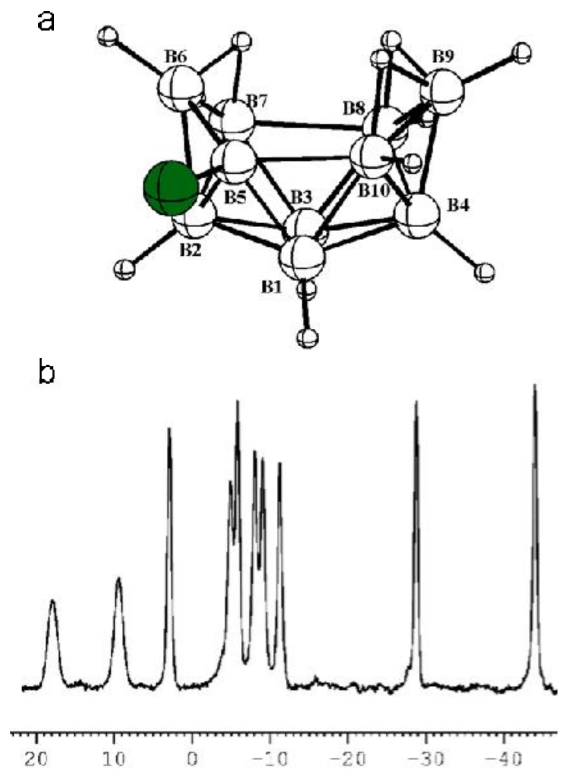

Figure 4.3.3. (a) The lowest energy structure of **5Cl⁻** (B3LYP/6-311G(d)). (b) $^{11}B\{^{1}H\}$ NMR of **5Cl⁻** (obs/cal): B6 (19.0/18.6), B5 (10.5/14.8), B1 (4.0/5.5), B3 (-3.8/-5.4), B8 (-4.8/-5.6), B10 (-7.1/-7.4), B7 (-7.9/-12.4), B9 (-10.1/-14.3), B2 (-27.6/-28.7) and B4 (-42.9/-47.5).

At lower temperatures, the spectra observed for **$6Cl^-$** (12 °C) and **$6F^-$** (27 °C) likewise match the GIAO calculated chemical shifts (**Tables 4.3.2** and **4.3.3**) for their DFT-optimized C_1-symmetric structures. However, the ^{11}B NMR spectra of both **$6Cl^-$** and **$6F^-$** changed as the temperature was increased, with the spectra observed at higher temperatures consistent with C_s-symmetric structures. Thus, the spectrum of **$6Cl^-$** at 32 °C (**Figure 4.3.4**) showed only the four sharp intensity-one resonances arising from the B2, B4, B6 and B9 borons, along with a single broad resonance of intensity 6 centered near -1 ppm. Upon raising the temperature to 67 °C, the broad resonance narrowed and resolved into three new intensity-two sharp peaks. A similar dynamic behavior was observed in the ^{11}B NMR spectra of **$6F^-$** (**Figure 4.3.5**) where at 67 °C the spectrum began to broaden and then at 97 °C, 6 of the original 10 sharp peaks were replaced by two new broad peaks centered at -6.1 ppm (intensity 4) and -15.0 ppm (intensity 2).

Table 4.3.2. Comparisons of the DFT/GIAO (B3LYP/6-311G(d)) calculated and experimentally observed chemical shifts in the ^{11}B NMR spectra of **6Cl^{-}**. Colors indicate which boron resonances are averaged.

Observed 12 °C	Calculated C_1-Structure	Observed 67 °C	C_1-Averaged C_s-Structure
27.6	30.1 (B6)	27.9	30.1 (B6)
0.6	**1.9 (B1)**	**-2.4(2)**	**-2.1 (B1,3)**
-1.7	**-3.4 (B5)**		
-4.0	**-3.5 (B8)**	**-4.6(2)**	**-7.4 (B5,7)**
-5.6	**-6.1 (B3)**		
-8.1(2)	**-8.4 (B10)**	**-6.3(2)**	**-6.0 (B8,10)**
	-11.4 (B7)		
-9.9	-14.0 (B9)	-8.1	-14.0 (B9)
-26.6	-27.5 (B2)	-26.3	-27.5 (B2)
-43.6	-46.4 (B4)	-43.5	-46.4 (B4)

Table 4.3.3. Comparisons of the DFT/GIAO (B3LYP/6-311G(d)) calculated and experimentally observed chemical shifts in the ^{11}B NMR spectra of **6F^{-}**. Colors indicate which boron resonances are averaged.

Observed 27 °C	Calculated C_1-Structure	Observed 97 °C	C_1-Averaged C_s-Structure
34.9	34.5 (B6)	34.9	34.5 (B6)
-1.2	**-3.2 (B8)**		
-4.4	**-3.5 (B1)**	**-5.9(4)**	**-5.0 (B8,10)**
-6.9	**-6.8 (B10)**		**-5.7 (B1,3)**
-7.9	**-7.9 (B3)**		
-11.8	**-13.8 (B5)**	-11.8	-18.1 (B9)
-12.6	-18.1 (B9)	**-15.0(2)**	**-17.0 (B5,7)**
-17.4	**-20.2 (B7)**		
-25.6	-26.3 (B2)	-25.4	-26.3 (B2)
-46.6	-49.3 (B4)	-46.5	-49.3 (B4)

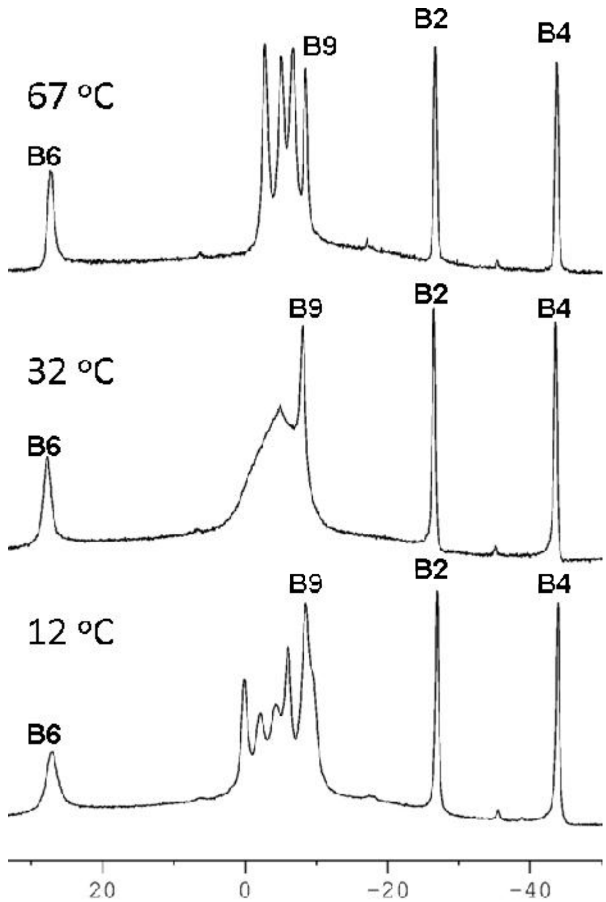

Figure 4.3.4. Variable temperature $^{11}B\{^{1}H\}$ NMR spectra of **6Cl⁻**.

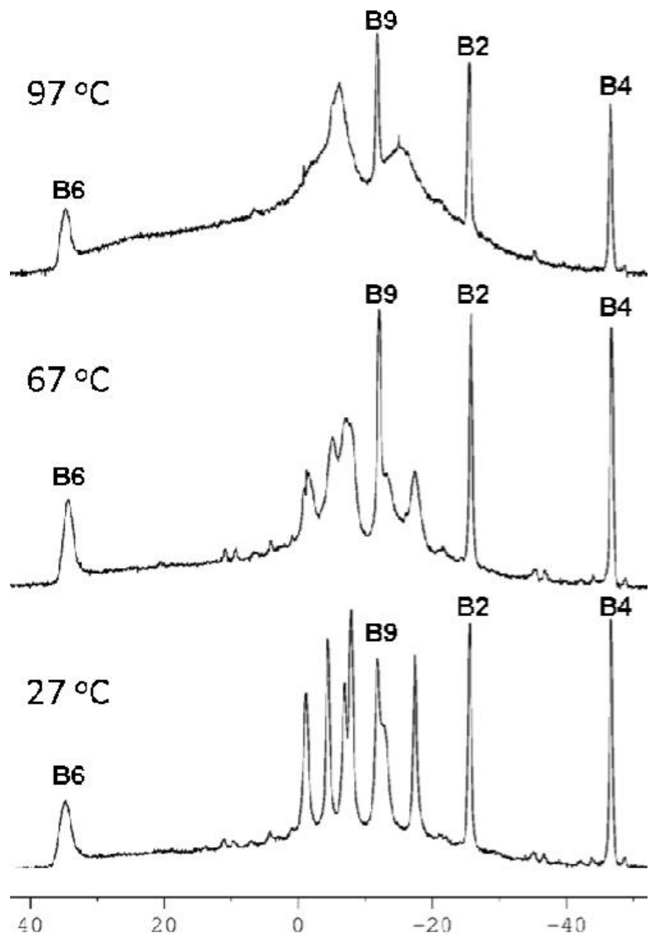

Figure 4.3.5. Variable temperature $^{11}B\{^{1}H\}$ NMR spectra of **6F⁻**.

The temperature dependent spectra observed for **6Cl$^-$** and **6F$^-$** suggest fluxional behavior, akin to that observed in the parent $B_{10}H_{13}^-$. DFT calculations identified the two pathways shown in **Figure 4.3.6** for hydrogen-migration in **6Cl$^-$** and **6F$^-$**. The top pathway is similar to that proposed by Schleyer[5] involving hydrogen-migration along only one side of the cage by a process in which a single bridge-hydrogen migrates across the B6-B5, B5-B10 and B10-B9 edges via the *endo*-B5-H (**TS1**) and *endo*-B10-H (**TS2**) transition states and the B5-H-B10 intermediate (**Int1**). The low barrier for this process supports its occurrence in **6Cl$^-$** (7.9 kcal/mol) and **6F$^-$** (6.8 kcal/mol); however, owing to the lower symmetry of the 6-X-$B_{10}H_{12}^-$ anions, such a process, unlike in the parent $B_{10}H_{13}^-$, will not average to give a C_s-symmetric ^{11}B NMR spectrum.

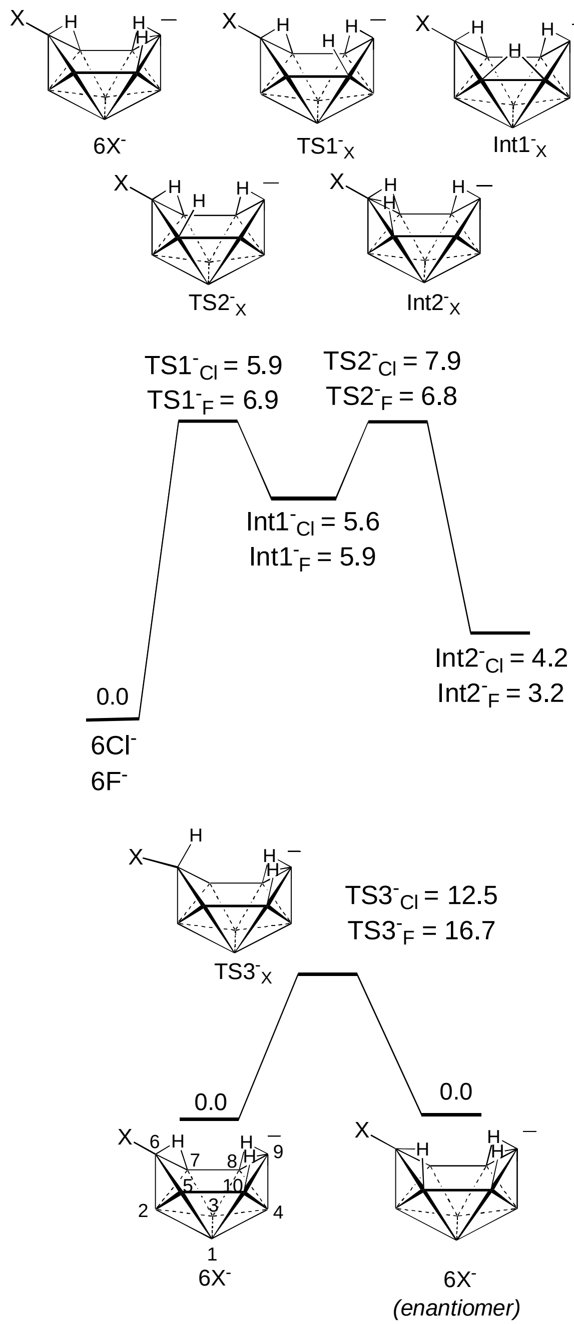

Figure 4.3.6. Calculated relative electronic energies (B3LYP/6-311G(d)) at 293.15 K for two hydrogen migration pathways in **6X$^-$** (X = Cl, F).

A second pathway for hydrogen migration, involving the movement of one bridging-hydrogen from the B6-B7 edge to its enantiomeric position on the B5-B6 edge is shown at the bottom of **Figure 4.3.6.** While the barrier going through the **TS3** transition state structure, which has an *endo*-hydrogen at B6, is higher in **6Cl⁻ (**12.5 kcal) and **6F⁻ (**16.7 kcal) than that of the first process, this barrier should still be accessible at the experimentally observed temperatures of fluxionality and, in the fast exchange limit, this process would produce a C_s-symmetric ^{11}B NMR spectrum. As shown in **Tables 4.3.2** and **4.3.3**, averaging the calculated shifts of the B5-B7, B10-B8 and B1-B3 pairs of boron atoms that would become equivalent in this process does indeed give excellent agreement with the values observed in the higher temperature spectra of **6Cl⁻** and **6F⁻**.

The relative barriers calculated for this process for **6Cl⁻** and **6F⁻** are likewise in agreement with the lower temperature required for **6Cl⁻** to reach the fast exchange limit. The parent $B_{10}H_{13}^-$ reaches the fast exchange limit at temperatures between those required for **6Cl⁻** and **6F⁻**, again in accordance with mechanism as $\mathbf{TS3_H}$ (15.1 kcal/mol)[5] is intermediate between $\mathbf{TS3_{Cl}}$ (12.5 kcal/mol) and $\mathbf{TS3_F}$ (16.7 kcal/mol). Likewise, the transition state for the conversion of the C_1-ground state to the C_s intermediate in $B_{10}H_{13}^-$ (5.4 kcal/mol) is slightly lower than $\mathbf{TS2_F}$ or $\mathbf{TS2_{Cl}}$ perhaps explaining the difficulties observing the static C_1 ground state in the parent anion.

4.4 Conclusions

In this chapter, the fluxional behavior of the 6-X-$B_{10}H_{12}^-$ (X = H, F, Cl) anions have been examined both computationally and by variable-temperature ^{11}B NMR. Although the predicted static ground-state isomer was not observed at low temperature for the parent $B_{10}H_{13}^-$, VT-^{11}B NMR provided the first evidence for the computationally predicted high-temperature fluxional process,[5] by which rapid movement of 3 bridging-hydrogens across the 4 bridging-positions leads to apparent C_{2v} symmetry on the NMR time scale.

Similar fluxional processes were computationally identified and experimentally observed for the halogenated **6F⁻** and **6Cl⁻** derivatives. Low temperature NMR showed compounds with static C_1-symmetry; however, as the temperature was increased a more dynamic spectrum was observed. At intermediate temperatures **6F⁻** and **6Cl⁻** undergo fluxional processes much like those observed for the parent $B_{10}H_{13}^-$ at room temperature, where hydrogen migration across one side of the cage is fast, but there isn't sufficient energy to overcome the higher activation energy (**TS3**). At the high temperature limit this transition state is achieved, and both compounds displayed average C_s-symmetry as predicted computationally.

4.5. References

1. Hermanek, S.; Plotova, H.; Plesek, J. *Collect. Czech. Chem. Comm.* **1975**, *40*, 3593-3601.

2. Hawthorne, M. F. Pitochelli, A. R.; Strahm, R. D.; Miller, J. J. *J. Am. Chem. Soc.* **1960**, *82*, 1825-1829.

3. (a) Sneddon, L. G.; Huffman, J. C.; Schaeffer, R. O.; Streib, W. E. *J. Chem. Soc. Chem. Comm.* **1972**, 474-475. (b) Wynd, A. J.; Welch, A. J. *Acta Cryst.* **1989**, *C45*, 615-617.

4. Siedle, A. R.; Bodner, G. M.; Todd, L. J. *J. Inorg. Nucl. Chem.* **1971**, *33*, 3671-3676.

5. Hofmann, M.; Schleyer, P. v. R. *Inorg. Chem.* **1998**, *37*, 5557-5565.

6. Ewing, W. C.; Carroll, P. J.; Sneddon, L. G. *Inorg. Chem.* **2008**, *47*, 8580-8582.

7. Ewing, W. C.; Carroll, P. J.; Sneddon, L. G. *Inorg. Chem.* **2010**, *49*, 1983-1994.

8. Frisch, M. J.; Trucks, G. W.; Schlegel, H. B.; Scuseria, G. E.; Robb, M. A.; Cheeseman, J. R.; Montgomery, J. A., Jr.; Vreven, T; Kudin, K. N.; Burant, J. C.; Millam, J. M.; Iyengar, S. S.; Tomasi, J.; Barone, V.; Mennucci, B.; Cossi, M.; Scalmani, G.; Rega, N.; Petersson, G. A.; Nakatsuji, H.; Hada, M.; Ehara, M.; Toyota, K.; Fukuda, R.; Hasegawa, J.; Ishida, M.; Nakajima, T.; Honda, Y.; Kitao, O.; Nakai, H.; Klene, M.; Li, X.; Knox, J. E.; Hratchian, H. P.; Cross, J. B.; Adamo, C.; Jaramillo, J.; Gomperts, R.; Stratmann, R. E.; Yazyev, O.; Austin, A. J.; Cammi, R.; Pomelli, C.; Ochterski, J. W.; Ayala, P. Y.; Morokuma, K.; Voth, G. A.; Salvador, P.; Dannenberg, J. J.; Zakrzewski, V. G.; Dapprich, S.; Daniels, A. D.; Strain, M. C.; Farkas, O.; Malick, D. K.; Rabuck, A. D.; Raghavachari, K.; Foresman, J. B.; Ortiz, J. V.; Cui, Q.; Baboul, A. G.; Clifford, S.; Cioslowski, J.; Stefanov, B. B.; Liu, G.; Liashenko, A.; Piskorz, P.; Komaromi, I.; Martin, R. L.; Fox, D. J.; Keith, T.; Al-Laham, M. A.; Peng, C. Y.;Nanayakkara, A.; Challacombe, M.; Gill, P. M. W.; Johnson, B.; Chen, W.; Wong, M. W.; Gonzalez, C.; Pople, J. A. *Gaussian 03*, revision B.05; Gaussian, Inc.: Pittsburgh PA, 2003.

Chapter 5

An Inorganic Analog of the S_N2' Reaction: Nucleophilic Attack of Alcohols on Haloboranes to Yield Boranyl Ethers

Abstract

The selective syntheses of new classes of decaboranyl ethers containing a range of functional groups substituted at the B5 or B6 positions were achieved through the reaction of alcohols with halodecaboranes. The surprising regioselectivity of the reaction, where the reaction of the 6-halodecaboranes (6-X-$B_{10}H_{13}$) with alcohols yielded the 5-substituted decaboranyl ethers (5-RO-$B_{10}H_{13}$) and the reaction with 5-halodecaboranes (5-X-$B_{10}H_{13}$) gave the 6-substituted decaboranyl ethers (6-RO-$B_{10}H_{13}$), was confirmed by NMR and X-ray crystallographic analyses. The crystallographic determinations also showed that the decaboranyl ethers had shortened B-O bonds and apparent sp^2 hybridization at oxygen indicating significant π-backbonding from oxygen to the cage boron. A possible substitution mechanism was computationally identified involving: (1) initial nucleophilic attack by the alcohol-oxygen at a site adjacent to the 5 or 6-halo-substituted boron, (2) movement of the terminal-hydrogen at the point of attack to a bridging-position, (3) formation of a 5-membered (B-O-H-Cl-B) cyclic transition state allowing the acidic methanolic-hydrogen to bond to the halogen, (4) release of HX, and finally (5) movement of a bridging-hydrogen into the vacated terminal-position. Deuterium labeling studies confirmed the movement of hydrogen from a bridging-position of the halodecaborane into the halogen-vacated terminal-position on the

decaboranyl ether product. The relative reaction rates of the 6-X-$B_{10}H_{13}$ compounds (X = F, Cl, Br, I) with alcohol were likewise found to be consistent with this mechanism.

5.1 Introduction

The selective, high yield syntheses of both 6-X-$B_{10}H_{13}$ (X = F, Cl, Br, I)[1] and 5-X-$B_{10}H_{13}$ (X = Cl, Br, I)[2] from *closo*-$B_{10}H_{10}^{2-}$ salts that were described in **Chapters 2** and **3** have now made these isomerically pure, monohalogenated compounds readily available. This chapter describes an example of the use of these monohalodecaboranes as reactive starting points for the syntheses of larger, more highly functionalized boranes, i.e. decaboranyl ethers.

In organic chemistry, the carbon-halogen bond is commonly utilized as a point of reactivity in substitution reactions. Whether it's the textbook S_N2 reaction (**Eq. 1**) with alkyl halides, or nucleophilic aromatic substitution (S_N2_{Ar}, **Eq. 2**), the reactivity toward nucleophilic attack imparted to a molecule by the presence of an electronegative halogen can be used to functionalize a substrate toward a number of ends.

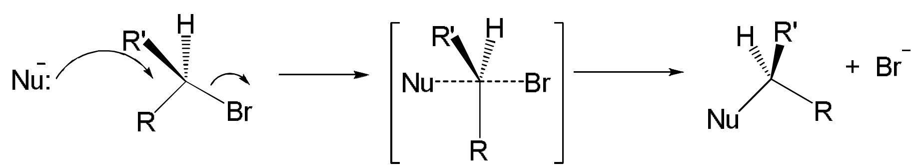

(1)

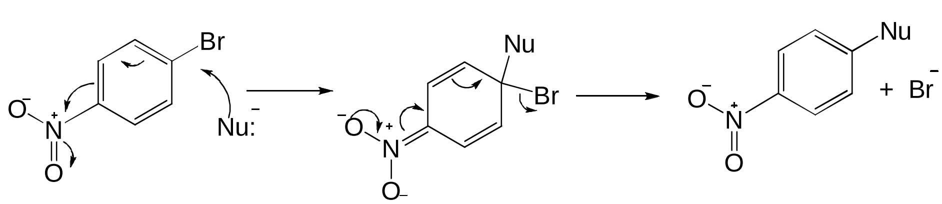

(2)

The S_N2' mechanism describes another type of substitution reaction that utilizes a halogen as a leaving group (**Eq. 3**), with the difference being that attack occurs at a position away from the leaving group. Nucleophilic attack at one end of a π-system leads to the movement of π-electrons, culminating in a relocation of the double bond, and expulsion of the leaving group.

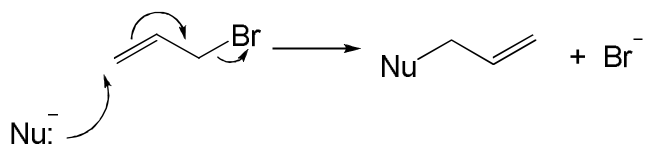

(3)

While not as nucleophilic as their deprotonated alkoxy counterparts, alcohols are known to attack highly electrophilic centers, although those reaction often require the aid of catalysts, and affect substitution chemistry.[3] These reactions, when carried out on carbon-electrophiles, yield organic ethers, eg. **Eq. 4**. Utilizing a B-X bond on the face of a polyhedral borane in a similar fashion could provide a new route to boranyl-ethers, bearing a B-O-R linkage.

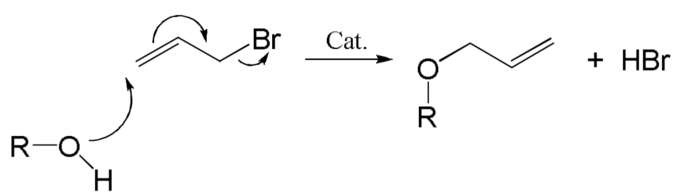

(4)

Recently, *p*-carboranes with ether linkages to a number of different alkyl and aryl organic groups have been synthesized in good yields through the palladium mediated coupling of alkoxides and aryloxides with 2-iodo-*p*-carborane.[4] Substitutions on *closo*-$B_{12}H_{12}^{2-}$ and $B_{10}H_{10}^{2-}$ salts have been carried out through a variety of reactions employing electrophilic substitution of terminal hydrides yielding *closo*-$B_{12}H_{(12-x)}(OR)_x^{2-}$ and *closo*-$B_{10}H_{(10-x)}(OR)_x^{2-}$.[5,6] Metalloboranes bearing the B-O-R (R = methyl, ethyl, isopropyl) moiety have also been synthesized in good overall yield through the cage-opening platination of *closo*-$B_{10}H_{10}^{2-}$ in alcoholic solutions yielding several isomers with the formula $L_2PtB_{10}H_{11}OR$ (R = Et, Me, iPr).[7]

Examples of organic/inorganic ethers containing *neutral* polyhedral boranes are rare. A limited number of decaboranyl ethers ($B_{10}H_{13}OR$) were synthesized in low yield (< 26%) and unconfirmed regiochemistry as a result of the reaction of sodium decaborate ($[Na^+][B_{10}H_{13}^-]$) with I_2 in organic ethers.[8] A mix of 5- and 6-C_2H_5O-$B_{10}H_{13}$ (15:85; **5OR**:**6OR**), in unreported yields, was also formed as a result of the oxidation of sodium decaborate with stannic chloride in diethyl ether.[9]

The strength of the B-O bond, and the tendency to form trialkoxyborates have limited the use of alcohols in reactions with neutral polyboranes such as decaborane. The only published account of the reaction of decaborane with alcohols reported degradation of the cage to $B(OR)_3$ compounds.[10]

This chapter reports the synthesis of new classes of decaboranyl ethers, i.e. 5-RO- and 6-RO-$B_{10}H_{13}$, via the nucleophilic substitution reactions of alcohols with halodecaboranes. In both the 5- and 6-halogenated systems, the reactivity imparted by the B-X bond allowed for nucleophilic attack by the alcohol, substituting alkoxide for halide. However, much like the organic S_N2' reaction, the site of the leaving group was not the site of the initial attack. Instead, attack occured away from the leaving group, inducing the movement of electrons which, in turn, moved toward and expelled the leaving group from the substrate. In the organic reaction, the electrons are contained in a π-system, but in boron hydrides they travel bound to hydrogen. The chemistry is robust, allowing for the syntheses of several potentially useful substituted decaboranes.

5.2 Experimental

Materials and Methods

Materials. The 5-X-$B_{10}H_{13}$ (**5X**) and 6-X-$B_{10}H_{13}$ (**6X**) (X = F, Cl, Br, I) compounds were synthesized according to literature procedures.[3,4] All alcohols, phenols, thiols, phenylthiols and deuterated alcohols (Aldrich) were used as received. Toluene, $NaHCO_3$, CH_2Cl_2, hexanes, pentane, $CDCl_3$ and D_2O (Fisher) were used as received. Silica gel (Fisher) was acidified according to literature prior to use.[11]

Physical Methods. ^{11}B NMR at 128.3 MHz and ^{1}H NMR at 400.1 MHz spectra were obtained on a Bruker DMX-400 spectrometer equipped with appropriate decoupling accessories. All ^{11}B chemical shifts were referenced to $BF_3{\cdot}OEt_2$ (0.0 ppm), with a negative sign indicating an upfield shift. All proton chemical shifts were measured relative to internal residual protons from the lock solvents (99.9% $CDCl_3$) and then referenced to $(CH_3)_4Si$ (0.0 ppm). High- and low-resolution mass spectra employing chemical ionization with negative ion detection were obtained on a Micromass AutoSpec high-resolution mass spectrometer. IR spectra were obtained on a Perkin-Elmer Spectrum 100 FT-IR spectrometer. Melting points were determined using a standard melting point apparatus and are uncorrected. Elemental analyses were carried out by Robertson Microlit Laboratories, Madison, NJ.

General Reaction Methods. Reactions were carried out in sealable 100 mL flasks equipped with a stir bar, side arm and Teflon stopcock (without a rubber o-ring), and were stirred after being sealed under N_2 at atmospheric pressure. In cases where chromatography was employed, 3 materials were isolated: (1) residual starting material, (2) the desired isomer (5- or 6-RO-$B_{10}H_{13}$) as the major product, and (3) the other isomer as a minor product. The order of elution was always the starting material, then 6-RO-$B_{10}H_{13}$, and lastly 5-RO-$B_{10}H_{13}$.

6-(CH_3O)-$B_{10}H_{13}$ (6OMe). A mixture containing methanol (31 mg, 0.94 mmol), **5Br** (150 mg, 0.75 mmol) and $NaHCO_3$ (63 mg, 0.75 mmol) in 7 mL of CH_2Cl_2 was stirred at 70 ^{o}C for 15 h. Additional methanol (15 mg, 0.26 mmol) was then added, and the reaction stirred another 12 h at 65 ^{o}C. The reaction was diluted with 7 mL of hexanes and filtered. The filtrate solvent was vacuum evaporated at 0 ^{o}C to give a clear oil that was then taken up in a minimal amount of a 10% CH_2Cl_2 in hexanes solution and chromatographed on acidic silica gel using the same eluent. For **6OMe**: 58 mg (0.38 mmol, 51%); clear oil; HRMS: *m/z* calcd for $^{12}C^{1}H_{16}{}^{11}B_{10}{}^{16}O$ 154.2131, found 154.2152. ^{11}B NMR (128.3 MHz, *J* = Hz, $CDCl_3$): δ 25.8 (s, 1B), 3.7 (d, *J* = ~125, 3B), 2.9 (d, *J* = ~125, 2B), -16.2 (d, *J* = 150, 2B), -32.6 (d, *J* = 158, 1B), -44.3 (d, *J* = 160, 1B). $^{1}H\{^{11}B\}$ NMR (400.1 MHz, *J* = Hz, $CDCl_3$): δ 3.91 (s, 1CH_3,1BH), 3.83 (s, 1BH), 3.23 (s, 4BH), 2.15 (s, 2BH), 1.42 (s, 1BH), 0.25 (s, 1BH), -0.52 (s, 2BHB), -1.81 (s, 2BHB). IR (KBr, cm^{-1}) 3004 (w), 2951 (w), 2858 (w), 2579 (vs), 1556 (w), 1466 (s), 1327 (s), 1292 (s), 1265 (s), 1173 (w), 1114 (w), 1037 (w), 1004 (m), 994 (m), 959 (w), 927 (w), 913 (w), 881 (w), 841 (w), 805 (w), 734 (w), 718 (w), 703 (w), 684 (w), 639 (w), 578 (w).

5-(CH_3O)-$B_{10}H_{13}$ (5OMe). A mixture containing methanol (31 mg, 0.94 mmol), **6Br** (80 mg, 0.40 mmol) and $NaHCO_3$ (33 mg, 0.4 mmol) in 7 mL of CH_2Cl_2 was stirred for 12 h at room temperature. The mixture was diluted with 7 mL of hexanes and filtered. The filtrate was concentrated at 0 ^{o}C to give a yellowish oil that was then taken up in a minimal amount of a 50% CH_2Cl_2 in hexanes solution and quickly filtered through a plug of acidic silica gel. The filtrate solvent was vacuum evaporated at 0 ^{o}C to give a clear oil that was then recrystallized from ~2 mL of pentane at -20 °C. For **5OMe:** 54 mg (0.36 mmol, 90%); white solid; mp 57-59 °C; HRMS: *m/z* calcd for $^{12}C^{1}H_{16}{}^{11}B_{10}{}^{16}O$ 154.2131, found 154.2312. ^{11}B NMR (128.3 MHz, *J* = Hz, $CDCl_3$): δ 21.8 (s, 1B), 12.6 (d, *J* = 149, 1B), 10.5 (d, *J* = 162, 1B), 2.5 (d, *J* = ~115, 1B), 2.0 (d, *J* = ~150, 1B), -3.4 (d, *J* = 172, 1B), -6.5 (d, *J* = 161, 1B), -11.3 (d, *J* = 150, 1B), -38.9 (d, *J* = 155, 2B). $^{1}H\{^{11}B\}$ NMR (400.1 MHz, *J* = Hz, $CDCl_3$): δ 3.99 (s, 1BH), 3.76 (s, CH_3), 3.66 (s, 1BH), 3.31 (s, 3BH), 2.76 (s, 1BH), 2.71 (s, 1BH), 0.99 (s, 1BH), 0.53 (s, 1BH), 0.34 (s, 1BHB), -1.98 (s, 1BHB), -2.22 (s, 1BHB), -2.38 (s, 1BHB). IR (KBr, cm^{-1}) 2995 (m), 2944 (m), 2849 (m), 2579 (vs), 1894 (br,w), 1549 (w), 1461 (s), 1258 (vs), 1170 (s), 1104 (w), 1068 (w), 1047 (w), 1012 (s), 980 (m), 932 (w), 913 (w), 859 (w), 816 (m), 781 (m), 716 (m), 682 (w), 620 (w).

6-(C_2H_5O)-$B_{10}H_{13}$. A mixture of ethanol (23 mg, 0.50 mmol), **5Br** (80 mg, 0.40 mmol) and $NaHCO_3$ (33 mg, 0.4 mmol) in 7 mL of CH_2Cl_2 was stirred at 70 °C for 12 h. The mixture was then diluted with 7 mL of hexanes and filtered. The filtrate solvent was vacuum evaporated at 0 °C to give an oil that was then dissolved in a minimal amount of a 10% CH_2Cl_2 in hexanes solution and chromatographed on acidic silica gel using the same eluent. For **6-(C_2H_5O)-$B_{10}H_{13}$**: 45 mg (0.27 mmol, 61%); clear oil; HRMS: *m/z* calcd for $^{12}C_2{}^{1}H_{18}{}^{11}B_{10}{}^{16}O$ 168.2287, found 168.2290. ^{11}B NMR (128.3 MHz, *J* = Hz, $CDCl_3$): δ 25.5 (s, 1B), 3.5 (d, *J* = ~125, 3B), 2.9 (d, *J* = ~125, 2B), -16.6 (d, *J* = 145, 2B), -32.4 (d, *J* = 153, 1B), -44.4 (d, *J* = 155, 1B). $^{1}H\{^{11}B\}$ NMR (400.1 MHz, *J* = Hz, $CDCl_3$): δ 4.16 (q, *J* = 7.0, CH_2), 3.82 (s, 1BH), 3.23 (s, 4BH), 2.12 (s, 2BH), 1.40 (t,s, *J* = 7.0, CH_3,1BH), 0.23 (s, 1BH), -0.47 (s, 2BHB), -1.81 (s, 2BHB). IR (KBr, cm^{-1}) 2983 (m), 2937 (w), 2901 (w), 2573 (vs), 2079 (br,w), 1900 (br,w), 1712 (w), 1556 (w), 1484 (m), 1443 (w), 1406 (m), 1375 (s), 1324 (s), 1359 (s), 1114 (w), 1094 (w), 1042 (m), 1017 (m), 1001 (s), 959 (m), 913 (w), 897 (w), 860 (w), 838 (w), 805 (w), 734 (w), 717 (m), 703 (m), 684 (m), 639 (w), 577(w).

6-($C_6H_{11}O$)-$B_{10}H_{13}$. A mixture of cyclohexanol (50 mg, 0.50 mmol), **5Br** (80 mg, 0.4 mmol) and $NaHCO_3$ (33 mg, 0.40 mmol) in 7 mL of CH_2Cl_2 was stirred at 70 ^oC for 20 h. The mixture was diluted with 7 mL of hexanes and filtered. The filtrate was concentrated in vacuo to give a clear oil that was then taken up in a minimal amount of a 40% CH_2Cl_2 in hexanes solution and quickly filtered through a small plug of acidified silica gel. The filtrate solvent was vacuum evaporated and the resulting oily solid was recrystallized from ~3 mL of pentane at -78 ^oC. For **6-($C_6H_{11}O$)-$B_{10}H_{13}$**: 42 mg (0.19 mmol, 48%); white solid; mp 66-68 ^oC; Anal. Calcd.: C, 32.72%, H, 10.91%. Found: C, 32.73%, H, 11.09%; HRMS: *m*/*z* calcd for $^{12}C_6{}^1H_{24}{}^{11}B_{10}{}^{16}O$ 222.2757, found 222.2782. ^{11}B NMR (128.3 MHz, *J* = Hz, $CDCl_3$): δ 25.5 (s, 1B), 3.4 (d, *J* = 134, 5B), -16.6 (d, *J* = 121, 2B), -31.9 (d, *J* = 145, 1B), -44.2 (d, *J* = 163, 1B). $^1H\{^{11}B\}$ NMR (400.1 MHz, $CDCl_3$): δ 4.19 (m, CH), 3.79 (s, 1BH), 3.21 (s, 4BH), 2.06 (s, 2BH), 2.00 (m, 2CH), 1.79 (m, 2CH), 1.56 (m, 4CH), 1.34 (m, 2CH,1BH), 0.21 (s, 1BH), -0.41 (s, 2BHB), -1.81 (s, 2BHB). IR (KBr, cm^{-1}) 2937 (s), 2859 (w), 2573 (vs), 1558 (w), 1489 (w), 1449 (w), 1392 (w), 1356 (m), 1330 (m), 1290 (m), 1258 (s), 1236 (m), 1112 (w), 1041 (w), 999 (m), 959 (m), 925 (w), 890 (w), 846 (w), 802 (w), 702 (w), 684 (w).

5-($C_6H_{11}O$)-$B_{10}H_{13}$. A mixture of cyclohexanol (63 mg, 0.63 mmol), **6Br** (100 mg, 0.50 mmol) and $NaHCO_3$ (43 mg, 0.50 mmol) in 7 mL of CH_2Cl_2 was stirred at room temperature for 24 h. The mixture was diluted with 7 mL of hexanes and filtered. The filtrate solvent was vacuum evaporated to give a pale yellow oil that was then taken up in a minimal amount of a 10% CH_2Cl_2 in hexanes solution and chromatographed on acidic silica gel using the same eluent. For **5-($C_6H_{11}O$)-$B_{10}H_{13}$**: 89 mg (0.41 mmol, 77%); white solid; mp 37-38 ^oC; HRMS: *m*/*z* calcd for $^{12}C_6{}^1H_{24}{}^{11}B_{10}{}^{16}O$ 222.2757, found 222.2728. ^{11}B NMR (128.3 MHz, *J* = Hz, $CDCl_3$): δ 21.3 (s, 1B), 12.6 (d, *J* = 155, 1B), 10.3 (d, *J* = 163, 1B), 3.3 (d, *J* = 148, 1B), 0.9 (d, *J* = 144, 1B), -3.9 (d, *J* = 145, 1B), -6.9 (d, *J* = 128, 1B), -11.8 (d, *J* = 156, 1B), -38.8 (d, *J* = 139, 2B). $^1H\{^{11}B\}$ NMR (400.1 MHz, *J* = Hz, $CDCl_3$): δ 3.99 (m, CH, BH), 3.62 (s, 1BH), 3.24 (s, 3BH), 2.70 (s, 1BH), 2.65 (s, 1BH), 1.92 (m, 2CH), 1.77 (m, 2CH), 1.55 (s, CH), 1.46 (m, 2CH), 1.29 (m, 3CH), 0.97 (s, 1BH), 0.49 (s, 1BH, 1BHB), -1.96 (s, 1BHB), -2.24 (s, 1BHB), -2.41 (s, 1BHB). IR (KBr, cm^{-1}) 2935 (s), 2858 (w), 2578 (s), 1452 (m), 1353 (w), 1328 (w), 1257 (vs), 1240 (w), 1151 (w), 1125 (w), 1102 (w), 1039 (m), 1019 (m), 1001 (s), 955 (w), 933 (w), 891 (w), 861 (w), 816 (w), 797 (w), 778 (w), 717 (w).

6-($(CH_3)_3CO$)-$B_{10}H_{13}$. A mixture containing *tert*-butanol (37 mg, 0.50 mmol), **5Br** (80 mg, 0.40 mmol) and $NaHCO_3$ (33 mg, 0.40 mmol) in 7 mL of CH_2Cl_2 was stirred at 70 ^oC for 14 h. The mixture was diluted with 7 mL of hexanes and filtered. The filtrate solvent was vacuum evaporated to give an oil that was then dissolved in a minimal amount of a 10% CH_2Cl_2 in hexanes solution and chromatographed on acidic silica gel using the same eluent. For **6-($(CH_3)_3CO$)-$B_{10}H_{13}$**: 32 mg (0.17 mmol, 42%); white solid; mp 63 ^oC; HRMS: *m*/*z* calcd for $^{12}C_4{}^1H_{22}{}^{11}B_{10}{}^{16}O$ 196.2601, found 196.2607. ^{11}B NMR (128.3 MHz, *J* = Hz, $CDCl_3$): δ 25.2 (s, 1B), 4.5 (d, *J* = ~135, 5B), -14.3 (d, *J* = 146, 2B), -30.9 (d, *J* = 154, 1B), -43.1 (d, *J* = 156, 1B). $^1H\{^{11}B\}$ NMR (400.1 MHz, *J* = Hz, $CDCl_3$): δ 3.79 (s, 1BH), 3.20 (s, 4BH), 2.11 (s, 2BH), 1.49 (s, 1$(CH_3)_3$), 1.41 (s, 1BH), 0.20 (s, 1BH), -0.40 (s, 2BHB), -1.82 (s, 2BHB). IR (KBr, cm^{-1}) 2994 (w), 2584 (s), 2565 (s), 2543 (m), 2518 (s), 1489 (w), 1396 (w), 1369 (m), 1338 (m), 1253 (w), 1169 (w), 1104 (w), 999 (w), 960 (w), 857 (w), 705 (w), 684 (w).

5-($(CH_3)_3CO$)-$B_{10}H_{13}$. A mixture containing *tert*-butanol (37 mg, 0.50 mmol), **6Br** (80 mg, 0.40 mmol) and $NaHCO_3$ (33 mg, 0.40 mmol) in 7 mL of CH_2Cl_2 was stirred for 14 h at room temperature. The mixture was diluted with 7 mL of hexanes and filtered. The filtrate solvent was vacuum evaporated to give an off-white solid that was then dissolved in ~5 mL of pentane and filtered again. Pure 5-($(CH_3)_3CO$)-$B_{10}H_{13}$ was recrystallized from the filtrate at -30 ^oC. For **5-($(CH_3)_3CO$)-$B_{10}H_{13}$**: 58 mg (0.30 mmol, 75%); white solid; mp 78-79 ^oC; HRMS: *m*/*z* calcd for $^{12}C_4{}^1H_{22}{}^{11}B_{10}{}^{16}O$ 196.2601, found 196.2604. ^{11}B NMR (128.3 MHz, *J* = Hz, $CDCl_3$): δ 20.4 (s, 1B), 13.4 (d, *J* = 149, 1B), 10.8 (d, *J* = 155, 1B), 6.0 (d, *J* = 170, 1B), 2.6 (d, *J* = 143, 1B), -1.8 (d, *J* = 147, 1B), -6.1 (d, *J* = 157, 1B), -11.0 (d, *J* = 145, 1B), -37.9 (d, *J* = 153, 2B). $^1H\{^{11}B\}$ NMR (400.1 MHz, *J* = Hz, $CDCl_3$): δ 3.92 (s, 1BH), 3.57 (s, 1BH), 3.25 (s, 3BH), 2.67 (s, 1BH), 2.60 (s, 1BH), 1.42 (s, $(CH_3)_3$), 0.96 (s, 1BH), 0.45 (s, 1BH, 1BHB), -1.94 (s, 1BHB), -2.21 (s, 1BHB), -2.37 (s, 1BHB). IR (KBr, cm^{-1}) 2983 (m), 2934 (w), 2588 (s), 2567 (s), 2531 (s), 1457 (w), 1389 (w), 1369 (m), 1281 (m), 1246 (m), 1179 (w), 1101 (w), 1162 (w), 1046 (w), 1000 (w), 970 (w), 923 (w), 873 (w), 856 (w), 826 (w), 782 (w), 741 (w), 718 (w).

5-($H_3CC{\equiv}CCH_2O$)-$B_{10}H_{13}$. A mixture containing 2-butyn-1-ol (27 mg, 0.4 mmol), **6Br** (80 mg, 0.4 mmol) and $NaHCO_3$ (33 mg, 0.4 mmol) in 7 mL of CH_2Cl_2 was stirred at 70 ^oC for 14 h. The mixture was diluted with 7 mL of hexanes and filtered. The filtrate was concentrated in vacuo to give a yellowish oil that was then taken up in a minimal amount of a 25% CH_2Cl_2 in hexanes solution and quickly filtered through a plug of acidic silica gel. The filtrate solvent was vacuum evaporated to give a white solid that was recrystallized from ~3 mL of pentane at -78 °C. For **5-($H_3CC{\equiv}CCH_2O$)-$B_{10}H_{13}$**: 55 mg (0.28 mmol, 72%); white solid; mp 53-55 °C; HRMS: *m/z* calcd for $^{12}C_4{}^1H_{18}{}^{11}B_{10}{}^{16}O$ 192.2287, found 192.2275. ^{11}B NMR (128.3 MHz, *J* = Hz, $CDCl_3$): δ 19.8 (s, 1B), 12.1 (d, *J* = 151, 1B), 10.0 (d, *J* = 162, 1B), 2.3 (d, *J* = 142, 2B), -2.6 (d, *J* = 155, 1B), -6.4 (d, *J* = 163, 1B), -11.3 (d, *J* = 153, 1B), -39.2 (d, *J* = 155, 2B). $^1H\{^{11}B\}$ NMR (400.1 MHz, *J* = Hz, $CDCl_3$): δ 4.53 (m, $1CH_2$), 3.99 (s, 1BH), 3.65 (s, 1BH), 3.37 (s, 2BH), 3.28 (s, 1BH), 2.79 (s, 1BH), 2.71 (s, 1BH), 1.89 (t, *J* = 2.2, $1CH_3$), 0.99 (s, 1BH), 0.54 (s, 1BH), 0.36 (s, 1BHB), -1.91 (s, 1BHB), -2.16 (s, 1BHB), -2.36 (s, 1BHB). IR (KBr, cm^{-1}) 2919 (vw), 2864 (vw), 2573 (vs), 2234 (w), 1556 (w), 1455 (w), 1382 (w), 1214 (s), 1154 (w), 1109 (w), 1045 (w), 1005 (m), 972 (m), 914 (w), 860 (w), 816 (w), 779 (w), 717 (w), 618 (w).

6-($HC{\equiv}C(CH_2)_3O$)-$B_{10}H_{13}$. A mixture containing 4-pentynol (40 mg, 0.48 mmol), **5Br** (80 mg, 0.40 mmol) and $NaHCO_3$ (33 mg, 0.4 mmol) in 7 mL of CH_2Cl_2 was stirred at 70 °C for 24 h. The mixture was diluted with 7 mL of pentane and filtered. The filtrate solvent was vacuum evaporated to give a clear oil that was then taken up in a minimal amount of a 15% CH_2Cl_2 in hexanes solution and chromatographed on acidified silica gel with the same eluent. For **6-($HC{\equiv}C(CH_2)_3O$)-$B_{10}H_{13}$**: 54 mg (0.26 mmol, 66%); clear oil; HRMS: *m/z* calcd for $^{12}C_7{}^1H_{24}{}^{11}B_{10}{}^{16}O$ 206.2444, found 206.2433. ^{11}B NMR (128.3 MHz, *J* = Hz, $CDCl_3$): δ 25.2 (s, 1B), 3.4 (d, *J* = ~130, 3B), 2.7 (d, *J* = ~115, 2B), -16.4 (d, *J* = 144, 2B), -32.7 (d, *J* = 158, 1B), -44.4 (d, *J* = 152, 1B). $^1H\{^{11}B\}$ NMR (400.1 MHz, *J* = Hz, $CDCl_3$): δ 4.22 (t, *J* = 6.1, CH_2), 3.82 (s, 1BH), 3.23 (s, 4BH), 2.37 (td, *J* = 6.8, 2.6, CH_2), 2.14 (s, 2BH), 2.00 (t, *J* = 2.6, CH), 1.95 (qn, *J* = 6.8, CH_2), 1.42 (s, 1BH), 0.24 (s, 1BH), -0.47 (s, 2BHB), -1.81 (s, 2BHB). IR (KBr, cm^{-1}) 3305 (m), 2959 (w), 2575 (s), 1713 (w), 1558 (w), 1495 (w), 1432 (w), 1404 (w), 1361 (w), 1263 (br, s), 1115 (w), 1041 (w), 1002 (m), 960 (w), 910 (w), 878 (w), 842 (w), 805 (w), 704 (w), 684 (w), 638 (m).

5-(HC≡C(CH_2)$_3$O)-$B_{10}H_{13}$. A mixture containing 4-pentynol (42 mg, 0.50 mmol), **6Br** (80 mg, 0.40 mmol) and $NaHCO_3$ (33 mg, 0.40 mmol) in 7 mL of CH_2Cl_2 was stirred for 24 h at room temperature. The mixture was diluted with 7 mL of hexanes and filtered. The filtrate solvent was vacuum evaporated to give a clear oil that was then taken up in a minimal amount of a 15% CH_2Cl_2 in hexanes solution and chromatographed on acidic silica gel using the same eluent. For **5-(HC≡C(CH_2)$_3$O)-$B_{10}H_{13}$**: 31 mg (0.15 mmol, 38%); clear oil; HRMS: *m*/*z* calcd for $^{12}C_7{}^{1}H_{24}{}^{11}B_{10}{}^{16}O$ 206.2444, found 206.2436. ^{11}B NMR (128.3 MHz, *J* = Hz, $CDCl_3$): δ 20.7 (s, 1B), 11.9 (d, *J* = 155, 1B), 9.8 (d, *J* = 162, 1B), 2.1 (d, *J* = ~125, 1B), 1.2 (d, *J* = ~130, 1B), -4.0 (d, *J* = 163, 1B), -7.1 (d, *J* = 148, 1B), -12.0 (d, *J* = 154, 1B), -39.5 (d, *J* = 155, 2B). $^{1}H\{^{11}B\}$ NMR (400.1 MHz, *J* = Hz, $CDCl_3$): δ 4.04 (t, *J* = 6.1, CH_2), 3.98 (s, 1BH), 3.63 (s, 1BH), 3.28 (s, 3BH), 2.74 (s, 1BH), 2.68 (s, 1BH), 2.35 (td, *J* = 6.9, 2.5, CH_2), 1.98 (t, *J* = 2.5, ≡CH), 1.90 (qn, *J* = 6.9, CH_2), 1.29 (s, 1BH), 0.52 (s, 1BH), 0.38 (s, 1BHB), -1.95 (s, 1BHB), -2.21 (s, 1BHB), -2.39 (s, 1BHB). IR (KBr, cm^{-1}) 3304 (m), 2957 (w), 2888 (w), 2579 (s), 1471 (m), 1359 (w), 1251 (s), 1035 (w), 1002 (m), 965 (w), 934 (w), 914 (w), 858 (w), 816 (w), 781 (w), 717 (w), 639 (m).

6-((CH_2=CHCH_2)$_2$HCO)-$B_{10}H_{13}$. A mixture containing 1,6-heptadiene-4-ol (48 mg, 0.50 mmol), **5Br** (80 mg, 0.40 mmol) and $NaHCO_3$ (33 mg, 0.40 mmol) in 7 mL of CH_2Cl_2 was stirred at 70 ^{o}C for 3 days. The mixture was diluted with 7 mL of hexanes and filtered. The filtrate solvent was vacuum evaporated to give a yellow oil that was then taken up in a minimal amount of a 5% CH_2Cl_2 in hexanes solution and chromatographed on acidic silica gel using the same eluent. For **6-((CH$_2$=CHCH$_2$)$_2$HCO)-B$_{10}$H$_{13}$**: 60 mg (0.26 mmol, 62%); clear oil; HRMS: *m*/*z* calcd for $^{12}C_7{}^1H_{24}{}^{11}B_{10}{}^{16}O$ 234.2757, found 234.2751. ^{11}B NMR (128.3 MHz, *J* = Hz, $CDCl_3$): δ 24.9 (s, 1B), 2.8 (d, *J* = 149, 5B), -17.0 (d, *J* = 146, 2B), -32.1 (d, *J* = 152, 1B), -44.5 (d, *J* = 161, 1B). ^{1}H{^{11}B} NMR (400.1 MHz, *J* = Hz, $CDCl_3$): δ 5.82 (m, 2 –CH=), 5.15 (m, 2 =CH_2), 4.27 (qn, *J* = 5.9, CH), 3.79 (s, 1BH), 3.20 (s, 4BH), 2.43 (m, 2CH_2), 2.06 (s, 2BH), 1.45 (s, 1BH), 0.22 (s, 1BH), -0.46 (s, 2BHB), -1.94 (s, 2BHB). IR (KBr, cm^{-1}) 3079 (w), 2980 (w), 2940 (w), 2912 (w), 2575 (s), 1642 (w), 1557 (w), 1489 (w), 1435 (w), 1385 (w), 1327 (s), 1300 (m), 1260 (m), 1113 (w), 1069 (w), 1001 (m), 960 (m), 922 (m), 854 (w), 806 (w), 703 (w), 684 (w)

5-((CH$_2$=CHCH$_2$)$_2$HCO)-B$_{10}$H$_{13}$. A solution containing 1,6-heptadiene-4-ol (48 mg, 0.50 mmol), **6Br** (80 mg, 0.40 mmol) and $NaHCO_3$ (33 mg, 0.40 mmol) in 7 mL of CH_2Cl_2 was stirred at room temperature for 48 h. The mixture was diluted with 7 mL of hexanes and filtered. The filtrate solvent was vacuum evaporated to give a yellow oil that was then taken up in a minimal amount of a 10% CH_2Cl_2 in hexanes solution and chromatographed on acidic silica using the same eluent. For **5-((C$_3$H$_5$)$_2$HCO)-B$_{10}$H$_{13}$**: 45 mg (0.19 mmol, 48%); clear oil; HRMS: *m*/*z* calcd for $^{12}C_7{}^1H_{24}{}^{11}B_{10}{}^{16}O$ 234.2757, found 234.2753. ^{11}B NMR (128.3 MHz, *J* = Hz, $CDCl_3$): δ 21.4 (s, 1B), 12.7 (d, *J* = 150, 1B), 10.4 (d, *J* = 146, 1B), 3.3 (d, *J* = ~150, 1B), 1.4 (d, *J* = 151, 1B), -3.6 (d, *J* = 136, 1B), -6.7 (d, *J* = 160, 1B), -11.7 (d, *J* = 154, 1B), -38.7 (d, *J* = 144, 2B). ^{1}H{^{11}B} NMR (400.1 MHz, *J* = Hz, $CDCl_3$): δ 5.80 (m, 2 –CH=), 5.12 (m, 2 =CH_2), 4.11 (qn, *J* = 6.0, CH), 3.96 (s, 1BH), 3.63 (s, 1BH), 3.25 (s, 3BH), 2.72 (s, 1BH), 2.64 (s, 1BH), 2.38 (m,

$2CH_2$), 0.99 (s, 1BH), 0.49 (s, 1BH, 1BHB), -1.96 (s, 1BHB), -2.25 (s, 1BHB), -2.41 (s, 1BHB). IR (KBr, cm^{-1}) 3079 (m), 3007 (w), 2980 (m), 2937 (m), 2911 (m), 2852 (w), 2580 (vs), 1642 (m), 1548 (w), 1455 (m), 1249 (vs), 1103 (w), 1065 (w), 1046 (w), 1002 (s), 974 (w), 919 (s), 860 (w), 816 (m), 780 (w), 717 (m), 619 (w).

6-(ClC_2H_4O-C_2H_4O)-$B_{10}H_{13}$. A mixture containing 2-(2-chloroethoxy)-ethanol) (62 mg, 0.50 mmol), **5Br** (80 mg, 0.40 mmol) and $NaHCO_3$ (33 mg, 0.40 mmol) in 7 mL of CH_2Cl_2 was stirred at 70 °C for 30 h. The reaction was diluted with 7 mL of hexanes and filtered. The filtrate was concentrated in vacuo to give a yellowish oil that was then taken up in a minimal amount of a 50% CH_2Cl_2 in hexanes solution and quickly filtered though a small plug of acidic silica gel. The filtrate solvent was vacuum evaporated to give an oil that was then recrystallized from pentane at -30 °C over 24 h. For **6-(ClC_2H_4O-C_2H_4O)-$B_{10}H_{13}$**: 61 mg (0.32 mmol, 63%), clear crystalline solid; mp 42-43 °C; Anal. Calcd.: C, 19.63%, H, 8.58%. Found: C, 19.77%, H, 8.63%; HRMS: *m*/*z* calcd for $^{12}C_4{}^{1}H_{21}{}^{11}B_{10}{}^{16}O_2{}^{37}Cl$ 248.2130, found 248.2128. ^{11}B NMR (128.3 MHz, *J* = Hz, $CDCl_3$): δ 25.1 (s, 1B), 3.9 (d, *J* = ~140, 1B), 3.1 (d, *J* = ~130, 2B), 2.3 (d, *J* = ~115, 2H), -16.2 (d, *J* = 148, 2B), -32.5 (d, *J* = 155, 1B), -44.4 (d, *J* = 159, 1B). $^{1}H\{^{11}B\}$ NMR (400.1 MHz, *J* = Hz, $CDCl_3$): δ 4.27 (t, *J* = 4.4, CH_2), 3.78 (s, 1BH), 3.73 (m, $2CH_2$), 3.61 (t, *J* = 4.8, CH_2), 3.20 (s, 4BH), 2.16 (s, 2BH), 1.40 (s, 1BH), 0.23 (s, 1BH), -0.30 (s, 2BHB), -1.79 (s, 2BHB). IR (KBr, cm^{-1}) 2961 (w), 2900 (w), 2869 (w), 2573 (s), 1914 (w), 1557 (w), 1494 (w), 1464 (w), 1430 (w), 1392 (w), 1367 (m), 1302 (s), 1262 (m), 1235 (s), 1199 (w), 1127 (m), 1070 (w), 1043 (w), 1019 (w), 1004 (m), 960 (w), 931 (w), 911 (w), 862 (w), 805 (w), 735 (w), 719 (w), 704 (w), 685 (w), 671 (w), 640 (w), 581 (w).

5-(ClC_2H_4O-C_2H_4O)-$B_{10}H_{13}$. A mixture containing 2-(2-chloroethoxy)-ethanol (62 mg, 0.50 mmol), **6Br** (80 mg, 0.40 mmol) and $NaHCO_3$ (33 mg, 0.4 mmol) in 7 mL of CH_2Cl_2 was stirred at room temperature for 30 h. The reaction mixture was diluted with 7 mL of hexanes and filtered. The filtrate was concentrated in vacuo to give a yellowish oil that was then dissolved in a minimal amount of a 50% CH_2Cl_2 in hexanes solution and quickly filtered through a short plug of acidic silica gel. The filtrate solvent was vacuum evaporated to give an oily solid that was then recrystallized from pentane at -30 ^oC over 24 h. For **5-(ClC_2H_4O-C_2H_4O)-$B_{10}H_{13}$**: 78 mg (0.32 mmol, 80%); clear crystalline solid; mp 44-46 ^oC; Anal. Calcd.: C, 19.63%, H, 8.58%. Found: C, 19.68%, H, 8.69%; HRMS: *m*/*z* calcd for $^{12}C_4{}^1H_{21}{}^{11}B_{10}{}^{16}O_2{}^{37}Cl$ 248.2130, found 248.2133. ^{11}B NMR (128.3 MHz, *J* = Hz, $CDCl_3$): δ 20.7 (s, 1B), 12.1 (d, *J* = 146, 1B), 10.1 (d, *J* = 167, 1B), 2.2 (d, *J* = 130, 2B), -3.0 (d, *J* = 138, 1B), -6.7 (d, *J* = 141, 1B), -11.6 (d, *J* = 163, 1B), -39.1 (d, *J* = 156, 2B). $^1H\{^{11}B\}$ NMR (400.1 MHz, *J* = Hz, $CDCl_3$): δ 4.11 (m, CH_2), 3.97 (s, 1BH), 3.76 (m, $2CH_2$), 3.65 (t, s, *J* = 5.1, $2CH_2$, 1BH), 3.30 (s, 3BH), 2.76 (s, 1BH), 2.67 (s, 1BH), 0.97 (s, 1BH), 0.61 (s, 1BH), 0.51 (s, 1BHB), -1.84 (s, 1BHB), -2.16 (s, 1BHB), -2.38 (s, 1BHB). IR (KBr, cm^{-1}) 2962 (w), 2939 (w), 2892 (w), 2868 (w), 2579 (s), 1916 (w), 1552 (w), 1456 (w), 1387 (w), 1362 (w), 1297 (m), 1254 (s), 1231 (s), 1129 (m), 1040 (m), 1001 (m), 966 (w), 914 (w), 877 (w), 858 (w), 815 (w), 782 (w), 717 (w), 667 (w), 620 (w).

6-(ICH_2CH_2O)-$B_{10}H_{13}$. A mixture containing 2-iodoethanol (86 mg 0.50 mmol), **5Br** (80 mg, 0.40 mmol) and $NaHCO_3$ (33 mg, 0.40 mmol) in 7 mL of CH_2Cl_2 was stirred at 70 ^oC for 30 h. The mixture was diluted with 7 mL of hexanes and filtered. The filtrate solvent was vacuum evaporated to give a yellowish oil that was then taken up in a minimal amount of a 4% CH_2Cl_2 in hexanes solution and chromatographed on acidified silica gel using the same eluent. For **6-(ICH_2CH_2O)-$B_{10}H_{13}$**: 52 mg (0.18 mmol, 45%); clear oil; HRMS: *m*/*z* calcd for $^{12}C_4{}^1H_{17}{}^{11}B_{10}{}^{16}O^{127}I$ 294.1253, found 294.1258. ^{11}B NMR (128.3 MHz, *J* = Hz, $CDCl_3$): δ 24.7 (s, 1B), 4.3 (d, *J* = ~140, 1B), 3.7 (d, *J* = 137, 2B), 2.8 (d, *J* = 138, 2B), -15.6 (d, *J* = 140, 2B), -32.5 (d, *J* = 156, 1B), -44.0 (d, *J* = 156, 1B). $^1H\{^{11}B\}$ NMR (400.1 MHz, *J* = Hz, $CDCl_3$): δ 4.37 (t, *J* = 6.4, CH_2), 3.85 (s, 1BH), 3.41 (t, *J* = 6.4, CH_2), 3.24 (s, 4BH), 2.18 (s, 2BH), 1.44 (s, 1BH), 0.27 (s, 1BH), -0.41 (s, 2BHB), -1.81 (s, 2BHB). IR (KBr, cm^{-1}) 2964 (vw), 2928 (vw), 2876 (vw), 2573 (s), 1552 (w), 1491 (w), 1467 (w), 1389 (w), 1300 (m), 1244 (m), 1187 (w), 1170 (w), 1114 (w), 1062 (w), 1003 (m), 971 (w), 923 (w), 883 (vw), 842 (w), 805 (w), 734 (vw), 719 (w), 703 (w), 684 (w), 636 (vw), 579 (vw), 507 (vw).

5-(ICH_2CH_2O)-$B_{10}H_{13}$. A mixture containing 2-iodoethanol (86 mg 0.50 mmol), **6Br** (80 mg, 0.40 mmol) and $NaHCO_3$ (33 mg, 0.40 mmol) in 7 mL of CH_2Cl_2 was stirred at room temperature for 20 h. The mixture was diluted with 7 mL of hexanes and filtered. The filtrate was concentrated in vacuo to give a yellowish oil that was then taken up in a minimal amount of 50% CH_2Cl_2 in hexanes and quickly filtered through a small plug of acidic silica gel. The filtrate solvent was vacuum evaporated to give a clear oil that was then recrystallized from pentane at -78 ^oC. For **5-(ICH_2CH_2O)-$B_{10}H_{13}$**: 82 mg (0.26 mmol, 69%); clear oil; HRMS: *m*/*z* calcd for $^{12}C_4{}^1H_{17}{}^{11}B_{10}{}^{16}O^{127}I$ 294.1253, found 294.1244. ^{11}B NMR (128.3 MHz, *J* = Hz, $CDCl_3$): δ 20.7 (s, 1B), 12.6 (d, *J* = 152, 1B), 10.7 (d, *J* = ~180, 1B), 2.5 (d, *J* = 141, 2B), -2.6 (d, *J* = 136, 1B), -6.1 (d, *J* = 156, 1B), -10.8 (d, *J* = 166, 1B), -38.7 (d, *J* = 155, 2B). $^1H\{^{11}B\}$ NMR (400.1 MHz, *J* = Hz, $CDCl_3$): δ 4.17 (t, *J* = 6.8, CH_2), 4.01 (s, 1BH), 3.65 (s, 1BH), 3.36 (t, *J* = 6.8, CH_2), 3.31 (s, 3BH), 2.78 (s, 1BH), 2.71 (s, 1BH), 0.99 (s, 1BH), 0.54 (s, 1BH), 0.43 (s, 1BHB), -1.91 (s, 1BHB), -2.17 (s, 1BHB), -2.36 (s, 1BHB). IR (KBr, cm^{-1}) 2963 (w), 2930 (w), 2867 (w), 2578 (s), 1893 (w), 1549 (w), 1463 (m), 1385 (w), 1286 (m), 1236 (s), 1184 (m), 1104 (w), 1059 (w), 1002 (m), 974 (w), 932 (w), 913 (w), 858 (w), 815 (m), 779 (w), 715 (m), 681 (w), 618 (w).

5-(($C_4H_4O_2N$)C_2H_4O)-$B_{10}H_{13}$. A mixture containing N-(2-hydroxyethyl)-succinimide (72 mg 0.50 mmol), **6Br** (80 mg, 0.40 mmol) and $NaHCO_3$ (33 mg, 0.40 mmol) in 7 mL of CH_2Cl_2 was stirred at room temperature for 30 h. The reaction mixture was diluted with 3 mL of hexanes and filtered. The filtrate was concentrated in vacuo to give a clear oil that was then dissolved in a minimal amount of 60% CH_2Cl_2 in hexanes and quickly filtered through a plug of acidic silica gel. The filtrate solvent was vacuum evaporated to give pure 5-(($C_4H_4O_2N$)C_2H_4O)-$B_{10}H_{13}$. For **5-(($C_4H_4O_2N$)C_2H_4O)-$B_{10}H_{13}$**: 78 mg (0.30 mmol, 74%); clear oil; HRMS: *m*/*z* calcd for $^{12}C_6{}^{1}H_{21}{}^{11}B_{10}{}^{16}O_3{}^{14}N$ 265.2451, found 265.2462. ^{11}B NMR (128.3 MHz, *J* = Hz, $CDCl_3$): δ 19.9 (s, 1B), 12.1 (d, *J* = 146, 1B), 10.0 (d, *J* = 158, 1B), 2.1 (d, *J* = 146, 2B), -3.4 (d, *J* = 133, 1B), -6.5 (d, *J* = 151, 1B), -11.8 (d, *J* = 145, 1B), -39.4 (d, *J* = 158, 2B). $^{1}H\{^{11}B\}$ NMR (400.1 MHz, *J* = Hz, $CDCl_3$): δ 4.11 (m, 2CH), 3.98 (s, 1BH), 3.80 (m, 2CH), 3.62 (s, 1BH), 3.27 (s, 3BH), 3.17 (s, 1BH), 2.75 (s, $2CH_2$), 2.66 (s, 1BH), 0.92 (s, 1BH), 0.47 (s, 1BH,1BHB), -1.82 (s, 1BHB), -2.14 (s, 1BHB), -2.36 (s, 1BHB). IR (KBr, cm^{-1}) 2959 (w), 2933 (w), 2874 (w), 2577 (s), 1777 (w), 1699 (s), 1464 (w), 1428 (w), 1402 (m), 1367 (w), 1330 (w), 1285 (m), 1237 (m), 1185 (m), 1111 (w), 1075 (w), 1052 (w), 1002 (w), 974 (w), 860 (w), 817 (w), 786 (w), 717 (w).

6-(HSC_2H_4O)-$B_{10}H_{13}$. A mixture containing 2-mercaptoethanol (39 mg, 0.50 mmol), **5Br** (80 mg, 0.40 mmol) and $NaHCO_3$ (33 mg, 0.40 mmol) in 7 mL of CH_2Cl_2 was stirred at 70 ^{o}C for 20 h. The mixture was diluted with 7 mL of hexanes and filtered. The filtrate solvent was vacuum evaporated to give an oil that was taken up in a minimal amount of 20% CH_2Cl_2 in hexanes and chromatographed on acidified silica gel using the same eluent. For **6-(HSC_2H_4O)-$B_{10}H_{13}$**: 35 mg (0.2 mmol, 49%); white solid; mp 33-34 ^{o}C; HRMS: *m/z* calcd for $^{12}C_2{}^{1}H_{18}{}^{11}B_{10}{}^{16}O_3{}^{32}S$ 200.2009, found 200.2020. ^{11}B NMR (128.3 MHz, *J* = Hz, $CDCl_3$): δ 24.5 (s, 1B), 3.0 (d, *J* = ~130, 3B), 2.2 (d, *J* = ~115, 2B), -16.5 (d, *J* = 151, 2B), -33.1 (d, *J* = 155, 1B), -44.8 (d, *J* = 154, 1B). $^{1}H\{^{11}B\}$ NMR (400.1 MHz, *J* = Hz, $CDCl_3$): δ 4.22 (t, *J* = 6.2, CH_2), 3.83 (s, 1BH), 3.23 (s, 4BH), 2.85 (m, CH_2), 2.16 (s, 2BH), 1.56 (t, *J* = 8.3, 1SH), 1.43 (s, 1BH), 0.26 (s, 1BH), -0.42 (s, 2BHB), -1.82 (s, 2BHB). IR (KBr, cm^{-1}) 2940 (w), 2884 (w), 2573 (s), 1557 (w), 1494 (w), 1470 (w), 1395 (w), 1310 (m), 1264 (m), 1235 (m), 1201 (w), 1115 (w), 1040 (w), 1017 (w), 1002 (m), 959 (w), 929 (w), 908 (w), 879 (w), 856 (w), 841 (w), 805 (w), 718 (w), 704 (w), 685 (w), 638 (w), 579 (w).

5-(HSC_2H_4O)-$B_{10}H_{13}$. A mixture containing 2-mercaptoethanol (39 mg, 0.50 mmol), **6Br** (80 mg, 0.40 mmol) and $NaHCO_3$ (33 mg, 0.40 mmol) in 7 mL of CH_2Cl_2 was stirred for 30 h at room temperature. The mixture was diluted with 7 mL of hexanes and filtered. The filtrate was concentrated in vacuo to give a yellowish oil that was taken up in a minimal amount of 40% CH_2Cl_2 in hexanes and quickly filtered through a small plug of acidified silica gel. The filtrate solvent was vacuum evaporated to give pure 5-(HSC_2H_4O)-$B_{10}H_{13}$. For **5-(HSC_2H_4O)-$B_{10}H_{13}$**: 61 mg (0.35 mmol, 88%); clear oil; HRMS: *m/z* calcd for $^{12}C_2{}^{1}H_{18}{}^{11}B_{10}{}^{16}O_3{}^{32}S$ 200.2009, found 200.2005. ^{11}B NMR (128.3

MHz, J = Hz, $CDCl_3$): δ 20.4 (s, 1B), 12.0 (d, J = 153, 1B), 10.0 (d, J = ~170, 1B), 2.0 (d, J = 138, 2B), -3.5 (d, J = 156, 1B), -6.7 (d, J = 157, 1B), -11.6 (d, J = 157, 1B), -39.3 (d, J = 155, 2B). $^1H\{^{11}B\}$ NMR (400.1 MHz, J = Hz, $CDCl_3$): δ 4.05 (t, J = 6.4, CH_2), 4.00 (s, 1BH), 3.64 (s, 1BH), 3.32 (s, 3BH), 2.81 (m, CH_2,1BH), 2.70 (s, 1BH), 1.57 (t, J = 8.4, SH), 0.98 (s, 1BH), 0.53 (s, 1BH), 0.41 (s, 1BHB), -1.92 (s, 1BHB), -2.20 (s, 1BHB), -2.37 (s, 1BHB). IR (KBr, cm^{-1}) 2937 (w), 2878 (w), 2573 (s), 1894 (w), 1550 (w), 1464 (m), 1416 (w), 1388 (w), 1299 (m), 1254 (s), 1233 (s), 1196 (m), 1104 (w), 1046 (w), 1028 (w), 1002 (m), 966 (w), 932 (w), 914 (w), 859 (w), 815 (m), 783 (w), 715 (m), 682 (w), 620 (w).

6,6'-($C_6H_{10}O_2$)-($B_{10}H_{13}$)$_2$. A mixture of 1,4-cyclohexandiol (mix of *cis* and *trans*, 46 mg, 0.40 mmol), **5Br** (160 mg, 0.80 mmol) and $NaHCO_3$ (33 mg, 0.4 mmol) in 7 mL of CH_2Cl_2 was stirred at 70 °C for 48 h. The mixture was diluted with 3 mL of hexanes and filtered. The filtrate was concentrated in vacuo to give a yellowish solid that was then dissolved in a minimal amount of a 50% CH_2Cl_2 in hexanes solution and quickly filtered through a small plug of acidified silica gel. The filtrate solvent was vacuum evaporated to give a white solid that was then washed twice with cold hexanes. The product is isolated as a mix of *cis*- and *trans*-isomers. For **6,6'-($C_6H_{10}O_2$)-($B_{10}H_{13}$)$_2$**: 36 mg (0.10 mmol, 25%); white solid. ^{11}B NMR (128.3 MHz, J = Hz, $CDCl_3$): δ 26.4 (s, 1B), 4.8 (d, J = ~140, 5B), -15.2 (d, J = 148, 2B), -31.0 (d, J = 153, 1B), -43.0 (d, J = 151, 1B). $^1H\{^{11}B\}$ NMR (400.1 MHz, $CDCl_3$): δ 4.38 (br, 2CH), 3.86 (s, 2BH), 3.27 (s, 8BH), 2.15 (m, 2CH, 4BH), 2.06 (m, 2CH), 1.86 (m, 2CH), 1.76 (m, 2CH), 1.47 (s, 2BH), 0.28 (s, 2BH), -0.38 (s, 4BHB), -1.75 (s, 4BHB). IR (KBr, cm^{-1}) 2946 (w), 2572 (s), 1522 (w), 1493 (w), 1444 (w), 1367 (w), 1259 (m), 1108 (w), 1044 (w), 1018 (w), 1000 (m), 958 (m), 923 (w), 911 (w), 883 (w), 842 (w), 800 (w), 703 (w), 683 (w), 639 (w).

5,5'-($C_6H_{10}O_2$)-($B_{10}H_{13}$)$_2$. A mixture of 1,4-cyclohexandiol (mix of *cis* and *trans*, 46 mg, 0.40 mmol), **6Br** (160 mg, 0.80 mmol) and $NaHCO_3$ (33 mg, 0.4 mmol) in 7 mL of CH_2Cl_2 was stirred at room temperature for 14 h. The mixture was diluted with 3 mL of hexanes and filtered. The filtrate was vacuum evaporated to give a yellow oily-solid that was then taken up in a minimal amount of a 50% CH_2Cl_2 in hexanes solution and quickly filtered through a small plug of acidified silica gel. The filtrate solvent was vacuum evaporated to give a white, oily solid that was then cooled at -40 ^{o}C and washed with cold hexanes. The product is isolated as a mix of *cis*- and *trans*-isomers. For **5,5'-($C_6H_{10}O_2$)-($B_{10}H_{13}$)$_2$**: 24 mg (0.07 mmol, 19%); HRMS: *m*/*z* calcd for $^{12}C_6{}^{1}H_{36}{}^{11}B_{20}{}^{16}O_2$ 360.4575, found 360.4574. ^{11}B NMR (128.3 MHz, *J* = Hz, $CDCl_3$): δ 21.2 (s, 1B), 12.8 (d, *J* = 148, 1B), 10.7 (d, *J* = ~165, 1B), 3.5 (d, *J* = 150, 1B), 1.3 (d, *J* = 149, 1B), -3.4 (d, *J* = 165, 1B), -6.3 (d, *J* = 170, 1B), -11.3 (d, *J* = 146, 1B), -38.6 (d, *J* = 153, 2B). ^{1}H{^{11}B} NMR (400.1 MHz, $CDCl_3$): δ 4.13 (s, 2CH), 3.98 (s, 2BH), 3.63 (s, 2BH), 3.25 (s, 6BH), 2.72 (s, 4BH), 1.94 (m, 4CH), 1.71 (m, 4CH), 0.97 (s, 2BH), 0.50 (s, 2BH, 2BHB), -1.94 (s, 2BHB), -2.22 (s, 2BHB), -2.39 (s, 2BHB). IR (KBr, cm^{-1}) 2944 (w), 2576 (s), 1446 (m), 1361 (w), 1328 (w), 1244 (s), 1102 (w), 1039 (w), 1022 (w), 1101 (m), 935 (w), 913 (w), 858 (w), 815 (w), 779 (w), 743 (w), 716 (w).

Reactions of 6F, 6Cl and 6I with CH_3OH. In three separate reactions, **6F**, **6Cl** and **6I** (50 mg each, 0.36, 0.32 and 0.20 mmol, respectively) were reacted with methanol (1.3 equiv.) at room temperature while being monitored by ^{11}B NMR. The reaction with **6F**

showed no change after 2 days. The reaction with **6Cl** was 25% complete after 2 days. The reaction with **6I** was complete after ~12 h.

Reactions of 6Br with phenol, 4-methoxyphenol, thiophenol and 1-octanethiol. 6Br (50 mg, 0.25 mmol) was separately reacted with phenol (28 mg, 0.30 mmol), 4-methoxyphenol (37 mg, 0.30 mmol), thiophenol (33 mg, 0.30 mmol) and 1-octanethiol (44 mg, 0.30 mmol) at both room temperature and at 70 ^{o}C in CH_2Cl_2 for at least 20 h. No reaction, other than trace isomerization from **6Br** to **5Br**, was observed by ^{11}B NMR for any of the reactions at either temperature.

Syntheses of μ-D_4-5-Br-$B_{10}H_9$ (μ-D_4-5Br) and μ-D_4-6-Br-$B_{10}H_9$ (μ-D_4-6Br). In separate reactions, **5Br** (50 mg, 0.25 mmol) and **6Br** (50 mg, 0.25 mmol) were stirred in a biphasic mixture of 2 mL of $CDCl_3$ and 0.5 mL of D_2O at room temperature. After 4 h, the ^{1}H{^{11}B} NMR spectra of the $CDCl_3$ layers showed the disappearance of the high-field signals for all 4 bridging positions (**Figures 5.3.18** and **5.3.19**). Neither ^{11}B NMR spectrum showed any change. The phases were separated, and the $CDCl_3$ layers containing the deuterated-decaborane products were then used without further workup in the subsequent experiments with CD_3OD and CH_3OH.

Reaction of μ-D_4-6Br with CD_3OD and CH_3OH. In two separate experiments, CD_3OD (~12 mg, 0.33 mmol) and CH_3OH (~10 mg, 0.33 mmol) were added to a solution of ~50 mg of **μ-D_4-6Br** in ~3 mL of $CDCl_3$ at room temperature. After the solution was stirred at room temperature for 10 h, ^{11}B NMR analysis indicated >90% conversion to μ-D_3-6-D-5-CD_3O-$B_{10}H_9$ and μ-D_3-6-D-5-CH_3O-$B_{10}H_9$, respectively. The $CDCl_3$ was vacuum evaporated at 0 ^{o}C. The products were then purified by recrystallization from pentane at -78 ^{o}C.

Reaction of 6Br with CD_3OD. CD_3OD (~12 mg, 0.33 mmol) was added to a solution of ~50 mg of **6Br** in 2 mL of $CDCl_3$. After the solution was stirred at room temperature for 10 h, ^{11}B NMR analysis indicated >90% conversion to 5-CD_3O-$B_{10}H_{13}$. The $CDCl_3$ was vacuum evaporated at 0 ^oC. The product was then purified by recrystallization from pentane at -78 ^oC.

Reaction of μ-D_4-5Br with C_2D_5OD. C_2D_5OD (~12 mg, 0.33 mmol) was added to a solution of ~50 mg of **μ-D_4-5Br** in ~3 mL of $CDCl_3$. After the solution was stirred at 70 ^oC for 10 h, ^{11}B NMR analysis indicated near quantitative conversion to μ-D_3-5-D-6-C_2D_5O-$B_{10}H_9$. The $CDCl_3$ was vacuum evaporated at 0 ^oC to give an oil that was then taken up in a minimal amount of a 10% solution of CH_2Cl_2 in hexanes and chromatographed on acidic silica gel using the same eluent. The solvent from the fractions containing the μ-D_3-5-D-6-C_2D_5O-$B_{10}H_9$ product was vacuum evaporated at 0 ^oC.

Crystallographic Data. All crystals were grown from cold pentane or by slow evaporation from heptane solution at -30 ^oC.

Collection and Reduction of the Data. Crystallographic data and structure refinement information are summarized in **Table 5.2.1**. X-ray intensity data for 6-(ClC_2H_4O-C_2H_4O)-$B_{10}H_{13}$ (Penn3371) and 5-(ClC_2H_4O-C_2H_4O)-$B_{10}H_{13}$ (Penn3367), 5-(CH_3O)-$B_{10}H_{13}$ (**5OMe**, Penn3364), and 5-($CH_3C\equiv CCH_2O$)-$B_{10}H_{13}$ (Penn3369) were collected on a Bruker APEXII CCD area detector employing graphite-monochromated Mo-K_α radiation. Rotation frames were integrated using SAINT,[12] producing a list of unaveraged F^2 and $\sigma(F^2)$ values which were then passed to the SHELXTL[13] program package for further processing and structure solution on a Dell Pentium 4 computer. The intensity data were corrected for Lorentz and polarization effects and for absorption using SADABS.[14]

The data for 6-($(CH_3)_3CO$)-$B_{10}H_{13}$ (Penn3349) and 6,6'-($C_6H_{10}O_2$)-($B_{10}H_{13}$)$_2$ (Penn3351) were collected on a Rigaku Mercury CCD area detector employing graphite-monochromated Mo-K_α radiation. Rotation frames were integrated using CrystalClear,[15] producing a list of unaveraged F^2 and $\sigma(F^2)$ values which were then passed to the CrystalStructure[16] program package for further processing and structure solution on a Dell Pentium 4 computer. The intensity data were corrected for Lorentz and polarization effects and for absorption using REQAB.[17]

Solution and Refinement of the Structures. The structures were solved by direct methods (SIR97[18]). Refinement was by full-matrix least squares based on F^2 using SHELXL-97.[19] All reflections were used during refinement (values of F^2 that were experimentally negative were replaced with $F^2 = 0$). For structures Penn3349, Penn3351, Penn3371, Penn3364, and Penn3367, all non-hydrogen atoms were refined anisotropically and hydrogen atoms were refined isotropically. For structure Penn3369, all non-hydrogen atoms were refined anisotropically and hydrogen atoms were refined isotropically, except for the methyl hydrogens which were refined using a riding model.

Bond lengths and angles for all the crystallographically studies structures are provided in **Tables 5.2.2-5.2.13**.

Table 5.2.1: Crystallographic data for structurally characterized compounds

	6-(ClC_2H_4O-C_2H_4O)-$B_{10}H_{13}$	**5-(ClC_2H_4O-C_2H_4O)-$B_{10}H_{13}$**	**5-CH_3O-$B_{10}H_{13}$**
Empirical formula	$C_4B_{10}H_{21}O_2Cl$	$C_4B_{10}H_{21}O_2Cl$	$CB_{10}H_{16}O$
Formula weight	244.76	244.76	152.24
Crystal class	Monoclinic	Triclinic	Monoclinic
space group	$P2_1/n$	$P\bar{1}$	$P2_1/c$
Z	4	2	4
a, Å	8.2214(10)	7.6495(15)	8.373(6)
b, Å	19.411(2)	9.7633(19)	9.848(9)
c, Å	9.2205(11)	11.127(3)	12.388(9)
α, deg		104.353(12)	
β, deg	103.768(5)	106.187(13)	102.34(4)
γ, deg		109.288(9)	
V, Å^3	1429.2(3)	698.3(3)	997.9(14)
D_{calc}, g/cm^3	1.138	1.164	1.013
μ, cm^{-1}	2.43	2.49	0.48
λ, Å (Mo-K_α)	0.71073	0.71073	0.71073
Crystal size, mm	0.28 x 0.25 x 0.08	0.35 x 0.30 x 0.08	0.44 x 0.35 x 0.08
F(000)	512	256	320
2θ angle, deg	4.20-50.18	4.12-54.50	4.98-50.26
temperature, K	143(1)	143(1)	143(1)
hkl collected	$-9 \leq h \leq 9$; $-23 \leq k \leq 23$; $-10 \leq l \leq 10$	$-9 \leq h \leq 8$; $-11 \leq k \leq 11$; $-13 \leq l \leq 13$	$-9 \leq h \leq 8$; $-8 \leq k \leq 11$; $-14 \leq l \leq 12$
No. meas reflns	23645	12464	3795
No. of unique reflns	2533 (R_{int}=0.0250)	2455 (R_{int}=0.0222)	1736 (R_{int}=0.0479)
No. parameters	239	239	174
R^a indices (F>2σ)	R_1=0.0243 wR_2=0.0682	R_1=0.0346 wR_2=0.0889	R_1=0.0471 wR_2=0.1143
R^a indices (all data)	R_1=0.0265 wR_2=0.0703	R_1=0.0383 wR_2=0.0928	R_1=0.0686 wR_2=0.1299
GOF^b	1.058	1.041	0.974
final difference peaks, e/Å^3	+0.166, -0.202	+0.444, -0.581	+0.206, -0.202

	6-((CH$_3$)$_3$CO)-B$_{10}$H$_{13}$	**5-(CH$_3$C≡CCH$_2$O)-B$_{10}$H$_{13}$**	**6,6'-(C$_6$H$_{10}$O$_2$)-(B$_{10}$H$_{13}$)$_2$**
Empirical formula	$C_4B_{10}H_{22}O$	$C_4B_{10}H_{18}O$	$C_6B_{20}H_{36}O_2$
formula weight	194.32	190.28	356.55
Crystal class	Monoclinic	Triclinic	Monoclinic
space group	P2$_1$	P$\bar{1}$	$P2_1$/c
Z	2	4	2
a, Å	5.8342(4)	7.094(3)	16.600(2)
b, Å	10.4766(7)	12.518(5)	6.6881(9)
c, Å	10.5591(7)	14.907(6)	10.1106(14)
α, deg		68.796(15)	
β, deg	96.879(2)	86.318(18)	91.691(3)
γ, deg		77.129(15)	
V, Å^3	640.75(7)	1202.9(9)	1122.0(3)
D_{calc}, g/cm^3	1.007	1.051	1.055
μ, cm^{-1}	0.49	0.52	0.51
λ, Å (Mo-K$_\alpha$)	0.71073	0.71073	0.71073
Crystal size, mm	0.30 x 0.22 x 0.08	0.42 x 0.25 x 0.15	0.38 x 0.32 x 0.03
F(000)	208	400	376
2θ angle, deg	5.25-50.08	3.72-50.26	6.56-50.00
temperature, K	143(1)	143(1)	143(1)
hkl collected	$0 \le h \le 6$; $0 \le k \le 12$; $-12 \le l \le 12$	$-8 \le h \le 8$; $-14 \le k \le 14$; $-17 \le l \le 17$	$-19 \le h \le 19$; $-7 \le k \le 7$; $-11 \le l \le 12$
No. meas reflns	10744	30153	11522
No. of unique reflns	2374 (R_{int}=0.0242	4260 (R_{int}=0.0215)	1968 (R_{int}=0.0340)
No. parameters	226	394	200
R^a indices (F>2σ)	R_1=0.0346 wR_2=0.0929	R_1=0.0416 wR_2=0.1176	R_1=0.0462 wR_2=0.1063
R^a indices (all data)	R_1=0.0361 wR_2=0.0937	R_1=0.0464 wR_2=0.1210	R_1=0.0580 wR_2=0.1141
GOF^b	1.113	1.042	1.053
final difference peaks, e/Å^3	+0.115, -0.145	+0.294, -0.252	+0.161, -0.168

$^aR_1 = \Sigma||F_o| - |F_c||/\Sigma|F_o|$; $wR_2 = \{\Sigma w(F_o^2 - F_c^2)^2/\Sigma w(F_o^2)^2\}^{1/2}$
^{b}GOF = $\{\Sigma w(F_o^2 - F_c^2)^2/(n-p)\}^{1/2}$ where n = no. of reflns; p = no. of params refined

Table 5.2.2. Bond lengths for 6-(ClC_2H_4O-C_2H_4O)-$B_{10}H_{13}$ (Å)

B1-B10	1.7519(17)	B1-B5	1.7534(17)	B1-B2	1.7659(17)
B1-B4	1.7701(17)	B1-B3	1.7706(17)	B1-H1	1.065(13)
B2-B6	1.7327(16)	B2-B3	1.7681(17)	B2-B5	1.8021(17)
B2-B7	1.8045(17)	B2-H2	1.077(14)	B3-B8	1.7468(18)
B3-B7	1.7581(16)	B3-B4	1.7820(17)	B3-H3	1.087(14)
B4-B9	1.7180(17)	B4-B10	1.7881(17)	B4-B8	1.7905(17)
B4-H4	1.069(13)	B5-B6	1.8025(17)	B5-B10	1.9631(18)
B5-H5	1.054(13)	B5-H56	1.217(13)	B6-O1	1.3548(13)
B6-B7	1.8045(16)	B6-H56	1.339(13)	B6-H67	1.374(12)
B7-B8	1.9776(18)	B7-H7	1.067(13)	B7-H67	1.182(12)
B8-B9	1.7862(19)	B8-H8	1.067(14)	B8-H89	1.234(14)
B9-B10	1.7924(19)	B9-H9	1.064(13)	B9-H89	1.257(14)
B9-H910	1.255(13)	B10-H10	1.062(13)	B10-H910	1.271(13)
C1-O1	1.4364(13)	C1-C2	1.4976(15)	C1-H1a	0.933(13)
C1-H1b	0.943(13)	C2-O2	1.4231(12)	C2-H2a	0.967(13)
C2-H2b	0.979(13)	C3-O2	1.4210(12)	C3-C4	1.4930(15)
C3-H3a	0.960(13)	C3-H3b	0.950(13)	C4-Cl1	1.7944(11)
C4-H4a	0.957(13)	C4-H4b	0.947(14)		

Table 5.2.3. Bond angles for 6-(ClC_2H_4O-C_2H_4O)-$B_{10}H_{13}$. (^{o})

B10-B1-B5	68.12(7)	B10-B1-B2	117.68(8)	B5-B1-B2	61.60(7)
B10-B1-B4	61.02(7)	B5-B1-B4	117.51(9)	B2-B1-B4	114.74(9)
B10-B1-B3	107.85(8)	B5-B1-B3	108.01(8)	B2-B1-B3	59.99(7)
B4-B1-B3	60.44(7)	B10-B1-H1	114.9(7)	B5-B1-H1	114.6(7)
B2-B1-H1	118.0(7)	B4-B1-H1	118.1(7)	B3-B1-H1	127.8(7)
B6-B2-B1	111.52(8)	B6-B2-B3	111.54(8)	B1-B2-B3	60.13(7)
B6-B2-B5	61.28(7)	B1-B2-B5	58.86(7)	B3-B2-B5	105.99(8)
B6-B2-B7	61.31(7)	B1-B2-B7	106.12(8)	B3-B2-B7	58.95(7)
B5-B2-B7	104.65(8)	B6-B2-H2	119.6(7)	B1-B2-H2	120.1(7)
B3-B2-H2	119.9(7)	B5-B2-H2	124.7(7)	B7-B2-H2	124.3(7)

B8-B3-B7	68.70(7)	B8-B3-B2	117.86(8)	B7-B3-B2	61.56(7)
B8-B3-B1	107.46(9)	B7-B3-B1	107.95(8)	B2-B3-B1	59.87(7)
B8-B3-B4	60.97(7)	B7-B3-B4	117.67(9)	B2-B3-B4	114.03(8)
B1-B3-B4	59.77(7)	B8-B3-H3	114.1(7)	B7-B3-H3	115.2(7)
B2-B3-H3	119.2(7)	B1-B3-H3	128.0(7)	B4-B3-H3	117.4(7)
B9-B4-B1	111.50(9)	B9-B4-B3	111.03(9)	B1-B4-B3	59.79(7)
B9-B4-B10	61.45(7)	B1-B4-B10	58.99(7)	B3-B4-B10	105.77(8)
B9-B4-B8	61.17(7)	B1-B4-B8	105.59(8)	B3-B4-B8	58.54(7)
B10-B4-B8	104.61(8)	B9-B4-H4	119.3(7)	B1-B4-H4	120.0(7)
B3-B4-H4	121.2(7)	B10-B4-H4	123.5(7)	B8-B4-H4	125.3(7)
B1-B5-B2	59.54(7)	B1-B5-B6	108.85(8)	B2-B5-B6	57.46(6)
B1-B5-B10	55.91(6)	B2-B5-B10	106.09(8)	B6-B5-B10	117.65(8)
B1-B5-H5	123.2(7)	B2-B5-H5	126.1(7)	B6-B5-H5	118.8(7)
B10-B5-H5	117.2(7)	B1-B5-H56	126.0(6)	B2-B5-H56	101.5(6)
B6-B5-H56	48.0(6)	B10-B5-H56	89.7(6)	H5-B5-H56	108.9(9)
O1-B6-B2	131.82(9)	O1-B6-B5	129.07(9)	B2-B6-B5	61.26(7)
O1-B6-B7	124.97(9)	B2-B6-B7	61.31(7)	B5-B6-B7	104.63(8)
O1-B6-H56	114.4(5)	B2-B6-H56	100.0(5)	B5-B6-H56	42.5(5)
B7-B6-H56	113.2(6)	O1-B6-H67	111.7(5)	B2-B6-H67	98.8(5)
B5-B6-H67	113.3(5)	B7-B6-H67	40.9(5)	H56-B6-H67	92.4(7)
B3-B7-B2	59.49(7)	B3-B7-B6	108.67(8)	B2-B7-B6	57.38(6)
B3-B7-B8	55.38(6)	B2-B7-B8	105.41(8)	B6-B7-B8	117.19(8)
B3-B7-H7	121.6(7)	B2-B7-H7	125.0(7)	B6-B7-H7	119.8(7)
B8-B7-H7	117.7(7)	B3-B7-H67	126.3(6)	B2-B7-H67	103.1(6)
B6-B7-H67	49.6(6)	B8-B7-H67	88.9(6)	H7-B7-H67	109.9(9)
B3-B8-B9	109.49(9)	B3-B8-B4	60.49(7)	B9-B8-B4	57.41(7)
B3-B8-B7	55.92(6)	B9-B8-B7	117.68(8)	B4-B8-B7	106.91(8)
B3-B8-H8	122.1(7)	B9-B8-H8	120.0(7)	B4-B8-H8	126.6(7)
B7-B8-H8	115.7(7)	B3-B8-H89	129.8(6)	B9-B8-H89	44.7(6)
B4-B8-H89	99.9(6)	B7-B8-H89	94.7(6)	H8-B8-H89	106.8(10)
B4-B9-B8	61.42(7)	B4-B9-B10	61.20(7)	B8-B9-B10	104.60(8)
B4-B9-H9	128.9(7)	B8-B9-H9	127.7(7)	B10-B9-H9	125.5(7)
B4-B9-H89	102.8(6)	B8-B9-H89	43.7(6)	B10-B9-H89	117.5(6)
H9-B9-H89	111.2(9)	B4-B9-H910	103.8(6)	B8-B9-H910	117.0(6)
B10-B9-H910	45.2(6)	H9-B9-H910	109.3(9)	H89-B9-H910	95.6(9)

B1-B10-B4	59.99(7)	B1-B10-B9	108.88(9)	B4-B10-B9	57.35(7)
B1-B10-B5	55.98(6)	B4-B10-B5	106.75(8)	B9-B10-B5	117.67(8)
B1-B10-H10	124.0(7)	B4-B10-H10	126.3(7)	B9-B10-H10	118.5(7)
B5-B10-H10	117.0(7)	B1-B10-H910	128.7(6)	B4-B10-H910	99.5(6)
B9-B10-H910	44.5(6)	B5-B10-H910	94.4(6)	H10-B10-H910	106.3(9)
B5-H56-B6	89.6(8)	B6-H67-B7	89.5(8)	B8-H89-B9	91.6(9)
B9-H910-B10	90.4(8)	O1-C1-C2	110.17(9)	O1-C1-H1a	109.8(7)
C2-C1-H1a	110.6(7)	O1-C1-H1b	106.6(8)	C2-C1-H1b	109.7(8)
H1a-C1-H1b	109.9(10)	O2-C2-C1	107.68(8)	O2-C2-H2a	110.1(7)
C1-C2-H2a	109.7(8)	O2-C2-H2b	109.1(7)	C1-C2-H2b	111.6(7)
H2a-C2-H2b	108.6(10)	O2-C3-C4	109.03(9)	O2-C3-H3a	109.1(7)
C4-C3-H3a	109.3(7)	O2-C3-H3b	110.0(7)	C4-C3-H3b	111.2(7)
H3a-C3-H3b	108.2(10)	C3-C4-Cl1	111.62(8)	C3-C4-H4a	113.1(7)
Cl1-C4-H4a	104.0(7)	C3-C4-H4b	109.6(8)	Cl1-C4-H4b	105.7(8)
H4a-C4-H4b	112.5(11)	B6-O1-C1	120.74(8)	C3-O2-C2	111.80(8)

Table 5.2.4. Bond lengths for 5-(ClC_2H_4O-C_2H_4O)-$B_{10}H_{13}$. (Å)

B1-B10	1.739(2)	B1-B5	1.770(2)	B1-B3	1.777(2)
B1-B4	1.790(2)	B1-B2	1.799(2)	B1-H1	1.077(18)
B2-B6	1.733(2)	B2-B3	1.765(2)	B2-B7	1.775(2)
B2-B5	1.826(2)	B2-H2	1.065(18)	B3-B7	1.747(2)
B3-B8	1.757(2)	B3-B4	1.780(2)	B3-H3	1.099(16)
B4-B9	1.723(2)	B4-B10	1.767(2)	B4-B8	1.792(2)
B4-H4	1.080(17)	B5-O1	1.3604(19)	B5-B6	1.810(2)
B5-B10	2.031(2)	B5-H56	1.342(17)	B6-B7	1.798(2)
B6-H6	1.072(18)	B6-H56	1.210(16)	B6-H67	1.261(19)
B7-B8	1.939(2)	B7-H7	1.072(18)	B7-H67	1.242(17)
B8-B9	1.794(3)	B8-H8	1.06(2)	B8-H89	1.261(18)
B9-B10	1.763(3)	B9-H9	1.077(19)	B9-H89	1.279(18)
B9-H910	1.281(19)	B10-H10	1.075(17)	B10-H910	1.240(19)
C1-O1	1.4372(17)	C1-C2	1.499(2)	C1-H1a	0.945(18)
C1-H1b	0.961(17)	C2-O2	1.4214(18)	C2-H2a	0.981(18)
C2-H2b	0.958(17)	C3-O2	1.4184(17)	C3-C4	1.490(2)

C3-H3a	0.963(19)	C3-H3b	1.00(2)	C4-Cl1	1.7873(15)
C4-H4a	0.950(17)	C4-H4b	0.943(18)		

Table 5.2.5. Bond angles for 5-(ClC_2H_4O-C_2H_4O)-$B_{10}H_{13}$. (^{o})

B10-B1-B5	70.73(10)	B10-B1-B3	107.60(12)	B5-B1-B3	108.26(11)
B10-B1-B4	60.05(9)	B5-B1-B4	118.35(11)	B3-B1-B4	59.84(9)
B10-B1-B2	118.79(11)	B5-B1-B2	61.53(9)	B3-B1-B2	59.15(9)
B4-B1-B2	113.18(12)	B10-B1-H1	115.5(9)	B5-B1-H1	113.7(10)
B3-B1-H1	127.1(9)	B4-B1-H1	119.5(10)	B2-B1-H1	117.4(9)
B6-B2-B3	111.42(12)	B6-B2-B7	61.62(10)	B3-B2-B7	59.14(9)
B6-B2-B1	110.13(11)	B3-B2-B1	59.81(9)	B7-B2-B1	105.74(11)
B6-B2-B5	61.08(9)	B3-B2-B5	106.33(11)	B7-B2-B5	105.63(11)
B1-B2-B5	58.45(8)	B6-B2-H2	120.9(10)	B3-B2-H2	119.5(10)
B7-B2-H2	124.5(10)	B1-B2-H2	120.0(9)	B5-B2-H2	123.8(10)
B7-B3-B8	67.19(10)	B7-B3-B2	60.72(9)	B8-B3-B2	116.26(12)
B7-B3-B1	107.90(11)	B8-B3-B1	107.25(11)	B2-B3-B1	61.04(9)
B7-B3-B4	116.93(12)	B8-B3-B4	60.89(10)	B2-B3-B4	115.40(12)
B1-B3-B4	60.44(9)	B7-B3-H3	115.7(8)	B8-B3-H3	114.7(9)
B2-B3-H3	119.3(9)	B1-B3-H3	128.0(8)	B4-B3-H3	116.9(8)
B9-B4-B10	60.67(10)	B9-B4-B3	110.98(12)	B10-B4-B3	106.31(11)
B9-B4-B1	109.59(12)	B10-B4-B1	58.54(9)	B3-B4-B1	59.72(9)
B9-B4-B8	61.35(10)	B10-B4-B8	105.11(11)	B3-B4-B8	58.92(9)
B1-B4-B8	105.18(11)	B9-B4-H4	121.7(9)	B10-B4-H4	125.1(9)
B3-B4-H4	118.6(9)	B1-B4-H4	120.5(10)	B8-B4-H4	124.0(10)
O1-B5-B1	121.13(12)	O1-B5-B6	125.81(12)	B1-B5-B6	107.99(11)
O1-B5-B2	132.56(13)	B1-B5-B2	60.02(9)	B6-B5-B2	56.94(9)
O1-B5-B10	111.63(11)	B1-B5-B10	53.93(8)	B6-B5-B10	115.19(11)
B2-B5-B10	104.18(10)	O1-B5-H56	110.3(7)	B1-B5-H56	126.2(8)
B6-B5-H56	41.9(7)	B2-B5-H56	96.4(7)	B10-B5-H56	94.4(7)
B2-B6-B7	60.34(10)	B2-B6-B5	61.98(9)	B7-B6-B5	105.36(11)
B2-B6-H6	127.8(10)	B7-B6-H6	124.7(10)	B5-B6-H6	127.0(10)
B2-B6-H56	106.8(8)	B7-B6-H56	118.2(8)	B5-B6-H56	47.8(8)

H6-B6-H56	110.3(13)	B2-B6-H67	101.9(8)	B7-B6-H67	43.7(8)
B5-B6-H67	118.8(8)	H6-B6-H67	109.7(13)	H56-B6-H67	95.3(11)
B3-B7-B2	60.14(9)	B3-B7-B6	109.25(12)	B2-B7-B6	58.04(9)
B3-B7-B8	56.63(9)	B2-B7-B8	107.18(11)	B6-B7-B8	116.56(11)
B3-B7-H7	122.3(10)	B2-B7-H7	123.8(10)	B6-B7-H7	118.7(10)
B8-B7-H7	118.4(10)	B3-B7-H67	129.4(8)	B2-B7-H67	100.5(9)
B6-B7-H67	44.5(9)	B8-B7-H67	93.4(8)	H7-B7-H67	107.5(13)
B3-B8-B4	60.19(9)	B3-B8-B9	108.74(12)	B4-B8-B9	57.43(9)
B3-B8-B7	56.18(9)	B4-B8-B7	107.30(12)	B9-B8-B7	117.41(12)
B3-B8-H8	122.5(10)	B4-B8-H8	123.9(10)	B9-B8-H8	119.0(10)
B7-B8-H8	117.8(10)	B3-B8-H89	128.5(9)	B4-B8-H89	100.5(8)
B9-B8-H89	45.4(8)	B7-B8-H89	93.2(8)	H8-B8-H89	108.1(13)
B4-B9-B10	60.90(10)	B4-B9-B8	61.22(10)	B10-B9-B8	105.18(12)
B4-B9-H9	131.4(10)	B10-B9-H9	126.5(10)	B8-B9-H9	126.6(10)
B4-B9-H89	103.4(8)	B10-B9-H89	118.4(9)	B8-B9-H89	44.6(8)
H9-B9-H89	108.4(13)	B4-B9-H910	102.8(9)	B10-B9-H910	44.7(9)
B8-B9-H910	117.3(8)	H9-B9-H910	109.3(13)	H89-B9-H910	95.8(12)
B1-B10-B9	110.12(12)	B1-B10-B4	61.41(9)	B9-B10-B4	58.44(10)
B1-B10-B5	55.34(8)	B9-B10-B5	115.75(11)	B4-B10-B5	107.01(10)
B1-B10-H10	122.7(9)	B9-B10-H10	121.5(9)	B4-B10-H10	129.0(9)
B5-B10-H10	114.1(9)	B1-B10-H910	127.3(9)	B9-B10-H910	46.6(9)
B4-B10-H910	102.2(9)	B5-B10-H910	89.8(9)	H10-B10-H910	106.6(13)
O1-C1-C2	111.27(12)	O1-C1-H1a	105.4(10)	C2-C1-H1a	109.1(10)
O1-C1-H1b	109.7(10)	C2-C1-H1b	110.1(10)	H1a-C1-H1b	111.2(14)
O2-C2-C1	107.99(12)	O2-C2-H2a	112.1(10)	C1-C2-H2a	109.0(9)
O2-C2-H2b	110.1(10)	C1-C2-H2b	110.7(10)	H2a-C2-H2b	107.0(14)
O2-C3-C4	108.60(12)	O2-C3-H3a	111.2(11)	C4-C3-H3a	112.2(12)
O2-C3-H3b	110.3(11)	C4-C3-H3b	109.8(11)	H3a-C3-H3b	104.7(15)
C3-C4-Cl1	111.26(10)	C3-C4-H4a	112.1(10)	Cl1-C4-H4a	104.6(10)
C3-C4-H4b	112.1(11)	Cl1-C4-H4b	105.8(11)	H4a-C4-H4b	110.4(14)
B5-O1-C1	122.93(11)	C3-O2-C2	113.67(11)	B5 H56 B6	90.2(11)
B6 H67 B7	91.8(12)	B8-H89-B9	89.9(12)	B9 H910 B10	88.7(12)

Table 5.2.6. Bond lengths for 5-(CH_3O)-$B_{10}H_{13}$. (Å)

B1-B10	1.746(3)	B1-B5	1.761(3)	B1-B3	1.785(3)
B1-B4	1.794(3)	B1-B2	1.810(3)	B1-H1	1.096(16)
B2-B6	1.732(3)	B2-B7	1.775(3)	B2-B3	1.780(3)
B2-B5	1.809(3)	B2-H2	1.097(17)	B3-B7	1.756(2)
B3-B8	1.757(3)	B3-B4	1.791(3)	B3-H3	1.104(17)
B4-B9	1.718(3)	B4-B10	1.776(3)	B4-B8	1.798(3)
B4-H4	1.111(15)	B5-O1	1.370(3)	B5-B6	1.826(3)
B5-B10	2.046(3)	B5-H56	1.376(17)	B6-B7	1.803(3)
B6-H6	1.078(15)	B6-H56	1.222(17)	B6-H67	1.312(18)
B7-B8	1.968(3)	B7-H7	1.083(15)	B7-H67	1.298(17)
B8-B9	1.788(3)	B8-H8	1.111(18)	B8-H89	1.277(17)
B9-B10	1.784(3)	B9-H9	1.042(17)	B9-H89	1.339(17)
B9-H910	1.288(18)	B10-H10	1.117(15)	B10-H910	1.245(17)
C1-O1	1.434(2)	C1-H1a	0.96(3)	C1-H1b	0.96(3)
C1-H1c	0.96(2)				

Table 5.2.7. Bond angles for 5-(CH_3O)-$B_{10}H_{13}$. (^{o})

B10-B1-B5	71.38(11)	B10-B1-B3	107.29(15)	B5-B1-B3	108.92(13)
B10-B1-B4	60.22(11)	B5-B1-B4	120.12(14)	B3-B1-B4	60.07(11)
B10-B1-B2	117.68(13)	B5-B1-B2	60.83(11)	B3-B1-B2	59.37(11)
B4-B1-B2	113.53(15)	B10-B1-H1	114.2(8)	B5-B1-H1	112.2(8)
B3-B1-H1	128.5(9)	B4-B1-H1	118.2(8)	B2-B1-H1	119.4(8)
B6-B2-B7	61.84(11)	B6-B2-B3	111.94(15)	B7-B2-B3	59.19(11)
B6-B2-B5	62.03(11)	B7-B2-B5	106.77(13)	B3-B2-B5	107.01(12)
B6-B2-B1	110.16(13)	B7-B2-B1	105.27(13)	B3-B2-B1	59.60(11)
B5-B2-B1	58.24(10)	B6-B2-H2	120.2(8)	B7-B2-H2	126.0(9)
B3-B2-H2	120.4(8)	B5-B2-H2	121.3(9)	B1-B2-H2	119.8(8)
B7-B3-B8	68.14(11)	B7-B3-B2	60.27(11)	B8-B3-B2	117.60(13)
B7-B3-B1	107.20(13)	B8-B3-B1	108.07(14)	B2-B3-B1	61.03(11)
B7-B3-B4	116.43(13)	B8-B3-B4	60.90(11)	B2-B3-B4	115.14(14)
B1-B3-B4	60.22(11)	B7-B3-H3	115.9(7)	B8-B3-H3	113.9(9)
B2-B3-H3	118.6(8)	B1-B3-H3	128.0(8)	B4-B3-H3	117.8(8)

B9-B4-B10	61.38(13)	B9-B4-B3	110.07(13)	B10-B4-B3	105.71(14)
B9-B4-B1	110.30(14)	B10-B4-B1	58.56(12)	B3-B4-B1	59.72(11)
B9-B4-B8	61.07(11)	B10-B4-B8	105.66(13)	B3-B4-B8	58.63(11)
B1-B4-B8	105.90(13)	B9-B4-H4	121.2(9)	B10-B4-H4	125.3(9)
B3-B4-H4	119.5(9)	B1-B4-H4	120.7(9)	B8-B4-H4	123.1(9)
O1-B5-B1	121.56(15)	O1-B5-B2	131.29(15)	B1-B5-B2	60.93(10)
O1-B5-B6	125.15(15)	B1-B5-B6	108.17(14)	B2-B5-B6	56.93(10)
O1-B5-B10	114.16(13)	B1-B5-B10	53.98(10)	B2-B5-B10	104.13(13)
B6-B5-B10	112.99(14)	O1-B5-H56	110.2(8)	B1-B5-H56	125.9(8)
B2-B5-H56	96.7(7)	B6-B5-H56	42.0(7)	B10-B5-H56	92.3(7)
B2-B6-B7	60.26(11)	B2-B6-B5	61.04(11)	B7-B6-B5	104.90(13)
B2-B6-H6	127.3(9)	B7-B6-H6	125.8(9)	B5-B6-H6	125.8(9)
B2-B6-H56	107.2(8)	B7-B6-H56	118.9(9)	B5-B6-H56	48.9(8)
H6-B6-H56	109.1(12)	B2-B6-H67	103.8(7)	B7-B6-H67	46.0(7)
B5-B6-H67	119.0(7)	H6-B6-H67	110.3(11)	H56-B6-H67	94.1(12)
B3-B7-B2	60.55(11)	B3-B7-B6	109.76(15)	B2-B7-B6	57.90(11)
B3-B7-B8	55.96(11)	B2-B7-B8	107.76(12)	B6-B7-B8	118.68(13)
B3-B7-H7	123.8(7)	B2-B7-H7	125.2(9)	B6-B7-H7	117.6(8)
B8-B7-H7	116.8(9)	B3-B7-H67	129.8(7)	B2-B7-H67	102.2(8)
B6-B7-H67	46.6(8)	B8-B7-H67	93.7(7)	H7-B7-H67	105.0(10)
B3-B8-B9	108.42(16)	B3-B8-B4	60.48(11)	B9-B8-B4	57.24(11)
B3-B8-B7	55.90(10)	B9-B8-B7	114.95(14)	B4-B8-B7	106.27(14)
B3-B8-H8	122.9(9)	B9-B8-H8	120.4(9)	B4-B8-H8	125.8(8)
B7-B8-H8	118.0(8)	B3-B8-H89	127.3(9)	B9-B8-H89	48.3(8)
B4-B8-H89	102.8(8)	B7-B8-H89	88.9(8)	H8-B8-H89	107.6(12)
B4-B9-B10	60.93(12)	B4-B9-B8	61.69(12)	B10-B9-B8	105.79(14)
B4-B9-H9	130.8(8)	B10-B9-H9	126.6(10)	B8-B9-H9	125.7(10)
B4-B9-H89	104.4(7)	B10-B9-H89	118.1(8)	B8-B9-H89	45.5(7)
H9-B9-H89	108.3(12)	B4-B9-H910	101.4(8)	B10-B9-H910	44.2(8)
B8-B9-H910	114.8(8)	H9-B9-H910	112.5(12)	H89-B9-H910	92.8(10)
B1-B10-B4	61.21(12)	B1-B10-B9	109.44(14)	B4-B10-B9	57.69(12)
B1-B10-B5	54.64(9)	B4-B10-B5	107.17(13)	B9-B10-B5	117.61(13)
B1-B10-H10	124.3(8)	B4-B10-H10	130.2(7)	B9-B10-H10	120.7(8)
B5-B10-H10	113.0(8)	B1-B10-H910	124.2(8)	B4-B10-H910	100.1(9)
B9-B10-H910	46.2(8)	B5-B10-H910	89.9(8)	H10-B10-H910	108.0(11)

B5-H56-B6	89.1(10)	B6-H67-B7	87.3(11)	B8-H89-B9	86.4(9)
B9-H910-B10	89.5(9)	O1-C1-H1a	109.3(15)	O1-C1-H1b	113.4(14)
H1a-C1-H1b	111(2)	O1-C1-H1c	112.5(13)	H1a-C1-H1c	109(2)
H1b-C1-H1c	101.4(18)	B5-O1-C1	120.82(15)		

Table 5.2.8. Bond lengths for 6-((CH_3)$_3$CO)-$B_{10}H_{13}$. (Å)

B1-B10	1.755(3)	B1-B5	1.764(3)	B1-B2	1.775(3)
B1-B4	1.778(3)	B1-B3	1.780(3)	B1-H1	1.10(2)
B2-B6	1.739(3)	B2-B3	1.774(3)	B2-B7	1.807(3)
B2-B5	1.806(3)	B2-H2	1.14(2)	B3-B8	1.748(3)
B3-B7	1.759(3)	B3-B4	1.785(3)	B3-H3	1.03(2)
B4-B9	1.718(3)	B4-B10	1.796(3)	B4-B8	1.795(3)
B4-H4	1.10(2)	B5-B6	1.826(3)	B5-B10	1.994(3)
B5-H5	1.04(2)	B5-H56	1.205(19)	B6-O11	1.335(2)
B6-B7	1.827(3)	B6-H56	1.44(2)	B6-H67	1.41(2)
B7-B8	1.977(3)	B7-H7	1.11(2)	B7-H67	1.25(2)
B8-B9	1.799(4)	B8-H8	1.04(2)	B8-H89	1.29(2)
B9-B10	1.793(3)	B9-H9	1.11(3)	B9-H89	1.26(3)
B9-H910	1.29(2)	B10-H10	1.07(2)	B10-H910	1.17(2)
O11-C12	1.470(2)	C12-C13	1.514(3)	C12-C15	1.516(3)
C12-C14	1.516(3)	C13-H13a	0.99(3)	C13-H13b	0.93(3)
C13-H13c	0.95(2)	C14-H14a	0.98(2)	C14-H14b	1.00(2)
C14-H14c	0.94(3)	C15-H15a	0.99(3)	C15-H15b	1.04(3)
C15-H15c	0.94(2)				

Table 5.2.9. Bond angles for 6-((CH_3)$_3$CO)-$B_{10}H_{13}$. (^{o})

B10-B1-B5	69.04(13)	B10-B1-B2	118.06(15)	B5-B1-B2	61.37(12)
B10-B1-B4	61.13(13)	B5-B1-B4	118.36(16)	B2-B1-B4	114.60(15)
B10-B1-B3	107.83(15)	B5-B1-B3	108.04(15)	B2-B1-B3	59.89(12)
B4-B1-B3	60.22(12)	B10-B1-H1	115.7(13)	B5-B1-H1	113.1(12)
B2-B1-H1	116.4(12)	B4-B1-H1	119.7(12)	B3-B1-H1	127.9(13)
B6-B2-B3	112.97(14)	B6-B2-B1	112.80(15)	B3-B2-B1	60.21(12)

B6-B2-B7	61.97(12)	B3-B2-B7	58.83(11)	B1-B2-B7	105.80(14)
B6-B2-B5	61.96(11)	B3-B2-B5	106.47(15)	B1-B2-B5	59.03(12)
B7-B2-B5	104.65(14)	B6-B2-H2	114.7(11)	B3-B2-H2	122.6(12)
B1-B2-H2	122.7(12)	B7-B2-H2	123.8(13)	B5-B2-H2	123.1(13)
B8-B3-B7	68.62(12)	B8-B3-B2	118.05(15)	B7-B3-B2	61.52(11)
B8-B3-B1	107.49(17)	B7-B3-B1	107.64(15)	B2-B3-B1	59.90(12)
B8-B3-B4	61.06(13)	B7-B3-B4	117.56(16)	B2-B3-B4	114.26(17)
B1-B3-B4	59.82(13)	B8-B3-H3	116.3(10)	B7-B3-H3	114.5(11)
B2-B3-H3	116.4(11)	B1-B3-H3	127.3(11)	B4-B3-H3	119.4(11)
B9-B4-B1	111.35(16)	B9-B4-B3	111.32(16)	B1-B4-B3	59.95(13)
B9-B4-B10	61.31(14)	B1-B4-B10	58.79(13)	B3-B4-B10	105.80(15)
B9-B4-B8	61.55(14)	B1-B4-B8	105.56(15)	B3-B4-B8	58.45(12)
B10-B4-B8	104.65(16)	B9-B4-H4	120.3(12)	B1-B4-H4	121.2(12)
B3-B4-H4	118.0(13)	B10-B4-H4	127.3(14)	B8-B4-H4	122.2(13)
B1-B5-B2	59.60(12)	B1-B5-B6	109.23(16)	B2-B5-B6	57.23(11)
B1-B5-B10	55.25(12)	B2-B5-B10	105.46(14)	B6-B5-B10	118.50(15)
B1-B5-H5	120.6(12)	B2-B5-H5	123.5(12)	B6-B5-H5	118.8(12)
B10-B5-H5	118.3(12)	B1-B5-H56	125.7(10)	B2-B5-H56	104.2(11)
B6-B5-H56	51.8(11)	B10-B5-H56	87.5(10)	H5-B5-H56	111.3(15)
O11-B6-B2	136.39(16)	O11-B6-B5	133.69(17)	B2-B6-B5	60.81(12)
O11-B6-B7	122.91(16)	B2-B6-B7	60.84(11)	B5-B6-B7	103.07(14)
O11-B6-H56	116.3(8)	B2-B6-H56	97.9(8)	B5-B6-H56	41.2(8)
B7-B6-H56	110.3(8)	O11-B6-H67	107.5(8)	B2-B6-H67	99.6(8)
B5-B6-H67	110.0(9)	B7-B6-H67	43.2(8)	H56-B6-H67	87.7(13)
B3-B7-B2	59.65(12)	B3-B7-B6	109.55(15)	B2-B7-B6	57.19(11)
B3-B7-B8	55.43(11)	B2-B7-B8	105.81(15)	B6-B7-B8	119.42(15)
B3-B7-H7	121.6(10)	B2-B7-H7	121.1(10)	B6-B7-H7	115.5(10)
B8-B7-H7	121.0(10)	B3-B7-H67	125.9(10)	B2-B7-H67	102.9(10)
B6-B7-H67	50.6(9)	B8-B7-H67	88.7(9)	H7-B7-H67	111.3(15)
B3-B8-B4	60.48(13)	B3-B8-B9	109.27(17)	B4-B8-B9	57.11(13)
B3-B8-B7	55.96(11)	B4-B8-B7	106.84(14)	B9-B8-B7	117.60(15)
B3-B8-H8	120.3(11)	B4-B8-H8	126.5(11)	B9-B8-H8	121.8(12)
B7-B8-H8	114.6(12)	B3-B8-H89	131.1(11)	B4-B8-H89	99.9(12)
B9-B8-H89	44.5(12)	B7-B8-H89	96.1(11)	H8-B8-H89	107.4(16)
B4-B9-B10	61.50(13)	B4-B9-B8	61.33(13)	B10-B9-B8	104.63(15)

B4-B9-H9	128.6(11)	B10-B9-H9	125.9(14)	B8-B9-H9	127.3(14)
B4-B9-H89	105.2(11)	B10-B9-H89	119.1(11)	B8-B9-H89	45.7(11)
H9-B9-H89	108.8(17)	B4-B9-H910	100.1(10)	B10-B9-H910	40.8(10)
B8-B9-H910	116.7(11)	H9-B9-H910	111.6(18)	H89-B9-H910	98.3(16)
B1-B10-B9	108.95(17)	B1-B10-B4	60.08(13)	B9-B10-B4	57.19(13)
B1-B10-B5	55.71(11)	B9-B10-B5	118.03(15)	B4-B10-B5	106.63(16)
B1-B10-H10	123.5(12)	B9-B10-H10	117.4(11)	B4-B10-H10	124.1(11)
B5-B10-H10	118.8(11)	B1-B10-H910	129.6(12)	B9-B10-H910	45.8(11)
B4-B10-H910	100.7(12)	B5-B10-H910	94.5(11)	H10-B10-H910	106.1(17)
B5-H56-B6	86.9(13)	B6-H67-B7	86.2(11)	B8-H89-B9	89.8(15)
B9-H910-B10	93.4(15)	B6-O11-C12	129.10(15)	O11-C12-C13	109.28(15)
O11-C12-C15	109.05(14)	C13-C12-C15	112.16(18)	O11-C12-C14	103.92(14)
C13-C12-C14	111.37(16)	C15-C12-C14	110.72(16)	C12-C13-H13a	112.9(14)
C12-C13-H13b	107.8(16)	H13a-C13-H13b	104(2)	C12-C13-H13c	109.4(14)
H13a-C13-H13c	112.1(18)	H13b-C13-H13c	110.2(19)	C12-C14-H14a	111.0(12)
C12-C14-H14b	107.3(14)	H14a-C14-H14b	112.1(17)	C12-C14-H14c	109.6(16)
H14a-C14-H14c	109(2)	H14b-C14-H14c	107(2)	C12-C15-H15a	107.5(14)
C12-C15-H15b	116.1(14)	H15a-C15-H15b	107(2)	C12-C15-H15c	112.3(13)
H15a-C15-H15c	110.5(19)	H15b-C15-H15c	103(2)		

Table 5.2.10. Bond lengths for 6,6'-($C_6H_{10}O_2$)-($B_{10}H_{13}$)$_2$. (Å)

B1-B10	1.748(2)	B1-B5	1.749(2)	B1-B2	1.768(2)
B1-B3	1.770(2)	B1-B4	1.775(2)	B1-H1	1.111(16)
B2-B6	1.733(2)	B2-B3	1.769(2)	B2-B7	1.798(2)
B2-B5	1.799(2)	B2-H2	1.118(16)	B3-B8	1.746(3)
B3-B7	1.760(2)	B3-B4	1.778(2)	B3-H3	1.083(16)
B4-B9	1.717(3)	B4-B10	1.789(2)	B4-B8	1.790(2)
B4-H4	1.094(16)	B5-B6	1.804(2)	B5-B10	1.980(2)
B5-H5	1.094(16)	B5-H56	1.202(16)	B6-O11	1.3549(19)
B6-B7	1.816(2)	B6-H56	1.353(15)	B6-H67	1.382(16)
B7-B8	1.991(2)	B7-H6	1.071(16)	B7-H67	1.221(17)
B8-B9	1.787(3)	B8-H7	1.088(17)	B8-H89	1.262(16)
B9-B10	1.794(3)	B9-H8	1.071(17)	B9-H89	1.274(16)

B9-H910	1.269(16)	B10-H9	1.099(16)	B10-H910	1.248(16)
O11-C12	1.4506(17)	C12-C13	1.517(2)	C12-C14	1.517(2)
C12-H12	0.993(15)	C13-C14	1.528(2)	C13-H13a	0.968(16)
C13-H13b	0.986(17)	C14-C12	1.517(2)	C14-H14a	0.983(17)
C14-H14b	1.002(17)				

Table 5.2.11. Bond angles for 6,6'-($C_6H_{10}O_2$)-($B_{10}H_{13}$)$_2$. (^{o})

B10-B1-B5	68.98(10)	B10-B1-B2	118.21(12)	B5-B1-B2	61.52(9)
B10-B1-B3	107.81(12)	B5-B1-B3	108.14(11)	B2-B1-B3	59.98(9)
B10-B1-B4	61.01(10)	B5-B1-B4	118.21(12)	B2-B1-B4	114.68(12)
B3-B1-B4	60.21(9)	B10-B1-H1	115.8(8)	B5-B1-H1	113.9(8)
B2-B1-H1	116.6(8)	B3-B1-H1	127.3(8)	B4-B1-H1	119.0(8)
B6-B2-B1	111.71(12)	B6-B2-B3	112.22(12)	B1-B2-B3	60.07(9)
B6-B2-B7	61.90(10)	B1-B2-B7	106.31(11)	B3-B2-B7	59.12(9)
B6-B2-B5	61.41(10)	B1-B2-B5	58.70(9)	B3-B2-B5	106.02(11)
B7-B2-B5	105.11(12)	B6-B2-H2	118.0(8)	B1-B2-H2	120.0(8)
B3-B2-H2	121.8(8)	B7-B2-H2	125.4(8)	B5-B2-H2	122.5(8)
B8-B3-B7	69.21(10)	B8-B3-B2	118.17(12)	B7-B3-B2	61.25(9)
B8-B3-B1	107.69(12)	B7-B3-B1	107.88(12)	B2-B3-B1	59.95(9)
B8-B3-B4	61.04(10)	B7-B3-B4	118.24(12)	B2-B3-B4	114.49(12)
B1-B3-B4	60.03(9)	B8-B3-H3	114.5(8)	B7-B3-H3	114.0(8)
B2-B3-H3	117.9(8)	B1-B3-H3	128.3(8)	B4-B3-H3	118.4(8)
B9-B4-B1	111.20(12)	B9-B4-B3	110.95(12)	B1-B4-B3	59.76(9)
B9-B4-B10	61.50(11)	B1-B4-B10	58.74(9)	B3-B4-B10	105.69(11)
B9-B4-B8	61.20(11)	B1-B4-B8	105.56(11)	B3-B4-B8	58.58(9)
B10-B4-B8	104.80(12)	B9-B4-H4	121.0(8)	B1-B4-H4	119.3(8)
B3-B4-H4	119.5(9)	B10-B4-H4	124.6(9)	B8-B4-H4	125.0(8)
B1-B5-B2	59.78(9)	B1-B5-B6	109.28(12)	B2-B5-B6	57.49(9)
B1-B5-B10	55.49(9)	B2-B5-B10	105.87(11)	B6-B5-B10	118.00(12)
B1-B5-H5	122.2(8)	B2-B5-H5	125.0(8)	B6-B5-H5	118.7(8)
B10-B5-H5	117.7(8)	B1-B5-H56	126.7(7)	B2-B5-H56	102.2(8)
B6-B5-H56	48.6(7)	B10-B5-H56	90.0(7)	H5-B5-H56	109.3(11)
O11-B6-B2	135.12(14)	O11-B6-B5	123.37(13)	B2-B6-B5	61.10(9)
O11-B6-B7	131.87(13)	B2-B6-B7	60.80(9)	B5-B6-B7	104.11(11)

O11-B6-H56	107.8(7)	B2-B6-H56	99.3(7)	B5-B6-H56	41.8(7)
B7-B6-H56	113.2(6)	O11-B6-H67	113.7(7)	B2-B6-H67	99.7(7)
B5-B6-H67	113.7(7)	B7-B6-H67	42.2(7)	H56-B6-H67	92.6(9)
B3-B7-B2	59.63(9)	B3-B7-B6	108.74(12)	B2-B7-B6	57.29(9)
B3-B7-B8	55.07(9)	B2-B7-B8	105.38(11)	B6-B7-B8	117.52(12)
B3-B7-H6	120.7(8)	B2-B7-H6	124.3(8)	B6-B7-H6	120.2(8)
B8-B7-H6	117.6(8)	B3-B7-H67	126.9(8)	B2-B7-H67	103.1(8)
B6-B7-H67	49.5(8)	B8-B7-H67	89.8(7)	H6-B7-H67	110.3(11)
B3-B8-B9	109.25(13)	B3-B8-B4	60.38(10)	B9-B8-B4	57.39(10)
B3-B8-B7	55.72(9)	B9-B8-B7	117.57(12)	B4-B8-B7	106.74(11)
B3-B8-H7	122.3(9)	B9-B8-H7	119.9(9)	B4-B8-H7	126.3(9)
B7-B8-H7	116.1(9)	B3-B8-H89	129.4(7)	B9-B8-H89	45.5(7)
B4-B8-H89	100.6(7)	B7-B8-H89	94.0(7)	H7-B8-H89	107.0(11)
B4-B9-B8	61.40(10)	B4-B9-B10	61.20(10)	B8-B9-B10	104.73(12)
B4-B9-H8	127.9(9)	B8-B9-H8	126.1(9)	B10-B9-H8	126.6(9)
B4-B9-H89	103.9(7)	B8-B9-H89	44.9(7)	B10-B9-H89	117.6(7)
H8-B9-H89	110.3(12)	B4-B9-H910	103.2(7)	B8-B9-H910	118.2(7)
B10-B9-H910	44.1(7)	H8-B9-H910	110.5(12)	H89-B9-H910	96.4(10)
B1-B10-B4	60.25(10)	B1-B10-B9	108.92(13)	B4-B10-B9	57.29(10)
B1-B10-B5	55.53(9)	B4-B10-B5	106.61(11)	B9-B10-B5	117.57(12)
B1-B10-H9	123.1(8)	B4-B10-H9	127.6(8)	B9-B10-H9	120.2(8)
B5-B10-H9	115.3(8)	B1-B10-H910	129.8(7)	B4-B10-H910	100.3(8)
B9-B10-H910	45.0(7)	B5-B10-H910	95.1(7)	H9-B10-H910	105.6(11)
B6-O11-C12	122.22(12)	O11-C12-C13	107.08(12)	O11-C12-C14’	110.62(12)
C13-C12-C14’	111.07(12)	O11-C12-H12	105.9(8)	C13-C12-H12	110.8(9)
C14’-C12-H12	111.2(9)	C12-C13-C14	110.60(13)	C12-C13-H13a	108.4(9)
C14-C13-H13a	109.3(9)	C12-C13-H13b	110.1(9)	C14-C13-H13b	110.0(9)
H13a-C13-H13b	108.5(13)	C12’-C14-C13	109.90(13)	C12’-C14-H14a	109.8(9)
C13-C14-H14a	111.6(9)	C12’-C14-H14b	109.6(9)	C13-C14-H14b	109.3(9)
H14a-C14-H14b	106.6(13)				

Table 5.2.12. Bond lengths for 5-($CH_3C{\equiv}CCH_2O$)-$B_{10}H_{13}$. (Å)

B1-B10	1.747(2)	B1-B5	1.7605(19)	B1-B3	1.774(2)
B1-B4	1.787(2)	B1-B2	1.791(2)	B1-H1	1.082(15)
B2-B6	1.726(2)	B2-B3	1.764(2)	B2-B7	1.782(2)
B2-B5	1.8118(19)	B2-H2	1.086(16)	B3-B7	1.743(2)
B3-B8	1.755(2)	B3-B4	1.782(2)	B3-H3	1.073(16)
B4-B9	1.720(2)	B4-B10	1.765(2)	B4-B8	1.791(2)
B4-H4	1.080(16)	B5-O1	1.3828(17)	B5-B6	1.793(2)
B5-B10	2.044(2)	B5-H56	1.305(14)	B6-B7	1.792(2)
B6-H5	1.064(16)	B6-H56	1.286(14)	B6-H67	1.245(17)
B7-B8	1.954(2)	B7-H7	1.089(15)	B7-H67	1.273(17)
B8-B9	1.787(2)	B8-H8	1.084(17)	B8-H89	1.276(17)
B9-B10	1.761(2)	B9-H9	1.052(16)	B9-H89	1.319(17)
B9-H910	1.293(14)	B10-H10	1.089(15)	B10-H910	1.240(14)
O1-C1	1.4336(15)	C1-C2	1.4586(18)	C1-H1a	0.953(15)
C1-H1b	0.957(16)	C2-C3	1.1889(19)	C3-C4	1.4585(19)
C4-H4a	0.9600	C4-H4b	0.9600	C4-H4c	0.9600
B1'-B5'	1.754(2)	B1'-B10'	1.755(2)	B1'-B3'	1.769(2)
B1'-B4'	1.787(2)	B1'-B2'	1.791(2)	B1'-H1'	1.069(15)
B2'-B6'	1.728(2)	B2'-B3'	1.765(2)	B2'-B7'	1.776(2)
B2'-B5'	1.807(2)	B2'-H2'	1.090(17)	B3'-B7'	1.743(2)
B3'-B8'	1.748(2)	B3'-B4'	1.783(3)	B3'-H3'	1.052(19)
B4'-B9'	1.717(2)	B4'-B10'	1.767(2)	B4'-B8'	1.791(2)
B4'-H4'	1.083(17)	B5'-O1'	1.3814(17)	B5'-B6'	1.794(2)
B5'-B10'	2.038(2)	B5'-H56'	1.301(15)	B6'-B7'	1.792(2)
B6'-H6'	1.076(16)	B6'-H56'	1.280(15)	B6'-H67'	1.258(16)
B7'-B8'	1.949(3)	B7'-H7'	1.098(16)	B7'-H67'	1.244(16)
B8'-B9'	1.790(3)	B8'-H8'	1.092(18)	B8'-H89'	1.251(16)
B9'-B10'	1.761(2)	B9'-H9'	1.067(19)	B9'-H89'	1.302(16)
B9'-H910'	1.293(16)	B10'-H10'	1.105(16)	B10'-H910'	1.216(16)
O1'-C1'	1.4316(15)	C1'-C2'	1.4593(18)	C1'-H1a'	0.970(16)
C1'-H1b'	0.992(17)	C2'-C3'	1.1894(19)	C3'-C4'	1.4590(19)
C4'-H4a'	0.9600	C4'-H4b'	0.9600	C4'-H4c'	0.9600

Table 5.2.13. Bond angles for 5-($CH_3C{\equiv}CCH_2O$)-$B_{10}H_{13}$. (°)

B10-B1-B5	71.28(8)	B10-B1-B3	107.25(10)	B5-B1-B3	108.24(10)
B10-B1-B4	59.90(8)	B5-B1-B4	119.16(10)	B3-B1-B4	60.05(8)
B10-B1-B2	118.95(10)	B5-B1-B2	61.33(8)	B3-B1-B2	59.32(8)
B4-B1-B2	113.85(10)	B10-B1-H1	116.4(8)	B5-B1-H1	113.4(8)
B3-B1-H1	126.8(8)	B4-B1-H1	119.4(8)	B2-B1-H1	116.5(8)
B6-B2-B3	111.33(11)	B6-B2-B7	61.43(9)	B3-B2-B7	58.88(9)
B6-B2-B1	109.89(10)	B3-B2-B1	59.86(8)	B7-B2-B1	105.10(10)
B6-B2-B5	60.84(8)	B3-B2-B5	106.42(10)	B7-B2-B5	104.97(10)
B1-B2-B5	58.50(7)	B6-B2-H2	120.7(8)	B3-B2-H2	119.8(8)
B7-B2-H2	125.1(8)	B1-B2-H2	120.4(8)	B5-B2-H2	123.7(8)
B7-B3-B8	67.91(9)	B7-B3-B2	61.05(9)	B8-B3-B2	117.78(11)
B7-B3-B1	107.50(10)	B8-B3-B1	107.62(10)	B2-B3-B1	60.82(8)
B7-B3-B4	116.83(11)	B8-B3-B4	60.83(9)	B2-B3-B4	115.43(10)
B1-B3-B4	60.32(8)	B7-B3-H3	117.8(9)	B8-B3-H3	115.5(8)
B2-B3-H3	118.3(8)	B1-B3-H3	125.9(9)	B4-B3-H3	116.1(9)
B9-B4-B10	60.71(9)	B9-B4-B3	110.57(11)	B10-B4-B3	106.17(10)
B9-B4-B1	110.04(10)	B10-B4-B1	58.95(8)	B3-B4-B1	59.63(8)
B9-B4-B8	61.17(9)	B10-B4-B8	105.16(10)	B3-B4-B8	58.84(9)
B1-B4-B8	105.54(10)	B9-B4-H4	121.7(8)	B10-B4-H4	124.6(8)
B3-B4-H4	119.3(8)	B1-B4-H4	120.0(8)	B8-B4-H4	124.3(8)
O1-B5-B1	126.77(10)	O1-B5-B6	119.65(10)	B1-B5-B6	108.27(10)
O1-B5-B2	131.45(11)	B1-B5-B2	60.17(8)	B6-B5-B2	57.22(8)
O1-B5-B10	116.37(10)	B1-B5-B10	54.06(7)	B6-B5-B10	114.93(10)
B2-B5-B10	104.32(9)	O1-B5-H56	104.4(6)	B1-B5-H56	126.1(6)
B6-B5-H56	45.8(6)	B2-B5-H56	100.0(6)	B10-B5-H56	91.0(6)
B2-B6-B7	60.81(8)	B2-B6-B5	61.94(8)	B7-B6-B5	105.31(10)
B2-B6-H5	129.0(8)	B7-B6-H5	127.1(8)	B5-B6-H5	125.3(8)
B2-B6-H56	105.4(6)	B7-B6-H56	116.6(7)	B5-B6-H56	46.7(6)
H5-B6-H56	109.5(10)	B2-B6-H67	103.9(8)	B7-B6-H67	45.2(8)
B5-B6-H67	118.8(8)	H5-B6-H67	109.6(11)	H56-B6-H67	93.7(10)
B3-B7-B2	60.07(8)	B3-B7-B6	109.23(10)	B2-B7-B6	57.76(8)
B3-B7-B8	56.34(8)	B2-B7-B8	107.45(10)	B6-B7-B8	118.14(10)
B3-B7-H7	122.1(8)	B2-B7-H7	126.6(8)	B6-B7-H7	120.4(8)

B8-B7-H7	114.7(8)	B3-B7-H67	129.8(8)	B2-B7-H67	99.7(8)
B6-B7-H67	44.0(8)	B8-B7-H67	95.5(8)	H7-B7-H67	107.0(11)
B3-B8-B9	108.71(11)	B3-B8-B4	60.32(8)	B9-B8-B4	57.46(8)
B3-B8-B7	55.75(8)	B9-B8-B7	116.23(10)	B4-B8-B7	106.54(10)
B3-B8-H8	123.0(9)	B9-B8-H8	119.0(9)	B4-B8-H8	124.5(9)
B7-B8-H8	118.6(9)	B3-B8-H89	127.5(8)	B9-B8-H89	47.5(8)
B4-B8-H89	102.1(8)	B7-B8-H89	90.4(8)	H8-B8-H89	107.8(12)
B4-B9-B10	60.90(9)	B4-B9-B8	61.37(9)	B10-B9-B8	105.45(11)
B4-B9-H9	131.2(9)	B10-B9-H9	125.8(8)	B8-B9-H9	126.9(8)
B4-B9-H89	104.0(8)	B10-B9-H89	117.8(8)	B8-B9-H89	45.5(8)
H9-B9-H89	109.2(11)	B4-B9-H910	102.5(6)	B10-B9-H910	44.7(6)
B8-B9-H910	116.7(6)	H9-B9-H910	109.6(11)	H89-B9-H910	94.0(10)
B1-B10-B9	109.95(10)	B1-B10-B4	61.15(8)	B9-B10-B4	58.39(9)
B1-B10-B5	54.66(7)	B9-B10-B5	116.61(10)	B4-B10-B5	106.63(9)
B1-B10-H10	122.1(8)	B9-B10-H10	122.3(8)	B4-B10-H10	129.5(8)
B5-B10-H10	113.0(8)	B1-B10-H910	126.7(7)	B9-B10-H910	47.2(7)
B4-B10-H910	102.5(7)	B5-B10-H910	90.0(7)	H10-B10-H910	107.4(10)
B5-O1-C1	117.61(10)	O1-C1-C2	111.30(10)	O1-C1-H1a	108.6(9)
C2-C1-H1a	109.1(8)	O1-C1-H1b	109.7(9)	C2-C1-H1b	110.1(9)
H1a-C1-H1b	108.0(12)	C3-C2-C1	171.61(13)	C2-C3-C4	179.10(14)
C3-C4-H4a	109.5	C3-C4-H4b	109.5	H4a-C4-H4b	109.5
C3-C4-H4c	109.5	H4a-C4-H4c	109.5	H4b-C4-H4c	109.5
B5-H56-B6	87.6(9)	B6-H67-B7	90.8(11)	B8-H89-B9	87.1(11)
B9-H910-B10	88.1(9)	B5'-B1'-B10'	71.00(9)	B5'-B1'-B3'	108.47(10)
B10'-B1'-B3'	107.15(11)	B5'-B1'-B4'	119.18(11)	B10'-B1'-B4'	59.84(9)
B3'-B1'-B4'	60.18(9)	B5'-B1'-B2'	61.30(8)	B10'-B1'-B2'	118.47(10)
B3'-B1'-B2'	59.42(9)	B4'-B1'-B2'	113.94(11)	B5'-B1'-H1'	113.7(8)
B10'-B1'-H1'	116.9(8)	B3'-B1'-H1'	126.3(8)	B4'-B1'-H1'	119.0(8)
B2'-B1'-H1'	116.6(8)	B6'-B2'-B3'	111.18(11)	B6'-B2'-B7'	61.48(9)
B3'-B2'-B7'	58.99(9)	B6'-B2'-B1'	109.62(10)	B3'-B2'-B1'	59.68(9)
B7'-B2'-B1'	105.18(11)	B6'-B2'-B5'	60.95(8)	B3'-B2'-B5'	106.31(11)
B7'-B2'-B5'	105.41(10)	B1'-B2'-B5'	58.33(8)	B6'-B2'-H2'	121.6(9)
B3'-B2'-H2'	119.1(8)	B7'-B2'-H2'	124.7(8)	B1'-B2'-H2'	120.1(8)
B5'-B2'-H2'	124.2(8)	B7'-B3'-B8'	67.88(10)	B7'-B3'-B2'	60.83(9)
B8'-B3'-B2'	117.63(11)	B7'-B3'-B1'	107.53(11)	B8'-B3'-B1'	107.87(11)

B2'-B3'-B1'	60.90(9)	B7'-B3'-B4'	116.83(12)	B8'-B3'-B4'	60.96(10)
B2'-B3'-B4'	115.44(11)	B1'-B3'-B4'	60.39(9)	B7'-B3'-H3'	114.4(10)
B8'-B3'-H3'	115.2(10)	B2'-B3'-H3'	116.7(10)	B1'-B3'-H3'	128.1(10)
B4'-B3'-H3'	119.3(10)	B9'-B4'-B10'	60.72(9)	B9'-B4'-B3'	110.54(12)
B10'-B4'-B3'	106.05(11)	B9'-B4'-B1'	110.33(11)	B10'-B4'-B1'	59.20(9)
B3'-B4'-B1'	59.43(9)	B9'-B4'-B8'	61.31(10)	B10'-B4'-B8'	105.03(11)
B3'-B4'-B8'	58.55(10)	B1'-B4'-B8'	105.25(11)	B9'-B4'-H4'	119.5(9)
B10'-B4'-H4'	122.8(9)	B3'-B4'-H4'	121.8(9)	B1'-B4'-H4'	120.9(9)
B8'-B4'-H4'	125.1(9)	O1'-B5'-B1'	126.89(11)	O1'-B5'-B6'	119.01(10)
B1'-B5'-B6'	108.32(10)	O1'-B5'-B2'	130.02(11)	B1'-B5'-B2'	60.37(8)
B6'-B5'-B2'	57.34(8)	O1'-B5'-B10'	117.75(10)	B1'-B5'-B10'	54.53(8)
B6'-B5'-B10'	114.20(10)	B2'-B5'-B10'	104.68(10)	O1'-B5'-H56'	105.4(6)
B1'-B5'-H56'	125.3(6)	B6'-B5'-H56'	45.5(6)	B2'-B5'-H56'	99.7(6)
B10'-B5'-H56'	89.8(6)	B2'-B6'-B7'	60.57(9)	B2'-B6'-B5'	61.71(8)
B7'-B6'-B5'	105.30(10)	B2'-B6'-H6'	127.5(8)	B7'-B6'-H6'	126.0(8)
B5'-B6'-H6'	125.7(8)	B2'-B6'-H56'	104.8(7)	B7'-B6'-H56'	116.5(7)
B5'-B6'-H56'	46.5(7)	H6'-B6'-H56'	111.5(11)	B2'-B6'-H67'	102.2(7)
B7'-B6'-H67'	44.0(7)	B5'-B6'-H67'	118.3(7)	H6'-B6'-H67'	111.2(11)
H56'-B6'-H67'	94.2(10)	B3'-B7'-B2'	60.18(9)	B3'-B7'-B6'	109.20(10)
B2'-B7'-B6'	57.94(8)	B3'-B7'-B8'	56.17(9)	B2'-B7'-B8'	107.45(11)
B6'-B7'-B8'	117.74(10)	B3'-B7'-H7'	124.5(9)	B2'-B7'-H7'	125.8(8)
B6'-B7'-H7'	117.9(9)	B8'-B7'-H7'	117.0(8)	B3'-B7'-H67'	128.8(7)
B2'-B7'-H67'	100.3(7)	B6'-B7'-H67'	44.6(7)	B8'-B7'-H67'	94.0(7)
H7'-B7'-H67'	105.6(11)	B3'-B8'-B9'	108.79(11)	B3'-B8'-B4'	60.48(10)
B9'-B8'-B4'	57.29(10)	B3'-B8'-B7'	55.95(9)	B9'-B8'-B7'	116.31(11)
B4'-B8'-B7'	106.78(11)	B3'-B8'-H8'	124.4(9)	B9'-B8'-H8'	118.0(9)
B4'-B8'-H8'	125.1(9)	B7'-B8'-H8'	118.8(9)	B3'-B8'-H89'	128.1(7)
B9'-B8'-H89'	46.7(7)	B4'-B8'-H89'	101.4(8)	B7'-B8'-H89'	91.4(7)
H8'-B8'-H89'	106.1(12)	B4'-B9'-B10'	61.04(10)	B4'-B9'-B8'	61.40(10)
B10'-B9'-B8'	105.33(12)	B4'-B9'-H9'	131.8(10)	B10'-B9'-H9'	127.3(10)
B8'-B9'-H9'	125.8(9)	B4'-B9'-H89'	103.2(7)	B10'-B9'-H89'	117.9(7)
B8'-B9'-H89'	44.3(7)	H9'-B9'-H89'	108.0(12)	B4'-B9'-H910'	102.4(7)
B10'-B9'-H910'	43.6(7)	B8'-B9'-H910'	118.6(7)	H9'-B9'-H910'	108.9(12)
H89'-B9'-H910'	97.2(10)	B1'-B10'-B9'	109.74(11)	B1'-B10'-B4'	60.97(9)
B9'-B10'-B4'	58.24(9)	B1'-B10'-B5'	54.47(8)	B9'-B10'-B5'	117.11(10)

B4'-B10'-B5'	106.53(10)	B1'-B10'-H10'	123.3(8)	B9'-B10'-H10'	121.3(8)
B4'-B10'-H10'	129.7(8)	B5'-B10'-H10'	113.4(8)	B1'-B10'-H910'	129.1(8)
B9'-B10'-H910'	47.2(8)	B4'-B10'-H910'	103.1(8)	B5'-B10'-H910'	92.7(8)
H10'-B10'-H910'	104.2(11)	B5'-O1'-C1'	118.07(10)	O1'-C1'-C2'	110.43(10)
O1'-C1'-H1a'	108.3(9)	C2'-C1'-H1a'	110.1(9)	O1'-C1'-H1b'	107.8(9)
C2'-C1'-H1b'	109.2(9)	H1a'-C1'-H1b'	111.0(13)	C3'-C2'-C1'	173.74(13)
C2'-C3'-C4'	179.46(15)	C3'-C4'-H4a'	109.5	C3'-C4'-H4b'	109.5
H4a'-C4'-H4b'	109.5	C3'-C4'-H4c'	109.5	H4a'-C4'-H4c'	109.5
H4b'-C4'-H4c'	109.5	B5'-H56'-B6'	88.1(9)	B6'-H67'-B7'	91.5(10)
B8'-H89'-B9'	89.0(10)	B9'-H910'-B10'	89.2(11)		

Computational Methods. Density Functional Theory (DFT) calculations were performed using the Gaussian 03 package.[20] All ground state, transition state, and intermediate geometries and both electronic and free energies were obtained at the B3LYP/6-311G(d) level without constraints for all H, C, B and Cl atoms. Both the B3LYP/6-311G(d) level and B3LYP/SDD pseudopotential were used for Br atoms (separate calculations), and only the B3LYP/SDD pseudopotential was used for I atoms. The NMR chemical shifts were calculated at the B3LYP/6-311G(d) level using the GIAO option within Gaussian 03 and are referenced to $BF_3 \cdot O(C_2H_5)_2$ using an absolute shielding constant of 102.24 ppm. Harmonic vibrational analyses were carried out on the optimized geometries at the same level to establish the nature of stationary points. True first-order saddle points possessed only one imaginary frequency. Intrinsic reaction coordinate (IRC) calculations were carried out in both the forward and reverse directions to confirm the reaction pathways from the located transition states.

The DFT optimized geometries and relevant energies of studied compounds, intermediates and transition states are provided in **Tables 5.2.14-5.2.35**.

Table 5.2.14. DFT optimized (B3LYP/6-311G*) coordinates for 5-CH_3O-$B_{10}H_{13}$.

Center Number	Atomic Number	X	Y	Z
1	5	-0.1989	1.177376	0.82709
2	5	1.909589	-0.95604	0.606089
3	5	1.507095	0.741345	0.997847
4	5	0.270978	-0.52843	1.190195
5	5	-1.01908	-0.23039	0.042592
6	5	0.456115	-1.65252	-0.13093
7	5	2.404772	0.393455	-0.47176
8	5	1.023251	1.778614	-0.31941
9	5	1.883965	-1.20992	-1.09418
10	5	-0.64942	1.33167	-0.83686
11	1	1.948756	0.009141	-1.64646
12	1	0.498522	1.47071	-1.49686
13	1	2.507396	-1.93889	-1.78602
14	1	0.074512	-2.77174	-0.10589
15	1	3.520224	0.737366	-0.66713
16	1	2.653517	-1.56239	1.299668
17	1	1.354008	2.910372	-0.42077
18	1	-0.72785	1.840988	1.65468
19	1	2.13998	1.270414	1.849791
20	1	-0.1156	-1.00214	2.206136
21	1	-1.4365	2.090587	-1.2904
22	1	0.587793	-1.3598	-1.41586
23	1	-0.84106	0.159954	-1.32711
24	8	-2.26901	-0.7629	0.160011
25	6	-3.44584	-0.05507	-0.21169
26	1	-4.29721	-0.67212	0.071886
27	1	-3.50706	0.907926	0.304002
28	1	-3.4742	0.117408	-1.29298

Table 5.2.15. DFT optimized (B3LYP/6-311G*) coordinates for 6-CH_3O-$B_{10}H_{13}$.

Center Number	Atomic Number	X	Y	Z
1	5	0.110119	0.094183	-1.48486
2	5	-2.451	-0.00851	0.06954
3	5	-1.3532	0.952024	-0.96199
4	5	-1.3487	-0.82961	-1.07112
5	5	0.19321	-1.40373	-0.47506
6	5	-1.5213	-1.46156	0.547473
7	5	-1.5279	1.37965	0.722238
8	5	0.18715	1.457483	-0.30106
9	5	-1.8475	-0.10616	1.676823
10	5	1.30089	0.019522	-0.24757
11	1	-0.9362	0.85601	1.791771
12	1	0.81846	0.949614	0.701141
13	1	-2.4258	-0.17142	2.706645
14	1	-1.9611	-2.5313	0.797937
15	1	-1.9725	2.408422	1.1024
16	1	-3.6173	0.000957	-0.13463
17	1	0.66359	2.520832	-0.50955
18	1	0.47404	0.165369	-2.60981
19	1	-1.8317	1.72723	-1.72173
20	1	-1.8225	-1.5098	-1.91961
21	1	-0.9314	-1.07152	1.671867
22	1	0.82388	-1.01427	0.581266
23	1	0.67868	-2.42785	-0.81677
24	8	2.65899	0.026272	-0.30999
25	6	3.48592	-0.05715	0.842972
26	1	3.29953	-0.98462	1.396466
27	1	4.52089	-0.05028	0.505017
28	1	3.32329	0.79887	1.507624

Table 5.2.16. DFT optimized (B3LYP/6-311G*) coordinates for **INT1**.

Center Number	Atomic Number	X	Y	Z
1	5	-0.3199	-0.05167	0.753903
2	5	2.62789	0.28475	0.337273
3	5	1.05515	1.120197	0.508716
4	5	1.34557	-0.36087	1.400802
5	5	0.35228	-1.70755	0.901254
6	5	2.21957	-1.45612	0.363821
7	5	1.81325	1.049118	-1.03891
8	5	-0.2106	1.008813	-0.67311
9	5	2.5985	-0.55343	-1.16777
10	5	-0.8162	-1.30494	-0.45405
11	1	1.62024	0.006755	-1.86615
12	1	1.91442	-1.65825	-0.92368
13	1	-0.4502	-1.34902	-1.58483
14	1	3.47474	-0.8163	-1.91839
15	1	2.98328	-2.31039	0.662418
16	1	2.2119	1.943446	-1.70531
17	1	3.60966	0.739644	0.81983
18	1	-0.4105	0.756761	-1.8132
19	1	-1.134	0.249036	1.569389
20	1	1.01344	2.165537	1.075773
21	1	1.55116	-0.37433	2.568165
22	17	-2.5404	-1.87577	-0.26853
23	1	0.00787	-2.3789	1.816686
24	1	0.12797	-2.36812	-0.13825
25	8	-1.1053	2.345892	-0.53947
26	1	-1.7156	2.378069	-1.28555
27	6	-1.7454	2.848346	0.679544
28	1	-0.9808	2.853201	1.445914
29	1	-2.08194	3.860524	0.464323
30	1	-2.56678	2.191672	0.956707

Table 5.2.17. DFT optimized (B3LYP/6-311G*) coordinates for **TS1**.

Center Number	Atomic Number	X	Y	Z
1	5	0.267054	0.132671	0.792744
2	5	-2.275	-1.34733	0.22204
3	5	-0.4918	-1.4317	0.279777
4	5	-1.3499	-0.36725	1.397394
5	5	-1.0398	1.323454	1.083732
6	5	-2.6705	0.373936	0.526374
7	5	-1.297	-1.42844	-1.25193
8	5	0.47081	-0.49784	-0.81354
9	5	-2.7227	-0.36676	-1.12362
10	5	0.13995	1.51036	-0.32653
11	1	-1.6108	-0.31123	-1.8902
12	1	-2.5998	0.885713	-0.69661
13	1	-0.2844	1.383387	-1.44165
14	1	-3.6546	-0.39848	-1.85091
15	1	-3.6968	0.761631	0.97094
16	1	-1.2695	-2.29224	-2.05861
17	1	-2.9295	-2.25658	0.604396
18	1	0.96712	-0.34899	-1.86667
19	1	1.18597	0.125766	1.545636
20	1	0.03038	-2.44794	0.594701
21	1	-1.501	-0.5928	2.550785
22	17	1.44809	2.767395	-0.22694
23	1	-1.0019	2.03338	2.030433
24	1	-1.096	2.07352	0.063729
25	8	2.4227	-1.52003	-0.50814
26	1	2.94795	-0.71233	-0.4466
27	6	2.78834	-2.39809	0.566648
28	1	2.27311	-3.33916	0.391245
29	1	3.86714	-2.57368	0.554386
30	1	2.487218	-1.99239	1.535905

Table 5.2.18. DFT optimized (B3LYP/6-311G*) coordinates for **INT2**.

Center Number	Atomic Number	X	Y	Z
1	5	-0.84753	-0.5188	-1.47821
2	5	-2.7677	0.8966	0.358746
3	5	-1.305	1.02868	-0.67086
4	5	-2.5269	-0.22897	-1.01056
5	5	-1.8063	-1.77791	-0.65739
6	5	-3.0732	-0.86258	0.534882
7	5	-1.1701	1.175525	1.065084
8	5	0.18522	0.234504	-0.20203
9	5	-2.3726	0.135131	1.850944
10	5	-0.0439	-1.54983	-0.35083
11	1	-1.0293	0.191993	1.935193
12	1	-2.3596	-1.18101	1.594399
13	1	0.81376	-2.33764	-0.55048
14	1	-2.8024	0.275843	2.943084
15	1	-4.1321	-1.36069	0.70696
16	1	-0.7632	2.138624	1.620578
17	1	-3.6153	1.720866	0.301164
18	1	0.30137	-0.8079	0.675494
19	1	-0.5396	-0.52548	-2.62194
20	1	-1.1422	2.037151	-1.27518
21	1	-3.3557	-0.23417	-1.85827
22	17	4.10458	-0.78545	0.486452
23	1	-2.1486	-2.80314	-1.13747
24	1	-1.0052	-2.13036	0.350592
25	8	1.47142	0.746482	-0.26875
26	1	2.98366	-0.19237	0.137886
27	6	1.73786	2.100819	-0.65086
28	1	1.16639	2.79603	-0.03262
29	1	2.80309	2.270103	-0.50072
30	1	1.487926	2.256313	-1.70204

Table 5.2.19. DFT optimized (B3LYP/6-311G*) coordinates for **TS2**.

Center Number	Atomic Number	X	Y	Z
1	5	0.050367	-0.78187	0.942919
2	5	2.55189	0.781775	0.442244
3	5	0.85621	0.79616	0.909617
4	5	1.80452	-0.67325	1.226787
5	5	1.20958	-1.97063	0.198005
6	5	2.89799	-0.88682	-0.10798
7	5	1.30996	1.396045	-0.69814
8	5	-0.312	0.468974	-0.33021
9	5	2.7814	0.491352	-1.23814
10	5	-0.5773	-1.33975	-0.5471
11	1	1.58733	0.725572	-1.80165
12	1	2.69614	-0.77621	-1.45704
13	1	-0.854	-2.09986	-1.39694
14	1	3.61901	0.938746	-1.94289
15	1	3.91649	-1.48582	-0.04869
16	1	1.19804	2.530253	-1.02677
17	1	3.30594	1.469805	1.042783
18	1	-0.3226	-0.20053	-1.41369
19	1	-0.644	-1.01567	1.873306
20	1	0.50446	1.618711	1.689373
21	1	2.181	-0.96802	2.311085
22	17	-2.9565	-1.15888	-0.16205
23	1	1.27087	-3.06253	0.660989
24	1	1.22093	-2.0025	-1.00706
25	8	-1.5979	1.227867	-0.37669
26	1	-2.347	0.466087	-0.30268
27	6	-1.8822	2.389539	0.451014
28	1	-1.0935	3.116677	0.282829
29	1	-2.8393	2.777185	0.11041
30	1	-1.9255	2.098928	1.498959

Table 5.2.20. DFT optimized (B3LYP/6-311G*) coordinates for **INT3**.

Center Number	Atomic Number	X	Y	Z
1	5	0.025651	-0.39253	-0.9844
2	5	2.710471	0.501692	-0.21002
3	5	1.770765	-0.59791	-1.24289
4	5	1.124836	1.002282	-0.82467
5	5	-0.30292	0.889979	0.231386
6	5	1.525724	1.371693	0.826213
7	5	2.546401	-1.25944	0.168563
8	5	0.841211	-1.92983	-0.51546
9	5	2.600976	0.038784	1.447759
10	1	2.160101	-1.16966	1.493576
11	1	1.512627	0.543707	1.924987
12	1	-0.34011	0.720172	1.414528
13	1	0.921198	-2.37968	0.597299
14	1	3.451214	0.163896	2.262282
15	1	1.64959	2.455023	1.284231
16	1	3.434955	-2.04086	0.180423
17	1	3.694501	1.001932	-0.64123
18	1	0.718917	-2.81863	-1.3000
19	1	-0.68798	-0.39822	-1.94874
20	1	2.161716	-0.81916	-2.33954
21	1	1.043834	1.870347	-1.62661
22	17	-1.68546	2.057239	-0.20249
23	8	-2.18442	-1.40909	-0.17239
24	1	-2.31092	-1.01039	-1.05087
25	6	-3.35327	-1.25597	0.698641
26	1	-4.205	-1.67773	0.170448
27	1	-3.13465	-1.8296	1.593182
28	1	-3.49549	-0.20117	0.925044
29	1	-0.74988	-1.37184	1.485923
30	5	-0.75847	-1.06526	0.34446

Table 5.2.21. DFT optimized (B3LYP/6-311G*) coordinates for **TS3**.

Center Number	Atomic Number	X	Y	Z
1	5	-0.06729	-0.67748	0.985359
2	5	-2.75064	0.46861	0.402024
3	5	-1.81696	-0.89007	1.124611
4	5	-1.1194	0.745388	1.016844
5	5	0.222111	0.734122	-0.11173
6	5	-1.55315	1.406552	-0.55445
7	5	-2.73956	-1.16765	-0.32672
8	5	-0.92169	-1.95989	0.03822
9	5	-2.79455	0.329871	-1.31226
10	1	-2.48142	-0.88112	-1.63483
11	1	-1.63989	0.811997	-1.74752
12	1	0.327372	0.245185	-1.2604
13	1	-0.85658	-1.85903	-1.16393
14	1	-3.6517	0.693397	-2.04226
15	1	-1.59865	2.56553	-0.78856
16	1	-3.63087	-1.94235	-0.4046
17	1	-3.66396	0.941642	0.989614
18	1	-0.8235	-3.0951	0.375795
19	1	0.589235	-0.90942	1.947699
20	1	-2.21236	-1.36847	2.13476
21	1	-0.96485	1.519287	1.900733
22	17	1.573543	1.959869	0.109614
23	8	2.530434	-1.09783	0.287046
24	1	2.589579	-0.44325	0.995866
25	6	3.684011	-1.02188	-0.56999
26	1	4.569941	-1.33072	-0.01299
27	1	3.510727	-1.7217	-1.38458
28	1	3.812561	-0.01326	-0.96702
29	1	1.170353	-1.51318	-1.46948
30	5	0.712376	-1.01011	-0.50354

Table 5.2.22. DFT optimized (B3LYP/ 6-311G*) coordinates for **INT4**.

Center Number	Atomic Number	X	Y	Z
1	5	0.857248	0.717585	1.286508
2	5	3.20741	-0.64828	0.036004
3	5	2.480644	0.885056	0.592233
4	5	1.975417	-0.65823	1.322096
5	5	0.305595	-0.94899	0.873028
6	5	1.869749	-1.84674	0.042293
7	5	2.69177	0.616398	-1.12377
8	5	1.11649	1.52875	-0.30332
9	5	2.535924	-1.13843	-1.47038
10	1	1.944722	-0.07162	-1.98744
11	1	1.382175	-1.73459	-1.19004
12	1	-0.44500	-1.6000	1.514541
13	1	0.360108	0.900092	-1.12234
14	1	3.036093	-1.73018	-2.36346
15	1	1.970861	-3.01202	0.217569
16	1	3.390458	1.279487	-1.81072
17	1	4.334804	-0.89843	0.296042
18	1	0.976227	2.688339	-0.49911
19	1	0.561004	1.289975	2.281205
20	1	3.190488	1.71363	1.056667
21	1	2.26498	-1.09867	2.384193
22	17	-4.15095	-1.13496	-0.1552
23	8	-1.66964	0.843733	-0.05765
24	1	-3.08619	-0.37737	-0.05649
25	6	-2.09721	2.207063	-0.19805
26	1	-1.73749	2.626213	-1.1406
27	1	-3.18556	2.200872	-0.19601
28	1	-1.73043	2.809382	0.635006
29	1	-0.2278	-0.81027	-0.30221
30	5	-0.33884	0.518317	0.059521

Table 5.2.23. DFT optimized (B3LYP/6-311G*) coordinates for **TS4**.

Center Number	Atomic Number	X	Y	Z
1	5	-0.12056	-0.14329	-1.02858
2	5	-2.88773	-0.55017	-0.08652
3	5	-1.82964	0.091953	-1.35315
4	5	-1.30477	-1.36666	-0.46463
5	5	0.101809	-0.9494	0.491145
6	5	-1.86996	-1.23157	1.16872
7	5	-2.54055	1.220124	-0.21584
8	5	-0.83485	1.497851	-1.01993
9	5	-2.66212	0.336447	1.383092
10	1	-2.06138	1.466856	0.991748
11	1	-1.5593	-0.16893	1.930973
12	1	0.54931	-1.11772	1.561484
13	1	-0.29008	2.088435	-0.02552
14	1	-3.40168	0.611482	2.26425
15	1	-2.06941	-2.12622	1.913748
16	1	-3.39871	2.011971	-0.41303
17	1	-3.91613	-1.04632	-0.39795
18	1	-0.63141	2.216274	-1.94084
19	1	0.636655	-0.40512	-1.89599
20	1	-2.21753	0.094249	-2.47187
21	1	-1.28344	-2.45061	-0.94736
22	17	2.466219	-1.66057	-0.1444
23	8	1.973855	1.110484	-0.15971
24	1	2.333339	0.065907	-0.24948
25	6	2.852892	1.899951	0.683679
26	1	2.806834	1.540293	1.711823
27	1	3.857664	1.793046	0.282165
28	1	2.531341	2.936935	0.620511
29	1	0.336447	1.116513	1.363779
30	5	0.537078	0.958522	0.19207

Table 5.2.24. DFT optimized (B3LYP/6-311G*) coordinates for 5-(CH_3S)-$B_{10}H_{13}$.

Center Number	Atomic Number	X	Y	Z
1	5	0.160797	1.178376	0.895158
2	5	2.177105	-1.01622	0.541956
3	5	1.859475	0.671552	1.028621
4	5	0.565055	-0.54805	1.158241
5	5	-0.69204	-0.13807	-0.00199
6	5	0.685751	-1.59956	-0.23665
7	5	2.732912	0.365998	-0.46094
8	5	1.408026	1.804595	-0.21988
9	5	2.146917	-1.17578	-1.17149
10	5	-0.27394	1.447735	-0.75397
11	1	2.262435	0.061956	-1.65834
12	1	0.882077	1.570127	-1.41131
13	1	2.746789	-1.89641	-1.89184
14	1	0.270546	-2.70641	-0.25887
15	1	3.85965	0.676876	-0.6456
16	1	2.888905	-1.69862	1.197229
17	1	1.785476	2.925191	-0.26478
18	1	-0.34557	1.813033	1.757653
19	1	2.514947	1.128972	1.904633
20	1	0.166961	-1.06727	2.145835
21	1	-1.03175	2.236718	-1.2023
22	1	0.854725	-1.26802	-1.50843
23	1	-0.50996	0.28116	-1.29385
24	6	-3.47145	0.586817	-0.32696
25	1	-4.49631	0.255636	-0.16341
26	1	-3.27487	1.460424	0.293655
27	1	-3.34872	0.84328	-1.37886
28	16	-2.39043	-0.81815	0.152811

Table 5.2.25. DFT optimized (B3LYP/6-311G*) coordinates for 5-($C_6H_{11}O$)-$B_{10}H_{13}$.

Center Number	Atomic Number	X	Y	Z
1	5	1.541644	-1.44265	0.015984
2	5	3.628201	0.450527	-1.03962
3	5	3.241142	-1.17259	-0.40248
4	5	1.987378	-0.23642	-1.25313
5	5	0.707708	0.155904	-0.11675
6	5	2.174783	1.435998	-0.80001
7	5	4.151287	-0.0559	0.602582
8	5	2.788755	-1.29657	1.277812
9	5	3.616905	1.618204	0.223259
10	5	1.119494	-0.63603	1.490944
11	1	3.702037	0.921052	1.363519
12	1	2.283121	-0.38437	2.090985
13	1	4.238647	2.612668	0.376037
14	1	1.779781	2.34736	-1.44218
15	1	5.273536	-0.22443	0.938967
16	1	4.356082	0.564441	-1.96681
17	1	3.135953	-2.18072	1.983897
18	1	1.013545	-2.45999	-0.28669
19	1	3.868067	-2.08752	-0.82275
20	1	1.582788	-0.41909	-2.35288
21	1	0.361066	-1.02074	2.314941
22	1	2.32232	1.911186	0.427755
23	1	0.924881	0.602186	1.251358
24	8	-0.53626	0.551101	-0.49425
25	6	-1.78034	0.090019	0.073466
26	6	-2.63248	1.307168	0.430246
27	6	-2.48224	-0.81393	-0.94083
28	1	-1.56953	-0.48401	0.983673
29	6	-4.02342	0.8884	0.929928
30	1	-2.72495	1.93144	-0.46608
31	1	-2.1157	1.911864	1.18279
32	6	-3.87196	-1.23673	-0.4415
33	1	-2.57175	-0.26136	-1.8832
34	1	-1.85885	-1.68942	-1.1453
35	6	-4.73591	-0.02115	-0.08043
36	1	-4.62518	1.779384	1.134839
37	1	-3.92498	0.359787	1.887131

38	1	-4.36741	-1.84543	-1.20424
39	1	-3.76432	-1.88135	0.440598
40	1	-5.70115	-0.34763	0.320226
41	1	-4.95627	0.550858	-0.99085

Table 5.2.26. DFT optimized (B3LYP/6-311G*) coordinates for 6-($C_6H_{11}O$)-$B_{10}H_{13}$.

Center Number	Atomic Number	X	Y	Z
1	5	-2.00105	-0.23371	-1.54581
2	5	-4.13364	-0.00822	0.550255
3	5	-3.35854	0.70594	-0.89252
4	5	-3.26695	-1.05337	-0.60914
5	5	-1.5966	-1.46088	-0.28313
6	5	-3.02951	-1.30547	1.100881
7	5	-3.17759	1.500704	0.651602
8	5	-1.74501	1.365021	-0.73852
9	5	-3.17831	0.266119	1.954009
10	5	-0.55245	-0.01063	-0.64099
11	1	-2.32813	1.236992	1.640505
12	1	-0.88131	1.107037	0.175046
13	1	-3.50417	0.428185	3.079579
14	1	-3.33361	-2.29535	1.674207
15	1	-3.58772	2.584683	0.89146
16	1	-5.31438	-0.05765	0.625914
17	1	-1.39847	2.357247	-1.28361
18	1	-1.91103	-0.41714	-2.71268
19	1	-4.04378	1.28344	-1.67
20	1	-3.87687	-1.91305	-1.15363
21	1	-2.22616	-0.66263	1.941333
22	1	-0.76828	-0.83625	0.483666
23	1	-1.13967	-2.53282	-0.49217
24	8	0.751788	0.003949	-1.01415
25	6	1.867142	0.000179	-0.09761
26	6	2.714675	-1.2478	-0.33762
27	6	2.679138	1.279777	-0.29407
28	1	1.480275	-0.02413	0.932426
29	6	3.964392	-1.24803	0.555757
30	1	3.003333	-1.26332	-1.39474
31	1	2.109337	-2.14267	-0.16393

32	6	3.929038	1.28806	0.598545
33	1	2.967595	1.336818	-1.34969
34	1	2.05004	2.152845	-0.0939
35	6	4.78864	0.035088	0.378582
36	1	4.575048	-2.12829	0.333073
37	1	3.663503	-1.34455	1.607218
38	1	4.513979	2.192281	0.404651
39	1	3.626624	1.341465	1.652671
40	1	5.640652	0.035866	1.065887
41	1	5.208923	0.058161	-0.63482

Table 5.2.27. DFT optimized (6-311G*) coordinates for TS2 (X=F).

Center Number	Atomic Number	X	Y	Z
1	5	0.049749	0.94508	0.894236
2	5	-2.02526	-1.16621	0.468471
3	5	-0.36693	-0.78063	0.89819
4	5	-1.62384	0.446018	1.220093
5	5	-1.40111	1.832903	0.177722
6	5	-2.78115	0.359755	-0.07207
7	5	-0.7007	-1.4843	-0.69631
8	5	0.704459	-0.23967	-0.34623
9	5	-2.34737	-0.93937	-1.20603
10	5	0.635626	1.588917	-0.57312
11	1	-1.12477	-0.86712	-1.77846
12	1	-2.56728	0.319511	-1.41278
13	1	0.640901	2.450392	-1.37518
14	1	-3.05756	-1.56745	-1.91335
15	1	-3.91796	0.679179	0.01107
16	1	-0.35142	-2.56605	-1.03526
17	1	-2.58218	-2.00915	1.08715
18	1	0.582312	0.459596	-1.43459
19	1	0.683483	1.329027	1.825947
20	1	0.169552	-1.49587	1.678797
21	1	-2.02688	0.651522	2.31616
22	1	-1.69855	2.869691	0.679595
23	1	-1.40408	1.891792	-1.02045
24	8	2.11856	-0.61517	-0.36783
25	1	2.57895	0.593475	-0.29458
26	6	2.671652	-1.65443	0.458186

27	1	2.121523	-2.57857	0.287793
28	1	3.708666	-1.78034	0.151796
29	1	2.617655	-1.3803	1.512503
30	9	2.436869	1.670674	-0.32415

Table 5.2.28. DFT optimized (B3LYP/SDD for Br, 6-311G* for B, H) coordinates for **TS2** (X=Br).

Center Number	Atomic Number	X	Y	Z
1	5	0.45332	-0.62907	0.963162
2	5	3.186423	0.44834	0.403592
3	5	1.52911	0.779037	0.89212
4	5	2.206096	-0.82375	1.239352
5	5	1.375847	-2.0319	0.261924
6	5	3.20907	-1.27012	-0.1095
7	5	2.055519	1.254426	-0.73405
8	5	0.305182	0.635287	-0.33196
9	5	3.331336	0.086001	-1.27252
10	5	-0.26129	-1.11286	-0.51029
11	1	2.204732	0.530586	-1.83402
12	1	3.009142	-1.1436	-1.46466
13	1	-0.6473	-1.79456	-1.38293
14	1	4.232906	0.358578	-1.98763
15	1	4.103181	-2.04288	-0.05627
16	1	2.143324	2.384971	-1.08237
17	1	4.063901	0.998736	0.97768
18	1	0.188328	-0.02007	-1.40456
19	1	-0.25971	-0.71579	1.903716
20	1	1.339195	1.662365	1.66024
21	1	2.536895	-1.14945	2.329396
22	1	1.24246	-3.09241	0.779608
23	1	1.402208	-2.1378	-0.93782
24	8	-0.82811	1.624833	-0.37285
25	1	-1.69858	1.056716	-0.29807
26	6	-0.88647	2.816817	0.466912
27	1	0.019401	3.386319	0.286103
28	1	-1.76258	3.372117	0.141482
29	1	-0.96571	2.52863	1.513008
30	35	-2.74746	-0.59312	-0.08488

Table 5.2.29. DFT optimized (B3LYP/SDD for I, 6-311G* for B, H) coordinates for **TS2** (X=I).

Center Number	Atomic Number	X	Y	Z
1	5	0.857905	-0.57687	0.962918
2	5	3.669714	0.264328	0.394468
3	5	2.049041	0.736545	0.892301
4	5	2.590795	-0.91316	1.242708
5	5	1.657659	-2.05572	0.277121
6	5	3.534384	-1.4525	-0.11515
7	5	2.606981	1.169107	-0.73547
8	5	0.813332	0.693921	-0.33032
9	5	3.774621	-0.10907	-1.28145
10	5	0.120963	-1.01046	-0.5161
11	1	2.699004	0.440099	-1.84248
12	1	3.344064	-1.30126	-1.47612
13	1	-0.29102	-1.63619	-1.41824
14	1	4.700065	0.08334	-1.99229
15	1	4.358465	-2.29983	-0.06994
16	1	2.790091	2.289416	-1.08011
17	1	4.594789	0.735877	0.964228
18	1	0.660537	0.0631	-1.40622
19	1	0.144709	-0.60049	1.905872
20	1	1.938007	1.628292	1.666861
21	1	2.895347	-1.25715	2.334641
22	1	1.433344	-3.09201	0.812207
23	1	1.704765	-2.19477	-0.9183
24	8	-0.23395	1.780337	-0.37002
25	1	-1.15312	1.315341	-0.30229
26	6	-0.18472	2.982392	0.45876
27	1	0.772521	3.459847	0.277451
28	1	-1.00242	3.614029	0.120921
29	1	-0.29757	2.712293	1.506349
30	53	-2.5413	-0.37411	-0.0534

Table 5.2.30. DFT optimized (B3LYP/6-311G*) coordinates for 6-F-$B_{10}H_{13}$.

Center Number	Atomic Number	X	Y	Z
1	5	-0.67787	-0.89149	1.118304
2	5	0.854866	0.0000	1.207452
3	5	-0.67787	0.891492	1.118304
4	5	-2.01124	0.0000	0.336083
5	5	0.661412	-1.43197	0.125147
6	5	1.6527	0.00000	-0.30981
7	5	0.661412	1.431972	0.125147
8	5	-1.25238	1.423166	-0.44482
9	5	-1.83035	0.00000	-1.37485
10	5	-1.25238	-1.42317	-0.44482
11	1	-0.93685	-1.62445	2.013636
12	1	1.503167	0.00000	2.198292
13	1	-0.93685	1.624449	2.013636
14	1	-3.08972	0.00000	0.823643
15	1	1.204796	-2.47383	0.26006
16	9	2.944321	0.00000	-0.66024
17	1	1.204796	2.473834	0.26006
18	1	-1.75472	2.476514	-0.6378
19	1	-2.64878	0.00000	-2.22813
20	1	-1.75472	-2.47651	-0.6378
21	1	0.998208	-0.98051	-1.04182
22	1	0.998208	0.98051	-1.04182
23	1	-0.96400	0.966908	-1.66024
24	1	-0.96400	-0.96691	-1.66024

Table 5.2.31. DFT optimized (B3LYP/SDD for Br, 6-311G* for B, H) coordinates for 6-Br-$B_{10}H_{13}$.

Center Number	Atomic Number	X	Y	Z
1	5	-1.78035	-1.20927	0.891772
2	5	-1.41014	0.291344	0.0000
3	5	-1.78035	-1.20927	-0.89177
4	5	-1.41029	-2.70987	0.00000
5	5	-0.44466	-0.21532	1.428076
6	5	0.284038	0.586579	0.00000
7	5	-0.44466	-0.21532	-1.42808
8	5	-0.44466	-2.2076	-1.42335
9	5	0.282458	-3.02129	0.00000
10	5	-0.44466	-2.2076	1.423349
11	1	-2.71119	-1.2013	1.62605
12	1	-2.16652	1.201238	0.00000
13	1	-2.71119	-1.2013	-1.62605
14	1	-2.18395	-3.60568	0.00000
15	1	-0.39157	0.336251	2.471979
16	35	1.293567	2.26247	0.00000
17	1	-0.39157	0.336251	-2.47198
18	1	-0.40213	-2.74345	-2.47688
19	1	0.875877	-4.04365	0.00000
20	1	-0.40213	-2.74345	2.476881
21	1	0.788726	-0.20207	0.96591
22	1	0.788726	-0.20207	-0.96591
23	1	0.799217	-2.26458	-0.96945
24	1	0.799217	-2.26458	0.969445

Table 5.2.32. DFT optimized (B3LYP/SDD for I, 6-311G* for B, H) coordinates for 6-I-$B_{10}H_{13}$.

Center Number	Atomic Number	X	Y	Z
1	5	-2.3907	-0.89049	1.062495
2	5	-0.8831	0.00000	1.416587
3	5	-2.3907	0.890493	1.062495
4	5	-3.5559	0.00000	0.047133
5	5	-0.8971	-1.42667	0.328184
6	5	0.15071	0.00000	0.038783
7	5	-0.8971	1.426669	0.328184
8	5	-2.6688	1.422609	-0.58272
9	5	-3.0566	0.00000	-1.60202
10	5	-2.6688	-1.42261	-0.58272
11	1	-2.8091	-1.62417	1.894557
12	1	-0.4203	0.00000	2.505457
13	1	-2.8091	1.624168	1.894557
14	1	-4.7064	0.00000	0.325119
15	1	-0.385	-2.47273	0.527927
16	53	2.31439	0.00000	-0.11272
17	1	-0.385	2.472727	0.527926
18	1	-3.1257	2.476128	-0.86598
19	1	-3.6929	0.00000	-2.5982
20	1	-3.1257	-2.47613	-0.86598
21	1	-0.3101	-0.96404	-0.76431
22	1	-0.3101	0.964036	-0.76431
23	1	-2.1463	0.968947	-1.71236
24	1	-2.1463	-0.96895	-1.71236

Table 5.2.33. Calculated free energies and electronic energies (298K) at B3LYP/6-311G* for starting materials, intermediates, transition states, and products of the reactions of **6Cl** to **5OMe** and **5Cl** to **6OMe**.

Reactions			
Free Energy			
	G (in Hartrees)		**G (in Hartrees)**
6Cl	-716.556894	**5Cl**	-716.556697
MeOH	-115.717905	**HCl**	-460.837449
TS1	-832.237981	**TS3**	-832.235336
INT1	-832.245029	**INT3**	-832.245796
TS2	-832.226957	**TS4**	-832.216440
INT2	-832.279627	**INT4**	-832.280961
5OMe	-371.448947	**6OMe**	-371.448731
Electronic Energy			
	E (in Hartrees)		**E (in Hartrees)**
6Cl	-716.523471	**5Cl**	-716.523384
MeOH	-115.695198	**HCl**	-460.819552
TS1	-832.198346	**TS3**	-832.196428
INT1	-832.206435	**INT3**	-832.206778
TS2	-832.189451	**TS4**	-832.179111
INT2	-832.238786	**INT4**	-832.239520
5OMe	-371.413763	**6OMe**	-371.411611

Table 5.2.34. Calculated free energies and electronic energies (298K) at B3LYP/6-311G* for 5-(CH_3S)-$B_{10}H_{13}$ and CH_3SH.

	G (in Hartrees)
5-(CH_3S)-$B_{10}H_{13}$	-694.417600
CH_3SH	-438.711916
	E (in Hartrees)
5-(CH_3S)-$B_{10}H_{13}$	-694.381374
CH_3SH	-438.687692

Table 5.2.35. Calculated free energies and electronic energies (298K) for 6-X-$B_{10}H_{13}$ at B3LYP/6-311G* (X=F) or B3LYP/SDD (X=Br, I).

	G (in Hartrees)
6-F-$B_{10}H_{13}$	-356.213582
6-Br-$B_{10}H_{13}$	-269.552521
6-I-$B_{10}H_{13}$	-267.736717
TS2 (X=F)	-471.871328
TS2 (X=Br)	-385.382605
TS2 (X=I)	-383.417938
HF	-100.465885
HBr	-13.986600
HI	-12.025099
	E (in Hartrees)
6-F-$B_{10}H_{13}$	-356.181130
6-Br-$B_{10}H_{13}$	-269.517752
6-I-$B_{10}H_{13}$	-267.701465
TS2 (X=F)	-471.834649
TS2 (X=Br)	-385.344033
TS2 (X=I)	-383.378340
HF	-100.449474
HBr	-13.967331
HI	-12.004940

5.3 Results and Discussion

5.3.1 Syntheses of 6OR and 5OR

The reaction of 5- and 6-halodecaboranes with alcohols led to the formation of decaboranyl ethers, with the loss of hydrogen halide. However, the observed regiochemistry was surprising, as the reaction of 6-X-$B_{10}H_{13}$ (**6X**) with an alcohol yielded 5-RO-$B_{10}H_{13}$ (**5OR**), while the reaction of 5-X-$B_{10}H_{13}$ (**5X**) produced the 6-RO-$B_{10}H_{13}$ (**6OR**) isomer (**Eq. 5** and **6**).

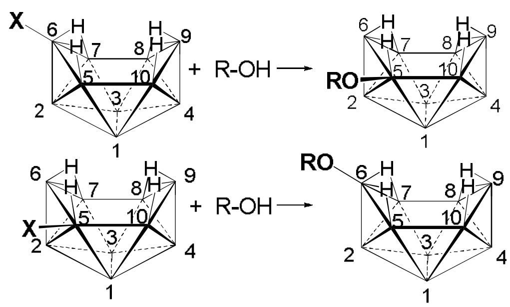

(5)

(6)

A variety of alkyl alcohols were employed as nucleophiles, resulting in the production of a range of boranyl ether compounds (**Table 5.3.1**).

Table 5.3.1. Isolated yields for a number of 6-RO-$B_{10}H_{13}$ and 5-RO-$B_{10}H_{13}$ compounds.

*N.I. indicates that the compound was not isolated due to complications in workup.

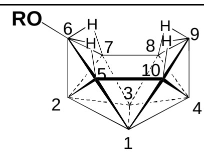		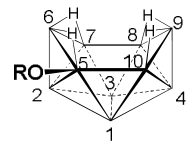	
-OR	% yield	-OR	% yield
-OCH_3	51	-OCH_3	90
-OC_6H_{11}	48	-OC_6H_{11}	77
-$OC(CH_3)_3$	42	-$OC(CH_3)_3$	75
-$O(CH_2)_3C{\equiv}CH$	66	-$O(CH_2)_3C{\equiv}CH$	38
-$O(CH_2C{\equiv}CCH_3)$	N.I.*	-$O(CH_2C{\equiv}CCH_3)$	72
-$OCH(CH_2CH{=}CH_2)_2$	62	-$OCH(CH_2CH{=}CH_2)_2$	48
-OC_2H_4SH	49	-OC_2H_4SH	88
-OC_4H_2I	45	-OC_4H_2I	69
-$OC_2H_4(NC_4H_4O_2)$	N.I.*	-$OC_2H_4(NC_4H_4O_2)$	74
-$OC_2H_4OC_2H_4Cl$	62	-$OC_2H_4OC_2H_4Cl$	80

In general, the syntheses of the 5-RO-$B_{10}H_{13}$ compounds were faster and required less purification than their 6-RO-$B_{10}H_{13}$ counterparts. Reactions starting with **6Br** proceeded quickly at room temperature, while those starting with **5Br** required heating (70 ^{o}C) to go to completion. Since alcohols are only mildly basic, the rate of the base-catalyzed isomerization between **5X** and **6X**, described in **Chapter 3**,[2] was slow at room temperature compared to the rate of substitution. However, at 70 ^{o}C the rate of isomerization from **5X** to **6X** was competitive with the substitution rate. The ^{11}B NMR spectra of the reactions of **5Br** with alcohols at 70 ^{o}C displayed small resonances for **6Br** after ~ 1 h. Accordingly, the room temperature reactions with **6Br** yielded comparatively pure **5OR** products, while the isomerization that occurred at 70 ^{o}C with **5Br** resulted in a mix of product isomers that, although favoring **6OR**, required more extensive purification resulting in decreased isolated yields.

In agreement with a previous report,[9] chromatographic separations resulted in greatly decreased yields, especially when used to isolate **5OR**, as these compounds were somewhat less stable and had longer retention times on the acidified silica gel columns than the **6OR** isomers. If the silica gel was not acidified prior to use, the **5OR** compounds degraded completely on the column. Best yields were found when the products were purified via crystallization, or simple filtration through a small plug of silica. Both **5OR** and **6OR** slowly degraded when left exposed to air for prolonged periods of time.

No substitution was seen in the reactions of phenol with **6Br** at temperatures up to 90 ^{o}C, likely as a result of the decreased basicity (ie. nucleophilicity) of the phenolic oxygen when compared to the oxygen on the alcohols. Even when the more strongly

Lewis-basic *p*-methoxyphenol was employed, still no reaction was observed. The role of the relative basicity of the nucleophilic oxygen was examined through comparisons of the reaction rates of β-halogenated alcohols with **6Br**. The presence of halogens on alcohols inductively alters the electron density, and Lewis basicity, at oxygen according to the electronegativity of the halogen.[21] In order of decreasing basicity, the tested alcohols rank: C_2H_5OH > IC_2H_4OH> BrC_2H_4OH> ClC_2H_4OH> FC_2H_4OH. Accordingly, the reaction of **6Br** with ethanol was largely complete after 12 h at room temperature, but reactions with 2-iodoethanol (~20 h), 2-bromoethanol (~40 h), 2-chloroethanol (~100 h) and 2-fluoroethanol (~125 h), all took significantly longer, in line with the predicted trend.

Mercapto-compounds also failed to react, despite their greater Lewis basicity than phenols. This result may be explained thermodynamically, as the formation of a non-dative B-S bond (85 – 90 kcal/mol),[22] which is comparatively weaker than a similar B-O bond (117 – 119 kcal/mol),[23] fails to provide a sufficient driving force for halogen substitution. DFT calculations showed that the reaction of methanol with **6Br** to yield **5OMe** was -10.0 kcal/mol downhill, while the reaction employing methylthiol was instead +5.6 kcal/mol uphill. This selectivity for oxygen allowed the synthesis of the potentially useful compounds 6- and 5-(HSC_2H_4O)-$B_{10}H_{13}$ through the reaction of **5Br** or **6Br** with 2-mercaptoethanol (**Eq. 7** and **8**). The free thiol group on these products could find utility as a pendant nucleophile, or as a way of tethering the polyborane to metallic surfaces.

Additionally, the pendant thiol group on a 10-boron cage may be a useful tool in anti-cancer research. Therapeutic agents for Boron Neutron Capture Therapy (BNCT) must be of both of high boron content[24] and be preferentially taken up in tumor cells, rather than healthy cells, once administered *in vivo*. To date, one of only two potential BNCT agents promising enough to undergo clinical trials is a thiolated polyborate ($[B_{12}H_{11}SH]^{2-}[Na]^{+}{}_{2}$).[25]

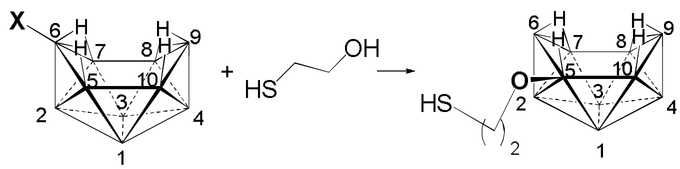

(7)

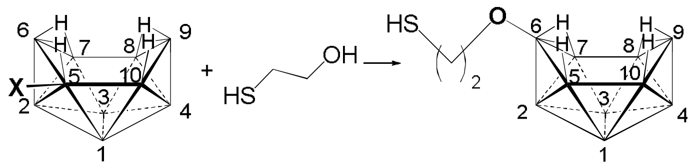

(8)

Particularly high-boron content can be achieved through the reactions of halodecaboranes with alcohols bearing more than one hydroxyl. The reaction of 1,4-cyclohexyldiol with both **5Br** and **6Br** yielded the high-boron content compounds 6,6'-(C_6H_{10})-$(B_{10}H_{13})_2$ (**Eq. 9**) and 5,5'-(C_6H_{10})-$(B_{10}H_{13})_2$ respectively.

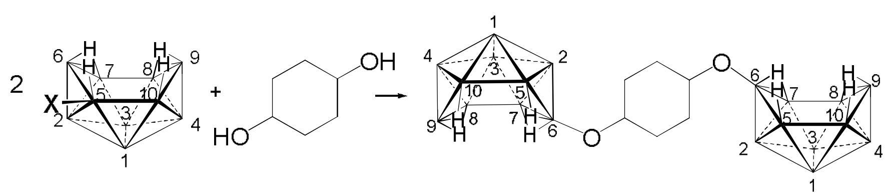

(9)

5.3.2 Characterization of 6OR and 5OR

Regardless of the identity of the alkyl ether unit, the ^{11}B NMR spectra of all of the **5OR** compounds looked similar, as did the spectra of the **6OR** ethers. Spectra of the **5OR** compounds, as illustrated by the ^{1}H-decoupled and coupled ^{11}B NMR spectra of 5-$(C_6H_{11}O)$-$B_{10}H_{13}$ in **Figs. 5.3.1a** and **5.3.1b**, displayed 9 peaks (B2 and B4 are coincident at ~40 ppm) consistent with the predicted C_1 symmetry, with the low-field singlet arising from the ether-substituted B5 vertex. When the cages were substituted with primary alcohols, the separation between the 2 resonances between 0.0 and +5.0 ppm decreased, and in some cases these peaks were coincident, but the shifts of the other resonances were nearly identical regardless of the alcohol employed. The ^{11}B NMR spectra of the **6OR** compounds showed only 5 resonances in 1:5:2:1:1 ratios, as can be seen in the spectra of 6-($C_6H_{11}O$)-$B_{10}H_{13}$ in **Fig. 5.3.1c** and **5.3.1d**, in line with the predicted C_s symmetry of this isomer. Again, the resonance for the ether-substituted vertex (B6) is at lowest-field.

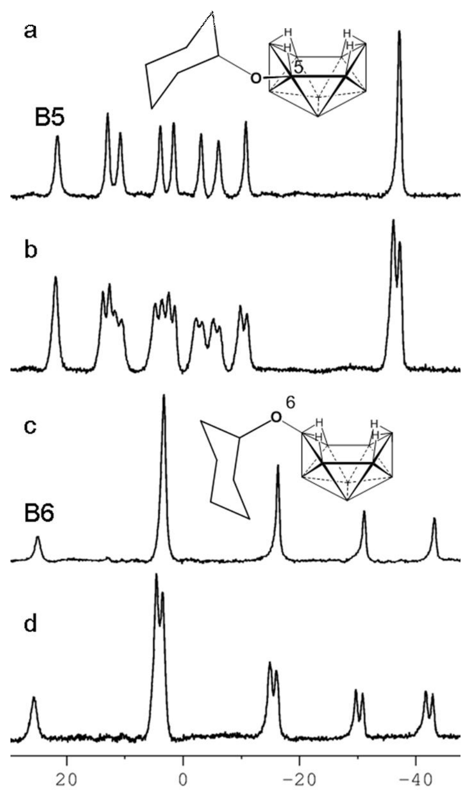

Figure 5.3.1. (a) $^{11}B\{^1H\}$ NMR spectrum of 5-($C_6H_{11}O$)-$B_{10}H_{13}$; (b) ^{11}B NMR spectrum (^1H coupled) of 5-($C_6H_{11}O$)-$B_{10}H_{13;}$ (c) $^{11}B\{^1H\}$ NMR spectrum of 6-($C_6H_{11}O$)-$B_{10}H_{13}$; (d) $^{11}B\{^1H\}$ NMR spectrum of 6-($C_6H_{11}O$)-$B_{10}H_{13}$. The spectra are typical of all compounds synthesized with similar regiochemistry.

Table 5.3.2 gives the calculated ^{11}B NMR shifts for **6OMe** and **5OMe**, along with the observed shifts for the assigned peaks. In contrast to the chemical shifts calculated for the 5- and 6-halodecaboranes, which showed excellent agreement with the observed experimental values, a number of the calculated decaboranylether resonances showed higher than normal discrepancies (>4 ppm) between the computationally predicted and experimentally observed shifts. Most notably, the calculated shifts for the ether-substituted B6 vertex of **6OMe** and its immediate neighbor borons (B2, B5, and B7) showed the poorest agreement. Nevertheless, the assignment of these resonances via 2D COSY ^{11}B-^{11}B NMR spectroscopy, discussed below, was found to be consistent the DFT assignments.

Table 5.3.2. DFT/GIAO (B3LYP/6-311G(d)) calculated and observed ^{11}B NMR shifts (ppm) of **6OMe** and **5OMe**. Assignments are based on the combination of DFT calculated values and 2D COSY ^{11}B-^{11}B NMR in **Figs. 5.3.2** and **5.3.3**.

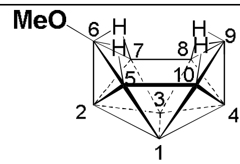			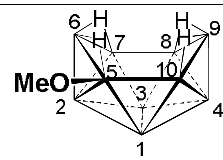		
	Calc.	Assign.		Calc.	Assign.
B1,3	6.6	3.7	B1	2.6	2.0
B2	-38.4	-32.6	B2	-41.9	-38.9
B4	-45.8	-44.3	B3	16.2	12.6
B5,7	-8.9	-16.2	B4	-42.0	-38.9
B6	19.1	25.8	B5	21.6	21.8
B8,10	1.4	2.9	B6	-8.6	-3.4
B9	3.9	3.7	B7	-12.9	-11.3
			B8	-6.4	-6.5
			B9	6.4	10.5
			B10	4.8	2.5

Fig. 5.3.2 shows the 2D COSY ^{11}B-^{11}B NMR spectrum of **6OMe** along with the DFT assignment of peaks (for numbering scheme see **Table 5.3.2**). The downfield singlet in the ^{1}H-coupled ^{11}B NMR spectrum, and can be unambiguously identified as B6. This peak showed a cross-peak with the resonance at -32.6 that, in agreement with the DFT prediction, identified this peak as B2. Accordingly, the B2 resonance showed cross-peaks with a resonance representing B1,3. Both B6 and B2 show cross-peaks with the resonance at -16.2 ppm, which identified this resonance as B5,7. In this instance, the DFT predicted value (~-9 ppm) was not in strong agreement with the observed spectrum, but integration of the peak (intensity-2), and the observed cross-peaks with B2 and B6, along with the lack of a cross-peak with B4 supported the assignment as B5,7. The weakness of the cross-peak observed between B5,7 and B6 was unsurprising, as ^{11}B-^{11}B COSY cross-peaks are often weak, or even absent, when the two boron atoms are bridged with hydrogen.[26] The set of peaks ranging from ~2-5 ppm were comprised of one intensity-2 peak and another resonance comprised of a coincident intensity-1 and intensity-2 peaks. From the symmetry of the compound, these resonances represented B8,10, B1,3 and B9. The upfield portion of the set, an intensity-2 peak, was assigned as B8,10 due to a cross-peak with B4, but not B2. The B8,10 resonance also showed weak cross-peaks with the B5,7 resonance, which was expected, as DFT calculations indicate that B5-B10 and B7-B8 bond distances are greater than 2 Å in this compound. The remaining resonance accounts for B1,3 and B9.

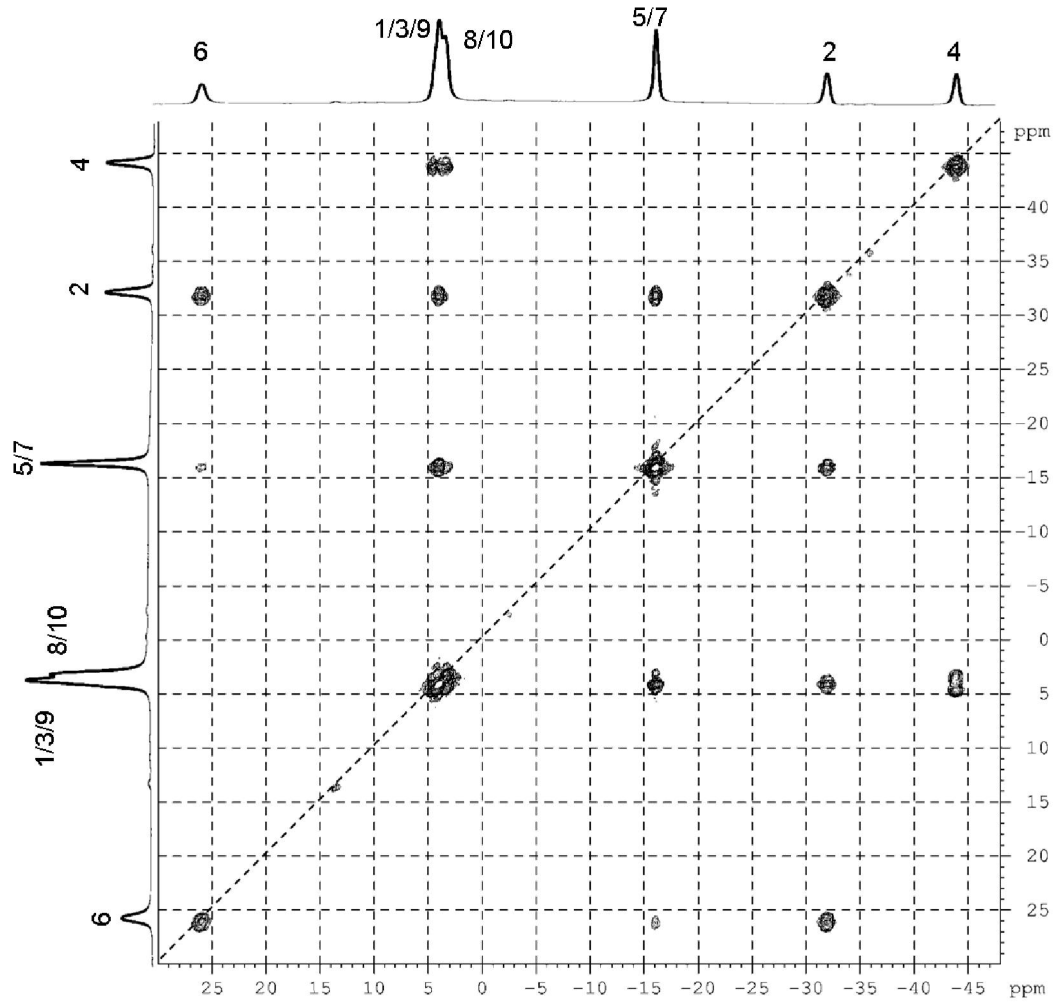

Figure 5.3.2. The 2D COSY ^{11}B-^{11}B NMR spectrum of **6OMe**. Observed cross-peaks: B6-B2; B6-B5,7 (weak); B1,3/B9 -B4; B1,3/B9-B2; B8,10-B4; B8,10-B5,7 (weak); B5,B7-B2; B5,7-B1,3/B9.

The 2D COSY ^{11}B-^{11}B NMR spectrum of **5OMe** is shown in **Fig. 5.3.3**. The coincident upfield peaks were easily identified as B2 and B4 based on the DFT predictions along with their observed cross-peaks to all other boron atoms present. The most downfield resonance, a singlet in the ^{1}H-coupled ^{11}B NMR spectrum, was unambiguously identified as B5. The B5 resonance showed cross-peaks with B1 and B10, and a weak cross-peak with B6, due to the presence of the bridging hydrogen between the B5 and B6. This weak cross-peak, and the stronger cross-peaks between the B2/4 resonance and B6 were the only cross-peaks found for B6, on account of the hydrogen-bridge between B6 and B7. The peak at 10.5 ppm was assigned as B9, as it only shows cross-peaks to the upfield B2/4 peak, and all other neighbors were hydrogen-bridged. The resonance assigned to B3 showed the expected cross-peaks with B7, B8 and B1. Unambiguous assignment of B7 and B8 could not be made based on the data in **Fig. 5.3.3**. Both showed the expected cross-peaks with one another, no cross-peaks with B1, B5, or B10; however, the telltale sign of a B8 cross-peak with B9 or a B7 cross-peak with B6 wasn't readily apparent, on account of bridging hydrogens. Calculations predicted the B7 peak to be the more upfield of the two, and the calculated value of -12.9 was in good agreement with the observed peak at -11.3 ppm. Likewise, the lower field resonance at -6.5 agreed with the predicted value for B8 (-6.4).

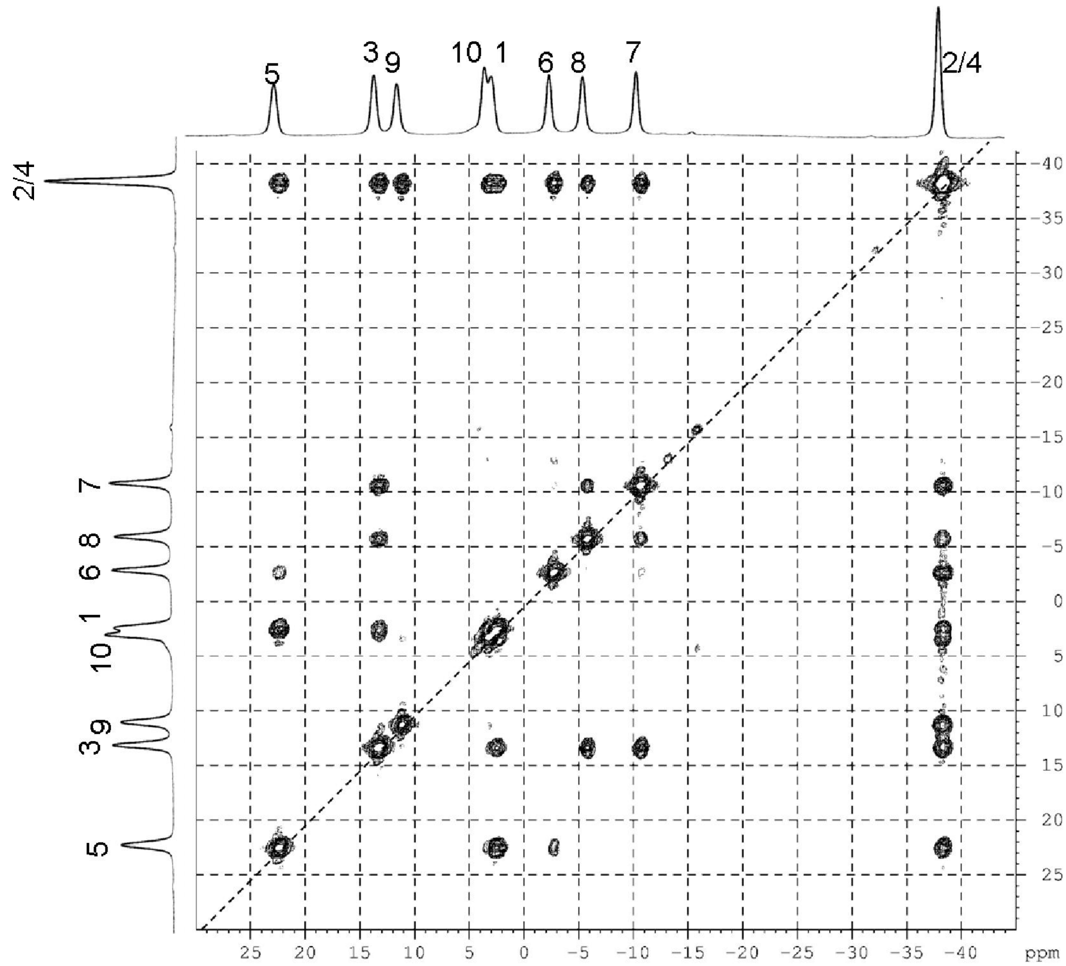

Figure 5.3.3. The 2D COSY ^{11}B-^{11}B NMR spectrum of **5OMe**. Observed cross-peaks: B5-B2/B4; B5-B6 (weak), B5-B1; B5-B10 (weak); B3-B2/B4; B3-B7, B3-B8; B3-B1; B9-B2/B4; B10-B2/B4; B1-B2/B4; B8-B2/B4, B8-B7; B7-B2/B4.

Figs. 5.3.4 and **5.3.5** show the $^{1}H\{^{11}B\}$ and ^{1}H NMR spectra of 6-$((CH_2{=}CHCH_2)_2HCO)$-$B_{10}H_{13}$ and 5-$((CH_2{=}CHCH_2)_2HCO)$-$B_{10}H_{13}$ respectively. The two intensity-2 bridging-hydrogen singlets above 0.0 ppm in **Fig. 5.3.4a** indicate a plane of symmetry, in line with the C_s-symmetry assigned to this isomer. In addition to the resonances originating from the organic portion of the ether, the ^{11}B-decoupled spectrum for the 6-substituted isomer shows 5 broad singlets in 1:4:2:1:1 ratios corresponding to the 9 terminal B-H protons. These resonances show coupling to boron in the ^{11}B-coupled ^{1}H NMR spectrum displayed shown in **Fig. 5.3.4b** with coupling constants (J > ~100 Hz) typical of terminal-hydrogen on polyboranes. The C_1-symmetric **5OR** isomer shows 4 broad, intensity-1 bridging-protons (**Fig. 5.3.5a**) in the 3-upfield/1-downfield pattern seen in the proton spectra of **5X** compounds.[2] The terminal B-H resonances display the lack of symmetry predicted for C_1-symmetry, as five intensity-1 singlets, an intensity 3-singlet (3 coincident resonances), and another intensity-1 singlet (coincident with the downfield bridging-hydrogen) all display coupling to boron. In both isomers, the two sets of vinyl multiplets, one allyl multiplet, and an intensity-1 quintet confirm the identity of the pendant R-groups.

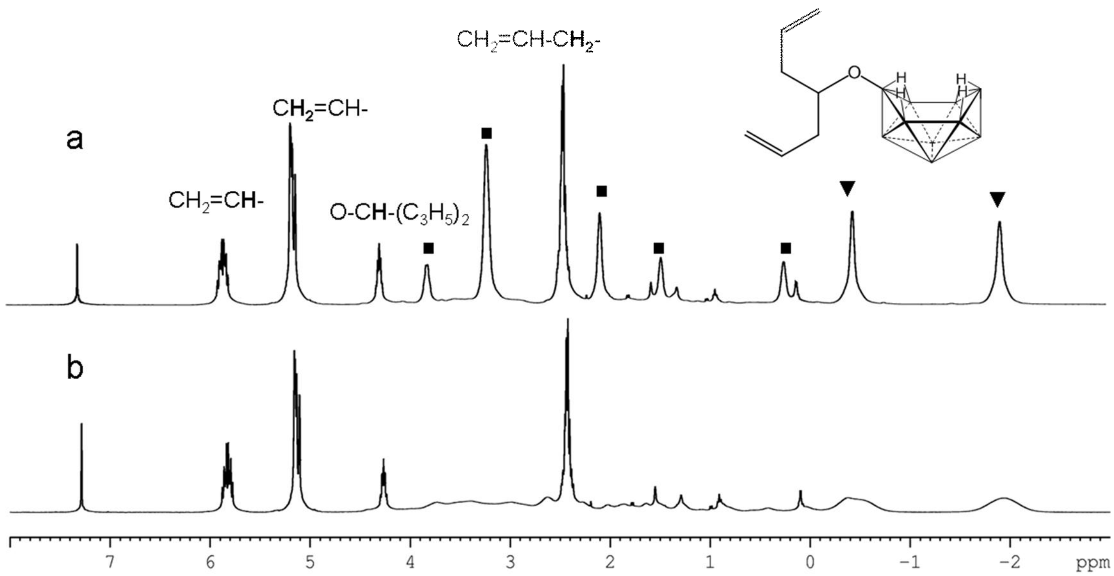

Figure 5.3.4. (a) $^{1}H\{^{11}B\}$ NMR spectrum of 6-($(CH_2{=}CHCH_2)_2HCO$)-$B_{10}H_{13}$ and (b) ^{1}H NMR spectrum of 6-($(CH_2{=}CHCH_2)_2HCO$)-$B_{10}H_{13}$. ■ – terminal B-H, ▼ – bridging B-H-B.

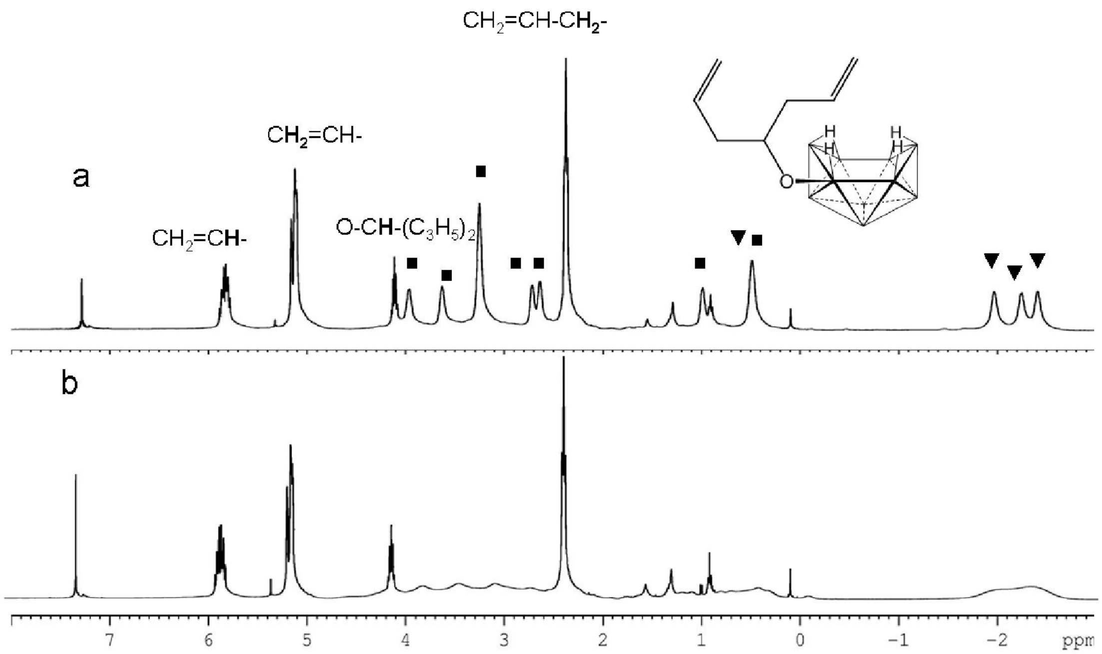

Figure 5.3.5. (a) The $^{1}H\{^{11}B\}$ NMR spectrum of 5-($(CH_2{=}CHCH_2)_2HCO$)-$B_{10}H_{13}$ and (b) the ^{1}H NMR spectrum of 5-($(CH_2{=}CHCH_2)_2HCO$)-$B_{10}H_{13}$. ■ – terminal B-H, ▼ – bridging B-H-B

Figures 5.3.6 and **5.3.7** show the heteronuclear (^{1}H, ^{11}B) correlated 2D NMR spectra of **6OMe** and **5OMe**, along with assignments of the proton resonances. In both cases the bridging protons can be assigned definitely based on cross-peaks with assigned ^{11}B resonances. Proton resonances at the lowest field in both spectra were those closest to the ether-substituted vertex. The only bridging-proton resonance to be downfield of 0.0 ppm is the proton between B5 and B6 in **5OMe**. As would be expected, the trend in the chemical shifts of the terminal hydrogens mirrors that seen in the boron atoms on which they sit. Lower-field (less shielded) boron atoms showed cross-peaks with lower-field protons, and vice-versa.

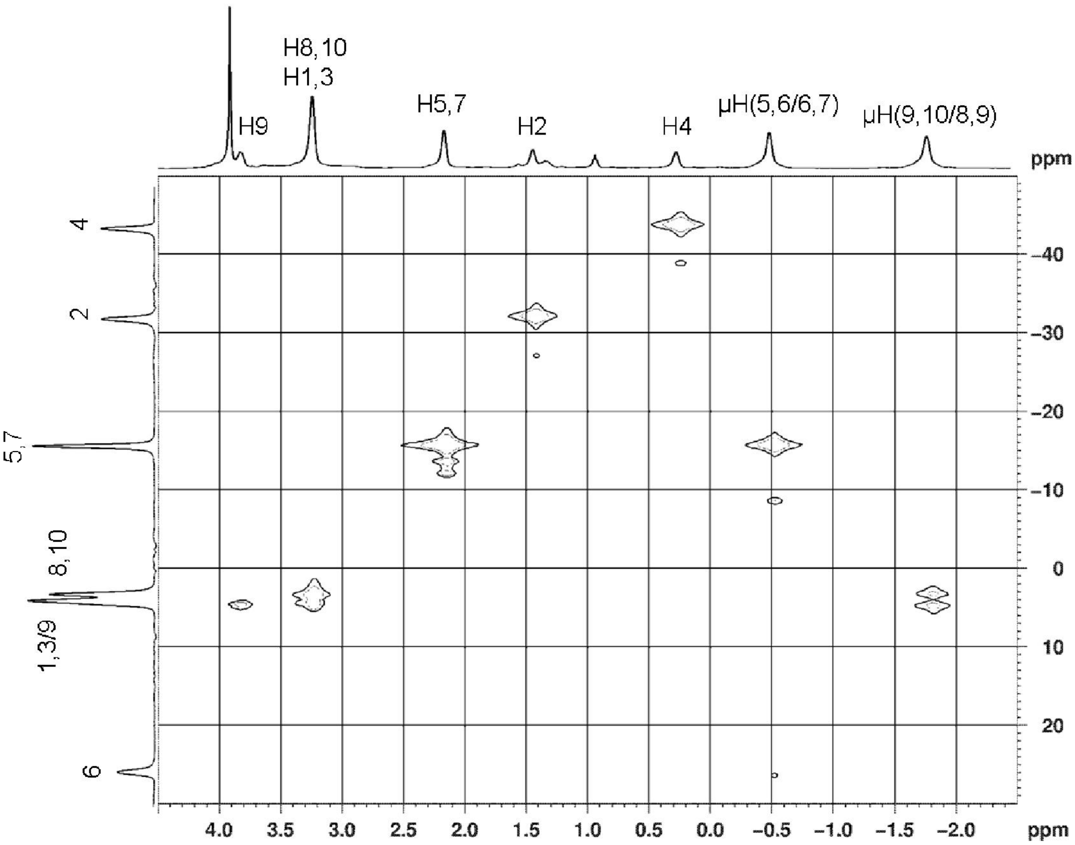

Figure 5.3.6. $^{11}B/^{1}H$ NMR 2D NMR spectra of 6-((CH_3O)-$B_{10}H_{13}$. $^{11}B\{^{1}H\}$ spectrum on the vertical axis, $^{1}H\{^{11}B\}$ spectrum on the horizontal axis.

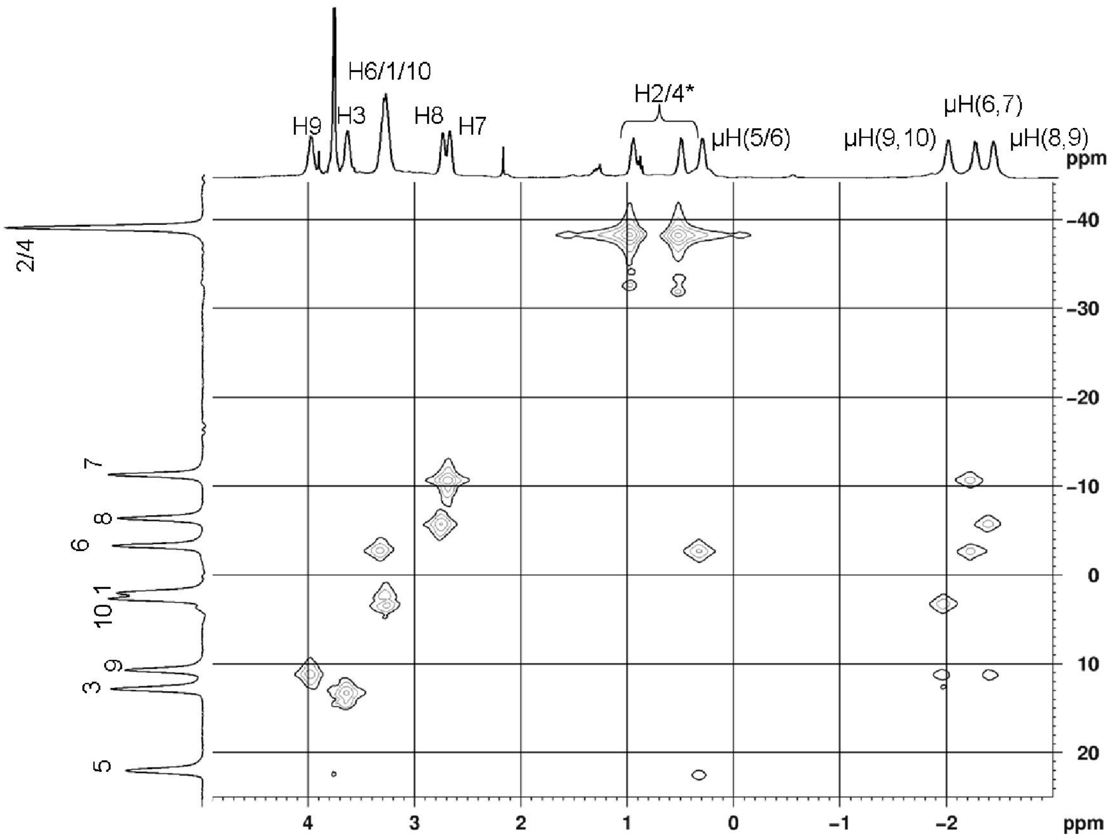

Figure 5.3.7. $^{11}B/^{1}H$ NMR 2D NMR spectra of 6-((CH_3O)-$B_{10}H_{13}$. $^{11}B\{^{1}H\}$ spectrum on the vertical axis, $^{1}H\{^{11}B\}$ spectrum on the horizontal axis. * - Assignment for H2 and H4 could not be made definitively.

5.3.3 Crystallographic Structure Determinations of 5- and 6-OR

Various **5OR** and **6OR** compounds were analyzed crystallographically. ORTEP drawings of the crystallographically determined structures of the structurally characterized ethers are shown in **Figs. 5.3.8-5.3.12**.

Comparisons of the B-B intracage bond distances in both the 5- and 6-substituted boranylethers with the **5X** and **6X** halodecaboranes respectively showed no consistently significant differences. Likewise, as was the case for the halodecaboranes, significant differences in the B-B bond lengths in **5OR** and **6OR** were not observed.

a

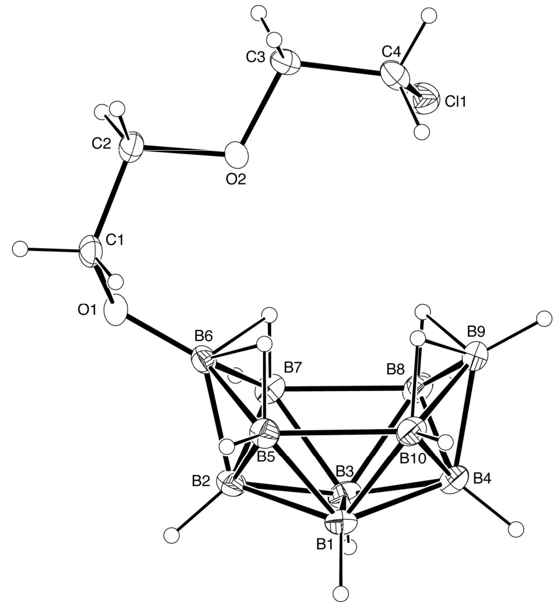

b

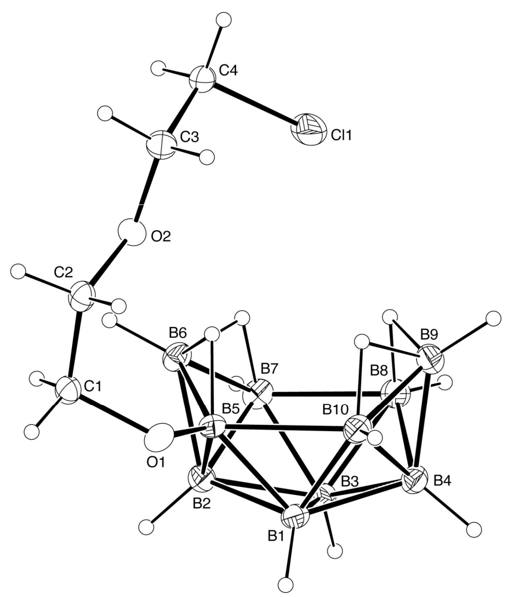

Figure 5.3.8. ORTEP drawings of the crystallographically determined structures of (a) **6-(ClC_2H_4O-C_2H_4O)-$B_{10}H_{13}$**, (b) **5-(ClC_2H_4O-C_2H_4O)-$B_{10}H_{13}$**. Selected bond distances (Å) and angles (^{o}) for: (a) B6-O1, 1.3548(13); O1-C1, 1.4246(13); B6-B5, 1.8025(17); B5-B10, 1.9631(18); B5-B2, 1.8021(17); B6-B2, 1.7327(16); B9-B10, 1.7924(19); B9-

B4, 1.7180(17); C1-O1-B6, 120.74(8); O1-B6-B5, 129.07(9); B6-B5-B10, 117.65(8); O1-B6-B2, 131.82(9); B5-B6-B7, 104.63(8); B8-B9-B10, 104.60(8). (b) B5-O1, 1.3604(19); O1-C1, 1.4372(17); B5-B6, 1.810(2); B5-B10, 2.031(2); B8-B7, 1.939(2); B6-B7, 1.789(2); B5-B2, 1.826(2); B5-B1, 1.770(2); B6-B2, 1.733(2); B4-B9, 1.723(2); B2-B7, 1.775(2); C1-O1-B5, 122.93(11); B6-B5-B10, 115.19(11); O1-B5-B2, 132.56(13); O1-B5-B1, 121.13(12); B5-B10-B9, 115.75(11); B5-B1-B10, 70.73(10); O1-B5-B10, 111.63(11); O1-B5-B6, 125.81(12); B5-B6-B7, 105.36(11); B8-B9-B10, 105.18(12).

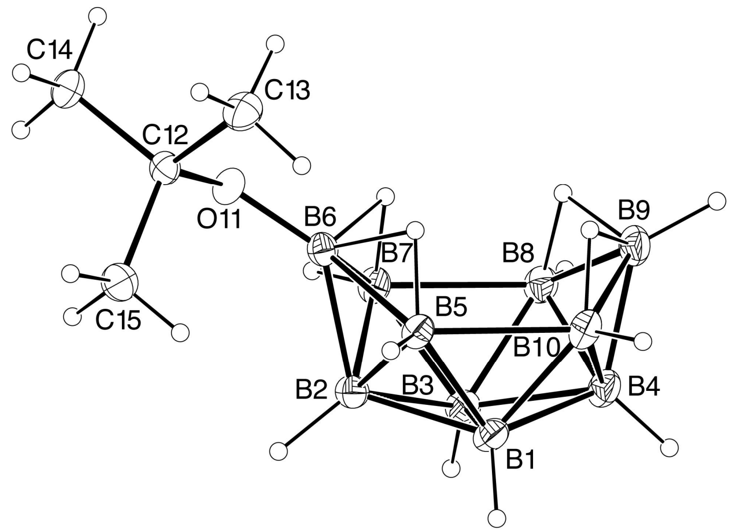

Figure 5.3.9. An ORTEP drawing of the crystallographically determined structure of 6-($(CH_3)_3CO$)-$B_{10}H_{13}$. Selected bond distances (Å) and angles (°): B6-O11, 1.3364(12); O11-C12, 1.4692(11); B6-B5, 1.8280(15); B5-B10, 1.9882(15); B5-B1, 1.7612(15); B5-B2, 1.8066(16); B6-B2, 1.7373(15); B9-B10, 1.7945(17); B9-B4, 1.7163(18); C12-O11-B6, 129.29(7); O11-B6-B5, 133.54(9); O11-B6-B7, 123.05(8); B6-B5-B10, 118.56(8); O11-B6-B2, 136.24(8); B5-B10-B9, 117.97(8), B5-B6-B7, 103.06(7); B10-B9-B8, 104.75(8).

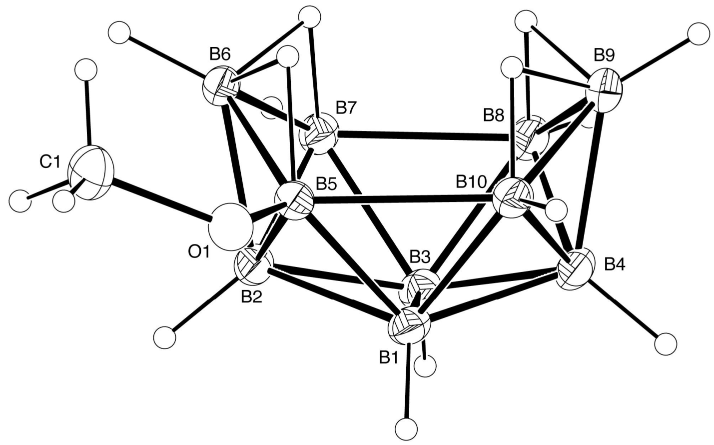

Figure 5.3.10. ORTEP drawings of the crystallographically determined structures of **5OMe**. Selected bond distances (Å) and angles (°): B5-O1, 1.370(3); O1-C1, 1.343(2); B5-B6, 1.828(3); B6-B7, 1.803(3); B5-B10, 2.046(3); B8-B7, 1.968(3); B5-B1, 1.761(3); B1-B10, 1.746(3); B8-B3, 1.757(3); B6-B2, 1.732(3); B2-B3, 1.780(3); B4-B9, 1.718(3); B7-B3, 1.756(2); C1-O1-B5, 120.82(15); B6-B5-B10, 112.99(14); O1-B5-B2, 131.29(15); O1-B5-B1, 121.56(15); B5-B10-B9, 117.61(13); B5-B1-B10, 71.38(11); B7-B3-B8, 68.14(11); B5-B6-B7, 104.90(13); B8-B9-B10, 105.79(14).

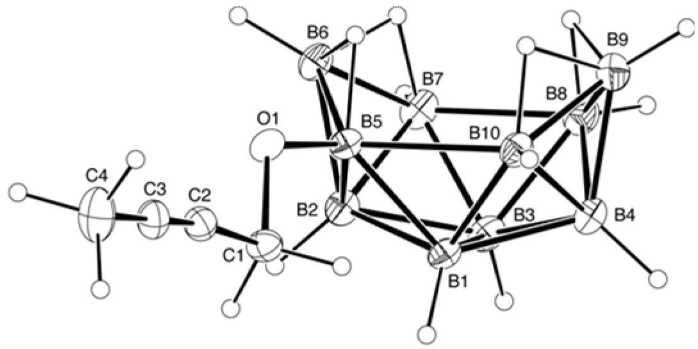

Figure 5.3.11. An ORTEP drawing of the crystallographically determined structure of **5-($CH_3C{\equiv}CCH_2O$)-$B_{10}H_{13}$**. Selected bond distances (Å) and angles (°): B5-O1, 1.3828(17); O1-C1, 1.4336(15); B5-B6, 1.793(2); B5-B10, 2.044(2); B8-B7, 1.954(2); B6-B7, 1.792(2); B5-B1, 1.7605(19); B1-B10, 1.747(2); B6-B2, 1.726(2); B4-B9, 1.720(2); B7-B3, 1.782(2); C1-O1-B5, 117.61(10); B6-B5-B10, 114.93(10); O1-B5-B2, 131.45(11); O1-B5-B1, 126.77(10); B5-B10-B9, 116.61(10); B5-B1-B10, 71.28(8); B7-B3-B8, 67.91(9); B5-B6-B7, 105.31(10); B8-B9-B10, 105.45(11).

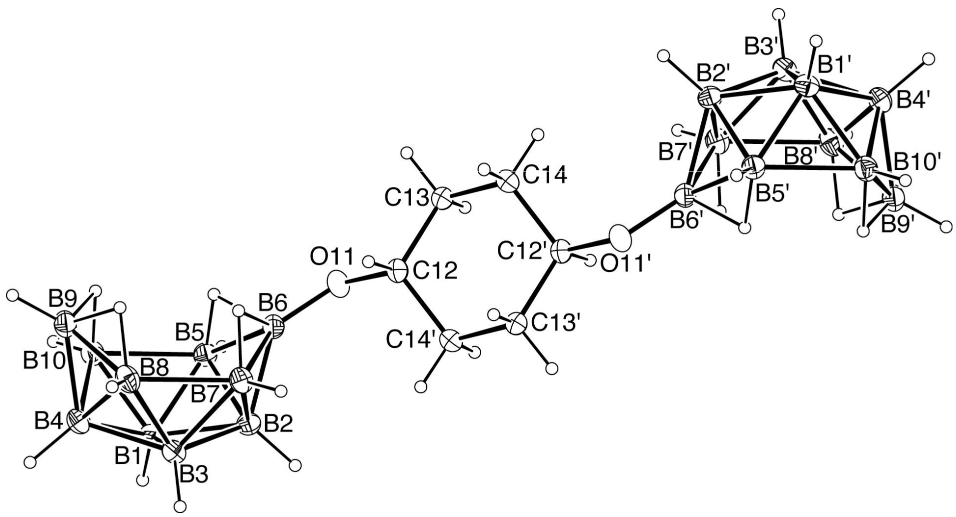

Figure 5.3.12. An ORTEP drawing of the crystallographically determined structure of **6,6'-($C_6H_{10}O_2$)-($B_{10}H_{13}$)$_2$**. Selected bond distances (Å) and angles (°): B6-O1, 1.3549(19); O11-C1, 1.4506(17); B6-B5, 1.804(2); B5-B10, 1.980(2); B5-B1, 1.749(2); B1-B10, 1.748(2); B5-B2, 1.799(2); B6-B2, 1.733(2); B9-B4, 1.717(3); C1-O11-B6, 122.22(12); O11-B6-B5, 123.37(13); B6-B5-B10, 118.00(12); B5-B6-B7, 104.11(11); B8-B9-B10, 104.73(12).

Backbonding from π-donating substituents on decaborane cages has been proposed in halogenated and amino-substituted compounds.[1,2,27] Backbonding from O to B in the boranyl ether compounds is evidenced in these compounds by short B-O bonds, and an sp^2 hybridized oxygen. **Table 5.3.3** gives the lengths of the B-O bonds and the measured B-O-C angles in all the structurally characterized compounds as well as the B-O length in $B(OCH_3)_3$,[28] where π-backbonding is strong, and the average of the B-O bonds of a few $B(OCH_3)_4^-$ tetrahedral anions,[29] where π-backbonding is impossible. The B-O bond lengths in both the 5- and 6-decabroanylethers range from ~1.33 Å to ~1.37 Å, similar to bonds in $B(OMe)_3$, and significantly shorter than the average B-O length for tetrahedral borates (~1.46 Å). The B-O-C bond angles in each of the crystallographically characterized ethers were all near 120^o indicating sp^2 hybridization of the cage-bound oxygen, as would be necessary for true π-backbonding. The B-O-C angle in trimethylborate is similar, at 119.7^o, while the same angle in tetramethylborate is only 116^o.

Also listed in **Table 5.3.3** are the B-O bond lengths and B-O-C angles in alkoxy-substituted examples of *closo*-dodecaborate, monocarboncarborane, and *p*-carborane. In the alkoxy-bearing polyhedral cages, back-donation from O to B should be less prevalent in electron-rich systems. This predicted trend is confirmed in comparisons of the B-O length in $(C_2H_5O)\text{-}B_{12}H_{11}^{2-}$ (1.442(5) Å), 2-(ClC_4H_8O)-1-$CB_{11}H_{11}^-$ (1.409(3) Å) and 2-(C_2H_5O)-1,12-$C_2B_{10}H_{11}$ (1.3884(16) Å). With the exception of 5-$(CH_3C{\equiv}CCH_2O)$-$B_{10}H_{13}$, which has a similar B-O bond length as the alkoxy *p*-carborane, the decaboranyl B-O bonds are shorter than any of these. The B-O-C angle in $(C_2H_5O)\text{-}B_{12}H_{11}^{2-}$ is

115.9(3)^o, in 2-(ClC_4H_8O)-1-$CB_{11}H_{11}^-$ is 118.4(2)^o, and is 119.76(10)^o in 2-(C_2H_5O)-1,12-$C_2B_{10}H_{11}$, again suggesting a decrease in backbonding with increase in electron density. With the exception of 5-($CH_3C{\equiv}CCH_2O$)-$B_{10}H_{13}$, the B-O-C angles in the decaboranylethers are larger (~120^o or greater) than any of these.

Table 5.3.3. Comparisons of the crystallographically determined B-O bonds lengths to trigonal and tetrahedral B-O bonds.

	B-O Length (Å)	C-O-B Angle (°)
$B(OCH_3)_3$[28]	1.359(6)	119.7
$[B(OCH_3)_4^-]$[29]	1.46 (avg)	116 (avg)
6-(ClC_2H_4O-C_2H_4O)-$B_{10}H_{13}$	1.3548(13)	120.74(8)
6-($(CH_3)_3CO$)-$B_{10}H_{13}$	1.3354(13)	129.39(8)
6,6'-($C_6H_{10}O_2$)-$(B_{10}H_{13})_2$	1.3549(19)	122.22(12)
5-(ClC_2H_4O-C_2H_4O)-$B_{10}H_{13}$	1.3604(19)	122.93(11)
5-((CH_3O)-$B_{10}H_{13}$ (**5OMe**)	1.370(3)	120.82(15)
5-($CH_3C{\equiv}CCH_2O$)-$B_{10}H_{13}$	1.3828(17)	117.61(10)
[(C_2H_5O)-$B_{12}H_{11}^{2-}$][30]	1.442(5)	115.9(3)
[2-ClC_4H_8O-1-$CB_{11}H_{11}^-$][31]	1.409(3)	118.4(2)
2-(C_2H_5O)-1,12-$C_2B_{10}H_{11}$[4]	1.3884(16)	119.76(10)

5.3.4 Computational Exploration of the Reaction Mechanism.

As described earlier, the substitution reactions in **Eqs. 5** and **6** proceeded with surprising regioselectivites. Nevertheless, it was possible to identify reasonable pathways for the transformations of **6X** to **5OMe** and **5X** to **6OMe** using DFT/IRC calculations. As can be seen in **Figure 5.3.13** for the reaction of **6Cl** with methanol, nucleophilic attack of the alcohol-oxygen at B5 pushes its terminal-hydrogen upward to form the **TS1** transition state. In **TS1**, the oxygen is still 2.23 Å from B5 and the B-Cl bond has only slightly lengthened from 1.78 Å to 1.82 Å. As the oxygen moves closer to B5, three hydrogens (the B5 terminal-hydrogen and 2 bridging-hydrogens) move to *endo*-positions on B5, B6 and B7 to form **INT1**. In **INT1**, the B-O bond decrease to 1.61 Å is accompanied by a corresponding increase in the B5-B6 distance from 1.81 Å to 2.40 Å, but at this point there is no additional lengthening of the B-Cl bond. As the oxygen moves closer (1.49 Å) to B6 to form **TS2**, the chlorine begins to detach (B6-O, 2.42 Å) from the cage and a five-membered B-Cl-H-O-B ring structure (**Figure 5.3.14**) forms that allows the Cl to initially bond with the methanolic hydrogen (1.74 Å). In the final step, the hydrogen is transferred from the oxygen to the chlorine (H-Cl,1.32 Å) with the elongated H-O bond length (1.82 Å) typical of those found for hydrogen-bonded ethers.[32] As a result of the chlorine leaving the cage, the *endo*-B6-H moves to the vacated terminal B6-position and the *endo*-hydrogens on B5 and B7 move into bridging-positions. The hydrogen-bonded HCl/decaboranyl-ether adduct is not stable under the experimental reaction conditions, since the HCl is immediately neutralized by $NaHCO_3$ to liberate the final decaboranyl ether.

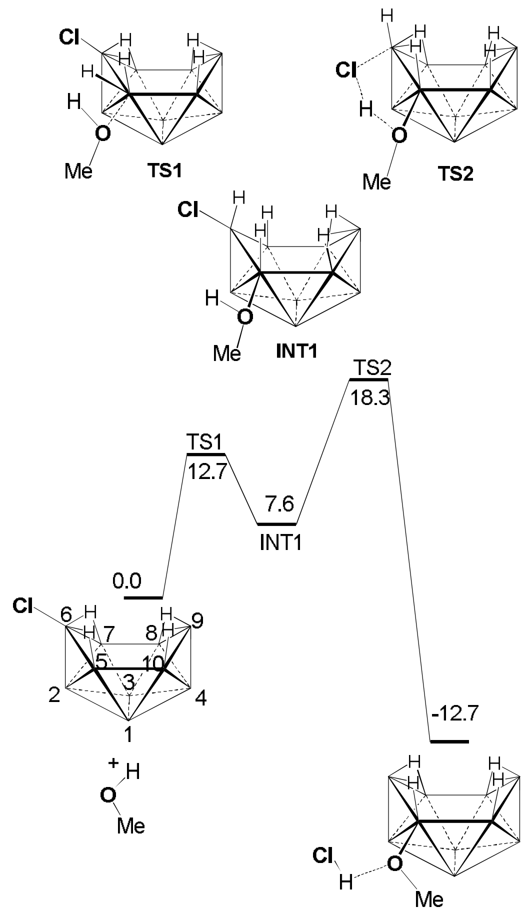

Figure 5.3.13. DFT calculated mechanism from **6Cl** to **5OMe**. Calculations performed at the B3LYP/6-311G(d) level of theory at 298 K. Electronic energies are given in kcal/mol.

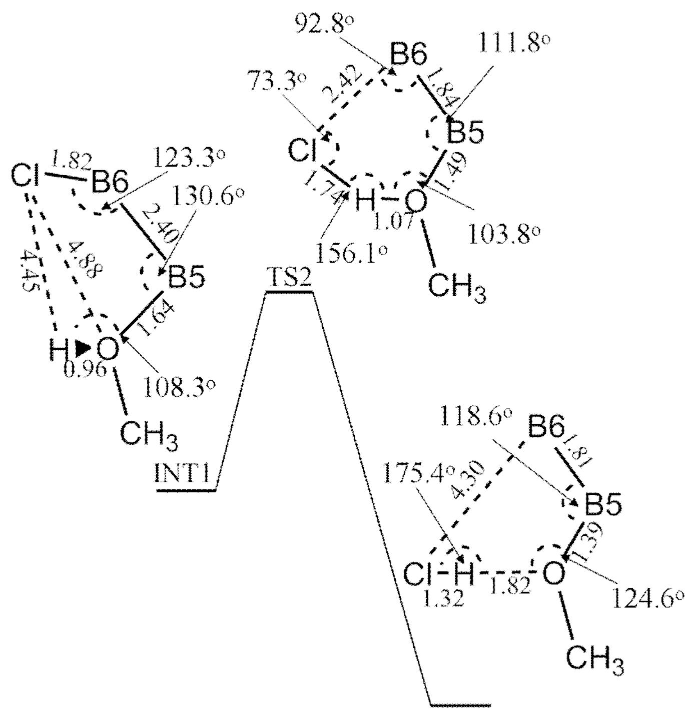

Figure 5.3.14. Bond distances and angles in the 5-membered ring portion of **INT1**, **TS2** and the hydrogen-bonded product.

An analogous pathway was found for the reaction of methanol with **5Cl** (**Figure 5.3.15**). Nucleophilic attack of the alcohol at B6 occurs through **TS3** to form **INT2**. The **INT2** structure is similar to **INT1**, with a 1.61 Å B6-O distance and three *endo*-hydrogens. As the oxygen moves closer to B6 (1.49 Å), the **TS4** transition state is formed, which, like **TS2,** has a cyclic five-membered configuration with an elongated B6-Cl (2.55 Å) distance (**Figure 5.3.16**) that facilities the initial H-Cl bonding interaction (H-Cl, 1.73 Å). In the final step, the hydrogen transfer from the oxygen (H-O, 1.87 Å) to the chlorine (H-Cl, 1.31 Å) is complete to again produce the hydrogen-bonded decaboranyl ether. The chlorine is no longer attached to the cage and the *endo*-B5-H has moved to the vacated terminal B5-position with the *endo*-hydrogens on B5 and B7 moving back into bridging-positions. Again, under the experimental reaction conditions the hydrogen-bonded HCl is neutralized by $NaHCO_3$ to liberate **6OMe**.

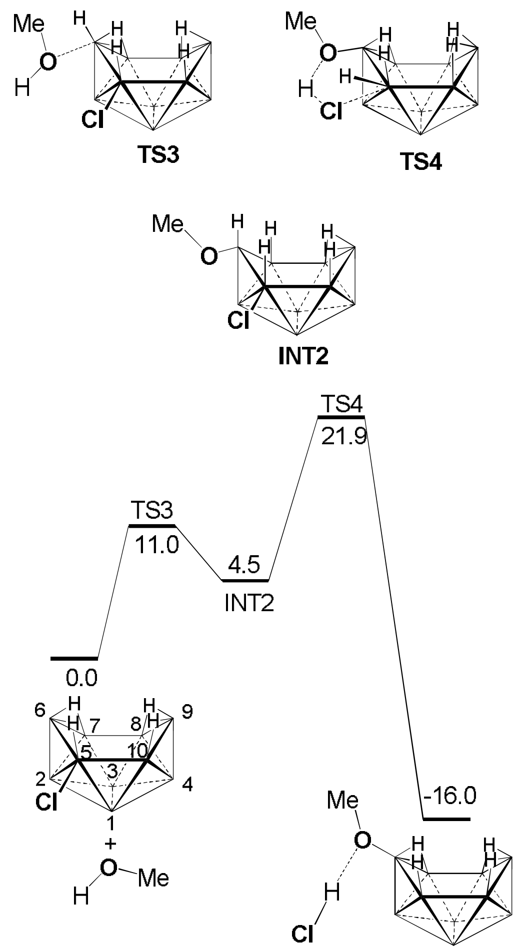

Figure 5.3.15. DFT calculated mechanism from **5Cl** to **6OMe**. Calculations performed at the B3LYP/6-311G(d) level of theory at 298 K. Electronic energies are given in kcal/mol.

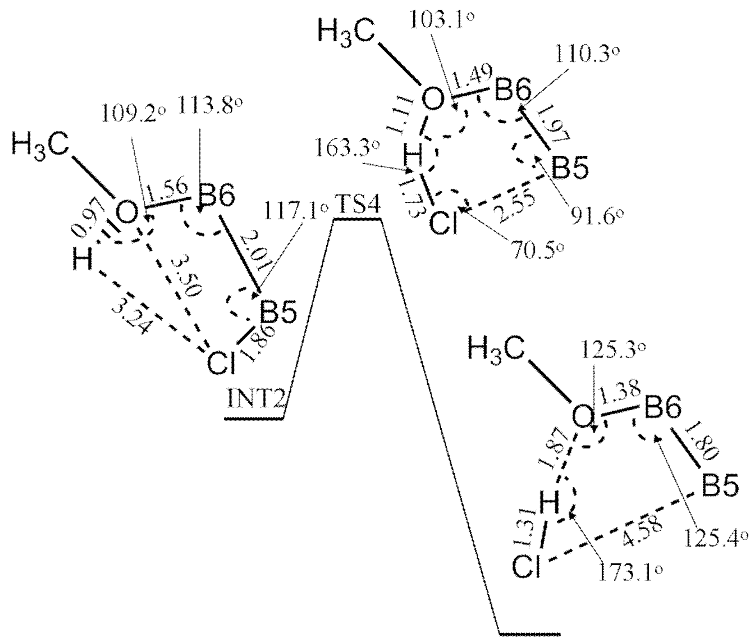

Figure 5.3.16. Bond distances and angles in the 5-membered ring portion of **INT2**, **TS4** and the hydrogen-bonded product.

For computational ease **5Cl** and **6Cl** were used as model compounds; however, within the halogenated series reactions involving the chlorinated compounds reacted more slowly than did their brominated and iodinated relatives. When **6Cl** reacted with methanol at room temperature the reaction was found to be only ~25% complete after 2 days. The same reaction with **6Br** was complete after ~12 h. When **6I** was employed, the starting material was consumed in ~12 h, but the relative rapidity of the isomerization of **6I** to **5I**[2] resulted in a mixture of final isomers, so a direct rate comparison could not be made. When **6F** was reacted with methanol no reaction was seen after 48 h at room temperature. A comparison of the DFT calculated activation energies (from starting materials to **TS2**, for each halogen) for the series is shown in **Fig. 5.3.17**. The trend in observed reaction rates is in agreement with the calculated activation energies, which show a relatively low activation energy for the reaction with **6I** and **6Br**, followed by a greater activation energy for **6Cl** and finally a much higher activation energy for **6F**.

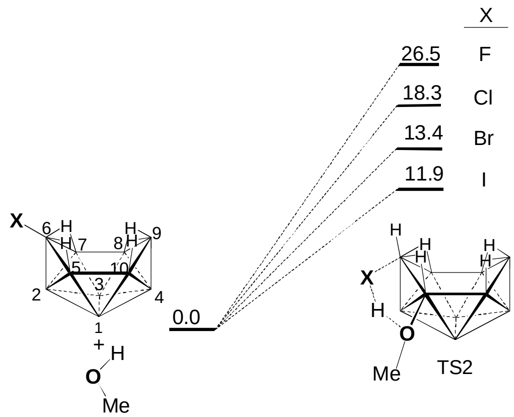

Figure 5.3.17. Comparison of the calculated activation energies for the reaction of methanol with **6X** (X = F, Cl, Br, I). Calculations of electronic energies were performed at the B3LYP/6-311G(d) level for **6F** and **6Cl**. For **6Br** and **6I** B3LYP/6-311G(d) was used for all B, C, O and H atoms, and the SDD psuedopotential was used for the halogens.

5.3.5 Substitution Reactions on Deuterated 6Br.

Reactions of alcohols with bridge-deuterated bromodecaboranes were carried out in order to test the computationally proposed mechanism. The complete deuteration of the bridging-hydrogens of $B_{10}H_{14}$ was previously achieved through stirring in a biphasic mixture of D_2O and dioxane.[33] While bridging-hydrogens were observed to undergo quick deuterium exchange, the terminal B-H bonds exchanged at a much slower rate. When **6Br** was stirred in a biphasic solution of $CDCl_3$ and D_2O, the disappearance of the upfield $^{1}H\{^{11}B\}$ NMR resonances indicated the exchange of the four bridging-hydrogens for deuterium, while ^{11}B NMR indicated no exchange at terminal B-H sites. **Figs. 5.3.18** and **5.3.19** show the $^{1}H\{^{11}B\}$ NMR spectra of **6Br** and **5Br** before and after deuteration. Interestingly, while the parent compound $B_{10}H_{14}$ was not found to undergo H/D exchange when stirred in mixtures of D_2O and non-ethereal solvents,[11] **6Br** quickly underwent bridge-deuteration with D_2O in $CDCl_3$. This is likely an indication of the enhanced acidity of the halogenated cages relative to $B_{10}H_{14}$.

According to the mechanisms shown in **Figs. 5.3.13** and **5.3.15**, reaction of the bridge-deuterated, halodecaboranes with methanol should result in one of the bridging-deuterons (specifically, the bridge-deuteron shown in bold) relocating to the position formerly occupied by the halogen (**Eq. 10** and **11**).

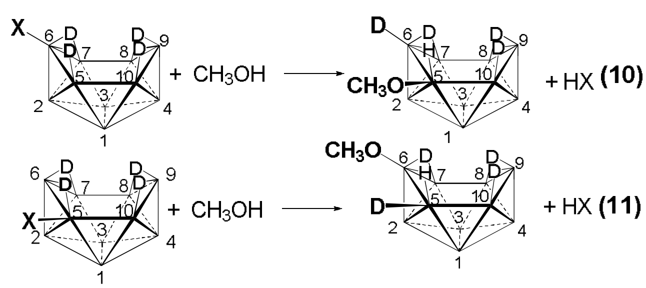

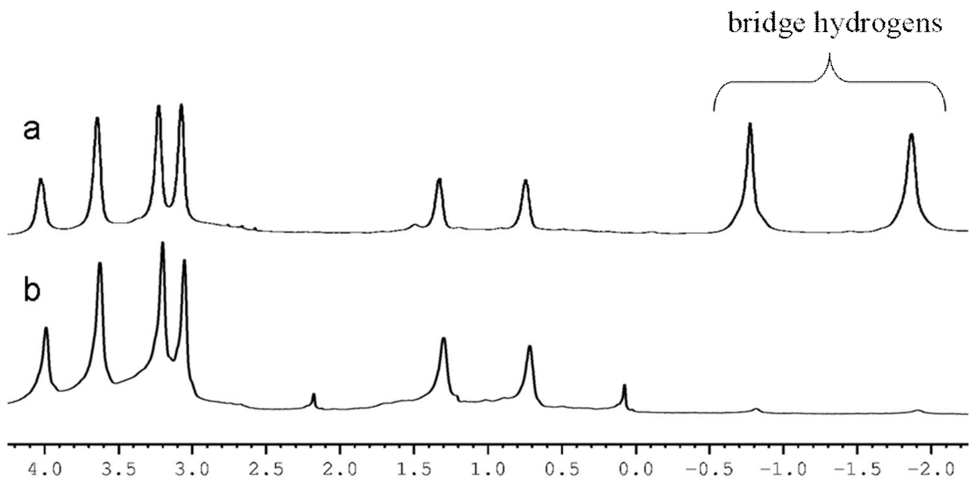

Figure 5.3.18. $^{1}H\{^{11}B\}$ NMR spectra of: (a) **6Br** and (b) **μ-D$_4$-6Br**

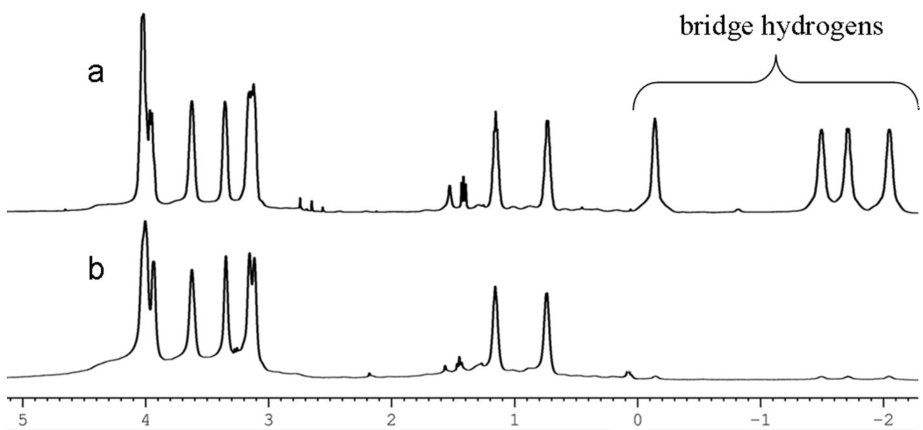

Figure 5.3.19. $^{1}H\{^{11}B\}$ NMR spectra of: (a) **5Br** and (b) **μ-D$_4$-5Br**

Since coupling between boron and deuterium is small (e.g. for BH_4^-: $J_{B\text{-}D}$ = ~12 Hz, $J_{B\text{-}H}$ = ~80 Hz)[34] and not readily observed, evidence for terminal deuteration can be found in the absence of clear B-H coupling normally seen in the ^{11}B NMR spectra of each decaboranylether. The ^{11}B NMR spectrum of **5OMe**, a product of the reaction of **6Br** with methanol, is shown in **Fig. 5.3.20a**. All of the cage-boron resonances, excepting the expected B5 singlet, appear as doublets as a result of the coupling to their terminal hydrogens. The ^{11}B NMR of the product of the reaction (**Eq. 10**, X = Br) of **μ-D$_4$-6Br** with methanol (**Fig. 5.3.20c**) showed that the B6-resonance (-3.68 ppm) had changed from a doublet to a broadened singlet indicating deuterium incorporation at the B6 terminal-position, in accordance with the proposed mechanism. When **μ-D$_4$-6Br** was reacted with CD_3OD (**Eq. 12**), the ^{11}B NMR spectrum of the product showed a much sharpened singlet for 6B (**Fig. 5.3.20d**). Reaction of un-deuterated **6Br** with CD_3OD gave a boranylether (**Eq. 13**) for which the ^{11}B NMR spectrum lacked the apparent-singlet indicative of a terminal B-D bond (**Fig. 5.3.20b**), indicating that deuterium incorporated into the terminal B6 position must come from the cage, and not from methanol.

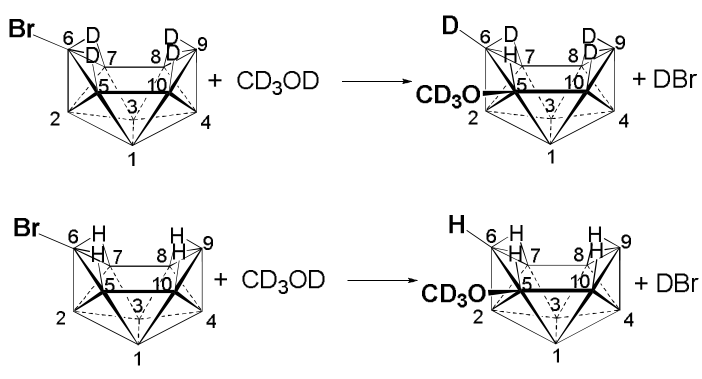

(12)

(13)

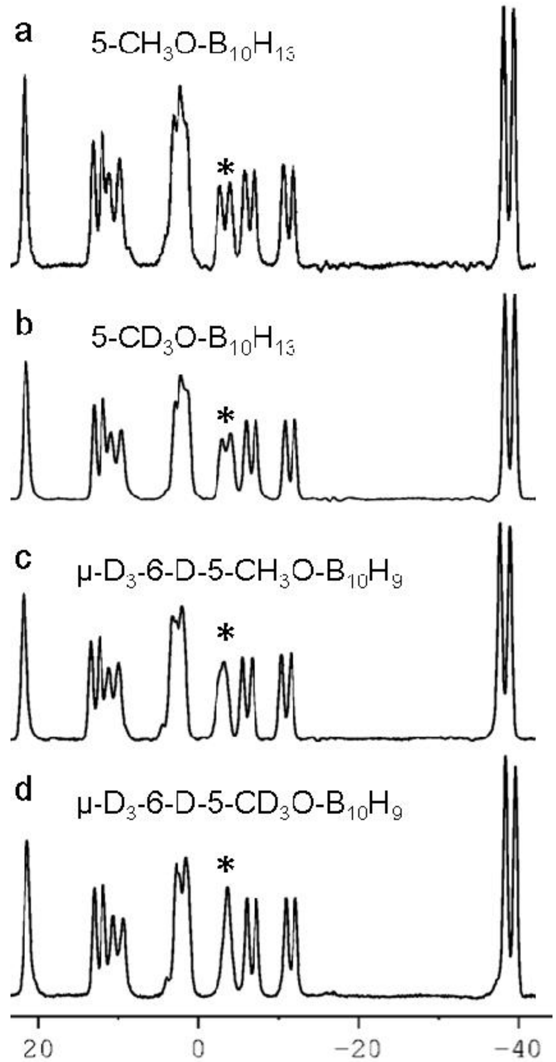

Figure 5.3.20. [11]B NMR spectrum of the products of the following reactions: (a) **6Br** + CH_3OH, (b) **6Br** + CD_3OD, (c) **μ-D₄-6Br** + CH_3OH, (d) **μ-D₄-6Br** + CD_3OD. The * denotes the 6B resonance.

The broadness of the singlet in **Fig. 5.3.20c** and the doublet in **Fig. 5.3.20b**, relative to the singlet in **Fig. 5.3.20d** and the doublet in **Fig. 5.3.20a**, indicates incorporation of a small amount of hydrogen in the B6 vertex of μ-D_3-6-D-5-CD_3O-$B_{10}H_9$, and deuterium in the B6 vertex of 5-CD_3O-$B_{10}H_{13}$. When **μ-D4-6Br** was treated with standard methanol, H/D exchange between the deuterated bridging positions of the cage and the hydroxyl-hydrogen led to small amounts of hydrogen incorporation at B6 of the products. Likewise, when **6Br** was treated with CD_3OD, a small amount of deuterium was exchanged into the bridging positions of the cage and was incorporated at B6, resulting in a broadened doublet in the ^{11}B NMR. Since fast H/D exchange only occurs in the bridging positions, observed broadening in cases where exchange might occur supports the mechanism presented in **Fig. 5.3.13**.

When **μ-D_4-5Br** was reacted with C_2D_5OD in $CDCl_3$ (**Eq. 14**) at 70 ^oC, the ^{11}B NMR spectrum of the μ-D_3-5-D-6-C_2D_5O-$B_{10}H_9$ product showed a broadened resonance at ~ -15.5 ppm (B5,7) indicating the incorporation of deuterium into one of these vertices (**Fig. 5.3.21b**). The reactions of **5Br** with CD_3OD, and **μ-D_4-5Br** with CH_3OH were carried out, but the increased rate of deuterium exchange between bridging H/D and alcohol H/D at the elevated temperatures necessary for the reaction resulted in products with a mix of H/D incorporation at B6. However, the observation of the inclusion of deuterium at B5 of the **μ-D_4-5Br**/CD_3OD reaction supports the mechanism shown in **Fig. 5.3.15**.

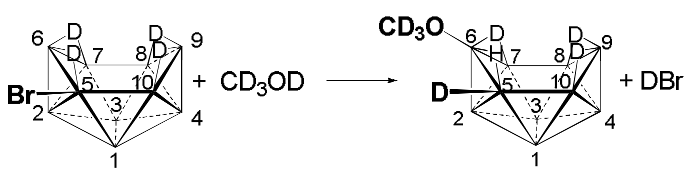

(14)

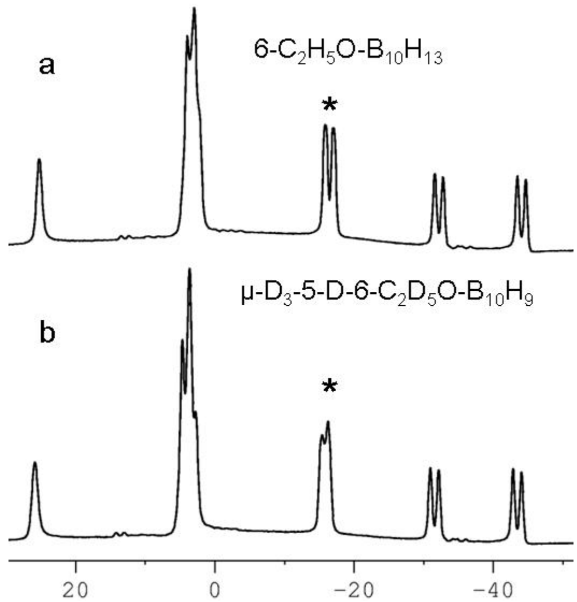

Figure 5.3.21. ^{11}B NMR spectrum of the products of the following reactions: (a) **5Br** + C_2H_5OH, (b) **μ-D_4-5Br** + C_2D_5OD. The * denotes the B5,7 coincident resonance.

5.4 Conclusions

A new method for the syntheses of a number of decaboranylether compounds has been described. A range of 1^o, 2^o and 3^o alcohols were successfully incorporated into the polyhedral cage, bearing polymerizable goups (alkenes, alkynes), nucleophiles (thiols), and electrophiles (alkyl halides, succinimide). The breadth of functional group inclusion shown in this chapter is only a small sampling of those that might be used, and may serve towards the incorporation of these neutral polyboranes into other chemistries.

The substitution mechanism displays a new type of reactivity in decaborane, in that, much like the S_N2' reaction, the substitution occurs through the movements of equivalents of electrons across the molecule. In the organic reaction (**Eq. 3**) these electrons are contained in π-system. In boron hydride systems, the lower electronegativity of boron means that electrons are bound to hydrogen, so movement of hydrogen around the open face of the cage represents an equivalent transformation.

5.5 References.

1. Ewing, W. C.; Carroll, P. J.; Sneddon, L. G. *Inorg. Chem.* **2008**, *47*, 8580-8582.

2. Ewing, W. C.; Carroll, P. J.; Sneddon, L. G. *Inorg. Chem.* **2010**, *49*, 1983-1994.

3. (a) Eames, J.; de las Heras, M. A.; Warren, S. *Tet. Lett.* **1996**, *37*, 4077-4080. (b) Trost, B. M.; Machacek, M. R.; and Tsui, H. C. *J. Am. Chem. Soc.* **2005**, *127*, 7014-7024. (c) Gumerova, D. F.; Mashevskaya, I. V.; Maslivets, A. N.; Kozlov; A. P. *Russ. J. Org. Chem.* **2003**, *39*, 995-997. (d) Kesharwani, T; Verma, A. K.; Emrich, D.; Ward, J. A.;

Larock, R. C. *Org. Lett.* **2009**, *11*, 2591-2593. (e) Dıaz, D.; Martın, T.; Martı´n, V. S. *Org. Lett.* **2001**, *3*, 3289-3291. (f) Spivey, A. C.; Andrews, B. I. *Agnew. Chem. Int. Ed.* **2001**, *40*, 3131-3134.

4. Kabytaev, K. Z.; Mukhin, S. N.; Glukhov, I. V.; Starikova, Z. A.; Bregadze, V. I.; Beletskaya, I. P. *Organomet.* **2009**, *28*, 4758-4763.

5. Siveav, I. B.; Bregadze, V. I.; Sjoberg, S. *Coll. Czech. Chem. Comm.* **2002**, *67*, 679-727 and references therein.

6. Sivaev, I. B.; Prikaznov, A. V.; Naoufal, D. *Coll. Czech. Chem. Comm.* **2010**, *75*, 1149-1199 and references therein.

7. (a) Nie, Y.; Hu, C-H.; Li, X.; Yong, W.; Dou, J-M.; Sun, J.; Jin, R-S.; Zheng, P-J. *Acta Cryst.* **2001**, *C57*, 897-899. (b) Paxon, T. E.; Hawthorne, M. F. *Inorg. Chem.* **1975**, *14*, 1604-1607.

8. Hawthorne, M. F.; Miller, J. J. *J. Am. Chem. Soc.* **1960**, *82*, 500.

9. Loffredo, R. E.; Drullinger R. F.; Slater, J. A.; Turner, C. A.; Norman, A. D. *Inorg. Chem.* **1976**, *15*, 478-480.

10. Beachell, H. C.; Schar, W. C. *J. Am. Chem. Soc.* **1958**, *80*, 2943-2945.

11. Stuchlik, J.; Hermanek, S.; Plesek, J.; Stibr, B. *Coll. Czech. Chem. Comm.* **1970**, *35*, 339-343.

12. *SAINT*: Bruker Corporation, 2009.

13. *SHELXTL*: Bruker Corporation, 2009.

14. Sheldrick, G. M. *SADABS.* University of Gottingen, Germany, 2007.

15. CrystalClear: Rigaku Corporation, 1999.

16. CrystalStructure: Crystal Structure Analysis Package

17. REQAB4: Jacobsen, R. A. 1994.

18. *SIR97*: Altomare, A.; Burla, M. C.; Camalli, M.; Cascarano, M.; Giacovazzo, C.; Guagliardi, A.; Moliterni, A.; Polidori, G. J.; Spagna, R. *J. Appl. Cryst.* **1999**, *32*, 115-119.

19. Sheldrick, G. M. *SHELXL-97*: Program for the Refinement of Crystal Structures; University of Göttingen: Germany, 1997.

20. Frisch, M. J.; Trucks, G. W.; Schlegel, H. B.; Scuseria, G. E.; Robb, M. A.; Cheeseman, J. R.; Montgomery, J. A., Jr.; Vreven, T; Kudin, K. N.; Burant, J. C.; Millam, J. M.; Iyengar, S. S.; Tomasi, J.; Barone, V.; Mennucci, B.; Cossi, M.; Scalmani, G.; Rega, N.; Petersson, G. A.; Nakatsuji, H.; Hada, M.; Ehara, M.; Toyota, K.; Fukuda, R.; Hasegawa, J.; Ishida, M.; Nakajima, T.; Honda, Y.; Kitao, O.; Nakai, H.; Klene, M.; Li, X.; Knox, J. E.; Hratchian, H. P.; Cross, J. B.; Adamo, C.; Jaramillo, J.; Gomperts, R.; Stratmann, R. E.; Yazyev, O.; Austin, A. J.; Cammi, R.; Pomelli, C.; Ochterski, J. W.; Ayala, P. Y.; Morokuma, K.; Voth, G. A.; Salvador, P.; Dannenberg, J. J.; Zakrzewski, V. G.; Dapprich, S.; Daniels, A. D.; Strain, M. C.; Farkas, O.; Malick, D. K.; Rabuck, A. D.; Raghavachari, K.; Foresman, J. B.; Ortiz, J. V.; Cui, Q.; Baboul, A. G.; Clifford, S.; Cioslowski, J.; Stefanov, B. B.; Liu, G.; Liashenko, A.; Piskorz, P.; Komaromi, I.; Martin, R. L.; Fox, D. J.; Keith, T.; Al-Laham, M. A.; Peng, C. Y.;Nanayakkara, A.; Challacombe, M.; Gill, P. M. W.; Johnson, B.; Chen, W.; Wong, M. W.; Gonzalez, C.; Pople, J. A. *Gaussian 03*, revision B.05; Gaussian, Inc.: Pittsburgh PA, 2003.

21. Ingold, C. K. *Chem. Rev.* **1934**, *15*, 225-274.

22. Finch, A.; Gardner, P. J.; Watts, G. B. *Trans. Farad. Soc.* **1967**, *63*, 1603-1607.

23. Fenwick, J. T. F.; Wilson, W. *J. Chem Soc. Dalt. Trans.* **1972**, *13*, 1324-1326.

24. (a) Sivaev, I. B.; Bregadze, V. I. *Eur. J. Inorg. Chem.* **2009**, *11*, 1433-1450 and references therein. (b) Ma, L.; Hamdi, J.; Wong, F.; Hawthorne, M. F. *Inorg. Chem.* **2006**, *45*, 278-285.

25. (a) Barth, R. F. *Appl. Radiat. Iso.* **2009**, *67*, S3-S6. (b) Hatanaka, H.; Nakagawa. Y. *Int. J. Radiat. Oncol. Biol. Phys*. **1994**, *28*, 1061–1066.

26. Goodreau, B. H.; Spencer, J. T. *Inorg. Chem.* **1992**, *31*, 2612-2621.

27. (a) Li, Y.; Sneddon, L. G. *J. Am. Chem. Soc.* **2008**, *130*, 11494-11592. (b) Roth, A.; Meyer, F.; Paetzold, P. *Collect. Czech. Chem. Commun.* **1997**, *62*, 1299-1309. (c) Paetzold, P. *Eur. J. Inorg. Chem.* **1998**, *2*, 143-154. (d) Garrett, P. M.; Ditta, G. S.; Hawthorne, M. F. *J. Am. Chem. Soc.* **1971**, *93*, 1265-1266.

28. Hartl, M. A.; Williams, D. J.; Acatrinei, A. I.; Stowe, A.; Daemen, L. L. *Z. Anorg. Allg. Chem.* **2007**, *633*, 120-126.

29. Alcock, M. W.; Hagger, R. M.; Harrison, W. D.; Wallbridge, M. G. H. *Acta Cryst.* **1982**, *B38*, 676-677.

30. Peymann, T.; Lork, E.; Gabel, D. *Inorg. Chem.* **1996**, *35*, 1355-1360.

31. Mair, F. S.; Morris, J. H.; Gaines, D. F.; Powell, D. *J. Chem. Soc. Dalton Trans.* **1993**, 135-141.

32. (a) Legon, A. C. *Farad. Discuss.* **1994**, *97*, 19-33. (b) Ferreira, F.C.; Oliveira, B. G.; Ventura; E.; do Monte, S. A.; Braga, C. F.; Araujo, R. C. M. U.; Ramosc, M. N. *Spectrochim. Acta A*, **2006**, *64*, 156-160. (c) Antolõnez, S. A.; Lopez, J. C.; Alonso, J. L. *Chem. Phys. Lett.* **2001**, *334*, 250-256.

33. Hawthorne, M. F.; Miller, J. J. *J. Am. Chem. Soc.* **1958**, *80*, 754.

34. Than, C.; Morimoto, H.; Andres, H.; Williams, P. G. *J. Labelled Compd. Radio. Pharm.* **1998**, *38*, 693-711.

Chapter 6

Regeneration of Spent Ammonia Borane Hydrogen Fuels

Abstract

Spent fuel materials resulting from ammonia borane H_2-release were successfully digested in a number of strong acid systems to produce, according to ^{11}B NMR analysis, materials containing tetrahedral boron atoms devoid of remaining hydrogen. The digestate from the reaction of spent fuel with trifluoroacetic acid was found to react with dimethylethylamine alane to form dimethylethylamine borane; however, the dimethylethylamine could not be displaced by ammonia to produce ammonia borane (AB). Digestion of spent fuels resulting from only ~1 equivalent of AB H_2-release with superacidic $AlBr_3/HBr/CS_2$ solutions yielded BBr_3 which could be distilled out of the reaction mixtures; however, the digestion of more highly dehydrogenated spent fuels with ~2 equivalents of H_2-release could not be attained. Boron-halide reduction studies demonstrated that complexes readily formed upon reaction of BBr_3 with dialkylsulfides and that these R_2S-BBr_3 adducts could be quantitatively reduced to R_2S-BH_3 with either tin hydrides or silanes. The dialkylsulfides were then easily displaced from R_2S-BH_3 by ammonia to yield ammonia borane.

6.1 Introduction.

The thermal decomposition of ammonia borane (AB) leads to the production of linked forms of BNH_x compounds and free H_2. Whereas transition metal catalyzed dehydrocoupling reactions may yield specific, defined architectures,[1] solid state pyrolysis of AB leads to a number of products, as shown in **Figure 6.1.1**.

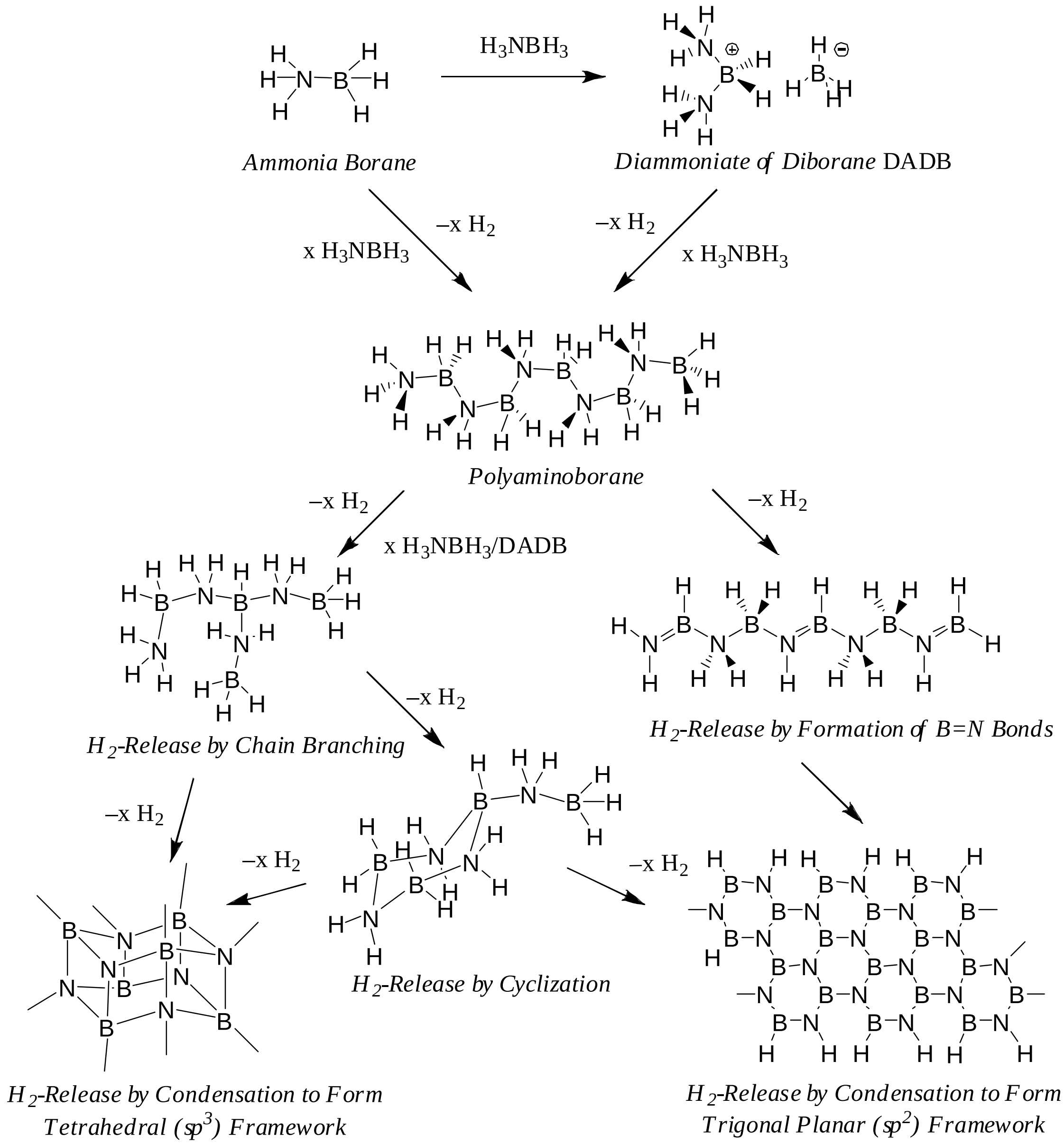

Figure 6.1.1. Possible end-products of the dehydrogenation of ammonia borane.

The exact polymeric form of the spent fuel, polyaminoborane (PAB), is not well defined, and depends on the degree of dehydrogenation achieved at the pyrolysis temperature. Thermochemical analysis showed that hydrogen was released from heated AB in 2 steps, with the first equivalent lost just under 100 ^{o}C, and a second equivalent completely lost around 200 ^{o}C.[2] Solid state ^{11}B NMR data indicated that at 88 ^{o}C, the temperature regime wherein only 1 equivalent of H_2 was released, the nonvolatile products of decomposition were linear and/or cyclic oligomers (**Eq. 1**).[3]

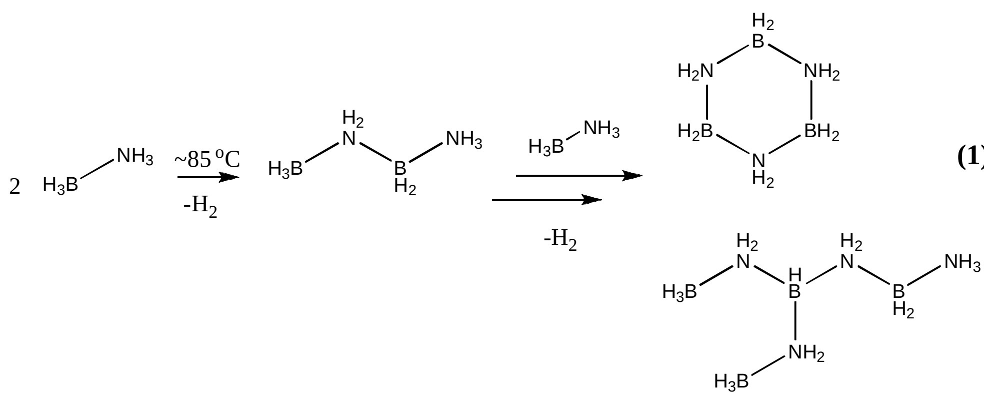

(1)

Pyrolysis at higher temperatures resulted in further release of H_2 and a shift in the structure of the products from polymers containing largely sp^3-hybridized boron to those with sp^2-hybridized boron. Solid state ^{11}B NMR of these products indicated the formation of polyborazylene, a linked network of borazine ($B_3N_3H_3$) monomers (**Eq 2**.).[4] Pyrolysis of AB, or dehydrogenated products, under very high temperatures (~ 1000 ^{o}C) results in the formation of ceramic hexagonal boron nitride.[5]

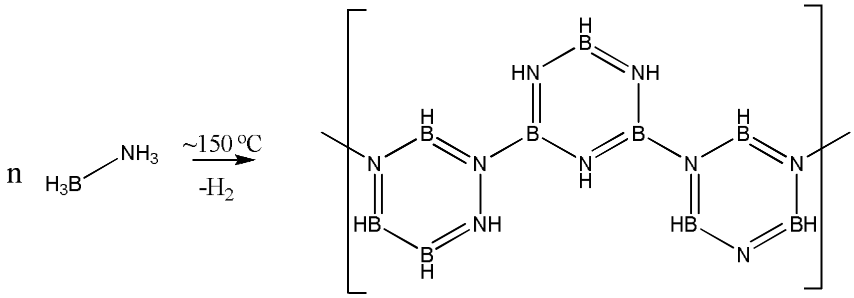

(2)

The decomposition of solid AB to an $(NH_2BH_2)_x$ polymer (PAB) was exothermic by ~5 kcal/mol at, and below, 90 °C.[6] High-level calculations indicate that nearly all possible dehydrogenation reactions of AB are exothermic. For example, the ΔH for the reaction linking 2 molecules of AB as shown in the first step of **Eq. 1** was calculated to be -20.5 kcal/mol at 0 °C, while the reaction of 3 molecules of AB to the cyclic trimer, cyclotriborazane (CTB), was calculated to be -55.9 kcal/mol at 0 °C.[7]

This exothermic nature of the dehydrogenation of AB poses challenges for any scheme to rehydrogenate spent fuel. Any potential process involving AB seeks to utilize as much of the bound hydrogen on the molecule as possible, but dehydrogenation reactions resulting in high degrees of chain-linking and unsaturation are thermodynamically down-hill, and yield comparatively low-energy products.[6] Regeneration of these products becomes increasingly challenging as the material is increasingly dehydrogenated.

Any viable regeneration process must be applicable to all spent-fuel materials and, in addition, avoid the formation of difficult to reduce intermediates. This chapter discusses an approach to AB regeneration from spent fuels involving: (1) the digestion of the spent AB fuels by strong acids to form BX_3 species; (2) base coordination of BX_3 and subsequent reduction of the base-BX_3 adduct to base-BH_3; and finally (3) displacement of the base from the base-BH_3 adduct by ammonia to produce AB.

6.2 Experimental

Materials. Ammonia borane (AB) was purchased from Aviabor and milled to a fine powder in a commercial coffee grinder. Trifluoroacetic acid (TFA) was purchased from Fisher and used as received. Aluminum bromide, HBr (anhydrous), BBr_3 (neat), triethylsilane (TES), and tributyltin hydride (TTH) were purchased from Aldrich and used as received. Ammonia (anhydrous) was purchased from Air Gas and used as received. Triethylamine, CS_2, and CH_2Cl_2 were purchased from Fisher and dried as described elsewhere.[8]

Computational Methods. Density Functional Theory (DFT) calculations were performed using the Gaussian 03 package.[9] Structures were optimized with the B3LYP method utilizing the 6-311G* basis set for all B, H, and S atoms, and the SDD psuedopotential for all Br atoms.

Physical Methods. ^{11}B NMR at 128.3 MHz and ^{1}H NMR at 400.1 MHz spectra were obtained on a Bruker DMX-400 spectrometer equipped with appropriate decoupling accessories. All ^{11}B chemical shifts are referenced to $BF_3 \cdot OEt_2$ (0.0 ppm), with a negative sign indicating an upfield shift. All proton chemical shifts were measured relative to internal residual protons from the lock solvents (99.9% $CDCl_3$) and then referenced to $(CH_3)_4Si$ (0.0 ppm).

Synthesis of Polyaminoborane at 85 ^{o}C (PAB1). In a typical experiment AB (200 mg, 6.49 mmol) was loaded into a round bottom flask equipped with a sidearm and Teflon stopcock. The flask was evacuated on a high vacuum and sealed, at which point it was heated at 85 ^oC under static vacuum for 14 h. The flask was evacuated and left under dynamic vacuum on a high vacuum for 12 h, yielding a white solid (198 mg) corresponding to the loss of 11 mg of H_2 (5.50 mmol, 0.85 eq).

Synthesis of Polyaminoborane at 120 ^{o}C (PAB2). After an identical setup to the 85 ^oC experiment the flask is heated at 120 ^oC under static vacuum for 12 h, evacuated, and held under dynamic vacuum on a high vacuum for 12 h. In a typical experiment 200 mg **AB** (6.49 mmol) was found yield 180 mg PAB2, corresponding to a loss of 20 mg H_2 (9.74 mmol, 1.5 eq).

Digestion of Spent Fuel with Trifluoroacetic Acid (TFA). (a) PAB1 (150 mg) was loaded into a 100 mL round bottom flask equipped with a sidearm and stir bar. The flask was connected to a high vacuum where TFA (~6 mL) was vacuum transferred. The mixture was heated at 60 ^oC for 12 h, during which time the solid PAB1 dissolved giving a monophasic, pale yellow solution. The TFA was removed in vacuo, yielding 803 mg of a yellow solid. (b) In an identical setup, PAB2 (100 mg) was stirred in ~6 mL of TFA at 60 ^oC for 12 h. All of the PAB2 dissolved giving products with identical ^{11}B NMR spectra as those found in (a). The TFA was removed in vacuo yielding 538 mg of a yellow solid. ^{11}B NMR (128.3 MHz, TFA): δ -0.40 (s), -1.60 (s).

Digestion of Spent Fuel with Other Oxyacids

PAB1 and PAB2 were digested in a number of other oxygen-containing acids of varying strength. The conditions and results of these experiments are summarized in **Table 7.3.1**.

Digestion Reactions with Anhydrous HCl. (a) In separate experiments, PAB1 (50 mg), PAB2 (50 mg) and h-BN (50 mg) were stirred in liquid anhydrous HCl (~7 mL) in a closed Fischer and Porter thick-walled pressure vessel at -78 ^{o}C for 4 h. The HCl was removed in vacuo and the product was pumped to dryness through a trap held at -90 ^{o}C. In each case, no boron containing species could be observed by ^{11}B NMR in the material in the cold trap and gravimetric analysis of the solids remaining in the flasks indicated no reaction had occurred. (b) Polyborazylene (97 mg) was stirred in liquid anhydrous HCl (~10 mL) in a closed pressure vessel at -78 ^{o}C for 4 h. The HCl was removed in vacuo yielding 231 mg of a white material that was insoluble in common solvents. The observed gravimetric uptake of the solid corresponded to an approximate formula $(B_3N_3H_9Cl_3)_x$ which would be consistent with the addition of one HCl molecule to 91% of all the unsaturated B-N units in polyborazylene. The material slowly lost HCl when held at room temperature.

Digestion Reactions with Superacidic HCl in Ionic Liquids. An acidic $AlCl_3$/BmimCl solution was prepared by the addition of $AlCl_3$ (473 mg, 3.5 mmol, 55 mol%) to BmimCl (500 mg, 2.9 mmol) as described elsewhere.[10] In two separate experiments, PAB1 (50 mg) samples were added to $AlCl_3$/BmimCl solutions in reaction vessels equipped with a gas inlet and outlet. The reactions were heated at (a) 65 ^{o}C and (b) 90 ^{o}C, respectively while anhydrous HCl was flowed through the reaction vessels with the exit gases being passed through -78 ^{o}C traps before being vented to the atmosphere through bubblers. After 2 h, the solutions were monophasic and all PAB1 had dissolved. No boron-species were found in the cold traps. The ^{11}B NMR analyses of the $AlCl_3$/BmimCl solutions diluted with CH_2Cl_2 showed new peaks at: (a) δ -31.2 (s), 0.2 (s), 0.0 (s). (b) δ 1.3 (s), 0.2

(s), -0.8 (s), -1.3 (s). Attempts to separate the products from the $AlCl_3$/BmimCl solutions by distillation and/or extraction were unsuccessful.

Digestion Reactions with Superacidic $AlBr_3$/HBr/CS_2[11]. (a) PAB1 (50 mg) and $AlBr_3$ (2.5 g, 9.36 mmol) were dissolved in ~12 mL of dry CS_2 in a 100 mL Schlenk flask equipped with a gas inlet. The mixture was stirred while the flask was filled with gaseous HBr. Stirring was continued for 4 h, with fresh HBr being added to the system every 20 min. The white solid SF1 gradually dissolved, yielding a dense, bubbling yellow oil. The ^{11}B NMR spectra of the clear CS_2 layer revealed the presence of BBr_3. The mixture was fractionated on a high-vacuum line through consecutive -95 ^oC and -198 ^oC traps. Dry triethylamine (TEA) (~5 mL) was vacuum transferred to the -95 ^oC trap and the mixture allowed to warm to room temperature. The BBr_3-TEA adduct[12] was concentrated in vacuo, yielding 228 mg (0.65 mmol, a 40% yield based on a NH_2BH_2 formula for PAB1) and was identified by its characteristic ^{11}B NMR spectrum (128.3 MHz, $CDCl_3$): δ -6.1 (s). The yellow oil that had separated from the CS_2 layer was analyzed by ^{11}B NMR (128.3 MHz, neat): δ -9.4 (s). (b) PAB2 (50 mg) and $AlBr_3$ (2.5 g, 9.36 mmol) were dissolved in ~12 mL of dry CS_2 and similarly treated with HBr. No formation of BBr_3 could be observed in the CS_2 solution by ^{11}B NMR.

Digestion Reactions with Superacidic $AlCl_3$/HCl/CS_2. (a) PAB1 (50 mg) was added to a solution of $AlCl_3$ (200 mg, 1.50 mmol) in CS_2 (~8 mL). Anhydrous HCl was bubbled into the reaction mixture for 3 h at room temperature with the exit gases passing through a -78 ^oC trap before being vented to the atmosphere through a bubbler. No dissolution of PAB1 was observed and analysis of the CS_2 layer by ^{11}B NMR showed no formation of soluble boron containing species. No boron containing products were found in the cold trap. (b) Using an identical setup, PAB1 and $AlCl_3$ were treated with HCl in toluene instead of CS_2. Again, no dissolution of PAB1 was observed, and no new boron containing species were found by ^{11}B NMR. (c) Liquid anhydrous HCl (~7 mL) was condensed into a Fischer and Porter thick-walled pressure vessel containing PAB1 (50 mg) and $AlCl_3$ (100 mg, 0.75 mmol). The mixture was stirred at -78 ^{o}C for 4 h. The volatiles were removed in vacuo, and ^{11}B NMR analysis of these volatiles showed no boron-containing species. Likewise, no soluble boron containing species were found in the remaining solids by ^{11}B NMR.

Triethylamine (TEA) BX_3 Complexation and B-X Reduction by Tributyltin Hydride (TBTH). (a) The addition of TEA (1.3 mL, 9.6 mmol) to a stirred 1 M solution of BCl_3 in heptane (8 mL, 8 mmol) at 0 ^{o}C resulted in the immediately formation of a white precipitate. Volatiles were removed in vacuo, and ^{11}B NMR analysis of a CH_2Cl_2 solution of the white solid indicated the formation of the TEA-BCl_3 adduct. ^{11}B NMR analysis indicated that the reaction of the solids in a stirred CH_2Cl_2 (~15 mL) solution with TBTH (7.74 mL, 28.8 mmol) at 60 ^{o}C for 3 days resulted in only partial reduction. Addition of TBTH (10 mL, 37.1 mmol) with further reaction for 12 h at 60 ^{o}C brought the reaction to ~95% TEA-BH_3. Attempts to separate the adduct from the tributyltin chloride and residual TBTH were unsuccessful. For TEA-BCl_3: ^{11}B NMR: δ 7.7; TEA-BH_3: -13.6 (q, J = 87 Hz). (b) TEA (0.43 mL, 3.0 mmol) was added to a solution of BBr_3 (640 mg, 2.64 mmol) in CH_2Cl_2 (~10 mL) and stirred for 5 min at room temperature at which point ^{11}B NMR analysis showed the quantitative formation of TEA-BBr_3[12]. For TEA-BBr_3: ^{11}B NMR: δ -6.2. This mixture was then treated with additional TBTH (6.34 mL, 23.8

mmol) for 1 h at room temperature, but ^{11}B NMR analysis showed no reaction. The reaction was then heated at 45 ^{o}C for 2 h, leading to quantitative conversion to TEA-BH_3.

The TEA-BH_3 adduct was independently synthesized by the addition of TEA to an equimolar amount of BH_3-THF. The solvent was removed in vacuo, at which point anhydrous liquid ammonia (~8 mL) was condensed onto the adduct and the mixture stirred for 2 h at -78 ^{o}C. The ammonia was removed in vacuo, but analysis by ^{11}B NMR showed no displacement of TEA by NH_3.

N,N-Diethylaniline (DEA) BBr_3 Complexation, B-Br Reduction with Triethylsilane (TES) and NH_3 Displacement to Produce Ammonia Borane. A sample of BBr_3 (1.21 g, 4.7 mmol) was reacted with DEA (0.84 mL, 4.7 mmol) in CH_2Cl_2 (~10 mL) at 0 ^{o}C. Analysis by ^{11}B NMR showed a new peak at -25.2 ppm, indicative of adduct formation. TES (6.0 mL, 37.5 mmol) was then added and the mixture stirred at room temperature for 5 min. Analysis by ^{11}B NMR showed quantitative conversion to DEA-BH_3.[13] Ammonia was then bubbled though the reaction mixture for 40 min, causing the precipitation of a large amount of white solid. The reaction flask was closed and the mixture stirred for 2 additional hours under an ammonia atmosphere. The precipitate was filtered and washed 3 times with hexanes, and then extracted with ether until further ether washes showed no traces of products in the ^{11}B NMR. The combined ether washes were concentrated in vacuo to yield AB (121 mg, 3.9 mmol, 84%). Examination of the reaction solution by ^{1}H NMR also revealed the formation of small amounts of para-bromodiethylaniline as a result of bromination of DEA.

General Complexation of BBr_3 with Dialkylsulfides and Reduction of Adducts. The reactions of BBr_3 in CH_2Cl_2 with equimolar amounts of a number of dialkylsulfides, including dimethyl, diethyl, dibutyl, dihexyl, diisopropyl and diisobutyl-sulfides and tetrahydrothiophene, resulted in the clean formation of their corresponding sulfide-BBr_3 adducts. The adducts all showed a single ^{11}B NMR resonance near -12 ppm. Each adduct could then be reduced with just over 3 molar equivalents of TES yielding BH_3-adducts with a single ^{11}B NMR resonance near -21 ppm. Complete reductions of the (*n*-alkyl)$_2$S-BBr_3 adducts with TES at 55 ^oC took 12-15 h, while the TES reductions of the R_2S-BBr_3 (R = isopropyl, isobutyl) adducts took 4 h at 55 ^oC to complete. As presented in the following two sections, the dialkylsulfide properties were selected to give the appropriate vapor pressure for efficient vacuum fractionation.

Synthesis of AB from BBr_3-Adducts with Triethylsilane (TES). BBr_3 (4.43 g, 17.7 mmol) and CH_2Cl_2 (~ 8 mL) were vacuum transferred into a 100 mL round-bottom flask equipped with a sidearm, stopcock and stirbar. This mixture was put under dry N_2 on a Schlenk-line and held at 0 ^oC while dihexyl sulfide (21.3 mmol, 5.06 mL) was added. The mixture was brought to room temperature and triethylsilane (68.3 mmol, 10.9 mL) was added under flowing N_2. The vessel was sealed and heated with stirring at 55 ^oC for 4 h at which point ^{11}B NMR analysis showed complete reduction of the BBr_3 to form the Hex_2S-BH_3 adduct. The mixture was fractionated on a high-vacuum line through consecutive -25 ^oC, -78 ^oC and -196 ^oC traps. The Hex_2S-BH_3 adduct was retained in the reaction flask (4.65 g, 17.7 mmol, ~100%), while triethylsilyl bromide (10.7 g, 5.2 mmol, 98%) was trapped at -25 ^oC and excess TES (1.6 g, 14.1 mmol, 96%) at -78 ^oC. The reaction flask was put back under N_2 and held at -78 ^oC while anhydrous NH_3 (8-10 mL) was condensed in. The mixture was stirred at -78 ^{o}C for 10 min, then the excess NH_3 was removed in vacuo. The resulting slurry was taken up in hexanes (~10 mL), filtered, washed 2 times with hexanes and dried in vacuo to yield AB (0.5 g, 16.9 mmol, 96%).

Synthesis of AB from BBr_3-Adducts with Tributyltin Hydride (TBTH). BBr_3 (1.41g, 5.6 mmol) was vacuum transferred into a two-neck, round-bottom flask equipped with a septum, vacuum adapter and stirbar. The flask was held at -78 ^{o}C while diethyl sulfide (0.91 mL, 8.4 mmol) was added. The mixture was warmed to 0 ^{o}C, then TBTH (4.75 mL, 17.6 mmol) was added and the reaction stirred for 10 min. The mixture was fractionated on a high-vacuum line through consecutive -78 ^{o}C and -198 ^{o}C traps. All tin products (6.4 g, 16.8 mmol tributyltin bromide + 0.8 mmol TBTH) remained in the reaction vessel while the Et_2S-BH_3 adduct (0.6 g) was collected at -78 ^{o}C. The adduct was vacuum transferred back into a round-bottom flask, and anhydrous NH_3 was condensed into the flask at -78 ^{o}C. The reaction was stirred for 10 min, then all excess NH_3 and diethyl sulfide were removed in vacuo, leaving behind AB (0.17 g, 5.6 mmol, ~100%).

6.3 Results and Discussion

At the outset of this project a possible general scheme, summarized in **Figure 6.3.1**, for the regeneration of ammonia borane from spent BNH_x fuels was proposed. The two key steps in the process were: 1) initial digestion of the AB spent-fuel with strong acids to form BX_3, followed by 2) a reduction-process to be carried out in one reaction vessel, involving coordination of the BX_3 to a base, reduction of the coordinated B-X bonds, and finally exchange of the base by ammonia to regenerate NH_3BH_3.

First Step: Acid Digestion of Spent Fuels

$$BNH_x + 4\,HX \longrightarrow BX_3 + NH_4X$$

Second Step: One-Pot Conversion of BX_3 to AB

Coordination of BX_3

$$BX_3 + \text{Base} \longrightarrow \text{BaseBX}_3$$

BX Reduction

$$\text{BaseBX}_3 + 3\,HMR_3 \longrightarrow \text{BaseBH}_3 + 3\,XMR_3$$

$M = Sn, Si$

Base Displacement by NH_3 to Yield AB

$$\text{BaseBH}_3 + NH_3 \longrightarrow H_3NBH_3 + \text{Base}$$

Figure 6.3.1 Overview of the proposed approach to AB regeneration.

6.3.1 Digestion of Spent Fuels with Acids. The first step envisioned in the regeneration process was the digestion of the polymeric spent fuel with acids, breaking B-N bonds via protonolysis (**Eq. 3**).

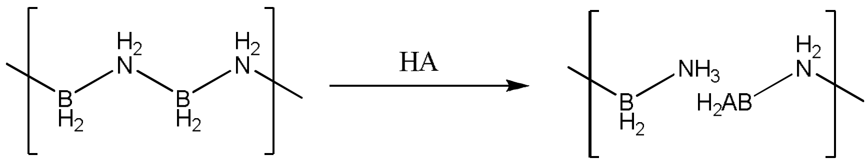

(3)

Ideally the protonolysis would effect only B-N bonds within the backbone, conserving remaining hydrogen on the PAB polymer; however, the hydridic nature of the B-H hydrogens resulted in the total dehydrogenation of boron yielding trigonal and/or tetrahedral species free of boron-bound hydrogen (BA_3, BA_4^-, NH_3BA_3, etc.). The oxophilic nature of boron, and the intrinsic strength of boron-halogen bonds, aided in the thermodynamics of digestion with oxyacids and hydrogen halides.

A number of acids/acidic systems with a range of strengths were tested (**Table 6.3.1**). Also listed are the ^{11}B NMR resonances found in the reaction mixture for each. All resonances were singlets in the ^{1}H-coupled ^{11}B NMR spectrum and, save the downfield resonances in the superacidic ionic liquid and the $HBr/AlBr_3$ systems, fell within the normal range for tetrahedral boron.

Table 6.3.1. List of acids and conditions employed in the digestion of PAB1 and PAB2, and the ^{11}B NMR resonances found in the digested mixture.

Acid	Spent Fuel Digested	Conditions	^{11}B NMR resonances
Superacidic Ionic Liquid	PAB1 and PAB2	65 ^{o}C, 2 h	31.2, 0.2, 0.0
Superacidic Ionic Liquid	PAB1 and PAB2	90 ^{o}C, 2h	1.3, 0.2, -0.8, -1.3
TFA	PAB1 and PAB2	Neat, 55 ^{o}C, 4-5 h	-0.4, -1.6
Triflic Acid	PAB1 and PAB2	Neat, 0 ^{o}C, mins	-3.88
Glacial Acetic Acid	PAB1	4:1 pyridine: acetic acid, 4 days	2.81, -0.06, -0.57
Glacial Acetic Acid	PAB1	neat, 60 ^{o}C, not fully solubilized	-0.06, -0.59
Formic Acid	PAB1	THF, excess formic acid	1.5
Chlorosulfonic	PAB2	Neat, 1h, 50 ^{o}C	-3.1, -4.6
$HBr/AlBr_3$	PAB1	CS_2, ~1 atm HBr	38, -9.5
$HBr/AlBr_3$	PAB2	CS_2, ~1 atm HBr	No digestion

6.3.1.1 Digestion with Oxyacids.

The reaction of both PAB1 and PAB2 in neat TFA at 55-60 ^{o}C led to the complete dissolution of the white polymer giving a monophasic solution that displayed a set of new ^{11}B NMR resonances (-0.4, -1.6) indicating tetrahedrally coordinated boron (**Figure 6.3.2)**.

The supernatant TFA was removed in vacuo, leaving a bubbly yellow oil that eventually solidified into a yellow solid. The product had gained mass, going from 150 mg initially, to 803 mg. Assuming the initial formulation as roughly $(BH_2NH_2)_x$, PAB took up just over 1 equivalent of TFA per B-N unit, though this assumes all retention of nitrogen in the sample, which is not necessarily the case. This lower than theoretical weight uptake precludes the formation of a simple boron-triester or triester-adduct. The products could not be identified further.

Both PAB1 and PAB2 were completely digested in neat triflic acid, giving an ^{11}B NMR spectrum with one sharp singlet at -3.9 ppm. The formation of a single product was attractive, but unlike TFA, triflic acid isn't volatile, and could not be removed in vacuo. Reactions of PAB1 and PAB2 in which stoichiometric amounts of triflic acid (1 equiv., 2 equiv., 3 equiv., and 4 equiv.) in hexanes gave products with peaks near 0.0 and a large broad peak near 20 ppm, diagnosed as trigonal $B\text{-}OTf_3$. As the amount of triflic acid added was increased, the resonances near 20 ppm decreased in intensity, and the singlets near 0.0 dominated indicating the conversion from trigonal to tetrahedrally coordinated boron.

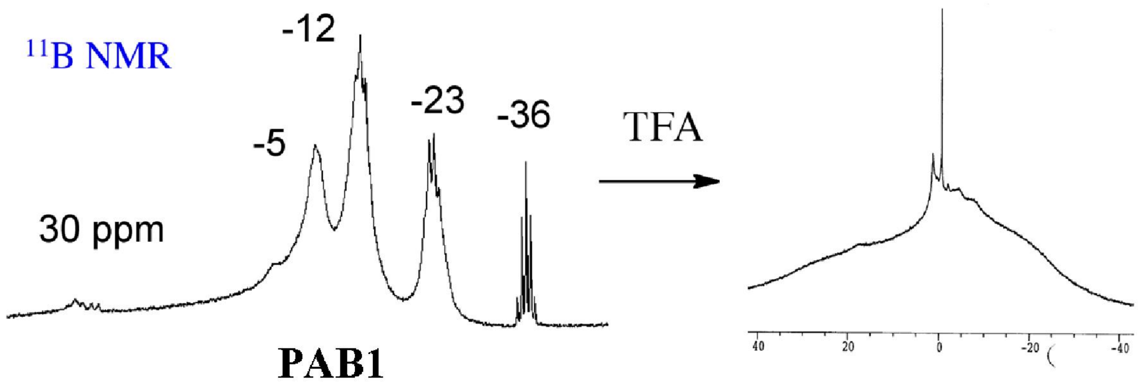

Figure 6.3.2 ^{11}B NMR analysis of the digestion of spent-fuel PAB1 with trifluoroacetic acid

When heated in neat glacial acetic acid the dissolution of the polymer was minimal, giving dilute ^{11}B NMR spectra with similar peaks to those seen in the digestion with TFA. However, when PAB1 was treated with a 4:1 mixture of pyridine:acetic acid, the polymer dissolved, giving a spectrum with 4 peaks ranging from 2.8 ppm to -0.6 ppm. Digestion in this mixture, which cannot be considered strongly acidic, points to the strength of the B-O bond as a driving force in polymer digestion, rather than simple protonolysis.

In hopes of yielding boron formate species which might be decomposed to B-H bonds and carbon dioxide, PAB1 was reacted with formic acid in THF. The product was a monophasic solution with one singlet in the ^{11}B NMR spectra at 1.5 ppm. The mixture was then heated to reflux, but analysis by ^{11}B NMR showed no signs of THF-BH_3. The volatiles were removed in vacuo, leaving a clear oil. This oil was then heated at 100 ^{o}C under vacuum, with volatiles collected at -198 ^{o}C. No boron was found in the cold trap, and the resulting viscous oil was no longer soluble in a range of normal organic solvents. After this experiment was carried out, calculations by collaborators showed that the degradation of B-$(OCOH)_3$ to BH_3 and CO_2 was energetically uphill, and as such efforts along these lines were halted.

Polymers PAB1 and PAB2 were both digested by neat chlorosulfonic acid ($ClSO_3H$), in hopes of promoting the reaction seen in **Eq. 6**.

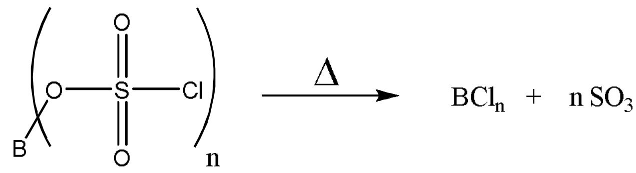 **(6)**

When dissolved in neat CSA the polymers gave ^{11}B NMR spectra with singlets slightly upfield of the other digestates (-3.1 ppm, -4.7 ppm), but isolation in vacuo followed by heating both in the presence and absence complexing agents, produced no decomposition to any identifiable boron-halide species.

6.3.1.2. Digestion with Haloacids.

As summarized in **Figure 6.3.2**, neither the spent-fuels (PAB1 and PAB2), nor commercial h-BN could be digested with anhydrous HCl. Polyborazylene did react with anhydrous HCl, but was not converted to molecular species. The observed HCl-uptake (mass balance) in the polyborazylene reaction instead suggested the production of a chlorinated cyclotriborazane polymer, such as shown in **Figure 6.3.2**, resulting from HCl-addition to the polyborazylene B=N units.

6.3.1.2.1 Digestion in Superacidic Ionic Liquid.

Ionic liquids constitute a set of organic salts with low melting points. One common class of ionic liquids are the 1-butyl-3-methylimadazolium halides (**Bmim.X**), that have melting points ranging from Bmim.Cl (~70 ^{o}C), to Bmim.Br (~60 ^{o}C), and Bmim.I which melts just below room temperature. It is known that the combination of aluminum halides and Bmim.X forms room temperature melts via **Eq. 4**, which, when combined with hydrogen halide (HX), become superacidic as a result of the equilibrium in **Eq. 5**.[10]

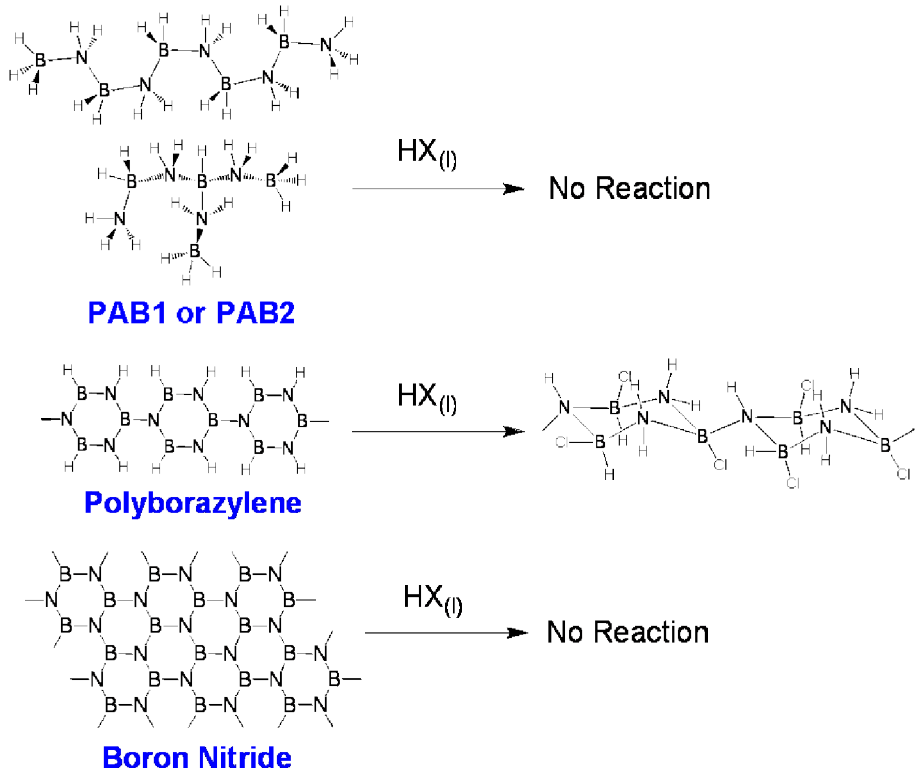

Figure 6.3.2. Summary of the results of the reactions of anhydrous HCl with spent-fuels, polyborazylene and boron nitride.

$$\text{Bmim.X} + 2\text{AlX}_3 \rightleftharpoons [\text{Al}_2\text{X}_7^-][\text{Bmim}^+] \quad \textbf{(4)}$$

$$\text{Al}_2\text{Cl}_7^- + \text{HX} \rightleftharpoons 2\text{AlCl}_4^- + \text{H}^+ \quad \textbf{(5)}$$

When either PAB1 or PAB2 were stirred in a mixture of $AlCl_3$ and Bmim.Cl under flowing HCl the white solid polymer dissolved with a good deal of bubbling. After a few minutes the bubbling stopped and the solution was monophasic.

When the reaction was run at 60 ^{o}C ^{11}B NMR analysis of the ionic liquid layer diluted with a small amount of CH_2Cl_2 gave the spectrum shown in **Figure 6.3.3**. The two upfield singlets, just downfield of 0.0, are likely $(H_2NBCl_2)_3$ and NH_3BCl_3 as these ^{11}B NMR resonances have been reported as 3.7[14] and 3.28[15] respectively. The downfield resonance near ~30 falls in the range for trigonal boron, and is similar to the reported shifts for B-trichloroborazine (30.3).[16]

When the digestion was performed at 90 ^{o}C , the downfield resonance disappeared, indicating the degradation of B-trichloroborazine. The four singlets present were centered around 0.0 ppm, but their identity could not be ascertained. In neither experiment were any boron-containing species separable from the ionic liquid.

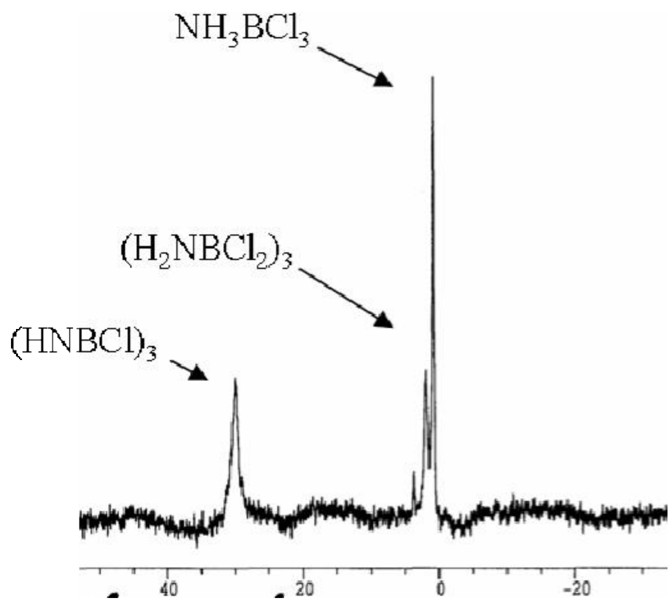

Figure 6.3.3. ^{11}B NMR spectrum of the products of the digestion of PAB at 60 °C in superacidic ionic liquid (Bmim.Cl/$AlCl_3$/HCl)

6.3.1.2.2. Digestion in Mixtures of $AlBr_3$/HBr.

In similar fashion to the superacidity of the Bmim.X/AlX_3/HX ionic liquid system, superacidity has also been reported when HBr was used in the presence of $AlBr_3$ in conventional solvents.[14] When 50 mg of PAB1 was added to a solution of 2.5 g $AlBr_3$ in CS_2 under ~1 atm of HBr the white polymeric solid bubbled slowly, eventually forming a yellow, immiscible oil at the bottom of the reaction vessel. Analysis of the supernatant CS_2 layer by ^{11}B NMR (**Figure 6.3.4**) showed the presence of BBr_3, which was removed in vacuo and complexed to triethylamine for quantification. A total of 228 mg of the BBr_3-TEA adduct was isolated, which accounts for ~40% of the boron in the sample of PAB1.

The remainder of the boron was contained in the viscous yellow oil. Analysis of the neat oil, insoluble in ethereal or chlorinated solvents, by ^{11}B NMR showed one singlet at -9.4 ppm. This peak was assigned, although not entirely definiteively, as hexabromocyclotriborazane, $(H_2N\text{-}BBr_2)_3$. This assignment fits the ^{11}B NMR trend found in brominated and chlorinated boron species, where brominated compounds show resonances somewhat upfield of their chlorinated analogues (**Table 6.3.2**). Even in the case of a mixed brominated and chlorinated species, $Et_2N\text{-}BClBr$, the ^{11}B resonance is between $Et_2N\text{-}BCl_2$ and $Et_2N\text{-}BBr_2$. A resonance of -9.5 ppm for $(H_2N\text{-}BBr_2)_3$ is reasonable as its chlorinated counterpart shows a resonance downfield of this, at 3.7 ppm.

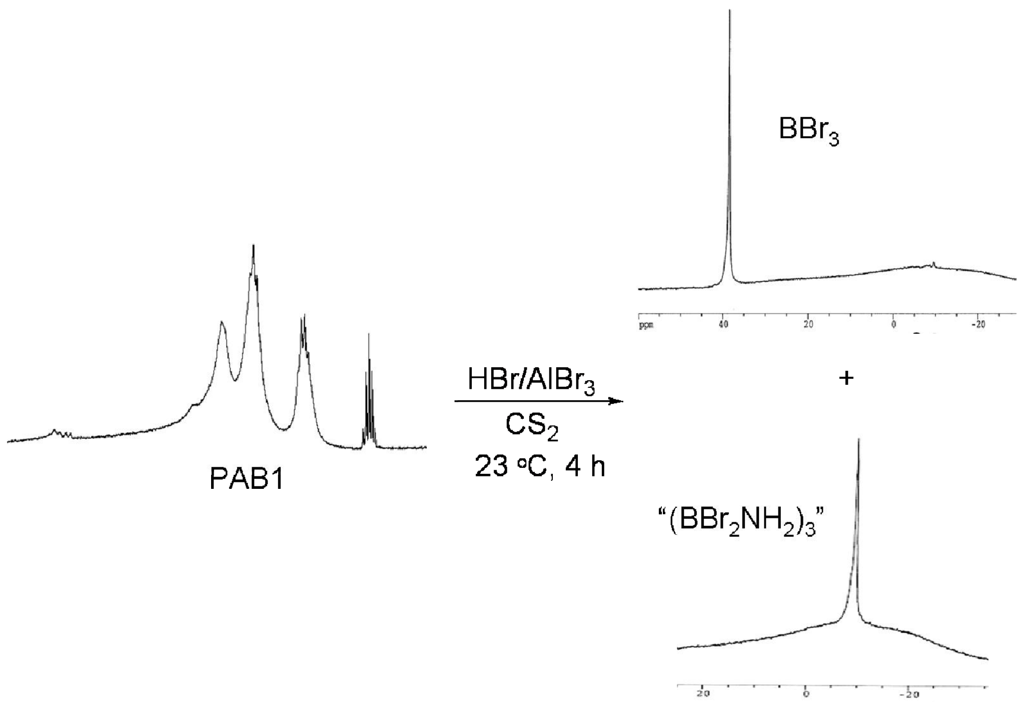

Figure 6.3.4. ^{11}B NMR of the reactants and products of the digestion of PAB1 in the $HBr/AlBr_3$ acidic system.

Table 6.3.2. ^{11}B NMR chemical shift comparison between some relevant chlorinated and brominated species. Values were taken from Noth and Wrackmeyer.[17]

Compound	δ (ppm)	Compound	δ (ppm)
BCl_3	41.9 - 48.0	BBr_3	38.5 - 44.0
$(HN\text{-}BCl)_3$	30.3 - 30.6	$(HN\text{-}BBr)_3$	28.6
$Et_3N\text{-}BCl_3$	10.0	$Et_3N\text{-}BBr_3$	-5.1
$Me_3N\text{-}BCl_3$	9.4 - 10.2	$Me_3N\text{-}BBr_3$	-3.1
$Et_2N\text{-}BCl_2$	30.3 - 30.8	$Et_2N\text{-}BBr_2$	25.6 - 26.7
$Et_2N\text{-}BClBr$	29.4		
$(BCl_2\text{-}NH_2)_3$	3.7		

This hexabrominated species has been reported only once, as the product of the treatment of borazine with Br_2.[18] The product, identified by characteristic IR stretches, is reported as a orange-yellow solid. This obviously differs from the yellow oil found in the degradation of PAB1, but this crude material likely contains a large amount of $AlBr_3$. Attempts to reduce the B-Br bonds to B-H bonds with tin hydrides or alanes, as will be described for other products of digestion later, were unsuccessful, most likely due to the presence of this $AlBr_3$.

When PAB2 was subjected to the same system no obvious decomposition was observed, and only very slight traces of BBr_3 were found in the CS_2 layer. It was clear that while this superacidic system was somewhat successful in digesting the less dehydrogenated, higher energy polymer, it was not successful with the more highly crosslinked, highly dehydrogenated material.

6.3.2 Recuction B-X and B-O Bonds.

Once the polymer is digested into monomeric units in the acidic system, the next step is to re-convert B-X bonds to B-H bonds (**Eq. 7**).

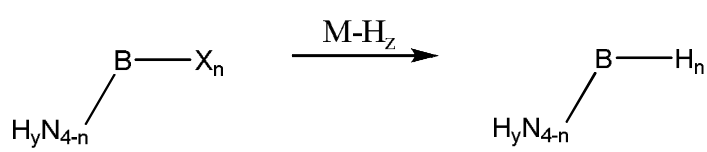

(7)

Collaborators have employed transition metal hydrides to this end with some success and have constructed a scale of hydride donor abilities to predict which hydride donors will energetically be able to displace which boron-bound species.[19] Highly energetic alkali metal hydrides are known to swap H^- for X^- as well.[20] Main group hydride metathesis is another route for re-hydrogenating digested polymer. Collaborators at Los Alamos have used tin-hydrides to displace boron-bound phenylthiols.[21] The use of tin,[22] aluminum[23] and silicon[24] hydrides for the metathesis of boron-halide bonds is likewise well known. We utilized these metathesis reactions in the treatment of spent fuels digested by TFA or in the HBr/$AlBr_3$ system.

6.3.2.1 Reduction of TFA-digestate with Alane. The room-temperature reaction of the TFA-digestate of PAB1 or PAB2 with an excess of a dimethylethylamine-alane adduct in toluene led to the reduction of all B-O bonds, yielding a product showing a quadruplet at -9.6 ppm in the ^{11}B NMR spectrum (**Figure 6.3.5**). Aside from the multiplicity of the peak indicating the presence of 3 boron-bound hydrogens, the assignment is further confirmed by the similarity in shift to other trialkylamino-boranes (eg. NMe_3-BH_3, $\delta = \sim -9$; NEt_3-BH_3, $\delta = \sim -13$).[17]

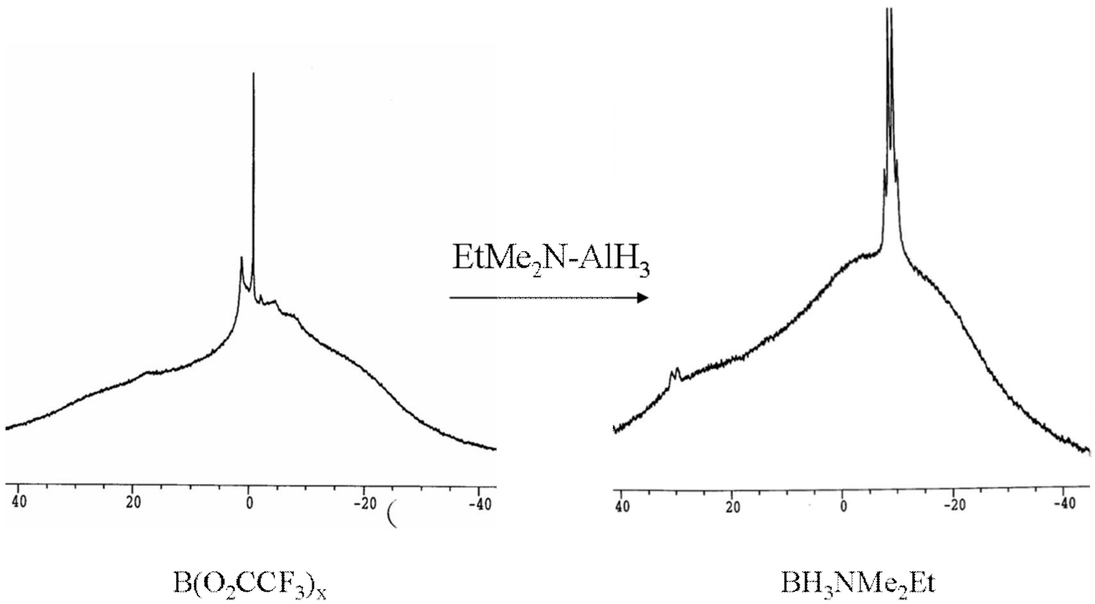

Figure 6.3.5. ^{11}B NMR spectra of the reactants and products of the reduction of TFA-digestate with dimethylethylamine-alane.

The amine-borane adduct is volatile, with a similar vapor pressure to the toluene solvent. This made isolation in vacuo difficult, as the temperatures used to trap the borane also trapped toluene. Ammonia borane is largely insoluble in toluene, so anhydrous ammonia was bubble through the system, but no displacement of the more-basic dimethylethylamine was found.

The TFA-digestate was not reduced when treated with either silicon or tin hydrides. This is likely due to the thermodynamic strength of the B-O bond. While the alane reduction took place under mild conditions with the TFA-digestate, the same treatment was unsuccessful in treatment of polymer digested in glacial acetic, or formic acids. The strength of the B-O bond is likely lower in the TFA-borate ester than in the non-fluorinated esters, as trifluoroacetate is significantly less basic than either acetate or formate.

6.3.2.2 Reduction of BBr_3 to AB. The release of boron as BBr_3 in the $AlBr_3$/HBr system exposed the need to find a pathway from BBr_3 to AB; however, complete reduction of BBr_3 would result in the formation and release of the dangerous, pyrophoric gas diborane (B_2H_6). Complexation of Lewis-acidic BBr_3 followed by reduction by hydrides would yield L-BH_3 species, circumventing the formation of diborane and enhancing the practical applicability of the process.

The ideal Lewis-base for this purpose is ammonia, as subsequent reduction would yield the target AB, however ammonia is not known to form adducts with BBr_3, and repeated attempts to synthesize NH_3-BBr_3 under a number of conditions only yielded intractable solids. Other bases employed for the sequestration of BBr_3 must form a sufficiently weak L-B bond so as to be displaced by ammonia downstream. This precludes the use of alkylamines, as they are more basic than ammonia, and impossible to displace. Two possible candidates were N,N-diethylaniline and dialkylsulfides. Each of these are Lewis-basic enough to complex both BBr_3 and BH_3, but form a bond sufficiently weak so as to be displaced by ammonia post-reduction.

The first attempts were made with N,N-diethylaniline (**Figure 6.3.6**), and while complexation, reduction with silane and displacement yielded AB, the overall reaction was hindered by unwanted Friedel-Crafts electrophilic aromatic substitution of bromine from BBr_3 on the aniline. Since recovery of starting materials is an important aspect of the overall regeneration process, attention was shifted toward reduction to sulfide-bound BBr_3.

It was found that BBr_3 formed stable complexes with every dialkylsulfide tested (eg. dimethyl, diethyl, dibutyl, dihexyl, diisopropyl, dicyclohexyl, diisobutyl, tetrahydrothiophene). These complexes were all soluble in a range of organic solvents, and all showed singlets in their respective ^{11}B NMR spectra around -12 ppm.

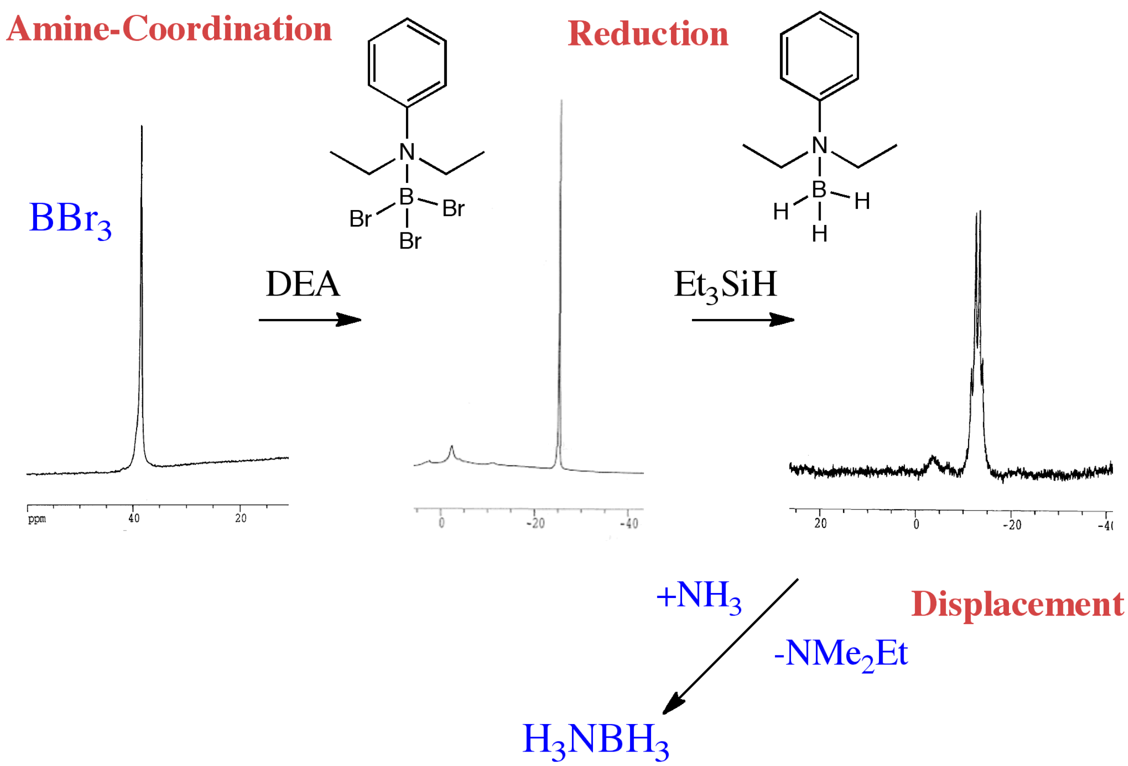

Figure 6.3.6. [11]B NMR analysis of the diethylaniline-based synthesis of ammonia borane from BBr_3 via coordination/reduction/displacement reactions.

The RS_2-BBr_3 adducts, when treated with 3.85 equivalents of triethylsilane (TES) at 55 °C in CH_2Cl_2 in a closed system for 12-15 h, gave a new boron species with a quartet around -23 ppm in its ^{11}B NMR spectrum. By comparison to similar compounds[17] this peak was assigned as R_2S-BH_3. The kinetics of the silane reduction differed depending on the steric bulk present near sulfur. In cases where R = *n*-alkyl (dimethyl, dibutyl, etc.), more than 12 h at 55 °C were needed for complete reduction. When diisopropyl sulfide was used as the Lewis base, the reaction was notably more vigorous (bubbling upon addition of the silane), and finished around 3-4 h. These kinetic differences point to a mechanism wherein the sulfide dissociates from the boron prior to B-X reduction, shown in **Eq. 8**.

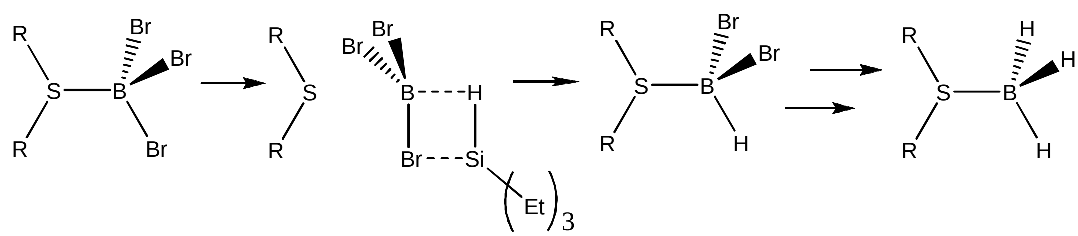

(8)

The bulk of the diispropylsulfide lengthens, and weakens, the B-S bond. Ground state DFT calculations of (i-Pr)$_2$S-BBr_3 show that the B-S bond is 2.106 Å long, notably longer than that calculated for Et_2S-BBr_3 (2.076 Å). The weakness of the B-S bond in (i-Pr)$_2$S-BH_3 was experimentally observed, as the compound was found to separate into its constitutive borane and sulfide under high-vacuum.

Tributyltin hydride (TBTH) was more reactive than TES in the reduction of the B-Br bonds, as this reduction was carried out at 0 °C, and was complete in minutes. As opposed to the silane, where ~3.85 equivalents were needed for efficient reduction, reduction with TBTH went to completion with almost exactly 3 equivalents, and could be run neat, simplifying the separation of products down the line. In the absence of solvent, reduction with TES was very slow.

6.3.2.3 Separation of Products from the Reduction of BBr_3. Once the tin or silane reduction was completed the products were separated via fractionation on a high-vacuum. Dialkylsufide-BH_3 adducts have a range of volatilities, depending on the size of the alkyl chain employed. Adducts of large sulfides, such as dihexylsulfide, have negligible vapor pressure, where as smaller sulfides are volatile under high vacuum.

The setup for the separation of the products of the reaction of $(C_6H_{13})_2S\text{-}BBr_3$ with 3.85 equivalents of TES is depicted in **Figure 6.3.7**. The dihexylsulfide-BH_3 adduct is not volatile, and remained in the reaction flask. The majority of the initial TES reacted to give triethylsilyl bromide, which is volatile at room temperature, but is stopped by a trap held at -25 ^oC. The remainder of the unreacted TES is sufficiently volatile to bypass the -25 ^oC trap, and is stopped at -78 ^oC.

As shown in **Figure 6.3.7**, the separation was very efficient, as greater than 90% of each of the products was isolated. From an engineering point of view, this is an important feature of the process. In the hydrogen economy, by-products such as silylbromide or excess TES need to be separated and sent to regeneration or back into the front end of the process. Physical separation eliminates waste streams that a chemical separation process (chromatography, etc.) would produce.

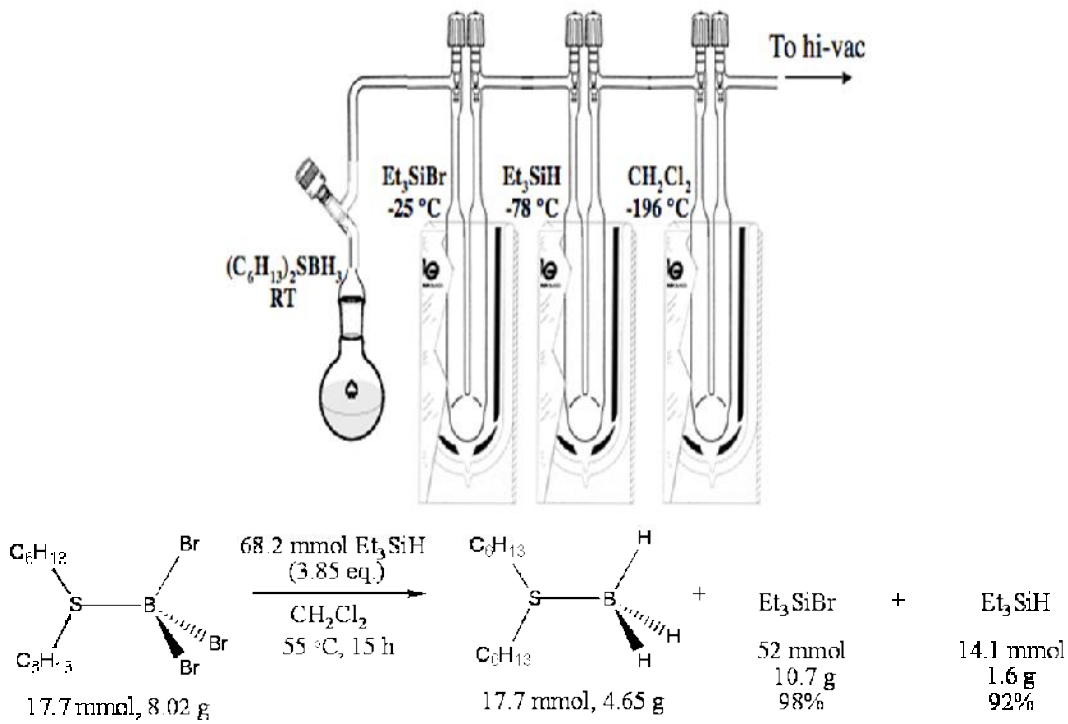

Figure 6.3.7. Reaction and product separation in the silane reduction of $(C_6H_{13})_2$-BBr_3

Neither TBTH nor tributyltinbromide have any significant vapor pressure at room temperature. In order to separate the sulfido-borane product from the tin by-products a Lewis-base was chosen to facilitate its removal by vacuum. The $(C_2H_5)_2S\text{-}BH_3$ adduct was sufficiently volatile and the products were separated as shown in **Figure 6.3.8**.

Again, full separation of the product borane from the tin by-products was achieved. While the tin hydride/bromide mixture could not be separated in vacuo, the efficiency of the reaction allowed for the use of just 3 equivalents of tin hydride, limiting the amount of residual hydride in the byproduct mixture.

6.3.2.4 Displacement of Sulfide with Ammonia. For both $(C_2H_5)_2S\text{-}BH_3$ and $(C_6H_{13})_2\text{-}BH_3$, stirring in liquid ammonia at -78 ^{o}C gave quantitative displacement of the sulfide and yielded AB (**Eq. 9**).

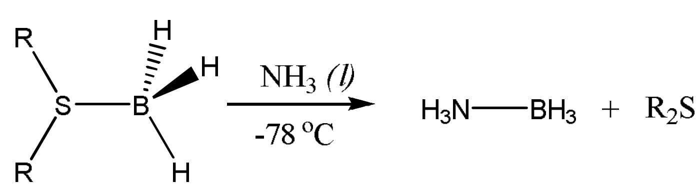

(9)

After the $(C_2H_5)_2\text{-}BH_3$ adduct was stirred in ammonia for 10 min the volatiles were vacuum-evaporated leaving pure AB. Unfortunately, dihexylsulfide is not volatile at room temperature, but the insolubility of AB in non-polar solvents such as hexanes allowed for the precipitation and filtration of AB. In both cases the yield of AB from initial BBr_3 was quantitative.

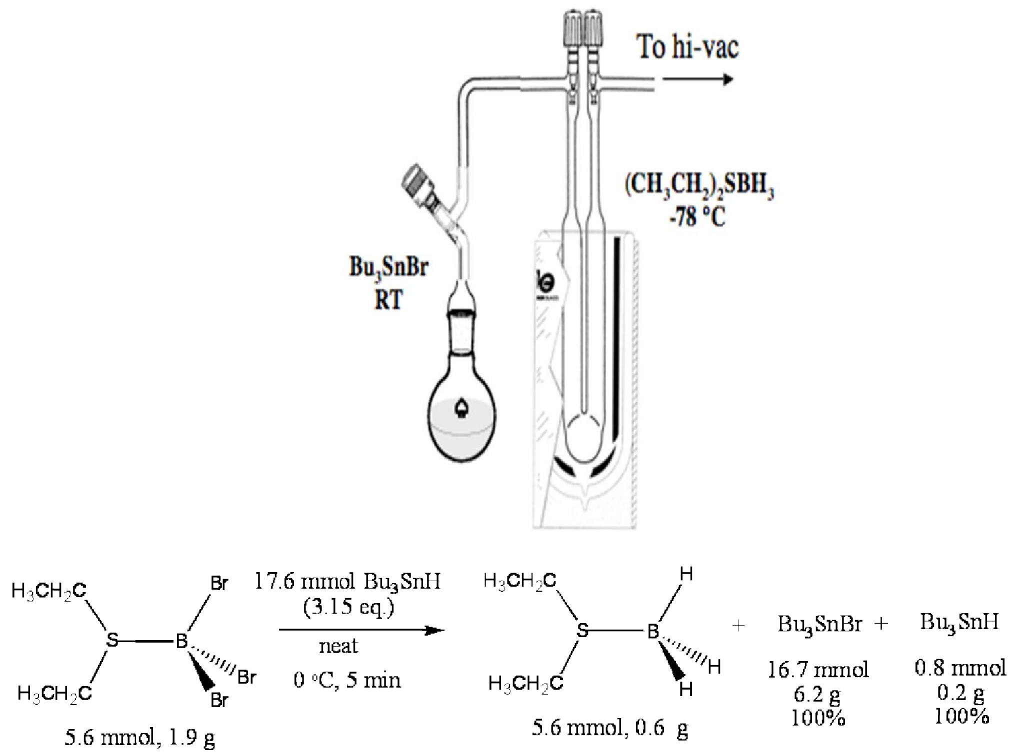

Figure 6.3.8. Reaction and separation method for the tin hydride reduction of $(C_2H_5)_2S$-BBr_3

6.4 Conclusions

The work presented here can be grouped into two areas, digestion and regeneration. The PAB polymer can be digested by a number of acids or varying strengths into monomeric units. The identity and composition of these units are ill-defined, but in most cases they bear sharp singlets around 0.0 ppm in the ^{11}B NMR indicative of tetracoordinate species.

The use of the $HBr/AlBr_3$ system in CS_2 allowed for the collection of some digested boron as BBr_3, but most of the original boron was contained in a thick, insoluble oil (designated as $(BBr_2NH_2)_3$). Digestion of the polymer into BBr_3 was attractive as there are a number of ways to reduce boron halide bonds. Complexing BBr_3 to dialkyl sulfides allowed for the reduction of the B-Br bonds without the formation of diborane by both silicon and tin hydrides. Sulfides were easily displaced by ammonia, and the production of AB from BBr_3 is quantitative. The acidic system, however, failed to digest more highly dehydrogenated spent fuels (PAB2).

The use of the strong reducing agent alane successfully reduced all B-O linkages in PAB/TFA digestate to B-H bonds. This reaction, though an important proof of concept, is less important in practical use. Aluminum-oxygen bonds, like boron-oxygen bonds, are strong and would need to be regenerated back to Al-H bonds if the process was to be cycled. Currently there is no energy efficient way to do this chemistry, and this problem would need solving before reduction with alanes can be seen as practical.

6.5 References

1. (a) Sloan, M. E.; Staubitz, A.; Clark, T. J.; Russell, C. A.; Lloyd-Jones, G. C.; Manners, I. *J. Am. Chem. Soc.* **2010**, *132*, 3831-3841. (b) Jaska, C. A.; Temple, K.; Lough, A. J.; Manners, I. *Chem. Comm.* **2001**, 962–963. Jaska, C. A.; Temple, K.; Lough, A. J.; Manners, I. *J. Am. Chem. Soc.* **2003**, *125*, 9424–9434.

2. Baitalow, F.; Baumann, J.; Jaenicke-Robler, K.; Leitner, G. *Thermochim. Acta* **2002**, *391*, 159-168.

3. Stowe, A. C.; Shaw, W. J.; Linehan, J. C.; Schmid, B.; Autrey, T. *Phys. Chem. Chem. Phys.* **2007**, *9*, 1831-1836.

4. Himmelberger, D. W.; Yoon. C. W.; Bluhm, M. E.; Carroll, P. J.; Sneddon, L. G. *J. Am. Chem. Soc.* **2009**, *131*, 14101-14110.

5. Fazen, R. J.; Remsen, E. E.; Beck, J. S.; Carroll, P. J.; McGhie, A. R.; Sneddon, L. G. *Chem. Mater.* **1995**, *7*, 1942-1956.

6. Wolf, G.; Baumann, J.; Baitalow, F.; Hoffmann, F. P. *Thermochim. Acta* **2000**, *343*, 19-25.

7. Matus, M. H.; Anderson, K. D.; Camaioni, D. M.; Autrey, S. T.; Dixon, D. A. *J. Phys. Chem. A* **2007**, *111*, 4411-4421.

8. Perrin, D. D.; Amarego, W. L. F. *Purification of Laboratory Chemicals*, 3rd ed.; Pergamon Press: New York, 1988.

9. Frisch, M. J.; Trucks, G. W.; Schlegel, H. B.; Scuseria, G. E.; Robb, M. A.; Cheeseman, J. R.; Montgomery, J. A., Jr.; Vreven, T; Kudin, K. N.; Burant, J. C.; Millam, J. M.; Iyengar, S. S.; Tomasi, J.; Barone, V.; Mennucci, B.; Cossi, M.; Scalmani, G.; Rega, N.; Petersson, G. A.; Nakatsuji, H.; Hada, M.; Ehara, M.; Toyota, K.; Fukuda,

R.; Hasegawa, J.; Ishida, M.; Nakajima, T.; Honda, Y.; Kitao, O.; Nakai, H.; Klene, M.; Li, X.; Knox, J. E.; Hratchian, H. P.; Cross, J. B.; Adamo, C.; Jaramillo, J.; Gomperts, R.; Stratmann, R. E.; Yazyev, O.; Austin, A. J.; Cammi, R.; Pomelli, C.; Ochterski, J. W.; Ayala, P. Y.; Morokuma, K.; Voth, G. A.; Salvador, P.; Dannenberg, J. J.; Zakrzewski, V. G.; Dapprich, S.; Daniels, A. D.; Strain, M. C.; Farkas, O.; Malick, D. K.; Rabuck, A. D.; Raghavachari, K.; Foresman, J. B.; Ortiz, J. V.; Cui, Q.; Baboul, A. G.; Clifford, S.; Cioslowski, J.; Stefanov, B. B.; Liu, G.; Liashenko, A.; Piskorz, P.; Komaromi, I.; Martin, R. L.; Fox, D. J.; Keith, T.; Al-Laham, M. A.; Peng, C. Y.; Nanayakkara, A.; Challacombe, M.; Gill, P. M. W.; Johnson, B.; Chen, W.; Wong, M. W.; Gonzalez, C.; Pople, J. A. *Gaussian 03*, revision B.05; Gaussian, Inc.: Pittsburgh PA, 2003.

10. Smith, G. P.; Dworkin, A. S.; Pagni, R. M.; Zingg, S. P. *J. Am. Chem. Soc.* **1989**, *111*, 525-530.

11. Farcasiu, D.; Fisk, S. L.; Melchior, M. T.; Rose, K. D. *J. Org. Chem.* **1982**, *47*, 453-457.

12. Gates, P. N.; McLaughlan, E. J.; Mooney, E. F. *Spectrochim. Acta* **1965**, *21*, 1445-1448.

13. Camacho, C.; Paz-Sandoval, M. A.; Contreras, R. *Polyhedron* **1986**, *5*, 1723-1732.

14. Gaines, D. F.; Schaeffer, R. *J. Am. Chem. Soc.* **1963,** *85*, 3592-3594.

15. Avent, A. G.; Hitchcock, P. B.; Lappert, M. F.; Liu, D.-S.; Mignani, G.; Richard, C.; Roche, E. *J. Chem. Sci., Chem. Comm.*. **1995**, 855-856.

16. Wrackmeyer, B.; Noth, H.; *Chem. Ber.* **1976**, *109*, 3480-3485.

17. Noth, H.; Wrackmeyer, B. in *NMR: Basic Principles and Progess*, Vol. 14; Deihl, P., Fluck, E., Kosfeld, R., Eds.; Springer-Verlag: Berlin, Germany, 1978.

18. Riley, R. F.; Schack, C. J. *Inorg. Chem.* **1964**, *3*, 1651-1653.

19. Mock, M. T.; Potter, R. G.; Camaioni, D. M.; Li, J.; Dougherty, W. G.; Kassel, W. S.; Twamley, B.; DuBois, D. L. *J. Am. Chem. Soc.* **2009**, *131*, 14454-14465.

20. (a) Jorg, K.; Noth, H. *J. Organomet. Chem.* **2000**, *214-215*, 168-187. (b) Douthwaite, R. E. *Polyhedron* **2000**, *19*, 1579-1583.

21. Davis, B. L.; Dixon, D. A.; Garner, E. B.; Gordon, J. C.; Matus, M. H.; Scott, B.; Stephens, F. H. *Agnew. Chem. Intl. Ed.* **2009**, *48*, 6812-6816.

22. Ashe III, A. J.; Klein, W.; Rousseau, R. *Organomet.* **1993**, *12*, 3225-3231. (b) Gaines, D. F.; Kunz, J. C.; Kulzick, M. J. *Inorg. Chem.* **1985**, *24*, 3336-3338.

23. (a) Herberich, G. E.; Baul, T. S. B.; Englert, U. *Eur. J. Inorg. Chem.* **2002**, 43-48. (b) Ashe III, A. J.; Butler, W.; Sandford, H. F. *J. Am. Chem. Soc.* **1979**, *101*, 7066-7067. (c) Bestmann, H. J.; Arenz, T. *Agnew. Chem.* **1986**, *98*, 571-572. (d) Pelter, A.; Singaram, S.; Brown, H. *Tet. Lett.* **1983**, *24*, 1433-1436. (e) Jadhav, P. K.; Kulkarni, S. U. *Heterocycles* **1982**, *18*, 169-173.

24. Parks, D. J.; Spence, R. E. v. H.; Piers, W. E. *Agnew. Chem. Intl. Ed.* **1995**, *34*, 809-811.